Engineering Nanoparticle Vaccines for Respiratory Infections

By

Frances Clare Knight

Dissertation

Submitted to the Faculty of the

Graduate School of Vanderbilt University

in partial fulfillment of the requirements

for the degree of

DOCTOR OF PHILOSOPHY

in

Biomedical Engineering

June 30, 2020

Nashville, Tennessee

Approved:

John T. Wilson, PhD

James E. Crowe, Jr., MD

Craig L. Duvall, PhD

Sebastian Joyce, PhD

Ethan Lippman, PhD

Helen Keipp Talbot, MD, MPH

This work is dedicated to my parents, who wholeheartedly supported my education (all thirty years of it), and my teachers and mentors through the years who inspired my interests and guided me along the way.

ACKNOWLEDGEMENTS

I couldn't have made it to the end of grad school without help from a lot of people. First, I want to thank my advisor, John Wilson, for bringing me into the lab as his third grad student (and first from biomedical engineering!) and trusting me to help set the lab on a course for success—and for the fun pizza parties. I am also thankful to my committee for providing insight on my research, collaborative opportunities, and career advice for the future. I am very grateful that I was able to incorporate my love of immunology into my graduate work.

I am thankful for those in my lab, in collaborating labs, and in the biomedical engineering, chemical engineering, and immunology departments who supported me, both in my work and as friends, including: Sema Sevimli, the best post-doc a lab could ever have; Dan Shae and Max Jacobson, my fellow "early grad students"; Kyle Garland and Carcia Carson, my office buddies who helped me through the final stretch of my PhD work; Jonah Rosch and Mohsin Rahim, for fun nights out and movie nights in; Ian Njoroge, who helped me finish my Saucer plate; and Pavlo Gilchuk and Amrendra Kumar, who were invaluable sources of expertise and knowledge on mouse work and flow cytometry. And, of course, all other labmates and collaborators who helped me with anything at any point along the way—I couldn't have done it without you! (I also want to thank my cat Rosie and every single dog and cat that I petted in the last six years, I couldn't have done it without you either.)

In particular I have to mention my fellow BME grad student cohort, who still feel like "new friends" until I think about the fact that we've now known each other for more than half a decade! It was an honor to go on this journey with you all. I especially want to mention my good friends who were there with me till the very end: Evan Kazura and Kristina Podesta, Wilson and Kat Adams (and Baby Ruth!), Kristy Walsh, Dan Gil, Tiffany Heaster, Jeremy Ford, and Meredith Jackson. I've loved every minute of Oktoberfests, Kay Bob's patio beers, game nights, kayaking, and New Year's Eves with y'all. Coronavirus had to show up and ruin our last few months (hmph), but I hope we'll all get to be together again in the future.

Of course, I also need to mention my good friends outside Vanderbilt who helped keep me sane: my best sister-friends, Maggie Faber and Megan Reape; my high school gaming buddies, Tom Gorman and Rick Dort; my Purdue friends: Ashley Laterza, Kara Luitjohan, Emma Kaiser, Sean Sullivan, and Amanda Schoolcraft; my cousin and vacation buddy, Gabrielle Prato; and my Nashville pals: Michael Leathers, Anushree Singh, and Mustache Man (Steve Jagla).

I also want to acknowledge the teachers and mentors who, in hindsight, very clearly shaped my path forward, especially: Ms. Chilton-Davis, my high school biology teacher, and Ms. Wasielewski, my two-times high school English teacher (writing is important too!); Prof. Alyssa Panitch, my first research mentor, and her grad student Jamie Brugnano, who taught me good research habits; Prof. Noel Murphy,

who helped make it possible for me go to Ireland for my master's degree, and Prof. Doug Heimburger, who welcomed me into the global health community at Vanderbilt. I also want to mention the support system I found in my later years at Vanderbilt that helped me through the final stretch: Stacey Satchell, Dean Ruth Schemmer, and Prof. Keipp Talbot—all women that I admire greatly.

Finally, and most importantly, I want to thank my parents who unquestioningly and unwaveringly supported me in going to school again…and again...and again. They encouraged academic success from an early age, they made me eat my veggies, they supported me financially, and they helped me become a successful and compassionate person. I also want to thank both sides of my extended family for their love and support and for giving me something to look forward to at the holidays—especially all the kiddos in my family who are going to grow up to be amazing humans and do amazing things.

To anyone I may have forgotten, I apologize deeply and it will keep me up at night, but know that you are loved and appreciated.

Finally, I would like to acknowledge my funding sources: NIH 5R21AI121626, NIH HL121139, NSF CBET-1554623, the Vanderbilt University Discovery Grant Program, the Vanderbilt University School of Engineering, Veteran's Affairs Merit Award BX001444, and the Stand Up To Cancer Innovative Research Grant No. SU2C-AACR-IRG 20-17. Stand Up To Cancer (SU2C) is a program of the Entertainment Industry Foundation; research grants are administered by the American Association for Cancer Research, the scientific partner of SU2C. Thanks also to the Vanderbilt Translational Pathology Shared Resource, the Flow Cytometry Shared Resource (especially Dave Flaherty and Brittany Matlock), the Institute for Nanoscale Science and Engineering (VINSE), and the Institute for Global Health (VIGH).

TABLE OF CONTENTS

Page

LIST OF TABLES

Table Page

LIST OF FIGURES

CHAPTER 1

Introduction

1.1 Background and Significance

In recent years, tissue-resident memory T cells have attracted a great deal of attention in the field of vaccine development. Many globally important diseases for which new or improved vaccines are needed, such as influenza and tuberculosis, require a robust T cell response to effectively fight off infection.[1, 2] In addition, the burgeoning field of cancer immunotherapy has benefited from technologies that can generate tumor-infiltrating T cells.[3-5] With regard to vaccine science, the importance of memory T cells is well-established.[6] For many years, memory T cells were divided into two types: central (T_{CM}), which circulate between lymphoid organs and the blood, and effector (T_{EM}), which circulate between the blood and peripheral tissues.[7] Now, a growing field of literature is showing that a separate and distinct subset of memory T cells—tissue-resident memory T cells, or T_{RM}—may be the ideal class of vaccine-induced T cell memory for combating many different pathogens and cancers (**Figure 1.1**). And, because T_{RM} often reside in the mucosal tissues that are common sites of pathogen encounter—for example, the lungs or urogenital tract—attention has also turned to developing methods for mucosal immunization that can promote a robust and long-lasting T_{RM} response.[8, 9] This is in contrast to traditional methods of vaccination that have been used for many years: intramuscular or systemic immunization primarily meant to elicit antibody responses. While antibody-producing vaccines remain important—immunization that generates neutralizing antibodies against pathogens such as influenza and HIV has shown great promise[10, 11]—it is becoming ever clearer that, for some pathogens, vaccines that can produce memory T cells or supplement other vaccines to produce both cellular and humoral immunity are greatly needed. In fact, Fang and Sigal showed that $CD8^+$ T cells and antibodies worked in concert to orchestrate a complete immune response that protected mice against lethal viral infection; the T cell response dominated the early phase of immunity, while antibodies were critical for later stages of protection against the virus.[12]

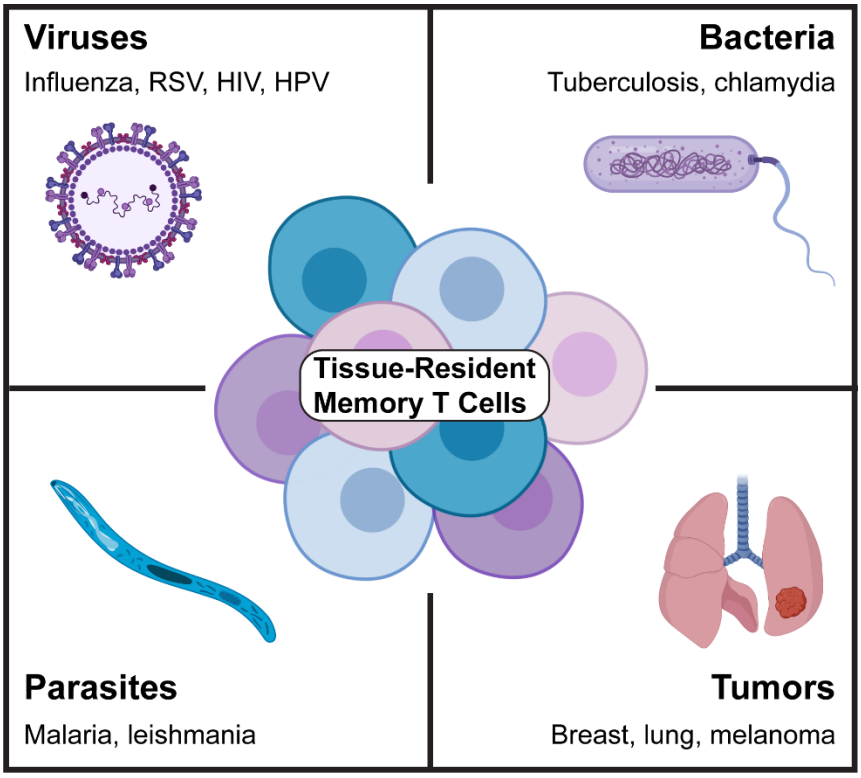

Figure 1.1 | Role of T_{RM} in infections and cancer. Tissue-resident memory T cells play a key role in defense against a range of viral, bacterial, and parasitic pathogens, as well as in cancers in multiple organs and mucosal tissues. Figure created with Biorender.com.

Although vaccines are often considered the single greatest contribution to public health, the field has also, in many ways, been slow to advance. For years, vaccines were exclusively made using either live attenuated or inactivated/killed microbes, which pose a variety of safety concerns.[13] In addition, until recently there was only one adjuvant approved for use in humans, alum, which has long been ill-defined—its precise mechanisms of action are still being studied today.[14] However, there has lately been a renaissance in vaccine development. In particular, materials science and engineering have intersected with vaccine design by way of immunoengineering: the application of engineering principles to study the immune system and design new and improved therapies to harness or modulate immune responses. New technologies such as stimuli-responsive polymers, virus-like particles, peptide nanofibers, lipid nanocapsules, and nanoparticles formed from naturally-occurring materials have shown promise for a new generation of vaccines that afford greater control over the immune responses they generate. In particular, they represent the potential for engineering vaccines that can specifically generate tissue-resident memory T cells and provide greater protection against pathogen encounter than many of the vaccines currently in use. They also offer the ability to minimize potential harmful side effects of adjuvants via targeted, localized delivery.

This chapter will provide an overview of tissue-resident T cell biology and commonly-used experimental techniques for demonstrating tissue residency, as well as lessons learned from studies of T_{RM} in viral infection and ways in which these lessons can be applied to vaccine design. It will also highlight reports of current technologies in the field of T_{RM}-targeted vaccines, focusing on viral vectors and engineered biomaterials.

1.1.1 Tissue-Resident T Cell Biology

Tissue-resident memory T cells are a specialized subset of memory cells with a phenotype and transcriptional signature distinct from those of central and effector memory T cells (T_{CM} and T_{EM}, respectively). Originally, memory T cells were thought to be maintained in circulation in the blood; later, they were divided into two distinct subsets according to their expression of CCR7, a lymph node homing receptor.[15] In this division of labor, T_{EM} ($CCR7^{lo}$) provide "protective memory" by migrating to inflamed peripheral tissues, where they exert immediate effector functions. Conversely, "reactive memory" is mediated by T_{CM} ($CCR7^{hi}$), which home to secondary lymphoid organs and rapidly proliferate and gain effector functions in response to antigen encounter.[16] This new model of T cell memory demonstrated that migration outside the blood could play an important role in protective cellular immunity. Later, further studies in mice uncovered both $CD8^+$ and $CD4^+$ "T_{EM}" cells distributed across multiple locations, including mucosal and barrier tissues such as the lungs, skin, and gut—however, these cells remained resident in the tissues even after infections had resolved, leading to them to be categorized as T_{RM}, a separate subset of T cell memory that provides localized protection in tissues. This has also led to the hypothesis that T_{RM} cells may in fact be derived from T_{EM}, rather than following a separate developmental pathway prior to memory formation.[7, 17]

The portals of entry for many infectious pathogens are the mucosal and barrier tissues in which T_{RM} make their home; thus, T_{RM} represent the ideal first line of defense against these pathogens, optimally positioned to respond more quickly than circulating T cells. T_{RM} are confined to their home tissues due to a combination of adhesion molecules that hold them there, and a lack of homing mechanisms for trafficking to distal lymphoid organs or circulating in the blood.[5] These cells have been identified in many organs in both mice and humans, including the skin, liver, kidneys, brain, and mucosal tissues such as the lungs, intestine, and urogenital tract.[15, 17, 18] There, they play a key role in protection against multiple infectious diseases for which new or improved vaccines are needed, including tuberculosis, influenza, malaria, respiratory syncytial virus, and HIV/AIDS;[19-24] in addition, T_{RM} are important in immunity against multiple types of tumors, including melanoma and breast, lung, and head and neck cancer.[25-28]

Work is ongoing to precisely define the factors needed for generation and maintenance of T_{RM} cells. They have been found to possess a unique transcriptional signature and an array of distinct surface markers, and multiple cytokines and other molecules play a role in their formation. T_{RM} can also be defined by the markers that they lack: for example, they do not express sphingosine-1-phosphate (S1P) receptor or CCR7, both of which are involved in T cell migration from tissues.[5, 17] CD69, a common T_{RM} marker, also serves to downregulate expression of the S1P receptor. While T_{CM} cells are often defined by a $CD62L^+CD44^+$ phenotype, T_{RM} express high levels of CD44 but lack CD62L, which is an adhesion molecule used for lymph node entry.[5] Low expression of KLRG1 also seems to be characteristic of T_{RM}; this may be due to the fact that its ligand is E-cadherin, which also binds the T_{RM} marker CD103.[17] CD103 is an adhesion molecule that may contribute to T_{RM} persistence in home tissues. While CD103 is often considered a canonical T_{RM} marker, it is not universally expressed on T_{RM} in all tissue compartments; for example, in the lungs, its expression can vary between the epithelium and parenchyma.[17, 29] Other adhesion molecules that may serve the same purpose include CD49a (VLA-1) and LFA-1.[5, 30]

Various transcription factors have been found to be up- or downregulated in T_{RM} populations. Eomesodermin and transcription factor 1 (TCF1) are expressed at lower levels in T_{RM} than in circulating memory T cells, and T_{RM} also lack Kruppel-like factor 2 (KLF2); both KLF2 and TCF1 activate genes for the S1P receptor, CCR7, and CD62L.[5, 17] T_{RM} also express low levels of transcription factors T-bet and Blimp1, while Nur77 and Hobit appear to be upregulated. T-bet can negatively regulate CD103 expression, while Hobit is multifunctional, suppressing expressing of S1P receptor, TCF1, CD62L, and CCR7.[5, 17]

Cytokines and chemokines also play a role in the generation and maintenance of T_{RM} cells. Studies indicate that maturation into T_{RM} occurs after activated T cells have migrated back to their home tissues from the lymph nodes, and that the presence of local inflammatory signals in the tissue drives this process.[18, 31, 32] Perhaps most importantly, TGFβ signaling has been found to be indispensable in many tissues for CD103 expression on T_{RM}.[33] In tandem with type I interferons, IL-33, and TNFα, TGFβ has been found to induce CD69 and downregulate S1P, KLF2, and T-bet expression.[5, 17] IL-7 and IL-15 are also important for T_{RM} maintenance in some tissues.[5, 33] In the lungs and skin, CXCR3 is needed for effector T cell localization to the epithelium and differentiation into T_{RM}, and entry of pre-T_{RM} cells into tissues is helped by IFNγ from $CD4^+$ T cells, which induces production of chemokines CXCL9 and CXCL10 to attract $CXCR3^+$ $CD8^+$ T cells.[5, 17]

While $CD8^+$ T_{RM} have largely been the focus of tissue-resident T cell research in recent years, due to their importance both in infection by viruses and other intracellular pathogens and in cancer immunity, $CD4^+$ T_{RM} also play a significant role in protection against certain diseases, including chlamydia, pertussis, leishmania, tuberculosis, and influenza.[34-40] $CD4^+$ T_{RM} are generally less well-

characterized than $CD8^+$ T_{RM}; work is still being to precisely determine the mechanisms by which they are established and maintained and how they provide protection.[33] Studies of influenza infection in the lungs showed that $CD4^+$ T_{RM} expressed increased levels of CD69, as well as CD11a;[40] however, in contrast to $CD8^+$ T_{RM}, $CD4^+$ T_{RM} typically do not express the adhesion molecule CD103.[33] Instead, $CD4^+$ T cells that persisted in the lungs after influenza infection were found to express VLA-1, as well as much greater levels of CD11a relative to circulating $CD4^+$ T_{EM}. [33, 41] It is also possible that lung $CD4^+$ T_{RM} do not require TGFβ for development, which could explain the lack of CD103 expression.[42] Further supporting this, $CD4^+$ T_{RM} found in white adipose tissue expressed the mucosal homing integrin α4β7, expression of which is inhibited by TGFβ.[42]

Pathogen-specificity and sites of tissue-residence also appear to play a role in characterizing $CD4^+$ T_{RM}; for example, $CD4^+$ T_{RM} found to be protective against *Leishmania major* infection produced IFNγ and recruited circulating T cells to the skin via CXCR3.[36] Conversely, protective $CD4^+$ T_{RM} in a model of *Mycobacterium tuberculosis* (Mtb) infection, while also $CXCR3^{hi}$, did not exert their protective effects via IFNγ—in this case, the researchers speculated the enhanced protective capacity of the tissue-resident cells may have been due to their ability to gain access to infected cells within granulomas.[39] In another study of Mtb infection after intranasal BCG immunization, $CD4^+$ T_{RM} were found to be $PD\text{-}1^+$ and $KLRG1^-$.[38] While it has been shown that $CD4^+$ T_{RM} can exhibit rapid recall functions upon antigen encounter, similar to $CD8^+$ T_{RM}, and can produce IFNγ and IL-17 cytokines, the full extent to which their functional profile differs from circulating memory T cells remains to be fully understood.[33] Interestingly, while $CD4^+$ T_{RM} have primarily been investigated for their role in infectious disease, there is also some evidence they may play a role in the pathogenesis of certain chronic inflammatory diseases, such as asthma, psoriasis, and inflammatory bowel disease.[33] This presents $CD4^+$ T_{RM} as a possible target for the design of immunotherapies to control these diseases.

Several experimental techniques have been reported in the literature for unambiguously establishing the tissue-residency of T cells (**Figure 1.2**). Perhaps the most robust approach is parabiosis: joining together the circulatory systems of two mice with different hematopoietic cell markers (typically CD45.1/CD45.2 or CD90.1/CD90.2). This allows identification of tissue-resident populations by their expression of only one of these markers—that is, non-resident cells in the first mouse will express either CD45.1 or CD45.2 after the two circulatory systems reach equilibrium, but $CD45.2^+$ tissue-resident cells will not travel from the second mouse to the first, and vice versa.[43] However, there are drawbacks to this approach. The kinetics of cell migration and establishment of tissue residence can vary between tissues, causing a cell population to appear “resident” when it may just have a slow turnover rate.[43] It is also a difficult and time-consuming technique and labs may face challenges in gaining IACUC approval to perform it. As such, several other simpler and less invasive techniques have come into widespread use. The first is fluorescent antibody staining for cell surface markers indicative

of T_{RM} cells—most commonly CD69 and CD103, although others have been used, including CD49a, CD11a, and the lack of expression of CCR7 or KLRG1.[7, 17, 40] These markers can be easily integrated into existing antibody panels for flow cytometry; a drawback is that complete characterization of the surface marker profiles of T_{RM} cells is still ongoing, and T_{RM} in some tissues have been found not to express certain markers (e.g., lack of $CD103^+$ T_{RM} in the lungs). This could lead to classifying cell populations as "non-resident" simply because they aren't expressing the right surface markers—a disadvantage that can be countered by performing transcriptional profiling of putative T_{RM} cells to unambiguously distinguish them from non-resident memory T cells.[32] Another technique that has been widely adopted is intravascular (i.v.) staining with an antibody for a marker only expressed on cells in the circulation—most often CD45. The antibody is administered i.v. to anesthetized mice and allowed to circulate for several minutes before sacrifice; thus, cells in the vasculature will be labeled as $CD45^+$, while tissue-resident cells are $CD45^-$.[44, 45] This is a simple technique that can also be easily integrated into existing flow cytometry panels and used in conjunction with, or instead of, staining for surface markers. Finally, treatment with FTY720, an analog of sphingosine-1-phosphate, has been used in infection challenge models to demonstrate whether protection is mediated by T_{RM} cells. FTY720 blocks the egress of non-resident T cells from the lymph nodes; if resident T cell populations are established in the mouse prior to challenge, and the level of protection observed is the same with or without FTY720 treatment, this indicates protection is dependent on T_{RM} cells rather than circulating memory T cells.[46] Researchers now possess an extensive toolbox for establishing the tissue-residency of T cells, and these tools can be put to use in studying the ability of new vaccines to generate T_{RM}.

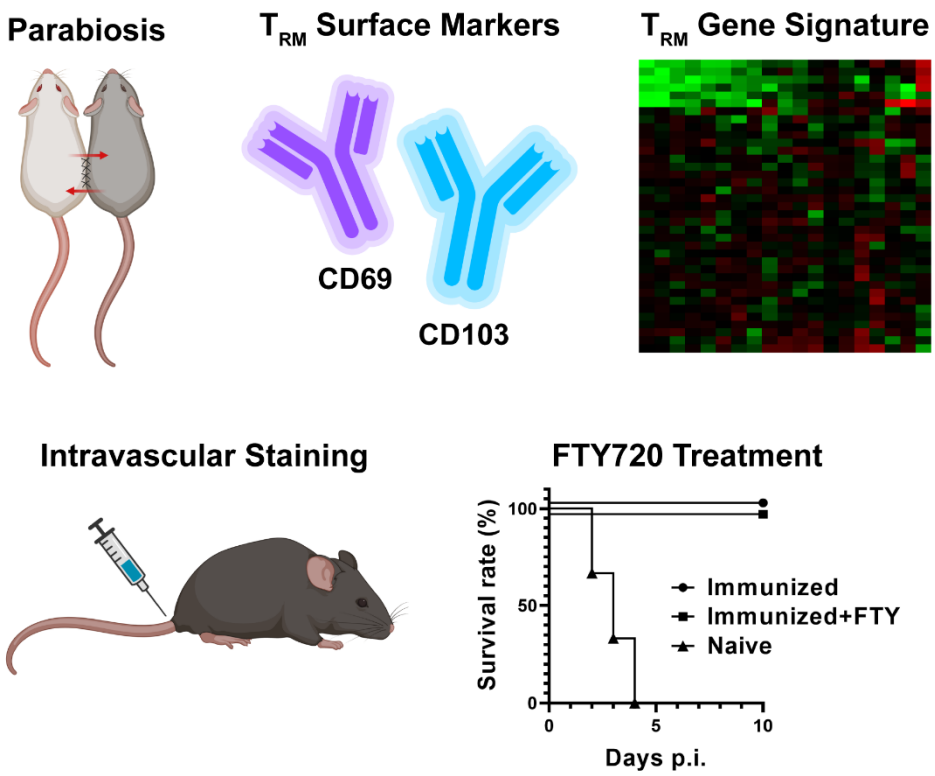

Figure 1.2 | Techniques for identifying T_{RM} cells. Common techniques for identifying T_{RM} populations include parabiosis, which joins the circulatory systems of two mice; staining with fluorescent antibodies for T_{RM}-associated surface markers; transcriptional profiling of putative T_{RM} cells; intravascular staining to differentiate cells in tissue from cells in vasculature; and FTY720 treatment to prevent egress of non-resident T cells from the lymph nodes. Figure created with Biorender.com.

1.1.2 Vaccine Design: Lessons from T_{RM} Biology

Findings from studies of tissue-resident T cell biology can be used to inform design choices when developing T_{RM}-targeted vaccines. For instance, cross-presenting dendritic cells (DCs) were found to be critical for priming of T_{RM} after infection with both vaccinia and influenza.[47] Taking inspiration from this, a vaccination approach using anti-DEC205 antibodies coupled with antigen targeted this subset of DCs in the lungs and successfully produced $CD8^+$ T_{RM} that protected against lethal influenza challenge.[48] Targeted antigen delivery with anti-Clec9a antibodies has also been used to generate $CD8^+$ T_{RM} in the liver and protect against malaria infection.[49] Delivery of antibodies using nanoparticle platforms offers the possibility of improved targeting to key antigen-presenting cell subsets and subsequent generation of tissue-resident T cell memory. In addition, the material properties of particulate delivery vehicles can be designed to promote antigen cross-presentation and cytosolic delivery, which could potentially supplement existing cross-presentation mechanisms.[8, 50, 51]

There is debate in the literature regarding the need for local antigen recognition in T_{RM} formation; this factor appears to be tissue-dependent. In some cases, $CD8^+$ T_{RM} have been found to persist long-

term in the absence of cognate antigen.[52-54] Conversely, generation of T_{RM} cells in the brain, genital mucosa, and lungs may be improved with persistent antigen presentation, and it has been proposed that local expression of CD69 on T_{RM} may be the result of continued encounters with antigen in the tissues.[33, 48, 55-57] Thus, while chronic antigen stimulation may inhibit T_{RM} formation in some cases, in other instances the presence of antigen "depots" may be beneficial.[5, 52] In either case, vaccines can be developed with this in mind. Nanoparticle delivery platforms may be designed to afford precise control over the release kinetics of cargo, promoting local antigen persistence in tissues, and perhaps could also feasibly be designed to "remove" remaining antigen after a certain period of time *via* biodegradability or other mechanisms. A polyanhydride nanoparticle has been used for this purpose, acting as an antigen depot and providing sustained release via surface erosion to generate $CD8^+$ and $CD4^+$ T_{RM} that protected against heterosubtypic influenza challenge.[58] Nanoparticles formed from a pH-responsive polymer have also shown increased residence time of vaccine cargo in pulmonary APCs, perhaps because of increased mucoadhesion due to the cationic nature of the polymer used.[8]

A multitude of cytokines and inflammatory molecules have been implicated in the generation and maintenance of T_{RM}. Vaccines can be used to deliver adjuvants that will stimulate a T_{RM}-biased cytokine profile, or they can be used to deliver the requisite cytokines themselves, such as TGFβ or IL-1β.[8, 59-61] The materials used for delivery are often also immunostimulatory, or "self-adjuvanting," and may offer further opportunities for generating T_{RM} using engineered vaccine platforms.[62] The precise relationships between adjuvant-mediated immune stimulation, cytokine production, and formation of T_{RM} merit further investigation.

Finally, complementary to the design of the vaccine itself, route of vaccine administration can play an equally important role in generating T_{RM} cells. In attempting to create vaccines that mimic natural viral infection, it follows that the natural portal of entry should be used for immunization as well. An ever-growing body of studies has demonstrated that mucosal immunization (e.g., intranasal, intravaginal, oral) is superior to systemic administration (e.g., intraperitoneal, intramuscular, subcutaneous) for installing tissue-resident memory populations.[8, 34, 63-68] There is also promise in the "prime and pull" method of parenteral immunization for the first dose, followed by boosting via a mucosal route.[49, 53] Interestingly, there is evidence that pulmonary or oral immunization can also generate T cell responses in distal mucosal tissues such as the urogenital tract, adding to the utility of mucosal administration for T_{RM} vaccines.[46, 64, 69]

1.1.3 Vaccines for Generating Tissue-Resident Memory T Cells

Much of what we know about tissue-resident memory T cells, we have learned from studying models of viral infection. As a result, many of these lessons have been applied to the design of T_{RM}-

targeted vaccines by utilizing viral vectors as a delivery platform. Engineering approaches have also been used to design T_{RM} vaccines comprised of virus-like particles or other bio-inspired materials. Overall, while the body of knowledge on tissue-resident T cell biology has grown rapidly in recent years, practical application of these findings to vaccine development has moved more slowly. This is especially true in terms of studying the ways in which material properties can be engineered to promote and fine-tune the T_{RM} response. In this section, we review T_{RM} vaccine technologies that currently exist in the literature, with a particular focus on engineered materials for T_{RM}-targeted vaccines (**Figure 1.3**).

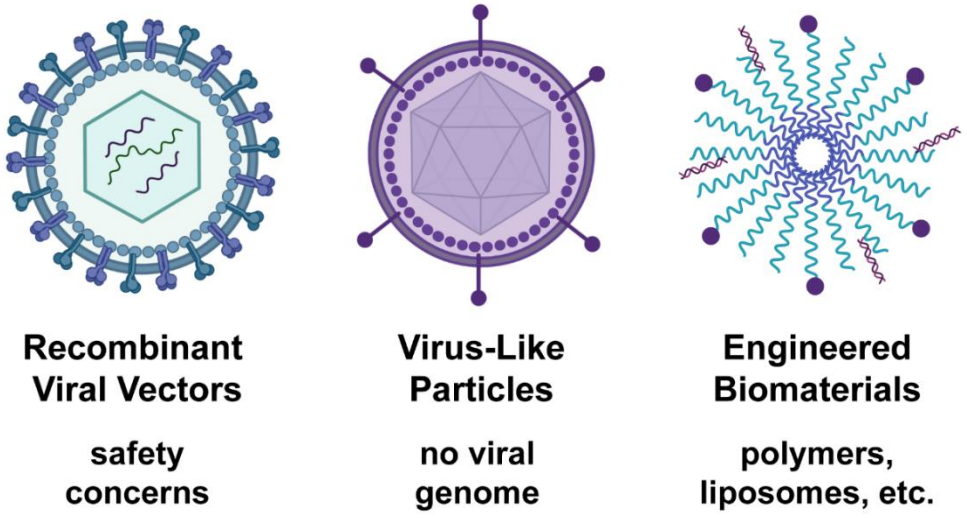

Figure 1.3 | Vaccine platforms used to generate T_{RM}. While viral vectors are common, they pose safety concerns regarding reversion to virulence and use in elderly or immunocompromised individuals. Virus-like particles address some of these safety concerns in that they mimic the structure and conformation of native viruses without containing the viral genome. Engineered biomaterials such as polymeric nanoparticles and liposomes have also found use as subunit vaccine delivery platforms for generating T_{RM}, and offer the advantages of rational design and modular loading of vaccine components such as protein antigens and nucleic acid adjuvants. Figure created with Biorender.com.

1.1.4 Viral Vector Vaccines

Infection models of viruses such as influenza and vaccinia have provided a great deal of insight into the biology of tissue-resident T cell memory. As a result, much of the literature on vaccines for generating T_{RM} has revolved around the use of viral vectors for antigen delivery. To date, some of the vectors used include human papilloma virus (HPV), influenza A virus, adenovirus, lentivirus, cytomegalovirus, vesicular stomatitis virus, and vaccinia virus. These experimental vaccines have shown efficacy in models of influenza, HIV, respiratory syncytial virus (RSV), tuberculosis and malaria.

Several viral vectors have been used to immunize against influenza, including murine cytomegalovirus (MCMV). Zheng *et al.* chose MCMV because this virus induces a highly robust $CD8^+$ T cell response, making it an ideal candidate for a vaccine to generate long-lasting tissue-resident cellular immunity.[70] A recombinant MCMV-influenza vector was created by inserting the sequence for an MCH-I-restricted epitope of the hemagglutinin (HA) antigen of Puerto Rico/A/8/1934 (PR8) influenza A virus (IAV) into the C-terminus of the MCMV *ie2* gene. In a previous report, this group showed that using a single peptide epitope in this setting provided greater protection than a vector expressing the full protein.[71] While intranasal (i.n.) immunization with the MCMV-influenza vaccine induced a lower magnitude $CD8^+$ T cell response relative to intraperitoneal (i.p.) immunization (shown by tetramer staining), only IN immunization provided robust protection against IN challenge with PR8 IAV. Surface staining for CD69 and CD103, as well as i.v. staining with CD45, was performed >3 months post-immunization to identify tissue-resident $CD8^+$ T cells, and the frequency of $CD69^+CD103^+$ in the lung tissue ($CD45^-$) was significantly higher after i.n. immunization relative to i.p. administration of the vaccine. Staining for the transcription factor Eomes also showed low levels in $CD8^+$ T_{RM}, which is in line with reports that T_{RM} downregulate this transcription factor.[17]

In another study, Macdonald *et al.* describe an immunization method that capitalizes on alveolar macrophages as antigen-presenting cells for priming a lung-resident T cell response to protect against influenza challenge.[72] This approach utilized a lentiviral vector (LV) based on HIV-1 that is replication-defective and can transduce alveolar macrophages after i.n. delivery. The LV was engineered to express PR8 nucleoprotein antigen along with a constitutive activator of the NFκB pathway, vFLIP. vFLIP was included because influenza infection of alveolar macrophages is known to stimulate NFκB-dependent secretion of chemokines that are necessary for T cell recruitment in response to influenza infection. One drawback of generating large numbers of T cells in the lungs is that it can also cause significant lung injury. This study explored the benefits of using a subcutaneous (s.c.) prime-i.n. boost immunization regimen to avoid high levels of inflammatory cytokines that have been shown to promote lung pathology during influenza infection (IFNy TNFa, IL-17, IL-4, IL-10). The LV-influenza vaccine successfully transduced large numbers of alveolar macrophages and recruited lung-resident T cells that conferred long-lasting protection without significant tissue injury. It is important to note that the T cell epitopes of viral antigens such as nucleoprotein are highly conserved, and so vaccines containing such antigens have potential for creating a universal influenza vaccine that provides heterosubtypic protection across multiple strains.[72]

In addition to its use in immunization against influenza, murine cytomegalovirus has also been utilized as a vaccine vector for RSV immunization. Morabito *et al*. have shown an MCMV vector expressing the RSV matrix (M) protein can generate $CD69^+CD103^{+/-}$ $CD8^+$ T_{RM} that protect against RSV challenge. They tested the efficacy of different routes of administration and found that IN but not IP

vaccination generated durable tissue-resident CD8T populations in the lungs.[73] Residency was established via IV staining with anti-CD45 antibody and FTY720 treatment. Generation of these $CD8^+$ T_{RM} by i.n. immunization resulted in faster T cell recall responses, IFNγ secretion, and effective viral clearance after challenge with RSV, providing further evidence that route of delivery is key to priming cellular immunity in the tissues where pathogens are first encountered. A notable advantage of the MCMV vector is that it persists and produces antigen for an extended period of time, which may contribute to a more robust T_{RM} response in the lungs due to the putative requirement for local antigen recognition.[74, 75] Another unique aspect of MCMV infection is its generation of two distinct waves of memory $CD8^+$ T cells: "conventional" cells, which expand during acute infection and then contract, and "inflationary" cells, which continue accumulating over time in the effector memory T cell compartment.[76] It is known that T_{RM} tend to wane over time in the lungs, in contrast to the more durable T_{RM} found in skin and other tissues, and so this "memory inflation" phenomenon may hold promise for MCMV-based vaccines that generating longer-lasting pulmonary T_{RM} immunity.[77, 78]

Influenza A viruses have also been used as a vaccine platform. Using a recombinant IAV vaccine expressing the immunodominant $CD4^+$ T cell epitope p25 from the Mtb antigen Ag85B, Flórido *et al*. investigated whether pulmonary immunization generated $CD4^+$ T_{RM} that could protect against Mtb challenge in the absence of circulating memory T cells.[79] Immunized mice were treated with FTY720 prior and during the first 17 days of Mtb challenge; while this significantly reduced the number of circulating T cells, it did not affect the frequency of Mtb-specific $CD4^+$ T_{RM} in the lung tissue, nor their ability to produce cytokines and protect against infection. Similar to other studies, IN but not IP immunization induced p25-specific $CD4^+$ T cells in the lung, which were found to be $CD69^+CD11a^+CD44^{hi}CD62L^{lo}$, consistent with a T_{RM} phenotype. Less than 5% of these cells expressed CD103, in agreement with findings that $CD4^+$ T_{RM} do not express this marker. Two-photon microscopy was used to confirm distribution of T_{RM} cells in lung parenchyma.

Generation of $CD8^+$ T_{RM} against Mtb has been achieved with a replication-deficient adenovirus vector expressing the immunodominant antigen Ag85A after i.n., but not intramuscular (i.m.), immunization.[20] In this study, Haddadi *et al*. found lung-resident $CD8^+$ T_{RM} to be characterized by VLA-1 as well as CD103, with the latter being acquired after the cells entered the lungs, while the former was acquired during priming in the lung draining lymph nodes. $CD8^+$ T_{RM} were identified via i.v. staining with anti-CD45 antibody. Blocking antibody for VLA-1 was used to show that although this integrin was not required for trafficking to the lungs and did not appear to play a major role in retaining the T_{RM} cells there, it did negatively regulate them in the contraction phase. Notably, VLA-1 is made up of CD49a and CD29, and CD49a has been used in other studies as an identifying marker for T_{RM} cells.

Vaccines that can install $CD8^+$ T_{RM} in the cervicovaginal mucosa hold promise for effective immunity against sexually-transmitted infections; as such, an influenza-based vector has also been

used as a vaccine for HIV. Tan *et al*. developed recombinant influenza viruses expressing the HIV-1 Gag protein p24 using two different strains, PR8 and X31; they primed i.n. with PR8-p24 and boosted intravaginally (ivag) with X31-p24.[80] Tetramer staining showed that this combination of mucosal doses generated durable $CD103^+$ $CD8^+$ T cells resident in the vaginal epithelial compartment rather than the submucosa, which is desirable for a rapid response against HIV encounter. Upon secondary antigen recognition in the vaginal mucosa, the HIV-specific $CD8^+$ T_{RM} rapidly upregulated expression of addressin on endothelial cells and recruited $CD4^+$ T cells, B cells, and NKT cells to the tissue.

Intravaginal immunization has also been demonstrated with HPV vectors; Çuburu *et al*. showed that ivag prime/boost with nonreplicating HPV16 and HPV45 "pseudovirions" encoding a fusion protein of the RSV M and M2 antigens generated significantly more cervicovaginal antigen-specific $CD8^+$ T cells than priming alone, and these cells were durable, waning by only 50% after six months.[81] The majority of the cells produced were located in the intra- or subepithelial compartment, produced both IFNγ and TNFα, and were protective against vaginal challenge with a recombinant vaccinia virus expressing M2 (VV-M2), reducing cervicovaginal viral titers by three orders of magnitude relative to controls. CD103/CD69 staining and FTY720 were used to establish tissue-residency. In a follow-up study, the same group developed a "prime-pull-amplify" vaccination strategy for maximizing both systemic and cervicovaginal $CD8^+$ T cells after immunization.[82] It was found that i.m. prime with an adenovirus vector and ivag boost with HPV16 could accomplish this (rather than ivag/ivag, i.m./i.m., or ivag/i.m.). Boosting with HPV was more effective at recruiting cervicovaginal $CD8^+$ T_{RM} than ivag installation of CXCR3 receptor ligands (CXCL9/10) or agonists for TLR3 (polyI:C), TLR7/8 (imiquimod), or TLR9 (CpG). It is also notable that these $CD8^+$ T_{RM} were induced in the absence of $CD4^+$ T cell help. This vaccine induced effective T cell responses against both HPV16 E7 oncoprotein and recombinant VV-M2 virus challenge, indicating its potential for use against both cancer and infectious disease.

In some instances, viral vectors have been combined with other molecules or delivery platforms for immunization. Fernando-Ruiz *et al*. put forth a vaccination strategy they called "prime-and-trap," in which anti-Clec9A antibodies were used for targeted i.v. delivery of a malaria peptide antigen to $CD8\alpha^+$ dendritic cells in the liver, and then recombinant adeno-associated virus (rAAV) containing the same malaria epitope was administered i.v. to "trap" T_{RM} cells in the liver.[49] A population of $CD69^+KLRG1^-$ $CD8^+$ T cells was identified that expressed the gene signature of T_{RM} cells and remained permanently in the liver, patrolling the sinusoids. It was found that these T_{RM} were essential for protection against liver-stage malaria and challenge with sporozoites. Notably, the liver T_{RM} population identified in this study did not express CD103. In some experiments, the adjuvants CpG or poly(I:C) were delivered with anti-Clec9A antibody+antigen; it was found that CpG induced a greater number of T_{RM} cells relative to poly(I:C).

A combination approach has also been used to develop an HIV vaccine that can simultaneously induce both antibodies and $CD8^+$ T cells. Petitdemange *et al*. hypothesized a vaccine that could generate both cellular and humoral immunity might provide enhanced protection against HIV.[83] To this end, three different experimental vaccines were tested via i.v. immunization in non-human primates: (1) sequential immunization with heterologous viral vectors (HVVs) comprising vesicular stomatitis virus, vaccinia virus, and adenovirus5 expressing mac239 Gag protein from simian immunodeficiency virus; (2) immunization with HIV-1 Env gp140 protein adjuvanted with poly(lactic-co-glycolic acid) (PLGA) nanoparticles containing 3M-052, a TLR7/8 agonist; and (3) a sequential combination of both. The HVV vaccine induced a high magnitude of Gag antigen-specific $CD8^+$ T cells in the blood and $CD8^+$ T_{RM} in the vaginal mucosa, while the Env+PLGA vaccine generated persistent antibody and innate immune responses. Vaccination with both provided enhanced protection, particularly in younger animals, and support the hypothesis that a holistic immune response can be more effective against HIV.

While viral vectors have seen extensive use as vaccine delivery platforms for generating tissue-resident T cell memory, and offer a convenient means of eliciting T cells via intracellular delivery of vaccine antigens, there are also several disadvantages to note. As vaccines are prophylactic, requirements for their approval for use in humans is stringent—they cannot harm a healthy recipient. The possibility of a viral vector reverting to virulence is a safety concern, and live virus vaccines cannot be given to immunocompromised individuals. Even in replication-deficient vectors, components of the virus may cause an undesirable inflammatory response.[13] Pre-existing immunity against the vector used may diminish vaccine efficacy, and large-scale manufacturing can prove difficult if delicate and time-consuming molecular biology or cell culture methods are needed to construct and produce the virus.[84, 85] Notably, the study by Petitdemange *et al.* discussed above used a combination vaccine regimen consisting of both viral vectors and synthetic polymeric nanoparticles formulated with antigen and adjuvant. The latter is an example of a subunit vaccine, a class of vaccine the circumvents many of the disadvantages of viral vectors. In recent years, significant progress has been made in the development and characterization of engineered biomaterials for subunit vaccines that can promote cellular immunity. The next section will cover these new technologies in more detail.

1.1.5 Engineered Biomaterials for Subunit Vaccines

Subunit vaccines have been widely studied as an alternative to vaccines containing live viruses, including in the context of mucosal delivery.[86] This type of vaccine consists of only the minimal components of a pathogen needed to stimulate an immune response—for example, a single protein or peptide antigen.[13] While this allows subunit vaccines to overcome many of the safety concerns of viral vectors, it comes at the cost of lower immunogenicity. Since subunit vaccines do not contain all of the

microbial molecules that contribute to eliciting an immune response, they are often supplemented with adjuvants; however, few adjuvants are currently approved for use in humans, and many in preclinical studies have demonstrated unfavorable safety profiles when administered mucosally.[34, 86, 87] In addition, this lower immunogenicity often means that more or higher doses must be given to achieve the same level of immunity as with a more potent live vaccine.[13]

Traditional subunit vaccine formulations typically consist of soluble antigen mixed with adjuvant. Several drug delivery barriers hinder the efficacy of these formulations, including rapid antigen clearance with poor uptake by antigen-presenting cells (APCs) and minimal accumulation in draining lymph nodes. In addition, subunit vaccines are particularly inept at eliciting $CD8^+$ T cells.[88] Generating a robust $CD8^+$ T cell response requires antigen presentation on major histocompatibility complex class I (MHC-I) by APCs in the context of additional molecular cues (co-stimulation, cytokines) that drive $CD8^+$ T cell expansion and differentiation.[89] To achieve presentation by MHC-I, administered antigen must either be endocytosed by specialized cross-presenting DC subsets or delivered to the classical cytosolic MHC-I antigen processing pathway. However, the predominant fate of soluble vaccine antigen after uptake is lysosomal degradation, with minimal presentation on MHC-I.[90] Despite this limited capacity for $CD8^+$ T cell generation, the superior safety profile of subunit vaccines continues to motivate strategies for improving their efficacy.[91] Biomaterials-based delivery systems have been developed that can enhance antigen uptake in APCs, promote antigen cross-presentation, or safely deliver adjuvants to promote a $CD8^+$ T cell response. These new approaches to vaccine delivery will be reviewed in the following section, divided into virus-like particle (VLP) and non-VLP technologies.

Virus-like particles represent an interesting middle ground between live viral vectors and fully synthetic vaccines. Features of traditional viral vectors that contribute to their efficacy include their particulate nature, repetitive surface geometry, and ability to replicate and to stimulate both innate and adaptive immune responses; VLPs retain most of these advantages but do not possess a viral genome and so cannot replicate and are safer than live viruses.[92] Their particulate nature allows them to overcome many of the delivery barriers for soluble antigens. Several vaccines currently approved for use in humans are formulated with VLPs, including vaccines against HPV, hepatitis B virus, and malaria. In recent years, a number of VLP vaccine platforms for generating T_{RM} cells have been published in the literature.

Respiratory pathogens such as influenza and RSV have been the primary target of VLP-based T_{RM} vaccines thus far. Lee *et al*. developed an experimental universal influenza vaccine using the highly conserved M2e antigen; termed M2e5x-VLP, the vaccine contains tandem repeats of M2e from human, swine, and avian flu viruses.[93] It was hypothesized that this strain-agnostic vaccine could provide broader but weaker protection that would result in cross-strain T cell-mediated protection. In comparison with the current strain-specific inactivated influenza vaccine (IIV), M2e5x-VLP administered IM was

superior in promoting heterosubtypic protection, and it generated $CD103^+CD69^+$ lung-resident memory $CD8^+$ T cells that produced IFNγ. It also generated M2e-specific antibodies, providing support for a platform capable of generating both cellular and humoral immunity, which may be particularly important for viruses like influenza.

Hodgins *et al*. have a described a strategy for vaccination with an VLP vaccine that contains influenza HA antigen and is produced in plants.[94] Various combinations of administration routes were explored, including "prime-pull" (IM prime/IN boost), "multi-modality" (IM and IN doses given simultaneously), and "traditional" (IM prime/IM boost). It was found that this plant-derived vaccine could induce both humoral and cellular T_{RM} responses that protected aged mice from lethal challenge. The VLP vaccine was also compared to commercially available IIV. In general, the VLP vaccine outperformed IIV; interestingly, these researchers found limited evidence supporting IN delivery of the VLP vaccine over IM administration, which contradicts much of the previous evidence supporting use of mucosal administration routes in generating T_{RM} but is in agreement with Lee *et al*., who also administered their influenza VLP vaccine intramuscularly.

While in many cases the VLP and vaccine antigen are the same, encapsulation of antigen within an unrelated VLP has been shown to enhance antigen availability for generation of $CD8^+$ T cells.[95] Schwarz *et al*. engineered a VLP derived from the *Salmonella typhimurium* bacteriophage P22 that can be genetically modified to allow for protein delivery, resulting in a ~60 nm diameter particle co-encapsulating two well-characterized RSV antigens, M and M2.[95] Delivery of multiple antigens may prove advantageous as it can avoid concentrating pressure for immune evasion on a single immunodominant epitope. Mice immunized IN with the P22-MM2 vaccine were found to have $CD103^+CD69^+$ lung-resident $CD8^+$ T_{RM} that were specific for both antigens, and the vaccine also decreased viral loads in the lung after IN RSV challenge.

Airway-resident memory T cells may also play an important role in protection against respiratory pathogens such as coronaviruses (COV). Zhao *et al*. showed that IN but not SC vaccination with alphavirus-derived Venezuelan equine encephalitis replicon particles (VRP) encoding a $CD4^+$ T cell epitope for SARS-COV could induce antigen-specific memory $CD4^+$ T cells in the airways that protected mice against lethal challenge via rapid local IFNγ production.[65] IL-10 produced by these airway-resident $CD4^+$ T cells was also key for optimal protection. It is important to note that there is some debate over whether airway-resident T cells represent "true" tissue-resident T cell memory; it has been estimated, for example, that influenza-specific $CD11a^{lo}CXCR3^{hi}$ airway T_{RM} have a high turnover rate, with a half-life of only 14 days and continual replenishment from circulating T_{EM} cells.[96, 97] In agreement with this, Zhao et al. show phenotypical and functional differences between CD4+ T cells in the airway vs. lung parenchyma, including lower expression of the markers CD11a, CD103, and CD69.[65] Nevertheless,

memory T cells in the airway are typically the first to encounter antigen during infection and so play a central role in protection at these sites of pathogen encounter.

Outside the realm of virus-like particles, vaccines that can effectively generate T cells have been engineered using a variety of materials, including stimuli-responsive polymers, peptide nanofibers, lipid nanocapsules, or nanoparticles derived from naturally-occurring materials. While many of these materials have coincidentally been found to also generate T_{RM}, the rational design of materials to explicitly promote and control the T_{RM} response is relatively unexplored. If it can be shown that material properties can directly affect the ways in which T_{RM} cells are generated, this will represent significant potential for the application of immunoengineering principles to vaccine development.

Synthetic polymeric nanoparticles (NP) have been utilized as a platform for vaccines to generate T_{RM}. The use of pH-responsive nanoparticles as a T_{RM} vaccine is presented in this dissertation; polyanhydride and PLGA NP have also been used for this purpose. In addition to the combination of viral vectors with adjuvanted PLGA NP by Petitdemange *et al*. as discussed earlier, PLGA NP have also been used in combination with an adenovirus vector in a "prime and target vaccination strategy" against malaria. Gola *et al*. evaluated the ability of the NP to promote localization of primed $CD8^+$ T_{EM} cells to the liver and protect against liver-stage malaria by first administering an antigen-expressing adenovirus vector IM, followed by IV administration of antigen-loaded PLGA NP.[98] FTY720 treatment was used to demonstrate that protection was mediated by tissue-resident cells in the liver, and these cells expressed the T_{RM} surface markers CXCR6, CD69, and CD44. Interestingly, the addition of adjuvants such as R848 and MPLA only minimally enhanced the number of liver-resident T cells.

While PLGA has found widespread use in a variety of biomedical applications, other polymer materials have been intentionally engineered for use in vaccines. Polyanhydride NP synthesized from the monomers 1,8-bis(*p*-carboxyphenoxy)-3,6-dioxoctane (CPTEG) and 1,6-bis-(*p*-carboxyphenoxy) hexane (CPH) and encapsulating influenza antigens HA and nucleoprotein (N) and the adjuvant CpG1668 were used to protect against heterosubtypic influenza A challenge in mice.[58] Similar to VLPs, polymeric particles such as these can in some ways be considered "virus-mimetic," due to their small size or ability to act as a depot providing sustained release of antigen over a long period of time. In fact, Zacharias *et al*. hypothesize that this depot effect could be crucial in promoting tissue-resident memory formation.[58] In this study, IN administration of the polyanhydride IAV vaccine was shown to be superior to IIV administered IM, and it induced both $CD8^+$ and $CD4^+$ T_{RM} responses in the lungs as well as IAV-specific antibodies in the airways and blood. IV staining with CD45 and surface staining for CD11a, CD69, and CD103 were used to identify T_{RM}.

Lipid-based materials have also been used in vaccines for generating T_{RM}. In a study by Woodworth *et al*., the subunit vaccine H56/CAF01 induced circulating $CD4^+$ T cells that localized to the lung parenchyma and protected against Mtb challenge.[99] This vaccine consists of a fusion protein (H56)

comprised of Mtb antigens Ag85B, ESAT-6, and Rv2660 and adjuvanted with CAF01 liposomes. IV staining with CD45 was used to differentiate T_{RM} in the lung parenchyma from cells in the vasculature, and these $CD4^+$ T_{RM} were found to be $KLRG1^-CXCR3^+$, consistent with the non-terminally differentiated phenotype of T_{RM} cells.[17] Vaccine-specific $CD4^+$ T cells were polyfunctional, producing combinations of IFNγ, TNFα, and IL-2, as well as IL-17 (CAF01 is a Th1/Th17-promoting adjuvant).

Similarly, an engineered lipid nanocapsule platform delivering protein or peptide antigen in combination with the adjuvants MPLA and poly(I:C) promoted the formation of antigen-specific, tissue-resident memory $CD8^+$ T cells after intratracheal administration.[46] Li *et al*. incorporated poly(I:C) as an adjuvant because it has been shown to increase DC cross-presentation.[100] They hypothesized that targeting a cross-presentation-promoting particulate vaccine to the pulmonary mucosa, home to a large population of APCs, could generate a robust cellular response in mucosal tissues. Pulmonary immunization with this platform, termed “interbilayer-crosslinked multilamellar vesicles” (ICMV), was able to generate $CD8^+$ T cells in both the lungs and vaginal tissue, consistent with the observation that intranasal immunization can elicit an immune response in distal mucosal sites.[101, 102] Intranasal ICMV immunization resulted in increased antigen transport to lung-draining lymph nodes relative to s.c. administration, and it increased expression of the mucosal homing integrin α4β7. Vaccine-induced T cells were protective against both tumor challenge with B16.F10-OVA melanoma and respiratory virus challenge with simian immunodeficiency virus (SIV) gag-expressing vaccinia. In the case of virus challenge, mice were immunized with the immunodominant MHC-I epitope from SIV gag, AL11, and the universal $CD4^+$ T cell helper epitope PADRE; interestingly, antibody depletion showed that protection was dependent on $CD8^+$ but not $CD4^+$ T cells. FTY720 treatment showed that protection was mediated by T_{RM}, many of which expressed CD103 and/or CD49a.

Peptide nanofibers have also been used as a vaccine platform for generating tissue-resident memory T cells. Previous studies of nanofibers have indicated that they can generate an immune response without the addition of adjuvants and without significant inflammation, which may prove advantageous in the delicate lung environment. The modularity of peptide nanofiber vaccines can also allow precise control over the strength and phenotype of the elicited immune response. Si *et al*. synthesized peptide nanofibers containing the self-assembling, beta-sheet-forming Q11 domain and the conserved MHC-I epitope from the acid polymerase (PA) antigen of H1N1 PR8 virus.[103] Notably, this nanofiber vaccine did not contain any $CD4^+$ T cell epitopes. The PA epitope was chosen because previous studies showed that PA-specific $CD8^+$ T cells were able to clear influenza virus infection in mice. Peptide nanofibers were taken up by DCs in the lung-draining lymph node (dLN) after i.n. immunization. Relative to s.c. immunization, i.n. immunization generated greater numbers of $CD8^+$ T cells in the dLN and persistent $CD8^+$ T_{RM} in the lung that protected against infection six weeks after

immunization. T_{RM} were identified using intravascular staining with anti-CD45 antibody, as well as surface expression of markers CD44 and CD69.

While viruses are frequently the target of T_{RM}-forming vaccines, non-viral pathogens may benefit from these technologies as well. Stary *et al*. developed a mucosal vaccine that protected against a bacterial pathogen, *Chlamydia trachomatis* (Ct), *via* two distinct "waves" of $CD4^+$ memory T cells.[34] After intrauterine immunization, a first wave of $CD4^+$ T cells trafficked to the uterine mucosa and became T_{RM}, while subsequent genital infection reactivated these uterine T_{RM} to recruit a second wave of circulating memory T cells. Both waves were required for optimal pathogen clearance. Previous attempts to immunize against chlamydia using UV-inactivated Ct have failed because mucosal exposure to UV-Ct generates regulatory T cells that exacerbate infection. In contrast, exposure to live Ct infection induces protective immunity dependent on IFNγ-producing $CD4^+$ T cells. Because live vaccines are often unsafe, the authors sought to convert UV-Ct into an immunogenic rather than tolerogenic vaccine platform. They did so by engineering charge-switching synthetic adjuvant particles (cSAPs), which self-assemble from a triblock copolymer of PLGA, poly(L-histidine) (PLH), and poly(ethylene glycol) (PEG). The adjuvant R848 (a TLR7/8 agonist) was included by covalently coupling it to poly(D,L-lactic acid) (PLA), which was incorporated into the particles. Acidification causes the cSAPs to become cationic and complex with negatively-charged UV-Ct bacteria, allowing all components to be delivered together. Previously, soluble mixtures of UV-Ct with adjuvant failed to provide protection against challenge, leading to the hypothesis that physical linkage of UV-Ct with adjuvant might allow the vaccine to cross the epithelial barrier and be taken up by mucosal DCs.

Finally, natural biomaterials have also found use as a platform for T_{RM}-targeted vaccines. Hart *et al*. used yellow carnauba wax particles (YC-NPs) coated with a fusion protein comprised of three Mtb antigens to protect against tuberculosis.[104] The fusion protein antigen consisted of Ag85b, an antigen expressed in early infection; Acr, expressed in latent infection; and the heparin-binding domain of HBHA, included as a means to "guide" the vaccine to epithelial tissue. The full vaccine is referred to as Nano-FP1. Intranasal administration of Nano-FP1 in mice primed with the BCG vaccine demonstrated enhanced protection against challenge with aerosolized Mtb. Control of bacterial burden in the lungs was associated with formation of $CD4^+$ and $CD8^+$ T_{RM} in the lungs and increased T cell polyfunctionality, and T_{RM} cells were identified by a $CD44^{hi}CD62L^{lo}CD69^+CD103^+$ phenotype. The authors also investigated the mechanisms of YC-NP immunogenicity; they hypothesized the NP could be acting as an adjuvant to induce APC activation and maturation. To test this, APCs were treated with YC-NP alone (no antigen), and activation markers were measured. YC-NP upregulated markers such as CCR7, CD86, PD-L1, and PD-L2, but did not stimulate production of IL-1β, IL-6, or TNFα. Based on these and other experiments, the authors concluded that YC-NP induced IRF-3-dependent maturation of APCs without the inflammation associated with NF-κB signaling, indicating a possible mechanism by which

the NP is immunologically active and enhances cellular immunity. This lends credence to the notion that delivery vehicles themselves can be designed to control the T_{RM} response.

1.2 Innovation

1.2.1 Nanoparticle-Mediated Dual-Delivery of Antigen and Adjuvant to Mucosal Tissue

Ample evidence exists in the literature that immunization via mucosal routes can provide an improved immune response over traditional systemic administration, particularly with regard to generation of T_{RM} cells. To our knowledge, this work represents the first use of a pH-responsive nanoparticle vaccine for mucosal immunization. Here, we extensively characterize the innate and adaptive pulmonary immune response to intranasal administration of a pH-responsive nanoparticle co-loaded with protein antigen and nucleic acid adjuvant. While dual-delivery of antigen and adjuvant on this particle was previously shown to be effective after systemic administration, its efficacy after mucosal immunization was not known. We demonstrate that intranasal administration of the nanoparticle vaccine is superior to subcutaneous immunization for generating a lung tissue-resident $CD8^+$ T cell response. In addition, the cytokine profile stimulated by the vaccine was found to be transient (no prolonged detrimental inflammation) and localized to the lungs, and it was supportive of a $CD8^+$ T_{RM}-biased response. Nanoparticle-mediated dual-delivery also increased co-localization and retention of vaccine cargo in pulmonary antigen-presenting cells that may play a key role in priming the T_{RM} response. Finally, this work presents the first demonstration that immunization with this nanoparticle vaccine can confer enhanced protection against morbidity and mortality in multiple mouse models of respiratory infection. Most notably, this enhanced $CD8^+$ T_{RM} response and subsequent protection is achieved after only a single intranasal dose, whereas most comparable nanoparticle-based vaccines in the literature utilize at least one booster dose to achieve a productive immune response. The single-dose efficacy of this vaccine provides importance translational advantages; for example, it could be useful for scenarios in which a rapid immune response is needed, such as during a pandemic or for biodefense applications.

1.2.2 Relationship Between pH-Responsive Activity and T_{RM} Formation

Precise engineering of the material properties of drug and vaccine delivery platforms, such as size and surface charge, can be used to control and modulate the immune response.[105-107] However, the specific impact of material properties on formation of tissue-resident memory T cells has not been studied. To our knowledge, the work presented in this dissertation is the first to demonstrate a direct link between an engineered nanomaterial and T_{RM} generation. The pH-responsive nanoparticle delivery platform used here leverages endosomal acidification after cellular uptake to release antigen into the

cytosol, where is can be processed by the MHC-I presentation pathway, resulting in a $CD8^+$ T cell response. By comparing this pH-responsive polymer with an analogous control polymer that does not respond to a decrease in pH, we were able to isolate the effect of this material property on generation of a tissue-resident $CD8^+$ T cell response in the lungs. Utilizing an intravascular staining technique to differentiate "true" resident cells in the lung interstitium from those in the lung vasculature, we demonstrated that immunization with the pH-responsive polymer generated tissue-resident $CD8^+$ T cells in the interstitium, whereas immunization with the control polymer did not. Interestingly, the two polymers were equally effective in the vasculature, indicating that this material property specifically impacts generation of tissue-resident cells. Since cross-presenting dendritic cells appear to play a key role in promoting T_{RM} cell formation, and the pH-responsive endosomal escape mechanism of the polymer "mimics" biological cross-presentation mechanisms, it is possible that this may be the cause of the enhanced T_{RM} response after immunization with the pH-responsive nanoparticle vaccine.

1.2.3 Delivery of Diverse Antigens and Adjuvants with a Modular Platform

A primary advantage of particulate-based delivery vehicles for subunit vaccines is the potential modularity of these platforms. They provide opportunities for accelerated development of vaccines against multiple distinct pathogens and offer a "plug-and-play" approach for testing various combinations of adjuvants and antigens to determine the best possible formulation. In this work, we demonstrate that the pH-responsive nanoparticle vaccine can accommodate multiple protein antigens and nucleic acid adjuvants with diverse physicochemical properties. Previously, this platform was used to deliver ovalbumin protein, a model antigen commonly utilized for studying murine immune responses. The net negative charge of this protein lends itself to association with the cationic polymer used to form the nanoparticle (DMAEMA), and an abundance of lysine residues on the surface of OVA also facilitates thiolation of the protein for covalent conjugation with pyridyl disulfide groups on the corona of the particle. However, while OVA has proven "ideal" for this application, other protein antigens may possess characteristics that would hinder formulation of protein-NP conjugates. This work presents the first evidence that our nanoparticle platform can be used to deliver other antigens. When conducting initial formulation studies of the pH-responsive nanoparticle with influenza nucleoprotein, an antigen with a net positive charge, we were concerned that this positive charge might prevent efficient conjugation to the particle or interfere with electrostatic complexation of the particle to nucleic acid adjuvants. Nevertheless, after minor optimization of reaction conditions, we were able to demonstrate efficient thiolation and conjugation of nucleoprotein, a clinically relevant antigen. Furthermore, although we did observe slight association of the positively-charged nucleoprotein with negatively-charged CpG adjuvant when mixed together (see Figure **B.1B**), this had no effect on the ability to complex CpG DNA with nucleoprotein-nanoparticle conjugates in order to formulate a dual-delivery influenza vaccine

(**Figure B.1**). Moreover, immunization with the nucleoprotein-containing vaccine conferred significant protection against lethal challenge with influenza virus, clearly demonstrating the success of particle-mediated delivery of this antigen.

In addition, this work also provides the first demonstration that nucleic acid adjuvants other than CpG DNA can be delivered using this nanoparticle platform. The adjuvants studied here possess diverse physicochemical features. CpG1826 is a small, single-stranded DNA molecule, while poly(I:C) is a large, double-stranded RNA molecule with heterogenous molecular weight, and nanoISD is a double-stranded DNA molecular intermediate in size to the other adjuvants. These adjuvants target distinct innate immune receptors in the endosome (TLR9, TLR3) and the cytosol (RIG-I, cGAS). Despite the varying size and structure of these adjuvants, we demonstrate that all three can stably complex with OVA-nanoparticle conjugates. Thus, this nanoparticle platform provides a tool for studying the ways in which delivery of adjuvants to targets in distinct intracellular compartments can affect the downstream immune response. In the final aim of this work, we begin investigating the impact of these adjuvants on the $CD8^+$ T_{RM} response in the lungs and their effect on antigen-presenting cell activation. We study whether the pH-responsive property of the vaccine is linked to the immunostimulatory activity of each adjuvant by comparing it with adjuvant-loaded control nanoparticles. This lays the groundwork for further study of the effects of single adjuvants, or adjuvant combinations, on innate immune activation, and the ways this can be harnessed to target key APC subsets and promote protective T_{RM} immunity.

1.3 Specific Aims

The overall goal of this to work is to develop a pH-responsive nanoparticle-based subunit vaccine that can generate tissue-resident memory T cells in the lungs and protect against respiratory infection. As part of this, we also seek to fully characterize the immune response to the nanoparticle vaccine, and to uncover possible relationships between material properties of the nanoparticle and its generation of a T_{RM} response. Although vaccines that can promote T_{RM} formation *via* a variety of mechanisms have been studied, the rational design of materials that can precisely tune the T_{RM} response is relatively unexplored.

Prior to initiation of the work described in this dissertation, work had been done on stimuli-responsive (“smart”) materials for overcoming a variety of barriers in drug delivery. In particular, pH-responsive materials were developed and used for several applications, including delivery of siRNA for gene therapy and delivery of protein antigen and nucleic acid adjuvant for systemic immunization.[50, 108] However, such materials had not yet been used with the purpose of applying principles of materials engineering and drug delivery to new knowledge regarding T_{RM} biology and vaccine design. As such, the work presented in this dissertation aimed to address several outstanding questions in the field,

namely: can this pH-responsive polymer nanoparticle system be used for mucosal (intranasal) immunization and co-delivery of antigen and adjuvant to the lungs? If so, can it be used to generate $CD8^+$ T_{RM} cells in the lungs, and are these cells protective against challenge with respiratory viruses? And finally, how can the material and delivery properties of the nanoparticle carrier (i.e., pH-responsive activity and nature of adjuvants delivered) be utilized to tune the T_{RM} response? What is the connection between activation of innate immunity and downstream production of T_{RM} cells?

The work presented here leverages a pH-responsive polymer to create a nanoparticle vaccine that can co-deliver antigen and adjuvant to a mucosal tissue, generate $CD8^+$ T cells that are resident in the lungs, and protect against respiratory infection. It also characterizes the innate and adaptive immune responses to the vaccine and demonstrates important links between material properties of the nanoparticle, cellular uptake and retention of vaccine cargo, and promotion of tissue-residency.

This nanoparticle vaccine is shown to be effective in two murine models of respiratory virus infection, vaccinia and influenza, *via* delivery of two different protein antigens, ovalbumin and influenza A nucleoprotein. Influenza is a clinically relevant pathogen that poses a serious global health threat, for which universal vaccines that can generate cellular immunity are greatly needed. The ability to effectively use the same nanoparticle platform to immunize against multiple pathogens demonstrates its modular capabilities. It can be loaded with antigens derived from any number of pathogens, including non-respiratory viruses and intracellular bacteria, and it can accommodate a variety of nucleic acid adjuvants for activation of diverse immune pathways. In addition, this platform has potential to be adapted for use in cancer vaccines *via* delivery of patient-specific tumor antigens.

Specific Aim 1: Determine whether mucosal antigen and adjuvant dual-delivery *via* pH-responsive nanoparticles can generate tissue-resident T cells in the lungs. Subunit vaccines containing protein antigens, while safer than live vectors, are also poorly immunogenic and require the addition of adjuvants to elicit a functional immune response. However, administration of soluble antigen and adjuvant results in poor cellular uptake and minimal generation of $CD8^+$ T cells; nanoparticle-mediated delivery can help mitigate this issue. While previous work has shown that non-mucosal delivery of vaccine cargo on pH-responsive nanoparticles generates a systemic $CD8^+$ T cell response, vaccines with translational potential will ideally generate tissue-resident cellular immunity in organs such as the lungs. This aim builds on previous work with pH-responsive nanoparticles by utilizing intranasal administration to determine whether a tissue-resident $CD8^+$ T cell response in the lungs can be produced. Extensive *in vivo* characterization of the immune response to mucosal immunization with this nanoparticle vaccine demonstrated that pH-responsive activity, route of administration, particulate dual-delivery of antigen and adjuvant, and persistence of vaccine cargo in pulmonary antigen-presenting cells all play a role in promoting a lung-resident $CD8^+$ T cell response.

Specific Aim 2: Evaluate the capacity of the nanoparticle vaccine to provide T_{RM}-mediated protection against viral respiratory pathogens. After this pH-responsive nanoparticle vaccine showed promise in generating a tissue-resident $CD8^+$ T cell response in the lungs, we further characterized the response at long-term memory timepoints after immunization *via* staining for common T_{RM} surface markers, CD103 and CD69. In addition, the protective capacity of the nanoparticle vaccine was tested in two models of murine respiratory virus infection. In a sublethal model, mice immunized with ovalbumin antigen were challenged with a recombinant vaccinia virus expressing the MHC-I epitope for OVA; in a lethal model, mice immunized with influenza A nucleoprotein were challenged with PR8 H1N1 virus. In both models, immunization with the nanoparticle vaccine exhibited significant improvement in morbidity and mortality relative to naïve mice or those receiving control formulations. Notably, this was achieved after immunization with only a single dose. The results of this aim indicate that the nanoparticle vaccine platform has potential for use against respiratory infections that require T_{RM}-mediated protection.

Specific Aim 3: Investigate the effect of material and adjuvant properties on innate immune cell activation and its relationship to T_{RM} generation. Evidence in the literature indicates that a multitude of innate immune cells and molecules may play a role in generation of tissue-resident memory T cell responses; however, much of the relationship between innate immunity and T_{RM} production remains unclear. In particular, the ways in which vaccines can be engineered to control innate immune activation and tailor it toward a T_{RM}-biased response are relatively unexplored. We previously showed that the pH-responsive activity of the nanoparticle vaccine impacted the magnitude of the lung-resident $CD8^+$ T cell response; in addition, this nanoparticle provides a platform for delivery of various nucleic acid adjuvants that target distinct innate immune pathways. In this aim, we demonstrated that both the pH-responsive nanoparticle (PH) and its non-pH-responsive control counterpart (CT) can be formulated with nucleic acid adjuvants that target receptors in either the endosome (CpG), cytosol (nanoISD), or both (poly[I:C]). Utilizing various combinations of PH and CT nanoparticles with each of these adjuvants, we probed the effects of the formulations on uptake and activation in dendritic cell subsets in the lungs and mediastinal lymph nodes. We also studied their effects on the pulmonary $CD8^+$ T_{RM} response at both short-term and long-term timepoints.

CHAPTER 2

Mucosal Dual-Delivery of Antigen and Adjuvant with a pH-Responsive Nanoparticle Vaccine Generates Lung Tissue-Resident CD8$^+$ T Cells

Text for Chapter 2 taken from:

Knight FC, Gilchuk P, Kumar A, Becker KW, Sevimli S, Jacobson ME, Suryadevara N, Wang-Bishop L, Boyd KL, Crowe JE, Jr., Joyce S, Wilson JT. Mucosal immunization with a pH-responsive nanoparticle vaccine induces protective CD8$^+$ lung-resident memory T cells. *ACS Nano*. Sep 25, 2019. PMID: 31553872.

2.1 Abstract

Tissue-resident memory T cells (T_{RM}) patrol non-lymphoid organs and provide superior protection against pathogens that commonly infect mucosal and barrier tissues, such as the lungs, intestine, liver, and skin. Thus, there is a need for vaccine technologies that can induce a robust, protective T_{RM} response in these tissues. Nanoparticle (NP) vaccines offer important advantages over conventional vaccines; however, there has been minimal investigation into the design of NP-based vaccines for eliciting T_{RM} responses. Here, we describe a pH-responsive polymeric nanoparticle vaccine for generating antigen-specific CD8$^+$ T cells that are resident in the lungs. With a single intranasal dose, the NP vaccine was able to elicit airway- and lung-resident CD8$^+$ T cells. In elucidating the contribution of material properties to the resultant immune response, we found that the pH-responsive activity of the carrier was important, as a structurally analogous non-pH-responsive control carrier elicited significantly fewer lung-resident CD8$^+$ T cells. We also demonstrated that dual-delivery of protein antigen and nucleic acid adjuvant on the same NP substantially enhanced the magnitude and functionality of the antigen-specific CD8$^+$ T cell response in the lungs. Compared to administration of soluble antigen and adjuvant, the NP also mediated retention of vaccine cargo in pulmonary antigen-presenting cells (APCs), enhanced APC activation, and increased production of T_{RM}-related cytokines. Overall, these data suggest a promising vaccine platform technology for rapid generation of CD8$^+$ T_{RM} cells in the lungs.

2.2 Introduction

Tissue-resident memory T cells (T_{RM}) are a specialized subset of memory cells with a distinct phenotype that reside in non-lymphoid tissues and act as a first line of defense against many pathogens.[18, 109, 110] T_{RM} cells remain localized in their home tissues due to a combination of adhesion

molecules and a lack of homing mechanisms for trafficking to distal lymphoid organs or circulating in the blood. As such, they are optimally positioned to respond more quickly than peripheral memory T cells. T_{RM} have been identified in several organs, including the skin, liver, kidneys, brain, and mucosal tissues such as the lungs, intestine, and female reproductive tract.[111, 112] These cells play a key role in protection against multiple infectious diseases for which new or improved vaccines are needed, such as influenza, tuberculosis, respiratory syncytial virus, and HIV/AIDS.[113-116] T_{RM} are also important in immunity against tumors, including breast cancer, melanoma, and lung cancer.[117-120] For several diseases, antibodies or non-resident memory T cells alone are not sufficient for optimal protection;[121-124] however, very few currently approved vaccines have been shown to generate T_{RM} cells.[63, 125] Therefore, there is a critical need to develop new vaccines that can induce protective T_{RM} in target tissues.

Pulmonary T_{RM} reside in both the lung interstitium and airways[126, 127] and are critical in mediating protection against respiratory pathogens.[63, 125, 128] Mucosal vaccination has garnered attention as a superior route of immunization over traditional intramuscular injections for several reasons, including its ability to mimic routes of pathogen entry and generate tissue-specific immune cells optimally positioned to fight off future infection.[120, 129] Specifically, pulmonary immunization *via* intranasal (i.n.) administration is advantageous for generating T_{RM} in the lungs.[59, 76] Additionally, there is evidence that pulmonary immunization can generate T cell responses in distal mucosal tissues.[46] Hence, the development of vaccine formulations that can be administered by mucosal routes holds great promise for a new generation of T_{RM}-targeted vaccines.

Protein-based subunit vaccines have been widely studied as a next-generation vaccine platform, including in the context of mucosal delivery.[130] A major drawback of protein-based subunit vaccines, however, is poor immunogenicity due to several drug delivery barriers, including rapid antigen clearance with poor uptake by dendritic cells and minimal accumulation in draining lymph nodes. Subunit vaccines are particularly inept at eliciting $CD8^+$ T cells, which are required for immunity against many pathogens and cancers.[88, 131] Eliciting a robust $CD8^+$ T cell response requires antigen presentation on major histocompatibility complex I (MHC-I) by dendritic cells (DCs) in the context of additional molecular cues (costimulation, cytokines) that drive $CD8^+$ T cell expansion and differentiation.[88, 132] To achieve presentation by MHC-I, administered antigen must either be endocytosed by specialized cross-presenting DC subsets or delivered to the classical cytosolic MHC-I antigen processing pathway. However, the predominant fate of soluble endocytosed antigen is lysosomal degradation, with minimal presentation on MHC-I.[90, 133]

Despite their limited capacity to generate $CD8^+$ T cells, the superior safety profile of subunit vaccines has motivated strategies to improve their efficacy.[91] Toward this end, a variety of nanoparticle (NP)-based vaccine delivery systems have been developed that utilize material properties to enhance

antigen uptake by DCs, promote antigen cross-presentation, and/or co-deliver immunostimulatory adjuvants in order to potentiate $CD8^+$ T cell responses to immunization.[50, 106, 134-137] This includes NP formulations that have been administered i.n. to generate pulmonary T cell responses in mouse models of infection and cancer.[138-140] However, to date only a few reports have evaluated the ability of NP-based subunit vaccines to specifically induce tissue-resident $CD8^+$ T cells in the lungs.[46, 58, 103] Moreover, while NP design principles for eliciting robust systemic T cell responses have largely been established, the ways in which properties of NP vaccines can be engineered to augment T_{RM} responses elicited by mucosal immunization have not been explored. This motivates the need for the design, optimization, and evaluation of NP vaccines for installing this unique memory T cell population in the lungs and other mucosal tissues.

While elucidation of the mechanisms underlying induction and maintenance of $CD8^+$ T_{RM} in the lungs remains an active area of investigation, lessons in vaccine design can be taken from studies of respiratory viral infections like influenza, in which robust and durable T_{RM} are often generated.[124, 141] These studies motivate the design of NP vaccines that can mimic viral infection by enhancing antigen uptake and cross-presentation in APCs, allowing for co-delivery of antigen and adjuvant, and/or increasing local antigen persistence in tissues.[74, 142-144] Therefore, in this study we leveraged a virus-mimetic polymeric NP vaccine delivery system that utilizes a pH-dependent endosomal escape mechanism to release cargo into the cytosol, resulting in enhanced antigen delivery to the MHC-I processing pathway.[50] Additionally, the corona of the NP is designed to enable dual-delivery of antigen and nucleic acid adjuvant from the same particle, further augmenting its ability to mimic pathogen encounter and enhance the $CD8^+$ T cell response.

Here, we demonstrate that the pH-responsive NP vaccine dual-loaded with ovalbumin protein antigen (OVA) and CpG DNA adjuvant enhanced the magnitude and functionality of the lung-resident $CD8^+$ T cell response in mice after a single dose. It also improved activation of pulmonary APCs and promoted antigen persistence in the lungs. Of significance to the design of T_{RM}-targeted NP vaccines, we show that the pH-responsive activity of the NP is important for induction of lung-resident $CD8^+$ T cells, demonstrating that a material property can be harnessed to install this important cell population in a mucosal tissue. Collectively, our results suggest a promising experimental vaccine platform for generating lung-resident $CD8^+$ T cells and offer evidence that NP properties can be modulated to augment tissue-resident immunity elicited by pulmonary immunization.

2.3 Results and Discussion

Intranasal antigen delivery with a pH-responsive nanoparticle carrier enhances the lung-resident $CD8^+$ T cell response

The nanoparticle described in this report is formulated using a pH-responsive diblock copolymer designed to enhance cytosolic delivery of vaccine cargo and strengthen the $CD8^+$ T cell response by promoting processing and presentation of antigen in the MHC-I pathway.[50] The polymer is composed of two functional blocks synthesized by RAFT polymerization (**Figure A.1A,B**). The first block is a hydrophilic copolymer of dimethylaminoethyl methacrylate (DMAEMA) and pyridyl disulfide ethyl methacrylate (PDSMA). PDSMA provides pyridyl disulfide groups on the surface of the particle for conjugation to thiolated protein antigen, and DMAEMA contributes cationic charge for electrostatic complexation with a nucleic acid adjuvant. The second block is a pH-responsive, endosomolytic copolymer of propylacrylic acid (PAA), butyl methacrylate (BMA), and DMAEMA, which drives micellar nanoparticle assembly due to its hydrophobic nature. After cellular uptake and in response to endosomal acidification, the micellar structure of the NP transforms to expose the membrane-destabilizing core (PAA-BMA-DMAEMA), which promotes endosomal escape and cytosolic antigen delivery to the MHC-I pathway.

While this mechanism of NP-mediated antigen cross-presentation was previously utilized to enhance the splenic $CD8^+$ T cell response *via* subcutaneous administration, whether pH-responsive activity can be leveraged to generate a lung-resident $CD8^+$ T cell response after intranasal antigen delivery is unknown. To evaluate this, both pH-responsive NP and non-responsive control NP (second block consisting only of BMA) were synthesized and characterized (**Figure A.1A-C**, **Table A.1, Figure A.2**), and a model protein antigen, ovalbumin (OVA), was thiolated and covalently conjugated to both NP carriers (**Figure A.3A,C**). Mice were immunized i.n. with antigen-NP conjugates made using either pH-responsive nanoparticles (OVA-NP_{pH}) or control nanoparticles (OVA-NP_{ctrl}). On d13 after immunization, mice were injected intravenously (i.v.) with αCD45.2 antibody to distinguish $CD45^+$ blood-borne cells in the marginated lung vasculature (MV) from tissue-resident $CD45^-$ cells in the lung interstitium (IST). By directly discriminating between cells residing in distinct lung compartments, this intravascular staining technique provides an accurate and robust method for establishing tissue residence.[44, 45, 66, 116] Broncheoalveolar lavage fluid (BAL) was also collected to differentiate $CD45^-$ cells resident in the airways (AW) from $CD45^-$ IST-resident cells[66] (**Figure 2.1A**).Cells obtained from lungs, BAL, and spleens were stained with fluorescent antibody against a panel of surface markers and with fluorescent MHC-I tetramer (Tet) containing SIINFEKL peptide (the immunodominant H-$2K^b$ epitope for OVA). They were then analyzed by flow cytometry to quantify antigen-specific $CD8^+$ T cells ($Tet^+CD8\alpha^+CD11b^-CD11c^-B220^-CD4^-$) in each lung compartment and the spleen (**Figures 2.1B and**

A.4A-C). Fluorescence microscopy was also used to confirm that OVA-NP conjugates reached the lower airways after i.n. administration. Conjugates formulated with Alexa Fluor 647-labeled OVA were visible in lungs harvested 24 h after immunization (**Figure 2.1C**). We found that the pH-responsive carrier elicited a significantly greater antigen-specific (Tet^+) $CD8^+$ T cell response than the control carrier in the AW (**Figure 2.2A**) and IST (**Figure 2.2B**), while there was no significant difference in the response between carriers in the MV (**Figure 2.2C**) and spleen (**Figure 2.2D**). These data indicate that the pH-responsive property of the NP is important for generating a tissue-resident $CD8^+$ T cell response in the lungs, and serve to demonstrate the importance of NP properties in development of T_{RM}-targeted vaccines.

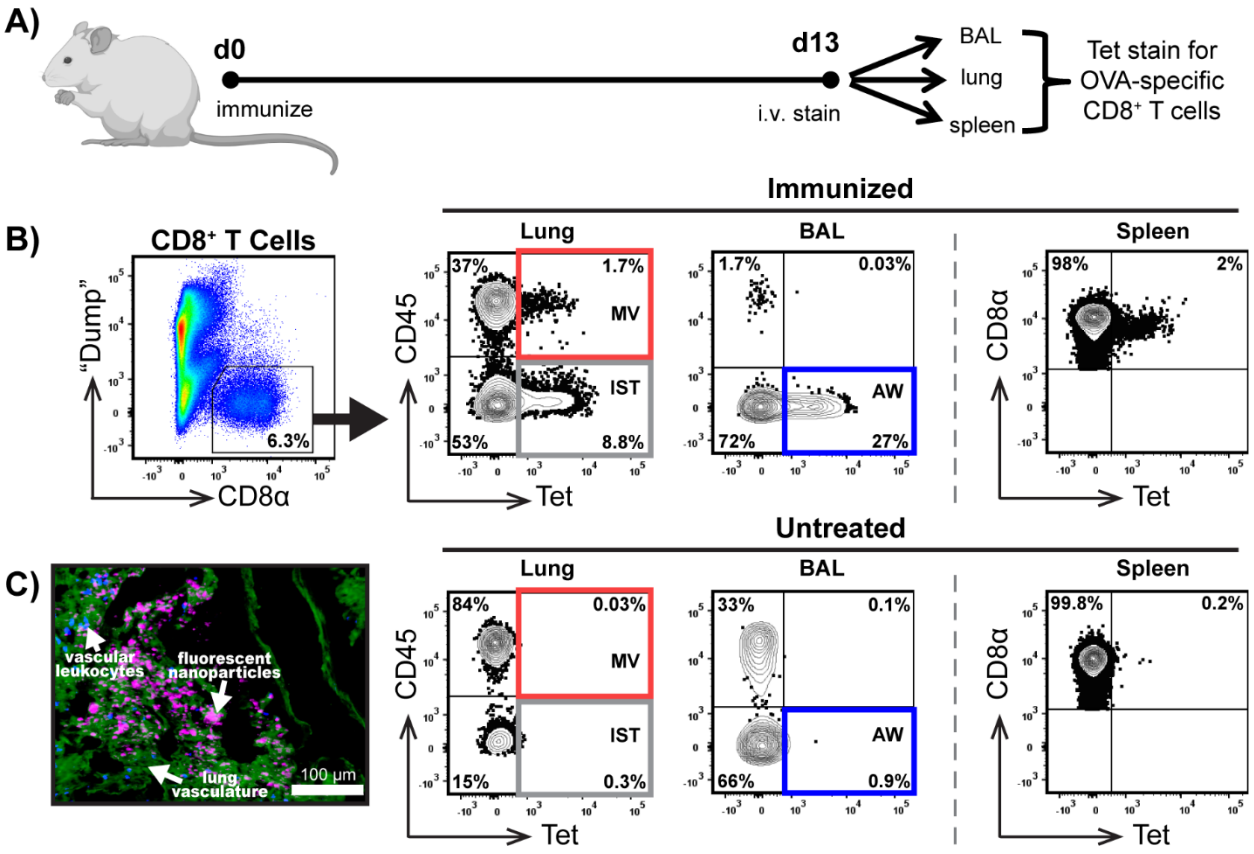

Figure 2.1 | Intravascular staining is used to determine localization of $CD8^+$ T cells in the lungs after intranasal vaccine delivery. Schematic of the experimental timeline. **(B)** Flow cytometry was used to identify antigen-specific (Tet^+) $CD8^+$ T cells in distinct lung compartments (airway, AW; interstitium, IST; marginated vasculature, MV) and the spleen. BAL was collected to discriminate AW *vs.* IST cells, and i.v. staining with αCD45 antibody discriminated IST ($CD45^-$) *vs.* MV ($CD45^+$) cells. Samples were stained with PE-labeled SIINFEKL/MHC-I tetramer to identify antigen-specific $CD8^+$ T cells. After gating out $CD11b^+$, $CD11c^+$, $B220^+$, and $CD4^+$ cells ("dump"), $CD8\alpha^+CD45^-Tet^+$ events in AW and IST, $CD8\alpha^+CD45^+Tet^+$ events in MV, and $CD8\alpha^+Tet^+$ events in the spleen were quantified. Dot plots are representative of the gating strategy used in at least ten experiments (see **Figure A.4A-C**).

(C) In conjunction with i.v. staining, microscopy was used to visualize fluorescent OVA-NP conjugates in the lower airways 24 h after immunization. Lungs were stained with αCD45 antibody, which labels vascular leukocytes, and tomato lectin, which binds to capillary endothelial cells and allows for visualization of lung structure. Purple: OVA-NP; blue: vascular leukocytes; green: lung vasculature. Scale bar = 100 µm. Microscopy experiment was performed once. Immunization dose: 25 µg NP, 7.5 µg OVA. Panel (A) created with Biorender.com.

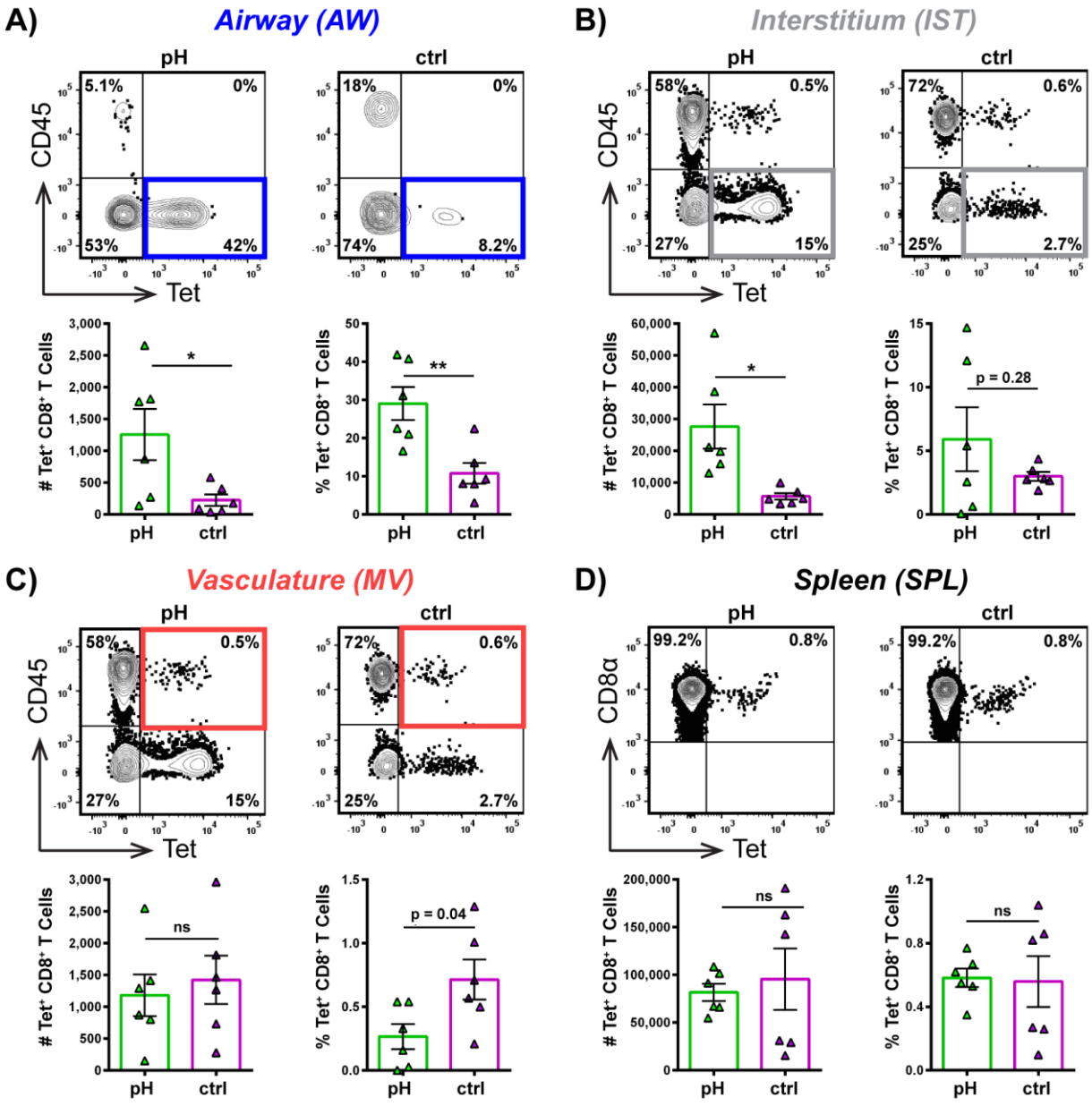

Figure 2.2 | Intranasal antigen delivery with pH-responsive nanoparticle enhances lung-resident CD8⁺ T cell response. Number (#) and frequency (%) of Tet⁺ CD8⁺ T cells in **(A)** AW, **(B)** IST, **(C)** MV, and **(D)** spleen were enumerated on d13 after i.n. administration of OVA-NP_{pH} or OVA-NP_{ctrl}. Representative dot plots are gated on viable CD8⁺ T cells. Immunization dose: 25 µg NP, 7.5 µg OVA. Data are mean ± SEM and representative of two independent experiments, with *n* = 6 per group. Limits

of detection: 1 cell (AW), 5 cells (IST/MV), 25 cells (spleen). *p<0.05, **p<0.01 by unpaired t-test. ns, not significant. See also **Figure A.4A-C**.

Intranasal dual-delivery of antigen and adjuvant with pH-responsive nanoparticles enhances magnitude and functionality of the lung-resident CD8$^+$ T cell response

After demonstrating the importance of pH-responsiveness in generating a robust lung-resident CD8$^+$ T cell response, we next asked whether dual-delivery of antigen and an immunostimulatory adjuvant on the same pH-responsive NP would further augment this response. While this pathogen-mimetic property has previously been shown to enhance the systemic CD8$^+$ T cell response,[50] to our knowledge the importance of NP dual-delivery for generating tissue-resident CD8$^+$ T cells has not been clearly demonstrated. Therefore, NP were co-loaded with OVA protein and a nucleic acid adjuvant, CpG ODN 1826 (a single-stranded DNA agonist for TLR9). CpG DNA has been shown to enhance the CD8$^+$ T cell response and has precedence for use in pulmonary immunization.[58, 138, 145] CpG was electrostatically complexed to OVA-NP conjugates (**Figure A.3B**), and this formulation is referred to henceforth as OVA-NP/CpG or the "nanoparticle vaccine."

On d0, mice were immunized i.n. with OVA-NP/CpG, OVA-NP conjugate, a mixture of soluble OVA+CpG, a mixture of soluble OVA+NP, or NP/CpG complex mixed with soluble OVA (NP/CpG+OVA) (**Figure 2.3A**). On d13 after immunization, mice were injected i.v. with αCD45.2 antibody and lungs, BAL, and spleens were collected and analyzed by flow cytometry as described above (**Figures 2.1A,B and A.4A-C**). Mice immunized with a single dose of OVA-NP/CpG produced significantly more Tet$^+$ CD8$^+$ T cells relative to all other formulations (**Figure 2.3B-E**). This increased response was observed in both the AW (**Figure 2.3B**) and IST (**Figure 2.3C**) lung compartments, as well as in the MV (**Figure 2.3D**) and spleen (**Figure 2.3E**). These data demonstrate that NP-mediated dual-delivery of antigen and adjuvant to the lungs enhances the CD8$^+$ T cell response over delivery of antigen alone (OVA-NP). This effect was particularly prominent in the IST, indicating the ability of the NP vaccine to induce lung-resident CD8$^+$ T cells. Simple mixing of components (OVA+CpG, OVA+NP) was ineffective, and dual-delivery on the same particle was crucial, as the formulation containing all three components without co-loading (NP/CpG+OVA) did not induce a robust response.

T cell functionality after immunization was assessed *via* intracellular cytokine staining (ICCS). Mice were immunized on d0 with OVA-NP/CpG, OVA-NP, OVA+CpG, or PBS, and lungs and spleens were collected on d13. Lung and spleen cells were re-stimulated with SIINFEKL peptide and analyzed by flow cytometry for production of IFNγ and TNFα (**Figure A.4D**). Mice immunized with OVA-NP/CpG had a greater percentage of polyfunctional (IFNγ$^+$TNFα$^+$) antigen-specific CD8$^+$ T cells in both the lungs and spleen, relative to all other formulations (**Figure 2.3F**). This further supports the importance of

antigen and adjuvant dual-delivery in generating a robust and functional $CD8^+$ T cell response, particularly in the lungs.

In addition, the $CD8^+$ T cell response in mice immunized i.n. with OVA-NP/CpG was compared to the response to subcutaneous (s.c.) immunization with the same formulation. It has been reported that systemic administration of antigenic protein and adjuvant *via* the intraperitoneal (i.p.) route generates low numbers of lung-resident $CD8^+$ T cells relative to i.n. administration.[66] We hypothesized that s.c. immunization with the NP vaccine would also be ineffective. On day 13 post-immunization, tetramer staining was used to analyze the antigen-specific $CD8^+$ T cell response to i.n. or s.c. administration of the NP vaccine. Responses in the AW (**Figure 2.4A**) and IST (**Figure 2.4B**) were significantly higher for mice immunized i.n., whereas there was no difference between administration routes for MV (**Figure 2.4C**) or spleen (**Figure 2.4D**). Consistent with previous reports, this demonstrates the importance of i.n. administration of the NP vaccine for generating a lung-resident $CD8^+$ T cell response.[46, 103, 140]

Pulmonary toxicity is an important consideration when evaluating the translational potential of mucosal vaccines. NP-based i.n. or intratracheal vaccine and/or CpG administration have previously been reported to be safe in mice.[46, 138, 139] In this work, mice immunized i.n. exhibited minimal weight loss within the first two days and recovered rapidly (**Figure A.5A**). In addition, lung tissue harvested at d1 and d12 after immunization with either OVA-NP/CpG or OVA+CpG was evaluated for immunopathology. Mild inflammation was induced by both formulations, with no signs of pathology or tissue damage, and findings were consistent between animals in the same treatment group (**Figure A.5B**). This mild inflammation was associated with infiltration of immune cells to the lungs (lymphocytes, macrophages, neutrophils at d1; lymphocytes, plasma cells, macrophages at d12) and is consistent with flow cytometry data showing recruitment of lymphoid cells in response to i.n. vaccine administration (**Figure 2.3B-E**).

Taken together, these data demonstrate that i.n. administration of the NP vaccine is safe and can significantly enhance the magnitude and functionality of the antigen-specific $CD8^+$ T cell response within 13 days and after a single dose. In addition to local lung-resident $CD8^+$ T cells, the NP vaccine can also induce systemic immunity *via* i.n. administration. Importantly, pathogen-mimetic dual-delivery of antigen and adjuvant on the same particle is integral to the magnitude and functionality of this response.

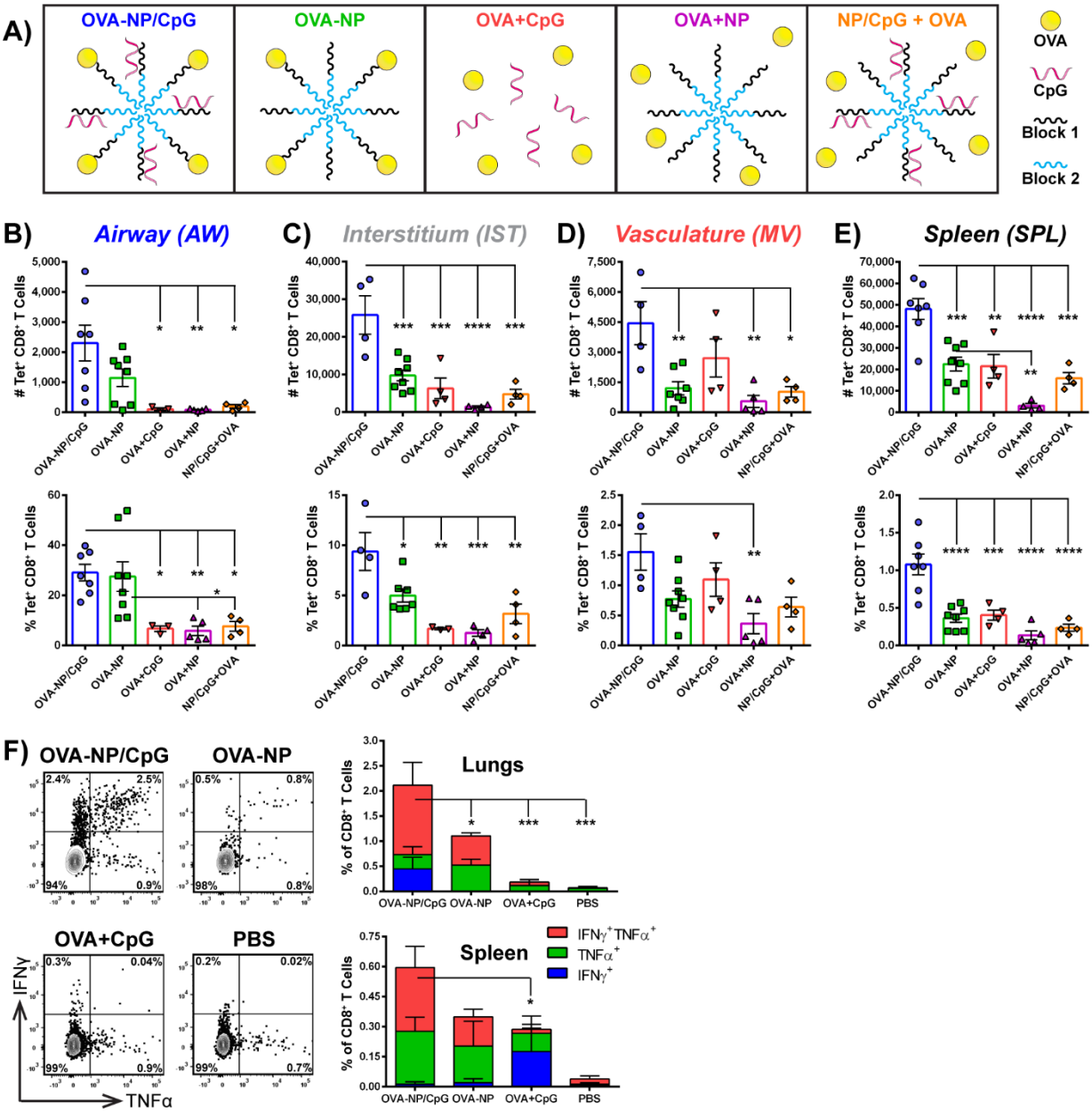

Figure 2.3 | Intranasal dual-delivery of antigen and adjuvant *via* nanoparticle vaccine enhances magnitude and functionality of lung-resident CD8⁺ T cell response. (A) Mice were immunized on d0 with the NP vaccine or control formulations, and lungs, spleens, and/or BAL were collected on d13 for analysis of the immune response by tetramer staining or ICCS. **(B-E)** Number (#) and frequency (%) of Tet⁺ CD8⁺ T cells in **(B)** AW, **(C)** IST, **(D)** MV, and **(E)** spleen were enumerated on d13 after i.n. administration of OVA-NP/CpG or control formulations. **(F)** ICCS was used to identify % CD8⁺ T cells positive for IFNγ and/or TNFα after *ex vivo* restimulation of lungs and spleen with SIINFEKL peptide. Statistical significance is shown for IFNγ⁺TNFα⁺ group only. Data are mean ± SEM and representative of one to three independent experiments, with **(B-E)** *n* = 4-7 per group and **(F)** *n* = 2-4 per group. Immunization dose: 25 µg NP, 7.5 µg OVA, 1.4 µg CpG. Limits of detection for **(B-E)**: 1 cell (AW), 5 cells (IST/MV), 25 cells (spleen). *p<0.05, **p<0.01, ***p<0.001, ****p<0.0001 by **(B-E)** ordinary one-way ANOVA with Tukey's multiple comparisons test or **(F)** ordinary two-way ANOVA with Tukey's multiple comparisons test. See also **Figure A.4A-D**.

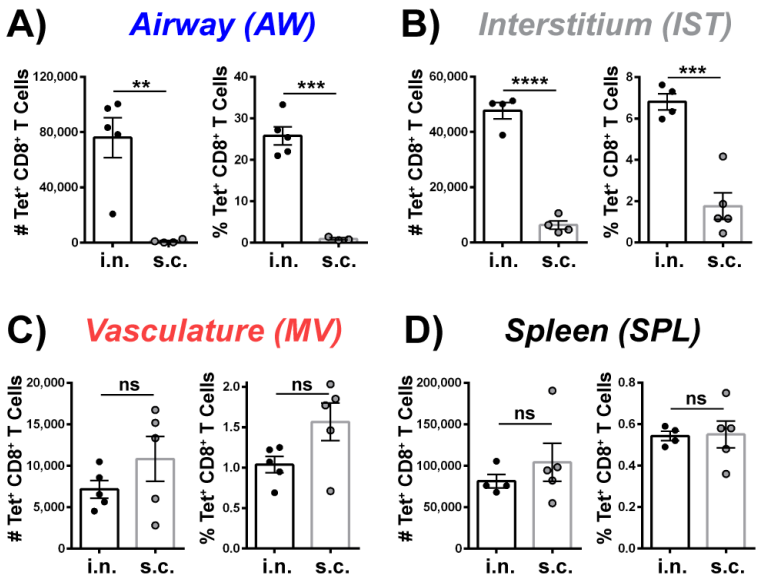

Figure 2.4 | Pulmonary immunization *via* intranasal administration is optimal for generating a lung-resident CD8⁺ T cell response. Number (#) and frequency (%) of Tet⁺ CD8⁺ T cells in **(A)** AW, **(B)** IST, **(C)** MV, and **(D)** spleen were enumerated on d13 after i.n. or s.c. administration of OVA-NP/CpG. Data are mean ± SEM, with *n* = 4-5 per group. Experiment was performed once. Immunization dose: 25 µg NP, 7.5 µg OVA, 1.4 µg CpG. Limits of detection: 1 cell (AW), 5 cells (IST/MV), 25 cells (spleen). **p<0.01, ***p<0.001, ****p<0.0001 by unpaired t-test.

Nanoparticle-mediated dual-delivery enhances persistence and co-localization of cargo and expression of activation markers in pulmonary antigen-presenting cells

We next asked what characteristics of the NP vaccine formulation could account for the enhanced lung-resident CD8⁺ T cell response. Previous reports have demonstrated the importance of antigen persistence in establishing T_{RM} populations in the lungs and other tissues.[18, 74, 143, 146] In addition, cross-presenting CD103⁺ DCs are involved in activation of precursor T_{RM}, and alveolar macrophages can promote formation of T_{RM} in the lungs.[47, 48, 72] We hypothesized that the NP formulation would increase vaccine residence time in the lungs, thereby promoting extended co-delivery of vaccine cargo (OVA and CpG) to pulmonary innate immune cells. We also postulated that this NP-mediated persistence would prolong activation of local APCs, thus leading to an improved downstream adaptive immune response and formation of T_{RM} in the lungs.[143]

To evaluate this, we labeled OVA with Alexa Fluor 647 (OVA_{647}) and CpG with Alexa Fluor 488 (CpG_{488}) and immunized mice i.n. with fluorescent formulations (OVA_{647}-NP/CpG_{488} or OVA_{647}+CpG_{488}) or PBS. First, to assess organ-level local and systemic biodistribution of the formulations, lungs and spleens were harvested at 24, 48, and 72 h post-immunization and imaged to determine whether the NP vaccine enhanced OVA retention relative to the soluble formulation. Quantification of OVA_{647} average radiant efficiency in fluorescent images demonstrated that antigen remained in the lungs longer

for mice immunized with the NP vaccine. At both 48 h and 72 h post-immunization, mice receiving OVA_{647}-NP/CpG_{488} had significantly more OVA_{647} fluorescence in the lungs relative to OVA_{647}+CpG_{488} (**Figure 2.5A**). There was negligible fluorescence present in the spleen (**Figure 2.5A**), liver, and kidneys (**Figure A.6**) at all time points, suggesting that i.n. administration leads to localized pulmonary delivery with minimal systemic distribution.

In addition to assessment of localization and retention at the organ level, lungs were also analyzed by flow cytometry to evaluate uptake of vaccine cargo in pulmonary APC subsets (**Figure A.7A**), as well as expression of the costimulatory marker CD86 in these populations. The cell types analyzed were: (1) alveolar macrophages (AMφ), (2) interstitial macrophages (IMφ), (3) $CD103^+$ dendritic cells ($CD103^+$ DC), (4) $CD11b^+$ dendritic cells ($CD11b^+$ DC), (5) a population of monocyte- and macrophage-like cells not encompassed by other subsets (Mono/Mφ), (6) granulocytes (Gran), and (7) "Other" (anything not included in previous categories).[147] We expected dual-delivery of OVA_{647} and CpG_{488} with the NP vaccine would increase their co-localization within cells, so we analyzed cells that were double-positive for both cargoes (OVA^+CpG^+) (**Figure A.7B**). Uptake was quantified for each cell subset as both "cell count" (# OVA^+CpG^+ events) and "relative uptake" (mean fluorescence intensity (MFI) of either OVA or CpG multiplied by # OVA^+CpG^+ events). Relative uptake was used to account for both the number of cells containing cargo (#) and the total amount of cargo taken up (MFI).[46] Initially, after 24 h, there was no difference in uptake between OVA-NP/CpG and OVA+CpG (**Figures 2.5B and A.7C, top row**). Starting at 48 h and increasing by 72 h post-immunization, there was significantly more cargo co-localization from the NP vaccine in several cell types, including $CD103^+$ DCs and $CD11b^+$ DCs at 48 h (**Figures 2.5B and A.7C, middle row**), and DCs, AMφ, IMφ, Mono/Mφ, and Gran at 72 h (**Figures 2.5B and A.7C, bottom row**). These data reflect the results obtained from fluorescent organ imaging (**Figure 2.5A**) and demonstrate that NP delivery prolongs antigen and adjuvant co-localization and retention in pulmonary APCs, suggesting that an NP-mediated increase in local antigen persistence may contribute to the generation of lung T_{RM}.

In addition, CD86 expression was significantly upregulated in certain cell subsets after immunization with OVA-NP/CpG relative to OVA+CpG, including $CD103^+$ DCs, IMφ, and Mono/Mφ (**Figure 2.5C**). The increase in expression was minimal in AMφ, $CD11b^+$ DCs, and Gran (**Figure A.7D**). This is particularly notable for $CD103^+$ DCs, since this cell subset exhibited lower levels of cargo uptake compared to, *e.g.*, Mφ populations, but the portion of $CD103^+$ DCs that did internalize the formulation appears to have been strongly activated, as CD86 expression remained high even after 72 h. Importantly, this cell subset has been implicated in the development of T_{RM} in the lungs.[148] Together, these data demonstrate that the NP vaccine enhances persistence and co-localization of vaccine cargo in pulmonary innate immune cells, as well as activation of APCs that can promote a T_{RM} response.

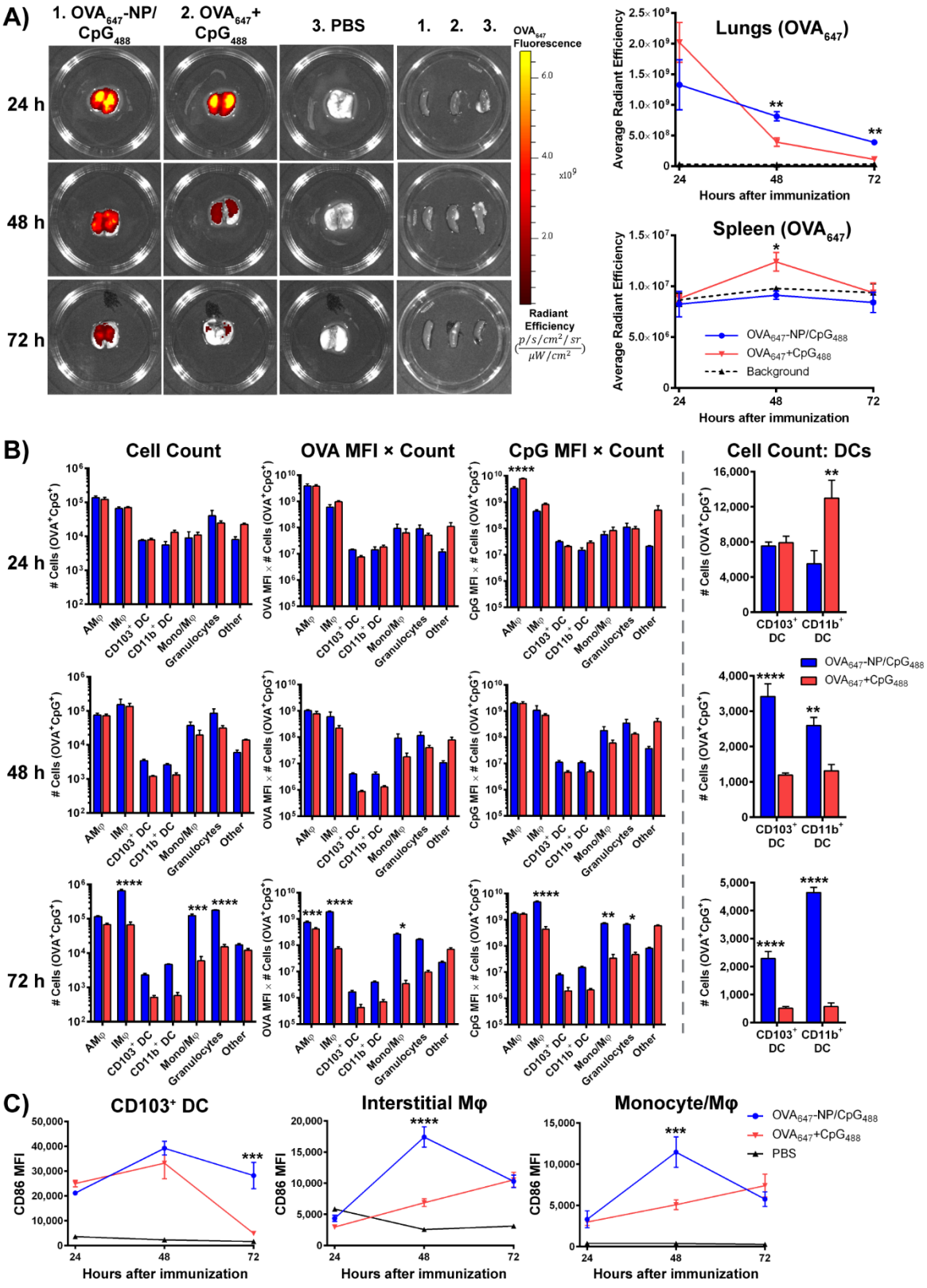

Figure 2.5 | Nanoparticle-mediated dual-delivery enhances co-localization and retention of cargo in pulmonary APCs and expression of activation markers. Lungs and spleens were imaged at 24, 48, and 72 h post-immunization to quantify uptake of OVA_{647}. Representative images of lungs and spleens from each treatment group at each timepoint (left) and quantification of OVA_{647} fluorescence in

lungs and spleens over time (right). **(B)** Flow cytometry was used to quantify the # of pulmonary APCs positive for both OVA_{647} and CpG_{488} (OVA^+CpG^+) at each time point ("cell count"). Cell counts were also multiplied by either OVA MFI or CpG MFI to determine "relative uptake" of each cargo (MFI × cell count). Bar graphs for $CD103^+$ DC and $CD11b^+$ DC are replicated for visibility. **(C)** Expression of CD86 was measured for several cell subsets in the lungs. Data are mean ± SEM and representative of four independent experiments, with n = 3-4 per group. Immunization dose: 25 μg NP, 7.5 μg OVA, 1.4 μg CpG. *p<0.05, **p<0.01, ***p<0.001, ****p<0.0001 by **(A)** unpaired t-test at each timepoint comparing OVA-NP/CpG *vs.* OVA+CpG, with Holm-Sidak multiple comparisons test, **(B)** ordinary two-way ANOVA with Sidak's multiple comparisons test, or **(C)** ordinary two-way ANOVA with Tukey's multiple comparisons test (significance shown for OVA-NP/CpG *vs.* OVA+CpG). See also **Figure A.7**.

The acute cytokine response to the nanoparticle vaccine is localized to the lungs and supports generation of lung-resident $CD8^+$ T cells

The innate immune response generated by a vaccine plays a critical role in shaping the magnitude and phenotype of the resulting adaptive immune response, and this innate response can be characterized in terms of the cytokine profile induced by the vaccine. Evidence suggests that maturation into T_{RM} occurs after activated T cells have migrated back to their home tissue from the lymph nodes, and that the presence of local inflammatory signals in the tissue drives this process.[5, 18, 31, 32] A number of cytokines are important for generating $CD8^+$ T cell responses (IFNγ, type I interferons (IFNα/β), IL-12, IL-1, IL-6)[149-153] and for the induction and maintenance of T_{RM} (IL-33, IFNα/β, TNFα, IL-12, TGFβ, IL-7, IL-15).[5, 18, 32, 146, 154] In particular, several of these cytokines are involved in upregulating T_{RM} surface markers CD69 and CD103; type I IFN, IL-33, and TNFα induce CD69 upregulation on T cells, TGFβ has been shown to induce CD103 expression on T_{RM} precursors, and IL-12 may play a role in differentiation of $CD103^-CD69^+$ T_{RM}. Many of these cytokines are also important for rapid activation of pulmonary APC subsets that that have been implicated in T_{RM} generation.[105, 155]

We hypothesized that the NP vaccine would increase local production of key cytokines in the lungs, supporting an improved pulmonary $CD8^+$ T_{RM} response. To evaluate this, mice were immunized i.n. with OVA-NP/CpG, OVA+CpG, or PBS, and multiplexed cytokine analysis was used to quantify cytokine levels in lung homogenate, BAL, and serum at 6 h, 24 h, 48 h, and 7 d post-immunization. Overall, i.n. administration of the NP vaccine generated 2.5- to 375-fold higher concentrations of cytokines in the lungs and BAL relative to concentrations in the serum, indicating local cytokine production with minimal systemic inflammation (**Figure 2.6**). The response peaked at either 24 h or 48 h for most cytokines before returning to baseline by d7 post-immunization. The local and acute nature of this cytokine response corroborates histological analyses demonstrating a favorable safety profile for the NP vaccine (**Figure A.5B**). At 24 h or 48 h post-immunization, OVA-NP/CpG generated 2- to 10-fold higher levels of cytokines associated with $CD8^+$ T cells (IFNγ, IFNα/β, IL-12p70, IL-1β, IL-6) in the lungs and/or BAL, relative to OVA+CpG. Similarly, concentration of cytokines related to T_{RM}

generation (IL-33, TNFα, IFNα/β, IL-12p70) were 2- to 15-fold higher in the lungs and/or BAL at 24 h or 48 h after immunization with OVA-NP/CpG, relative to OVA+CpG.

We also compared the cytokine response generated by OVA-NP *vs.* OVA-NP/CpG. Overall, the OVA-NP formulation generated little to no response above baseline levels, whereas for the majority of cytokines tested, OVA-NP/CpG stimulated significantly higher cytokine concentrations than OVA-NP at the 48 h timepoint (**Figure A.8**). Thus, CpG appears to be an integral component of stimulating the cytokine profile observed after immunization with OVA-NP/CpG. Taken together, these data demonstrate that immunization with the NP vaccine generates a local cytokine milieu that may support induction of $CD8^+$ T cells with a T_{RM} phenotype.

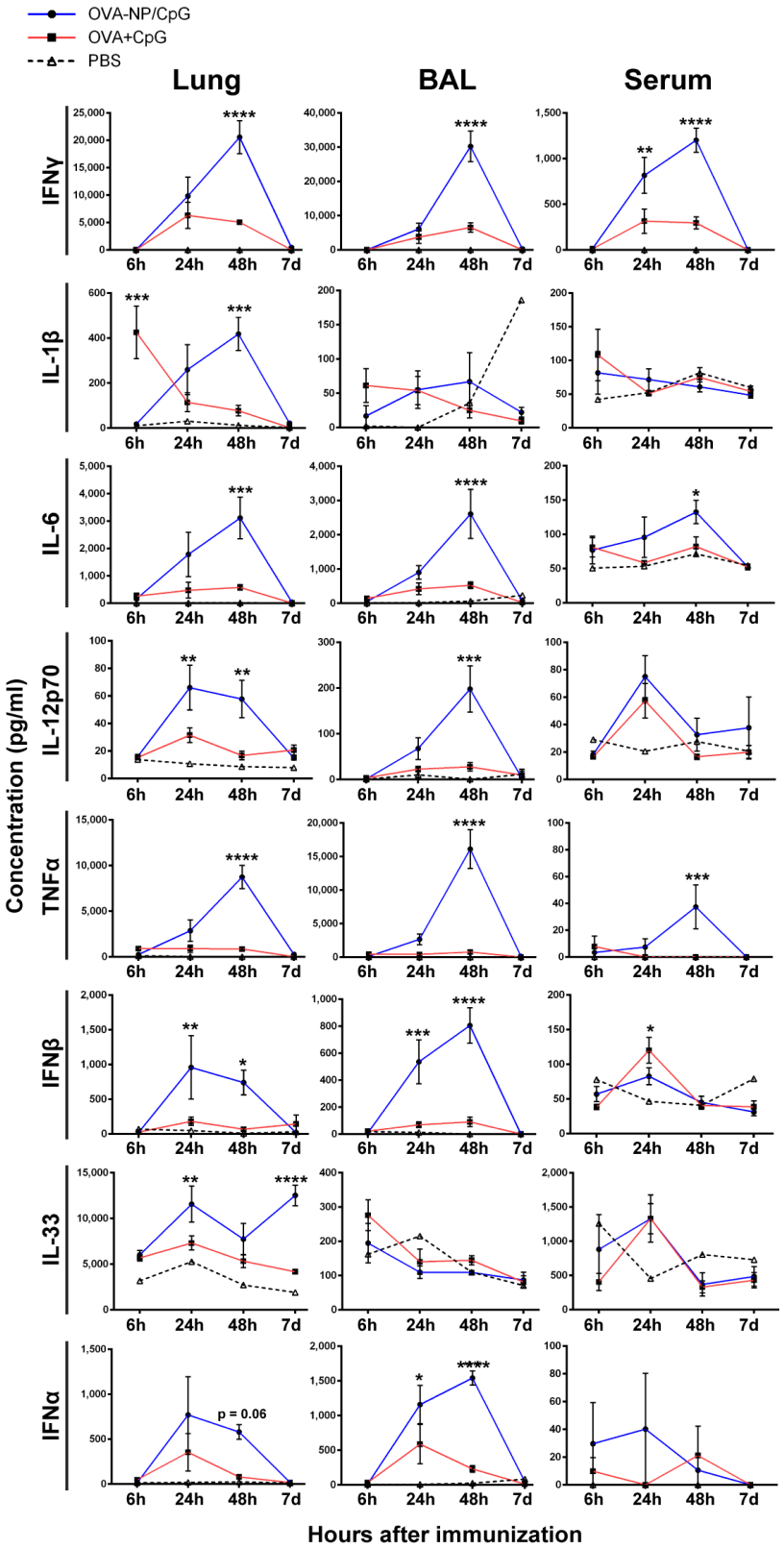

Figure 2.6 | Acute cytokine response to the nanoparticle vaccine is localized, transient, and supportive of lung-resident CD8⁺ T cells. Cytokines associated with $CD8^+$ T cells (IFNγ, IL-1β, IL-6, IL-12p70) and T_{RM} generation (TNFα, IFNβ, IL-33, IFNα) were measured in lungs, BAL, and serum obtained 6 h, 24 h, 48 h, or 7 d after i.n. administration OVA-NP/CpG or OVA+CpG. Data are mean ±

SEM and representative of two independent experiments, with *n* = 4-5 per group. Immunization dose: 25 µg NP, 7.5 µg OVA, 1.4 µg CpG. *p<0.05, **p<0.01, ***p<0.001, ****p<0.0001, by ordinary two-way ANOVA with Tukey's multiple comparisons test. Statistical differences shown are for comparison of OVA-NP/CpG *vs.* OVA+CpG. See also **Figure A.8**.

2.4 Conclusion

As the importance of tissue-resident memory T cells in defense against disease becomes increasingly clear, efforts are turning toward developing mucosal vaccines that can induce a durable and protective T_{RM} response against infectious pathogens and cancers.[46, 49, 53, 58, 73, 103, 120, 156] Here, using a mouse model of pulmonary immunization, we demonstrated that a single dose of a pH-responsive nanoparticle vaccine provided extended co-delivery of antigen and adjuvant to pulmonary APCs, produced a cytokine milieu supportive of $CD8^+$ T_{RM} cells, and enhanced generation of polyfunctional antigen-specific $CD8^+$ T cells that were resident in the lung tissue and airways, as shown by a combination of intravascular staining and perfusion. Both the pH-responsive functionality of the carrier and its capacity for dual-delivery were crucial for inducing a tissue-resident $CD8^+$ T cell response, which highlights the significance of engineering nanomaterial properties in the design of T_{RM} vaccines. We also showed that the route of administration was important for generating lung-resident cells; i.n. administration of the NP vaccine induced more antigen-specific $CD8^+$ T cells in the IST and AW than did s.c. immunization. Notably, unlike previous reports of T_{RM} vaccines in which multiple doses are typically administered, these results were obtained with a single dose, which offers potential translational advantages such as increased compliance and dose reduction.

Our findings suggest that several key properties of the NP vaccine are linked to the resulting tissue-resident $CD8^+$ T cell response. It has been proposed that local antigen recognition and persistence in non-lymphoid tissues, including the lungs, can promote formation of T_{RM} cell populations.[57, 74, 146, 157] Takamura *et al.* found that $CD8^+$ T cell encounter with cognate antigen in the lung, but not in the lung-draining lymph node, was critical for conversion from circulating to resident cells.[126] Notably, the NP we describe here increased retention of vaccine cargo in pulmonary APCs for up to three days after immunization. This finding suggests that NP-mediated delivery can extend antigen residence in the lungs over soluble antigen formulations and enhance the lung-resident $CD8^+$ T cell response. This could be due to the cationic surface charge of the NP, which may confer mucoadhesive properties that extend residence time in the lung.[105, 158] It could also reflect the capacity of pH-responsive NP carriers to prolong intracellular residence time by avoiding endosomal recycling and lysosomal degradation.[139] Longer-term studies that further examine the duration of antigen persistence and its effects on the T_{RM} response are warranted, and may motivate the use of pH-responsive materials as particle depots to control antigen release and delivery.

It has also been reported that certain pulmonary APC subsets, including $CD103^+$ DCs and alveolar macrophages, can promote establishment of lung T_{RM}.[47, 48, 72] In our experiments, alveolar macrophages took up large amounts of OVA and CpG over the course of 72 h and therefore may have contributed to the tissue-resident response. More importantly, we observed uptake in $CD103^+$ dendritic cells, the predominant cross-presenting DC subset in mucosal tissues.[159, 160] The pH-responsive nature of the NP, which allows it to transport antigen to the cytosol, potentially facilitated cross-presentation and priming of lung-resident $CD8^+$ T cell responses by $CD103^+$ DCs. The relative contributions that NP-mediated cytosolic antigen delivery *vs.* intrinsic mechanisms of DC cross-presentation provide in the induction of a $CD8^+$ T_{RM} response in the lungs merit further investigation. We speculate that both mechanisms contribute to the response. In addition, we found that $CD103^+$ DCs were the cell type most potently activated by the NP vaccine, with CD86 expression sustained for at least three days post-immunization. NP delivery enhanced co-localization of CpG with OVA in $CD103^+$ DCs during this time, which likely contributed to robust CD86 expression.[161] Methods of guiding vaccine delivery specifically to $CD103^+$ DCs (*e.g.*, antibody targeting) may be a promising approach for increasing vaccine uptake in this APC subset that is important for promoting T_{RM} formation.[48]

In conclusion, this report demonstrates generation of tissue-resident $CD8^+$ T cells in the lungs and airways with a single mucosally-administered dose of a pH-responsive nanoparticle vaccine. Intranasal dual-delivery of antigen and adjuvant with the pH-responsive NP was shown to enhance the quantity and functionality of $CD8^+$ T cells in the lungs and increase antigen persistence and activation in pulmonary APCs. Identification of lung interstitium-resident cells *via* intravascular staining has enabled relationships between NP material properties and the generation of tissue-resident $CD8^+$ T cells to be established. There are several practical advantages to this system that lend themselves to the possibility of scale-up and translation, such as the ability to synthesize NP on a large scale and sterilize them by filtration.[162] It would also be feasible to develop this vaccine as a needle-free aerosol formulation, to facilitate clinical translation and simple administration without the need for skilled healthcare workers.[64] Overall, this NP system represents a promising technology for the development of T_{RM} vaccines against respiratory infections, other pathogens that target non-lymphoid tissues, and mucosal cancers.

2.5 Materials and Methods

RAFT Synthesis of (PDSMA-*co*-DMAEMA)-*b*-(PAA-*co*-DMAEMA-*co*-BMA). RAFT copolymerization of pyridyl disulfide ethyl methacrylate (PDSMA) and dimethylaminoethyl methacrylate (DMAEMA) was conducted under a nitrogen atmosphere in dioxane (40 wt % monomer) at 30 °C for 18 h, as previously described.[50] PDSMA monomer was synthesized according to a previously reported procedure.[163] The RAFT chain transfer agent (CTA) used was 4-cyano-4-(ethylsulfanylthiocarbonyl)sulfanylpentanoic acid (ECT) and the initiator used was 2,2'-azobis(4-methoxy-2,4-dimethylvaleronitrile) (V-70) (Wako Chemicals, Richmond, VA). The initial molar ratio of DMAEMA to PDSMA was 92:8, and the initial monomer ($[M]_0$) to CTA ($[CTA]_0$) to initiator ($[I]_0$) ratio was 100:1:0.05. The resultant poly(PDSMA-*co*-DMAEMA) macro-chain transfer agent (mCTA) was isolated by precipitation (6×) into pentane. A schematic of the mCTA polymerization reaction can be found in **Figure A.1A**.

Purified mCTA was dried *in vacuo* for one week and used for block copolymerization with DMAEMA, propylacrylic acid (PAA), and butyl methacrylate (BMA) to create a pH-responsive polymer, as described previously.[50, 164] DMAEMA (30%), PAA (30%), and BMA (40%) ($[M]_0/[mCTA]_0 = 450$) were added to the mCTA dissolved in dimethylacetamide (DMAc) (40 wt % monomer and mCTA) along with V-70 initiator ($[mCTA]_0/[I]_0 = 2.5$). Polymerization took place under a nitrogen atmosphere for 24 h at 30 °C. The resultant diblock copolymer was isolated by dialysis against acetone using a 3.5 kDa MWCO membrane, followed by dialysis against deionized water. The purified diblock copolymer was lyophilized for 72 h prior to use. A schematic of the pH-responsive polymerization reaction can be found in **Figure A.1B**.

Polymer composition and monomer conversion of both the mCTA and diblock copolymer were characterized by ^{1}H NMR spectroscopy ($CDCl_3$) on a Bruker AV400 spectrometer (**Figure A.2A,B**). Gel permeation chromatography (GPC, Agilent) with DMF containing 0.1 M LiBr as the mobile phase and in-line light scattering (Wyatt) and refractive index (Agilent) detectors was used to determine molecular weight (MW) and polydispersity indices (PDI) of both the mCTA and diblock copolymer (**Figure A.2D and Table A.1**). Molecular weights were determined using d*n*/d*c* values calculated previously (0.071 for mCTA and 0.065 for diblock). Characterization was done according to previously published methods.[50] Representative NMR spectra, GPC traces, and a summary of polymer properties can be found in **Figure A.2** and **Table A.1**.

RAFT Synthesis of (PDSMA-*co*-DMAEMA)-*b*-(BMA). Purified mCTA used for the synthesis described above was also used for block copolymerization with poly(butyl methacrylate) (pBMA) to create a non-pH-responsive control polymer. Monomer was added to mCTA ($[M]_0/[mCTA]_0 = 300$) and dissolved in dioxane (40 wt % monomer and mCTA) along with V-70 initiator ($[mCTA]_0/[I]_0 = 20$), then polymerized

under a nitrogen atmosphere for 24 h at 35 °C. The resultant diblock copolymer was isolated by dialysis as described above. The purified polymer was then lyophilized, and its composition, molecular weight, and polydispersity index were analyzed using ^{1}H NMR ($CDCl_3$) spectroscopy and GPC (**Figure A.2C,D and Table A.1**), according to previously published methods.[165] The control polymerization reaction can be seen in **Figure A.1C**.

Preparation and Characterization of Nanoparticles. Self-assembled micellar nanoparticles (NP) were obtained by first dissolving lyophilized polymer at 50 mg/ml in 100% ethanol, then rapidly pipetting dissolved polymer into 100 mM phosphate buffer (pH 7) to a final concentration of 10 mg/ml. Nanoparticles were formulated in the same way for both pH-responsive (NP_{pH}) and control (NP_{ctrl}) polymers. For *in vivo* studies, ethanol was removed by buffer exchange into PBS (pH 7.4) *via* 3 cycles of centrifugal dialysis (Amicon, 3 kDa MWCO, Millipore), and NP solutions were then sterilized *via* syringe filtration (Whatman, 0.22 µm, GE Healthcare). Final polymer concentration was determined with UV-Vis spectrometry (Synergy H1 Multi-Mode Reader, BioTek) by measuring absorbance of aromatic PDS groups at 280 nm. Size of the NP was measured *via* dynamic light scattering (DLS). NP solutions were prepared at a concentration of 0.1-0.2 mg/ml in PBS (pH 7.4) and the hydrodynamic radius was measured using a Malvern Instruments Zetasizer Nano ZS Instrument (Malvern, USA). Representative DLS data for both polymers at physiological pH (7.4) can be found in **Figure A.2E**. In addition, size change of NP_{pH} but not NP_{ctrl} at pH 5.8, as measured by DLS, can be seen in **Figure A.2F** (left).

Erythrocyte Lysis Assay. The degree to which the pH-responsive polymer was able to induce pH-dependent lysis of lipid bilayer membranes (thus leading to cytosolic delivery) was assessed *via* a red blood cell hemolysis assay as previously described.[166] Briefly, polymers (10 µg/ml) were incubated for 1 h at 37 °C in the presence of human erythrocytes in 100 mM sodium phosphate buffer. Buffers in the pH range of the endosomal processing pathway (7.4, 7.0, 6.6, 6.2, and 5.8) were used. Extent of cell lysis (*i.e.*, endosomolytic activity) was determined *via* UV-Vis spectrometry by measuring the amount of hemoglobin released (Abs = 541 nm) (**Figure A.2F,** right). Absorbances were normalized to a 100% lysis control (1% Triton X-100). Samples were run in quadruplicate.

Preparation of Antigen-Nanoparticle Conjugates. A model antigen, ovalbumin protein (OVA), was conjugated to pendant PDS groups on NP *via* thiol-disulfide exchange. For conjugate characterization, OVA from chicken egg white (MilliporeSigma) was used; for *in vivo* studies, endotoxin-free (<1 EU/mg) EndoFit™ OVA (Invivogen) was used. In some experiments, OVA was labeled with fluorescein isothiocyanate isomer (FITC; Sigma) for evaluating conjugation efficiency *via* fluorescent imaging of SDS-PAGE gels, or with Alexa Fluor 647-NHS ester (AF647; Thermo Fisher Scientific) for tracking

conjugates after *in vivo* administration. Following manufacturer's instructions, dye was added to OVA for a degree of labeling of ~1 FITC/OVA or ~0.5 AF647/OVA.

To prepare OVA for conjugation, free amines on the protein were thiolated by incubation with ~25 molar excess of 2-iminothiolane (Traut's Reagent, Thermo Fisher Scientific) in reaction buffer (100 mM phosphate buffer, pH 8, supplemented with 1 mM EDTA) as previously described.[50] Unreacted 2-iminothiolane was removed by buffer exchanging thiolated OVA into 1X PBS (pH 7.4) using Zeba™ Spin desalting columns (0.5 ml, 7 kDa MWCO, Thermo Fisher Scientific). For *in vivo* studies, thiolated OVA was sterilized *via* syringe filtration (0.22 µm, Millipore). Following manufacturer's instructions, the molar ratio of thiol groups to OVA protein was determined with Ellman's reagent (Thermo Fisher Scientific) to be ~3-5 thiols/OVA. Polymer NP solutions were reacted with thiolated OVA at various molar ratios of pH-responsive NP:OVA (5:1, 10:1, 20:1) or control NP:OVA (3.5:1, 7:1, 14:1) to make OVA-NP_{pH} and OVA-NP_{ctrl} conjugates, respectively. The conjugation ratio for the control polymer was adjusted to maintain a constant dose of antigen for both carriers. Conjugation was done overnight, in the dark, at room temperature, and under sterile conditions (when needed), as previously described.[50] Antigen conjugation was verified *via* non-reducing SDS-polyacrylamide gel electrophoresis (SDS-PAGE) using 4-20% Mini-Protean TGX Precast Protein Gels (Bio-Rad) (**Figure A.3A**). Gels were run at 130 V for 1 h and imaged with a Gel Doc™ EZ System (Bio-Rad). A conjugation ratio of 5:1 (pH) or 3.5:1 (ctrl) was used for all *in vivo* formulations in order to maximize the amount of antigen delivered. DLS was used to measure the size of OVA-NP conjugates, as described above (**Figure A.3C,** left).

Formation of Nanoparticle/Adjuvant Complexes. NP/adjuvant complexation was carried out by combining CpG ODN 1826 (Invivogen) with NP, OVA-NP, or Flu-NP in PBS at room temperature for at least 30 min. Theoretical charge ratios (+/-) of 4:1 and 6:1 were tested. The charge ratio was defined as the molar ratio between protonated DMAEMA tertiary amines in the first block of the copolymer (positive charge; assuming 50% protonation at physiological pH) and phosphate groups on the CpG backbone (negative charge).[50] The charge ratios at which complete complexation of CpG to the polymer occurred were determined *via* an agarose gel retardation assay (**Figure A.3B**). Free CpG, NP/CpG, and OVA-NP/CpG prepared at various charge ratios were loaded into lanes of a 4% agarose gel and run at 90 V for 30 min. Gels were stained with GelRed® Nucleic Acid Gel Stain (Biotium, Fremont, CA) for 20 min and visualized with a Gel Doc™ EZ System (Bio-Rad). A charge ratio of 6:1 was used for all *in vivo* studies in order to maximize the stability of the formulation. DLS was used to measure the size of the OVA-NP/CpG formulation (**Figure A.3C,** right).

Animals. Male C57BL/6J mice were purchased from the Jackson Laboratory (Bar Harbor, ME), maintained at the animal facilities of Vanderbilt University under either conventional, specific pathogen-

free (SPF barrier facility), or animal biosafety level 2 (ABSL-2) conditions, and experimented upon in accordance with the regulations and guidelines of Vanderbilt University Institutional Animal Care and Use Committee (IACUC).

Immunization. Endotoxin-free OVA (<1 EU/mg, EndoFit™), sterile buffer solutions (1X PBS, pH 7.4), and sterile polymer solutions with ethanol removed were used for vaccine formulations. Experimental groups were: (**1**) nanoparticles loaded with covalently-conjugated OVA and complexed with CpG DNA (**OVA-NP/CpG**); (**2**) nanoparticles conjugated to OVA (**OVA-NP**); (**3**) a mixture of OVA (non-thiolated) and nanoparticles (**OVA+NP**); (**4**) a mixture of CpG-complexed nanoparticles and non-thiolated OVA (**NP/CpG+OVA**); (**5**) a mixture of non-thiolated OVA and CpG (**OVA+CpG**); (**6**) OVA conjugated to non-pH-responsive control polymer (**OVA-NP$_{ctrl}$**); and (**7**) **PBS** for sham mice. For all groups containing "**NP**," this denotes the pH-responsive polymer. Conjugates were prepared 1-2 days before use and stored at 4 °C. OVA was thiolated and used immediately for conjugation to NP at a molar ratio of 5:1 or 3.5:1 (NP:OVA), as described above. On the day of use, CpG was complexed to conjugates at a 6:1 charge ratio *via* rapid pipetting of CpG DNA (~0.5 mg/ml) into the conjugate solution, as described above. The formulation was allowed to react for at least 30 min at room temperature for complete complexation of CpG before administration to mice.

Male mice (8-12 weeks old) were anesthetized with ketamine/xylazine (10 mg/ml ketamine hydrochloride, Vedco; 1 mg/ml xylazine hydrochloride, Vanderbilt Pharmacy) by intraperitoneal (i.p.) injection (~200 µl anesthesia/22 g mouse weight). Anesthetized mice were immunized intranasally (i.n.) on day 0 with formulations containing 7.5 µg OVA and/or 1.4 µg CpG with or without 25 µg polymer. In dosing pilot studies, doses of 50 µg polymer (15.1 µg OVA, 2.8 µg CpG) and 12.5 µg polymer (3.8 µg OVA, 0.7 µg CpG) were also tested; the 25 µg polymer dose was ultimately selected for its ability to induce a robust $CD8^+$ T cell response with minimal toxicity. Vaccine formulations in a total volume of 80 µl PBS were delivered *via* pipette through the nostrils into the lungs of mice; inoculation with this volume allows formulations to reach the lower airways.[167] The dose was applied at the center of the nose to allow inhalation into both nostrils at a rate of ~8 µl/s. In some cases, anesthetized mice were instead immunized with a subcutaneous (s.c.) injection at the base of the tail. Animals were monitored either daily or thrice weekly for weight loss and signs of morbidity.

Measurement of Antigen-Specific $CD8^+$ T Cell Responses. On day 13 after immunization, mice were anesthetized and intravenously (i.v.) injected with 200 µl of anti-CD45.2-APC antibody (clone 104; Tonbo) at 0.01 mg/ml (2 µg αCD45 antibody per mouse), as previously described.[66] This was done to stain marginated vascular leukocytes (MV; $CD45^+$) and differentiate them from those resident in the lung interstitium (IST; $CD45^-$).[44] To allow for circulation of αCD45 antibody, mice were rested for 3-5

min after i.v. injection and prior to CO_2 euthanasia. Prior to organ harvest, lungs of euthanized mice were perfused with PBS to collect broncheoalveolar lavage fluid (BAL) from the airway compartment (AW) while maintaining IST and MV populations in the lung parenchyma.[66] Lungs and spleens were then harvested and processed as previously described.[168] Briefly, lungs were minced with a scalpel and incubated for 1 h at 37 °C in complete RPMI medium (cRPMI [RPMI+10% FBS]; Gibco) supplemented with 2 mg/ml collagenase (Sigma) and 50 nM dasatinib (LC Laboratories, Woburn, MA). Lungs and spleens were treated with ACK lysing buffer (Gibco) and passed through 70 µm cell strainers to generate single cell suspensions.

Cell suspensions from BAL, lungs, and spleens were stained for 1 h at 4 °C with anti-B220-FITC (clone RA3-6B2; BD Biosciences), anti-CD4-FITC (clone H129.19; BD Biosciences), anti-CD11b-FITC (clone M1/70; Tonbo), anti-CD11c-FITC (clone N418; Tonbo), anti-CD8α-Pacific Blue (clone 53-6.7; BD Biosciences), and 1.5 µg/ml PE-labeled $OVA_{257-264}$ (SIINFEKL)-H-$2K^b$ tetramer (Tet) prepared according to a previously reported procedure.[169] Antibodies labeled with FITC (B220/CD4/CD11b/CD11c) were referred to as the "dump" channel and were used to exclude B cells, $CD4^+$ T cells, dendritic cells, and macrophages from gating. After staining, cells were washed with FACS buffer (PBS supplemented with 2% FBS and 50 nM dasatinib) and stained with propidium iodide (BD Biosciences) to discriminate live *vs.* dead cells. AccuCheck counting beads (Thermo Fisher Scientific) were included in samples to allow for calculation of absolute cell counts. The frequency of antigen-specific $CD8^+$ T cells was determined using a 3-laser LSR-II flow cytometer (BD). All data were analyzed using FlowJo Software (version 10.4.2; Tree Star, Inc., Ashland, OR). Cells were gated by forward and side scatter to exclude debris and doublets. Viable antigen-specific $CD8^+$ T cell populations were defined as follows: AW = $CD8\alpha^+CD45^-Tet^+$ cells in BAL samples; IST = $CD8\alpha^+CD45^-Tet^+$ cells in lung samples; MV = $CD8\alpha^+CD45^+Tet^+$ cells in lung samples; SPL = $CD8\alpha^+Tet^+$ cells in spleen samples. All cells in the $CD8\alpha^+$ gate were also $B220^-CD4^-CD11b^-CD11c^-$ ("dump channel"). Representative gating for each sample type can be found in **Figure A.4A-C**.

Intracellular Cytokine Staining of Antigen-Specific $CD8^+$ T Cells. On day 13 after immunization, lungs and spleens were harvested and processed to obtain single-cell suspensions. Cells were plated in 96-well V-bottom plates at 3×10^6 cells/well (lung) or 2×10^6 cells/well (spleen) in cRPMI and re-stimulated with 10 µM of MHC class I epitope SIINFEKL peptide ($OVA_{257-264}$; Invivogen). Instead of treatment with peptide, positive controls were treated with PMA (50 ng/ml; Invivogen) and ionomycin (2 µg/ml; Sigma) and negative controls were treated with cRPMI. Cells were incubated at 37 °C and 5% CO2 for 1 h 30 min. BD GolgiPlug™ protein transport inhibitor (BD Biosciences) was then added to each well and cells were incubated for an additional 5 h 30 min.[50] After incubation, cells were washed with PBS and stained with eFluor® 450 fixable viability dye (eBioscience) for 30 min at 4 °C. Cells were

next washed with FACS buffer (PBS+2% FBS) and stained with anti-CD8α-APC/Cy7 (clone 53-6.7; Tonbo) and anti-CD3ε-PerCP/Cy5.5 (clone 145-2C11; Tonbo), as well as Fc-block (anti-CD16/CD32, clone 2.4G2; Tonbo), for 1 h at 4 °C. Cells were washed 2× in FACS buffer, then fixed and permeabilized by incubating for 10 min at 4 °C with BD Cytofix/Cytoperm (BD Biosciences), according to manufacturer instructions. Cells were then washed 2× with 1X BD Perm/Wash Buffer (BD Biosciences) and incubated for 1 h at 4 °C with antibodies against intracellular cytokines: anti-IFNγ-APC (clone XMG1.2; BD Biosciences) and anti-TNFα-PE (clone MP6-XT22; BD Biosciences). Finally, cells were washed once with 1X Perm/Wash buffer, resuspended in FACS buffer supplemented with 50 nM dasatinib, and analyzed using a 3-laser LSR-II flow cytometer (BD) and FlowJo software (v.10.4.2). Data are reported as the percentage of $CD8\alpha^+CD3\varepsilon^+$ cells that are $IFN\gamma^+$ and/or $TNF\alpha^+$ after subtraction of background values from negative (unstimulated) controls. Representative gating for lungs and spleens can found in **Figure A.4D.**

Histology. Lungs from mice immunized with OVA-NP/CpG or OVA+CpG, or from untreated mice, were harvested on d1 and d12 post-immunization. Tissue was fixed in 10% neutral buffered formalin, processed routinely, sectioned at 5 µm, and stained with hematoxylin and eosin (H&E). Sections were evaluated by an experienced veterinary pathologist blinded to the composition of the groups. Representative images are provided in **Figure A.5B**.

Fluorescence Microscopy. Mice were immunized i.n. with antigen-NP conjugates containing OVA labeled with Alexa Fluor 647 (OVA_{647}-NP). After 24 h, mice were injected i.v. with anti-CD45-Brilliant Violet 421 antibody (clone 30-F11; BD Biosciences) and Alexa Fluor 488-labeled tomato lectin (Vector Laboratories) to visualize intravascular lung leukocytes and the lung vasculature, respectively.

Mice were euthanized and lungs were harvested and fixed by inflation with 1 mL of 4% paraformaldehyde followed by 15% sucrose administered through the trachea. Lungs were frozen in OCT (Fisher Scientific). Ten-micron tissue sections were evaluated by fluorescence microscopy using an Axioplan widefield microscope (Zeiss) equipped with a 20x objective, 405-, 488-, 532-, and 633-nm laser lines, and a Hamamatsu ORCA-ER monochrome digital camera.

Uptake and Activation in Pulmonary Innate Immune Cells. To identify the effects of the NP vaccine on innate immune cell uptake and activation in lungs, mice were immunized with fluorescently labeled OVA_{647}-NP/CpG_{488} or OVA_{647}+CpG_{488}, or with PBS (control). In the fluorescent formulations, OVA was labeled with Alexa Fluor 647 as described above (OVA_{647}). Alexa Fluor 488-labeled CpG (CpG_{488}) was purchased from Integrated DNA Technologies (IDT; Skokie, IL). After 24, 48, or 72 h, mice were euthanized and lungs were harvested, as well as spleens, kidneys, and livers (to assess systemic

biodistribution). Organs were imaged using an IVIS Lumina III Imaging System (PerkinElmer, Waltham, MA) to visualize and quantify tissue-level OVA_{647} fluorescence after immunization. IVIS image files were analyzed using Living Image® software (version 4.5.5, PerkinElmer).

After imaging, lungs were processed as described above to obtain single-cell suspensions. Lung samples were stained for flow cytometric analysis of pulmonary immune cells using a modified version of the panel described by Misharin *et al*.[147] This panel was used to distinguish seven different cell types: **(1)** alveolar macrophages (**AMφ**); **(2)** interstitial macrophages (**IMφ**); **(3)** $CD103^+$ dendritic cells (**$CD103^+$ DC**); **(4)** $CD11b^+$ dendritic cells (**$CD11b^+$ DC**); **(5)** monocytes/macrophages (**Mono/Mφ**); **(6)** granulocytes (**Gran**); and **(7)** cells not included in other populations (**Other**). It was also used to quantify the amount of cargo co-localization (OVA^+CpG^+ cells) and expression of activation marker CD86 in each cell subset and at each timepoint. The following antibodies were used: anti-CD64-PE (BioLegend; X54-5/7.1), anti-CD24-PE/Cy7 (BioLegend; M1/69), anti-CD11b-PerCP/Cy5.5 (BioLegend; M1/70), anti-CD11c-APC/Cy7 (Tonbo; N418), anti-I-A/I-E-Brilliant Violet 605 (BD; M5/114.15.2), anti-CD45.2-Brilliant Violet 650 (BioLegend; 104), and anti-CD86-PE/Dazzle™ 594 (BioLegend; GL-1). Ghost Dye™ Violet 510 (Tonbo) was used to discriminate live *vs.* dead cells and AccuCheck counting beads (Thermo Fisher Scientific) were included in samples to allow for calculation of absolute cell counts. Samples were stained with viability dye for 30 min at 4 °C, washed with FACS buffer (PBS+2% FBS, 50 nM dasatinib), incubated with Fc-block (anti-CD16/CD32, clone 2.4G2; Tonbo) for 15 min at 4 °C, and then stained for 1 h at 4 °C with the antibody panel listed above. Finally, cells were washed once, resuspended in FACS buffer, and analyzed by flow cytometry. Data were collected using a 3-laser Fortessa (BD) and analyzed with FlowJo software (v.10.4.2). Representative gating for OVA and CpG uptake in lung cell subsets can be found in **Figure A.7**.

Measurement of Cytokines. Cytokines were measured in serum, BAL, or lung homogenates using a LEGENDplex™ bead-based immunoassay (BioLegend). Mice were immunized i.n. and blood, BAL, and lungs were harvested 6 h, 24 h, 48 h, and 7 d after immunization. Blood was obtained by cardiac puncture and BAL was collected by lavage with 1 ml sterile PBS containing a cocktail of protease inhibitors (Roche cOmplete™ Mini EDTA-free Protease Inhibitor Cocktail, Sigma). The right side (4 lobes) of the lung was collected in 1 ml M-PER™ Mammalian Protein Extraction Reagent (Thermo Fisher Scientific) with protease inhibitors and homogenized using a gentleMACS™ Octo Dissociator and M tubes (Miltenyi Biotec), according to manufacturer instructions. Lung homogenates were then centrifuged for 10 min at 4200 rpm and supernatants were collected and frozen at -80 °C until analysis. BAL samples were frozen at -80 °C without further processing. Blood was centrifuged for 10 min at 14,000 rpm (2×), and sera were collected and frozen at -80 °C until analysis. Prior to use with LEGENDplex™ kits, samples were thawed and centrifuged for 10 min at 10,000-12,500 rpm to remove

debris. Lung samples were filtered through 40 µm cell strainers for additional debris removal. The following cytokines were measured: IFNγ, TNFα, IFNα, IFNβ, IL-6, IL-33, IL-12p70, and IL-1β. LEGENDplex™ kits were used according to manufacturer instructions. Flow cytometric data was collected with a 3-laser LSR II (BD) and analyzed with LEGENDplex Data Analysis Software (v.8.0).

Statistical Analysis. Statistical analyses were performed as indicated in figure legends. All analyses were done using GraphPad Prism software, version 6.07. Results are expressed as mean ± SEM with ****$p < 0.0001$, ***$p < 0.001$, **$p < 0.01$, *$p < 0.05$ being considered statistically significant.

CHAPTER 3

Nanoparticle Vaccine Promotes Formation of $CD8^+$ Lung-Resident Memory T Cells and Protects Against Challenge with Respiratory Pathogens

Text for Chapter 3 taken from:

Knight FC, Gilchuk P, Kumar A, Becker KW, Sevimli S, Jacobson ME, Suryadevara N, Wang-Bishop L, Boyd KL, Crowe JE, Jr., Joyce S, Wilson JT. Mucosal immunization with a pH-responsive nanoparticle vaccine induces protective $CD8^+$ lung-resident memory T cells. *ACS Nano*. Sep 25, 2019. PMID: 31553872.

3.1 Abstract

Models of viral infection in mice have shown that that tissue-resident memory T cells (T_{RM}) are generated by infection and can rapidly mount an immune response to protect against subsequent pathogen encounter after initial challenge. As such, synthetic vaccines that can safely mimic natural infection and install protective T_{RM} populations in mucosal tissues where pathogens are typically encountered, such as the lungs, would represent an important advance in vaccine development. While viral vectors have been studied extensively for this purpose, they present significant safety concerns. Nanoparticle (NP)-based subunit vaccines can overcome many of the disadvantages of live vectors, but have not yet seen widespread use as vaccines for eliciting T_{RM} responses. Here, we demonstrate that single-dose pulmonary immunization with a pH-responsive NP vaccine generated $CD8^+$ T_{RM} in the airways and lungs. These T_{RM} expressed memory markers CD69 and CD103 and persisted for up to nine weeks after immunization. The NP vaccine also protected mice against respiratory virus challenge in both sublethal (vaccinia) and lethal (influenza) infection models. Overall, these data suggest the NP platform has translational potential for use in mucosal vaccines to protect against viral pathogens.

3.2 Introduction

Studies of tissue-resident memory T cells in viral infection have found that T_{RM} are often indispensable for protection against these pathogens. This has been particularly shown for respiratory viruses like influenza. [22, 63, 75, 122, 124] Research has found that the existing live attenuated flu vaccine given intranasally, FluMist, mediates cross-strain protection via virus-specific T_{RM} cells in the lungs.[63] In a model of influenza infection, another group found that repeated exposure to antigen enhanced the durability of influenza-specific lung-resident T_{RM} after immunization with live PR8 virus.[75] Loss of

protection over time is a major limitation of T cell immunity to influenza, and this loss has been linked to a decrease in the size of the virus-specific T_{RM} population in the lungs.[78, 124] Based on our findings in the previous aim, nanoparticle-mediated delivery of the vaccine to pulmonary antigen-presenting cells appeared to extend the persistence of antigen in these cells; thus, this nanoparticle platform can potentially capitalize on the need for persistent antigen stimulation in forming a robust $CD8^+$ T_{RM} response in the lungs. In light of this, we assessed the ability of the nanoparticle vaccine to generate antigen-specific pulmonary $CD8^+$ T cells expressing T_{RM} markers, and we studied its capacity to protect against challenge in murine models of respiratory infection. Importantly, we used tools that support the conclusion that protection is mediated by $CD8^+$ T cells: in the first challenge model, we utilized a recombinant vaccinia virus that expresses the immunodominant MHC-I epitope of ovalbumin protein (SIINFEKL). Thus, mice that are protected from infection after immunization with an OVA-containing vaccine are likely protected by OVA-specific $CD8^+$ T cells. Likewise, in the second challenge model, we utilized the influenza A H1N1 virus known as PR8, and immunized mice with PR8 nucleoprotein antigen, which is known to contain many conserved MHC-I epitopes for influenza.

One of the major driving forces behind development of universal influenza vaccines is readiness in the case of a global pandemic, such as occurred with H1N1 swine flu in 2009. In these situations, it is crucial to have access to vaccine technologies that are both easy to manufacture and have dose-sparing capabilities, in order to respond quickly and provide vaccines to all who need them.[170] In this regard, nanoparticle vaccines present an important advantage; they can often produce a comparable or better immune response relative to soluble subunit vaccines using less material, and in the case of polymeric nanoparticles produced *via* RAFT synthesis, they also lend themselves to manufacturing scale-up and large scale production.[162] Generation of a robust immune response with a single dose of the vaccine is also important, both for increasing patient compliance and minimizing costs and production time.

In these studies, we delivered either a model antigen, ovalbumin, or a clinically relevant antigen, influenza nucleoprotein, with the nanoparticle vaccine. Immunization with both antigens generated a $CD8^+$ T_{RM} response in the lungs at memory timepoints (30 days or 60 days after immunization). The NP vaccine conferred protection against sublethal respiratory challenge with recombinant vaccinia virus and increased survival of mice in a lethal influenza A virus challenge model. Importantly, these results were achieved after immunization with only a single intranasal dose of the vaccine. Collectively, our results suggest a promising experimental vaccine platform for generating $CD8^+$ T_{RM} that can protect against respiratory infections.

3.3 Results and Discussion

Nanoparticle vaccine generates long-lasting populations of lung-resident antigen-specific CD8$^+$ T cells that express T_{RM} surface markers

We previously demonstrated the ability of a pH-responsive NP vaccine to enhance the lung-resident CD8$^+$ T cell response after 13 days (see **Figure 2.3**). This prompted us to determine whether antigen-specific CD8$^+$ T cells present in murine lungs at 30 and 60 days after immunization, which are considered memory T cells,[116] possessed a characteristic T_{RM} phenotype. In addition to being defined as CD45$^-$ by i.v. staining, lung T_{RM} have been defined by surface expression of CD69—an activation marker that limits tissue egress by inhibiting expression of sphingosine-1-phosphate receptor—and CD103—an adhesion molecule that binds E-cadherin on epithelial cells and retains T_{RM} in their home tissues.[5] Both CD103$^-$CD69$^+$ and CD103$^+$CD69$^+$ T_{RM} subsets in the lungs have been reported.[66, 122] To characterize the memory phenotype of Tet$^+$ CD8$^+$ T cells in the IST and AW, we immunized mice i.n. with a single dose of OVA-NP/CpG, OVA-NP, or OVA+CpG, and on d30 or d60 post-immunization, harvested lungs and spleens and quantified Tet$^+$ CD8$^+$ T_{RM}. Here, CXCR3 was used as a marker of airway residence, as previously reported.[66, 127, 171] Staining with αCD103 and αCD69 antibodies was used in conjunction with i.v. αCD45 antibody to identify T_{RM}, and αCXCR3 antibody was used to discriminate AW-resident cells (CXCR3^{hi}) from those resident in the IST (CXCR3^{lo}) (**Figure 3.1A**).

At both d30 (**Figure 3.1B-E**) and d60 (**Figure 3.1F-I**) post-immunization, there were significantly more Tet$^+$ CD8$^+$ T cells in the lungs of mice immunized with OVA-NP/CpG relative to those receiving OVA+CpG. There were also generally more cells in the OVA-NP/CpG group relative to mice receiving OVA-NP, although in certain instances this difference was not statistically significant, consistent with the intrinsic capacity of the NP to enhance the CD8$^+$ T cell response (see **Figure 2.3**). At d30, OVA-NP/CpG generated a significantly higher response than OVA+CpG in the AW and IST (**Figure 3.1B,C**), but not in the MV or spleen (**Figure 3.1D,E**). The number of cells present in the lungs of mice immunized with OVA-NP/CpG were significantly higher in the IST relative to OVA-NP (**Figure 3.1C**), but in the AW they were not significantly different (**Figure 3.1B**). While there was no significant difference between any group in the MV (**Figure 3.1D**), OVA-NP/CpG generated a significantly higher response than OVA-NP in the spleen (**Figure 3.1E**). At d60, there were significantly more cells in the IST for the OVA-NP/CpG group relative to both OVA-NP and OVA+CpG (**Figure 3.1G**), while the difference between groups in the AW was less pronounced (**Figure 3.1F**). Again, there was no significant difference between any group in the MV (**Figure 3.1H**), while OVA-NP/CpG continued to produce a significantly higher response in the spleen relative to OVA-NP (**Figure 3.1I**). While in many cases the OVA-NP formulation also produced a greater response than OVA+CpG, at d60 it remained inferior to OVA-NP/CpG in the IST, where the majority of CD8$^+$ T_{RM} are located. Overall, these data show that the NP

vaccine is able to enhance generation of lung-resident $CD8^+$ T cells that are maintained for at least 60 days after immunization.

We next asked whether these long-lasting antigen-specific $CD8^+$ T cells in the lungs expressed characteristic T_{RM} surface markers. At these same time points, AW ($CXCR3^{hi}$) and IST ($CXCR3^{lo}$) cells were analyzed for CD103 and CD69 expression (**Figure 3.2A**). At d30, i.n. administration of OVA-NP/CpG elicited significantly more AW and IST Tet^+ $CD8^+$ T_{RM} with both $CD103^-CD69^+$ and $CD103^+CD69^+$ phenotypes when compared to immunization with OVA+CpG (**Figure 3.2B**,**D**). There were also significantly more AW and IST $CD8^+$ T_{RM} of the $CD103^+CD69^+$ phenotype in the OVA-NP/CpG group relative to the OVA-NP group (green bars); for the $CD103^-CD69^+$ phenotype (blue bars), this difference was not significant, although the number of cells was still higher. At d60, in the IST, OVA-NP/CpG induced significantly more $CD8^+$ T_{RM} of both phenotypes than either control group (OVA-NP and OVA+CpG) (**Figure 3.2E**). In the AW, this difference was only significant for OVA-NP/CpG *vs.* OVA+CpG in the $CD103^-CD69^+$ phenotype, although OVA-NP/CpG still produced the highest number of cells in all cases (**Figure 3.2C**). These data indicate that the NP vaccine is superior to control formulations for generating antigen-specific $CD8^+$ T_{RM} in the lungs, particularly at 60 days after immunization. Notably, OVA-NP/CpG also appears to be more likely to produce T_{RM} cells with the $CD103^+CD69^+$ phenotype than does OVA-NP.

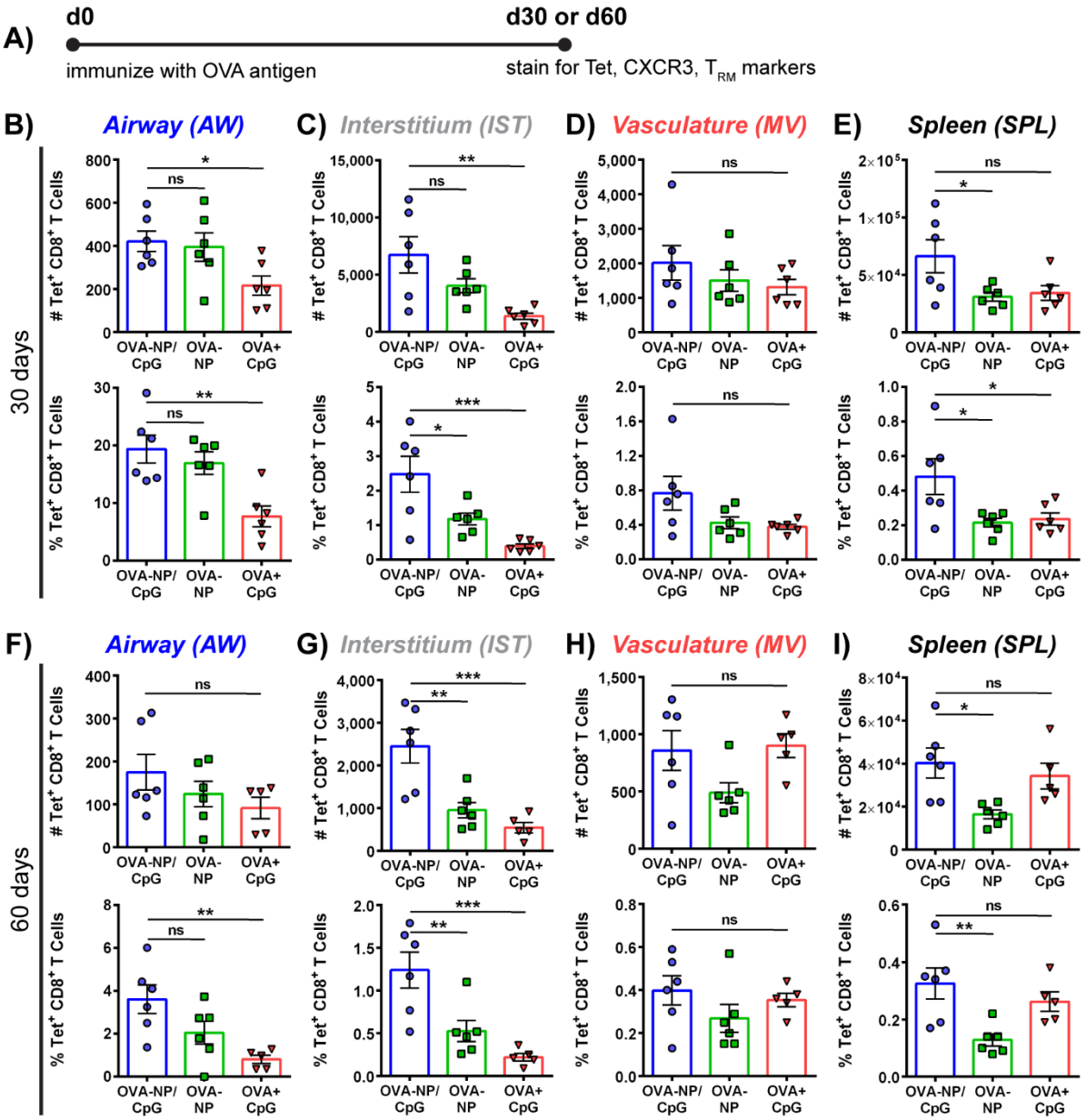

Figure 3.1 | OVA-specific CD8⁺ T cells are maintained at memory timepoints after immunization. **(A)** Mice were immunized i.n. with OVA-containing formulations on d0 and lungs and spleens were analyzed on d30 or d60 *via* tetramer and surface marker staining. CXCR3 was used as a marker of AW residence; CD45 was used to differentiate cells in IST *vs*. MV. **(B-E)** Number (#) and frequency (%) of Tet⁺ CD8⁺ T cells in **(B)** AW, **(C)** IST, **(D)** MV, and **(E)** spleen were enumerated on d30 after i.n. administration of OVA-NP/CpG, OVA-NP, or OVA+CpG. **(F-I)** Number (#) and frequency (%) of Tet⁺ CD8⁺ T cells in **(F)** AW, **(G)** IST, **(H)** MV, and **(I)** spleen were enumerated on d60 after i.n. administration of OVA-NP/CpG, OVA-NP, or OVA+CpG. Data are mean ± SEM and representative of four independent experiments, with *n* = 5-6 per group. Immunization dose: 25 µg NP, 7.5 µg OVA, 1.4 µg. CpG Limit of detection: 1 cell (AW), 5 cells (IST/MV), 25 cells (spleen). *p<0.05, **p<0.01, ***p<0.001, by ordinary one-way ANOVA with Tukey's multiple comparisons test. ns, not significant. Statistical comparisons are shown for OVA-NP/CpG only.

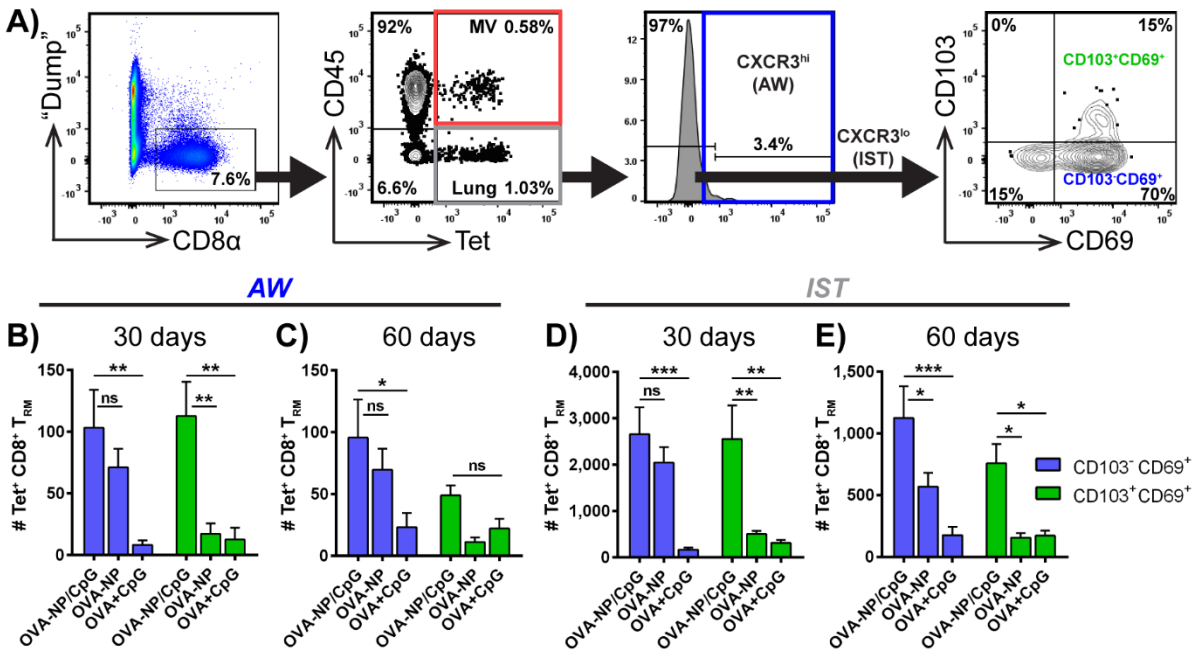

Figure 3.2 | OVA-specific CD8⁺ memory T cells express T_{RM} markers CD69 and CD103. Mice were immunized i.n. with OVA-containing formulations and lungs were analyzed on d30 or d60 *via* tetramer and surface marker staining. CD103 and CD69 were used as markers of tissue residency. **(A)** Flow cytometry was used to quantify Tet⁺ CD8⁺ T cells expressing T_{RM} markers (CD103, CD69) in the airway (CXCR3^{hi}) and lung interstitium (CXCR3^{lo}). **(B,C)** Number (#) of Tet⁺ CD8⁺ T cells expressing CD69±CD103 in AW was enumerated on **(B)** d30 or **(C)** d60 after immunization. **(D,E)** Number (#) of Tet⁺ CD8⁺ T cells expressing CD69±CD103 in IST was enumerated on **(D)** d30 or **(E)** d60 after immunization. Data are mean ± SEM and representative of four independent experiments, with *n* = 5-6 per group. Immunization dose: 25 µg NP, 7.5 µg OVA, 1.4 µg CpG. Limit of detection: 1 cell (AW), 5 cells (IST/MV), 25 cells (spleen). *p<0.05, **p<0.01, ***p<0.001, by ordinary two-way ANOVA with Tukey's multiple comparisons test. ns, not significant. Statistical comparisons are shown for OVA-NP/CpG only.

Single-dose pulmonary immunization with nanoparticle vaccine protects against sublethal respiratory virus challenge

Ultimately, an effective vaccine must generate T cells that protect against subsequent infectious challenge. Given the ability of a single i.n. dose of the NP vaccine to generate antigen-specific CD8⁺ T_{RM} and retain them in the lungs for up to 60 days post-immunization, we next determined whether these T_{RM} were protective against infection with a respiratory virus. To do this, we immunized mice i.n. with OVA-NP/CpG, OVA-NP, OVA+CpG, or PBS. On d30 or d60 post-immunization, mice were challenged i.n. with a recombinant vaccinia virus expressing influenza virus nucleoprotein, SIINFEKL peptide, and enhanced green fluorescent protein (VV.NP-S-EGFP). Since this virus expresses SIINFEKL, the immunodominant MHC-I epitope of OVA, it provides a tool for evaluating the ability of NP vaccine-induced CD8⁺ T cells to protect against i.n. challenge. Mice were inoculated with a sublethal

dose (1×10^7 pfu) of the virus and weighed daily through d6 post-inoculation (p.i.) (**Figure 3.3A**). On d6 p.i., lungs were harvested for quantification of viral load.

At both d30 and d60, mice immunized with the NP vaccine were significantly protected from challenge-induced weight loss relative to all other formulations. Mice immunized with OVA-NP/CpG lost ~5-7% of body weight by d6 p.i. *vs.* a loss of ~13-26% in other groups (**Figure 3.3B,C**). Additionally, the OVA-NP/CpG group in the 30-day cohort began regaining weight by d5 p.i. (**Figure 3.3B**).

To further validate these findings, viral load was quantified in lungs harvested from infected mice at d6 p.i. There was a 1-2 log reduction in viral burden in the lungs of mice immunized with OVA-NP/CpG, relative to the other formulations, at both d30 and d60 post-immunization (**Figure 3.3D,E**). Overall, these results demonstrate that a single dose of the NP vaccine provides significant $CD8^+$ T_{RM}-mediated protection against respiratory virus challenge in an antigen-specific manner.

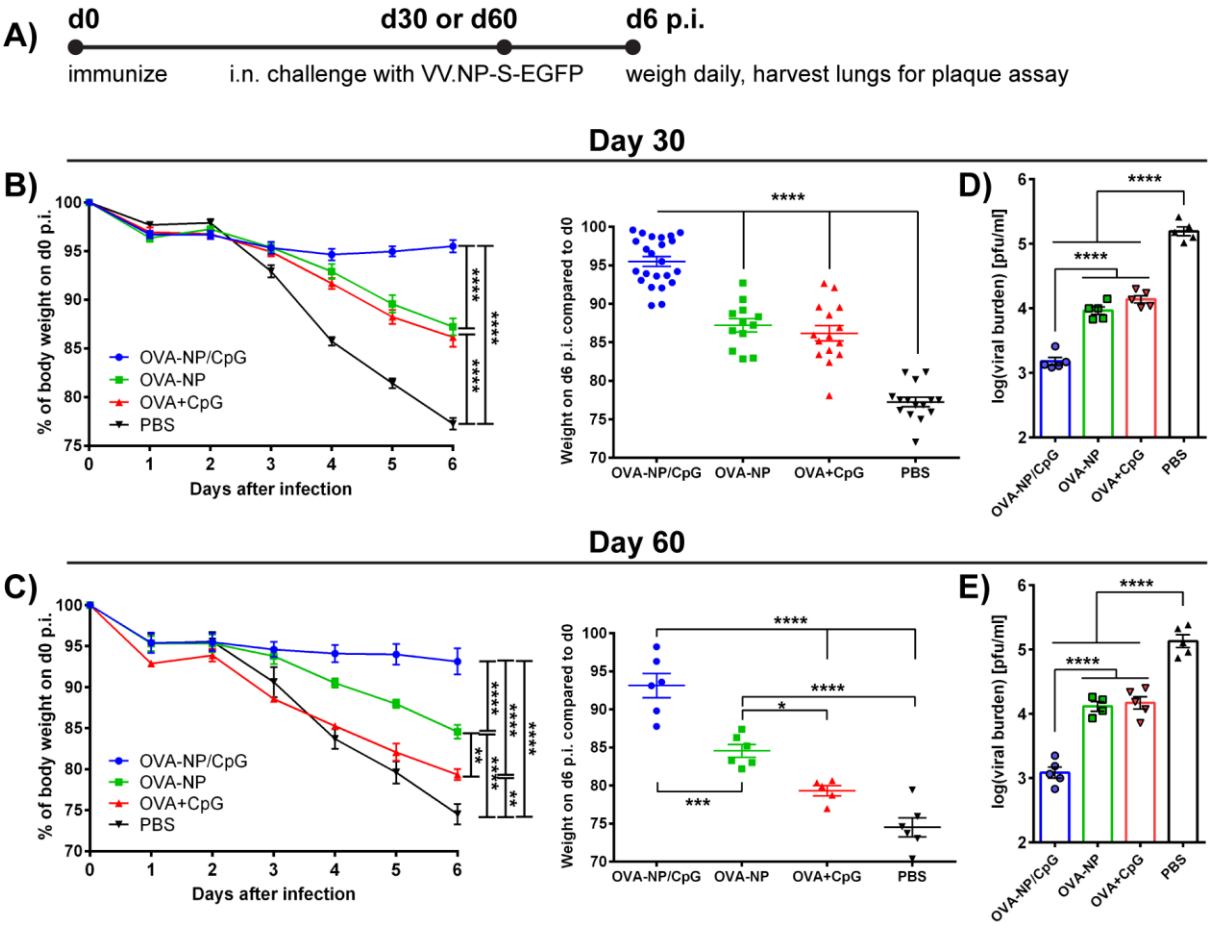

Figure 3.3 | Mice immunized with nanoparticle vaccine exhibit less weight loss and lower viral burden after intranasal challenge with recombinant vaccinia virus. (A) Mice immunized on d0 were challenged i.n. with recombinant SIINFEKL-expressing vaccinia virus (sublethal dose of 1×10^7 pfu/mouse) either 30 or 60 d post-immunization. Mice were weighed daily and lungs were harvested on d6 post-inoculation (p.i.). **(B,C)** Percent (%) weight loss in mice challenged on **(B)** d30 or **(C)** d60 after

i.n. administration. Left: weight loss over time. Right: weight at d6 p.i. expressed as % initial body weight. **(D,E)** Lungs of mice challenged on **(D)** d30 or **(E)** d60 post-immunization were harvested on d6 p.i. for quantification of viral load. Dots show titers for individual animals. Data are mean ± SEM, with **(B)** *n* = 12-23 per group, **(C)** *n* = 5-6 per group, and **(D,E)** *n* = 5 per group. Immunization dose: 25 µg NP, 7.5 µg OVA, 1.4 µg CpG. Data are pooled from one to four independent experiments. Limit of detection for plaque assay = 6 pfu. *p<0.05, **p<0.01, ***p<0.001, ****p<0.0001, by **(B,C left)** repeated measures two-way ANOVA with Tukey's multiple comparisons test or **(B,C right; D-E)** ordinary one-way ANOVA with Tukey's multiple comparisons test.

Nanoparticle vaccine containing influenza virus antigen generates antigen-specific $CD8^+$ T_{RM} in the lungs

After demonstrating the ability of the NP vaccine to generate $CD8^+$ T_{RM} in the lungs and protect against respiratory virus challenge using a model antigen (OVA), we next asked whether these findings could be applied to a more clinically relevant antigen and infection model. To this end, we shifted our focus to influenza, a respiratory infection of global importance and a significant public health challenge.[172] It is well-established that $CD8^+$ T_{RM} cells are important for generating heterosubtypic immunity against influenza A viruses in both mice and humans.[48, 59, 63, 122] To evaluate the ability of the NP vaccine to protect against this pathogen, we selected nucleoprotein, a structural protein from influenza A H1N1 virus (strain A/Puerto Rico/8/1934, or PR8), as the antigen, since there is precedent for using the PR8 strain in murine influenza challenge models. While surface proteins like hemagglutinin and neuraminidase are commonly used in experimental flu vaccines to generate a humoral response, internal viral antigens like nucleoprotein are known to contain the majority of influenza $CD8^+$ T cell epitopes.[173-175] Thus, using nucleoprotein as a vaccine antigen lends itself to specifically studying the protective effect of an immunization-induced $CD8^+$ T cell response. In addition, because $CD8^+$ T cell epitopes of influenza A virus are largely conserved across strains and subtypes, they may be particularly well-suited for providing broad protection, and while $CD8^+$ T cells typically do not generate sterilizing immunity, they are useful for reducing disease severity and pathogen transmission.[59, 173, 176, 177]

We will henceforth refer to the nucleoprotein antigen as "Flu" to avoid confusion with the "NP" abbreviation for nanoparticle. Thus, formulations will be indicated as Flu-NP/CpG (nucleoprotein conjugated to nanoparticle and complexed with CpG), Flu-NP (nucleoprotein conjugated to nanoparticle), and Flu+CpG (soluble nucleoprotein mixed with CpG). We first validated that the Flu antigen could be covalently conjugated to NP *via* the same chemistry used to load OVA protein. Flu protein was thiolated and reacted with pH-responsive NP to generate Flu-NP conjugates (**Figure B.1A**). Flu-NP conjugates were then electrostatically complexed with CpG to create Flu-NP/CpG (**Figure B.1B**). Both Flu-NP/CpG and Flu-NP were characterized by DLS (**Figure B.1C**).

We next assessed the ability of Flu-NP/CpG and related control formulations to generate antigen-specific $CD8^+$ T cells expressing lung T_{RM} markers at memory timepoints ($CD103^-CD69^+$ and $CD103^+CD69^+$ $CD8^+$ T_{RM}). To do this, we prepared a fluorescent MHC-I tetramer (Tet) containing ASNENMETM peptide, a known immunodominant H-$2D^b$ epitope for nucleoprotein from PR8 virus.[178] We then immunized mice i.n. with a single dose of Flu-NP/CpG, Flu-NP, or Flu+CpG, and on d30 or d60 post-immunization, harvested lungs and spleens and quantified Tet^+ $CD8^+$ T cells in the same manner as described for OVA (**Figure 3.4A**). Similarly, we also assessed expression of T_{RM} markers CD69 and CD103 on the antigen-specific $CD8^+$ T cell populations in the AW and IST lung compartments.

At d30, mice immunized with Flu-NP/CpG had significantly more Tet^+ $CD8^+$ T cells in the AW, IST, and MV compartments than mice immunized with Flu+CpG (**Figure 3.4B-E**). The difference between Flu-NP/CpG and Flu-NP groups was less pronounced, with significance only in the MV; however, a general trend of greater numbers of Tet^+ $CD8^+$ T cells produced by Flu-NP/CpG in the lungs was observed. There was no significant difference between treatment groups in the spleen. At d60, the number of cells generated by the Flu-NP/CpG, Flu-NP, and Flu+CpG groups were not significantly different in any lung compartment or in the spleen (**Figure 3.4F-I**), though in the IST both Flu-NP/CpG and Flu-NP exhibited higher cell counts than Flu+CpG (**Figure 3.4G**). These data show that, similarly to the NP vaccine containing OVA, the NP vaccine with Flu antigen is able to generate higher numbers of lung-resident $CD8^+$ T cells that are maintained for at least 30 days after immunization. However, by 60 days they have waned to similar levels as those seen in control groups. Regardless of the presence of adjuvant, NP-mediated delivery of Flu antigen generates more lung-resident $CD8^+$ T cells in the IST than soluble Flu+CpG at both timepoints, again demonstrating the importance of the particle's intrinsic ability to enhance the $CD8^+$ T cell response.

We next examined whether these long-lasting antigen-specific $CD8^+$ T cells in the lungs expressed T_{RM} surface markers. At 30d and 60d post-immunization, AW ($CXCR3^{hi}$) and IST ($CXCR3^{lo}$) cells were analyzed for CD103 and CD69 expression, as previously shown in **Figure 3.2A**. At d30, Flu-NP/CpG immunization generated more T_{RM} of both phenotypes ($CD103^-CD69^+$ and $CD103^+CD69^+$) in both the AW and IST (**Figure 3.5A,C**). Again, at d60, the differences between treatment groups were less pronounced, with the Flu-NP group in some instances producing equivalent or greater numbers of T_{RM} relative to the Flu-NP/CpG (**Figure 3.5B,D**). Both Flu-NP/CpG and Flu-NP were superior to Flu+CpG in the IST (**Figure 3.5C,D**). Overall, these data indicate that immunization with a nanoparticle-containing formulation is superior to a soluble formulation for generating Flu-specific $CD8^+$ T_{RM} in the lungs, and that addition of CpG adjuvant increases efficacy similarly to what was observed with model antigen (OVA).

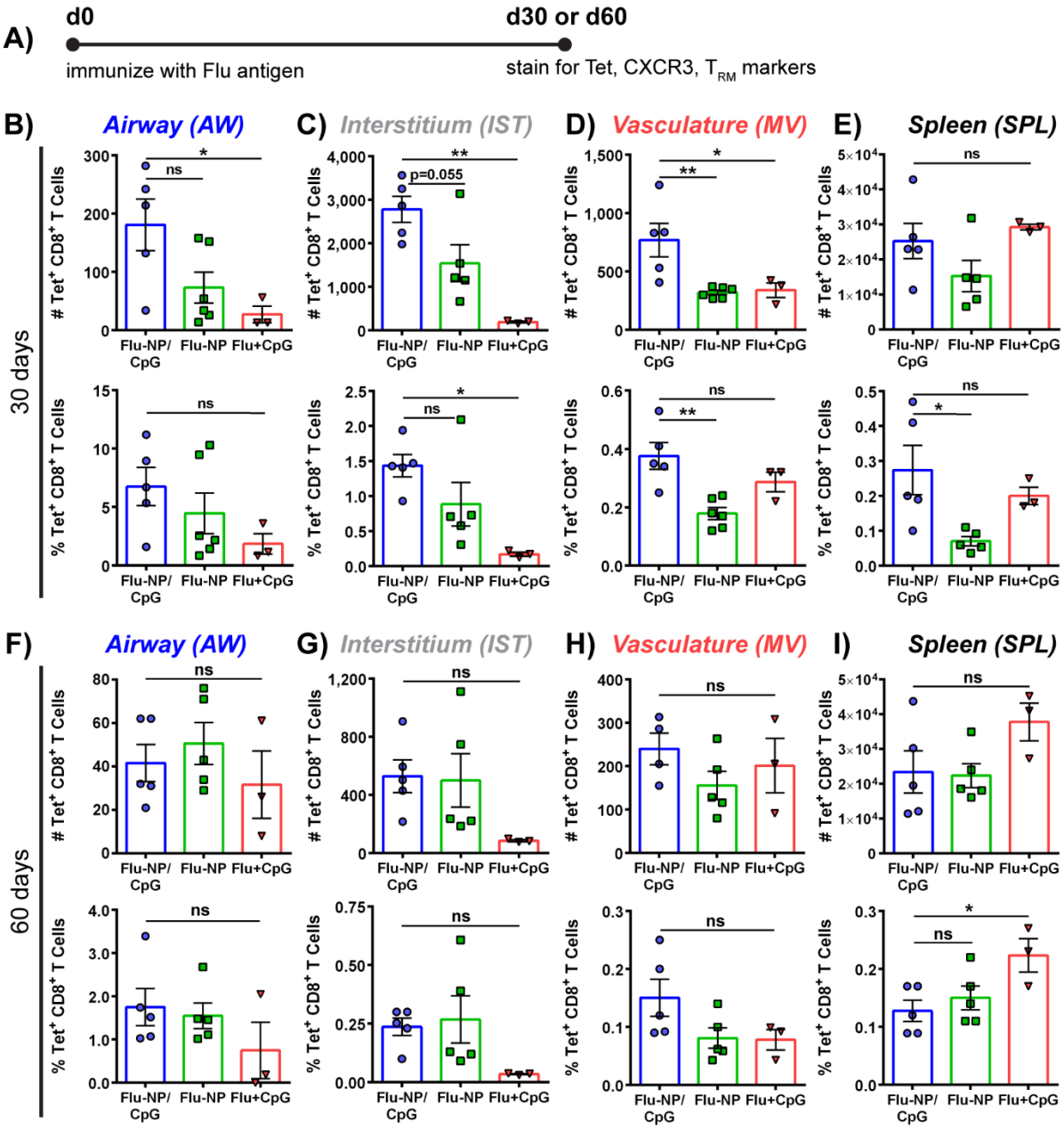

Figure 3.4 | Flu-specific CD8⁺ T cells are maintained at memory timepoints after immunization. **(A)** Mice were immunized i.n. with Flu-containing formulations on d0 and lungs and spleens were analyzed on d30 or d60 *via* tetramer and surface marker staining. CXCR3 was used as a marker of AW residence; CD45 was used to differentiate cells in IST *vs*. MV. **(B-E)** Number (#) and frequency (%) of Tet⁺ CD8⁺ T cells in **(B)** AW, **(C)** IST, **(D)** MV, and **(E)** spleen were enumerated on d30 after i.n. administration of Flu-NP/CpG, Flu-NP, or Flu+CpG. **(F-I)** Number (#) and frequency (%) of Tet⁺ CD8⁺ T cells in **(F)** AW, **(G)** IST, **(H)** MV, and **(I)** spleen were enumerated on d60 after i.n. administration of Flu-NP/CpG, Flu-NP, or Flu+CpG. Data are mean ± SEM, with *n* = 3-6 per group, and representative of two independent experiments. Immunization dose: 25 µg NP, 9.5 µg Flu, 1.4 µg CpG. Limit of detection: 1 cell (AW), 5 cells (IST/MV), 25 cells (spleen). *p<0.05, **p<0.01 by ordinary one-way ANOVA with Tukey's multiple comparisons test. ns, not significant. Statistical comparisons are shown for Flu-NP/CpG only.

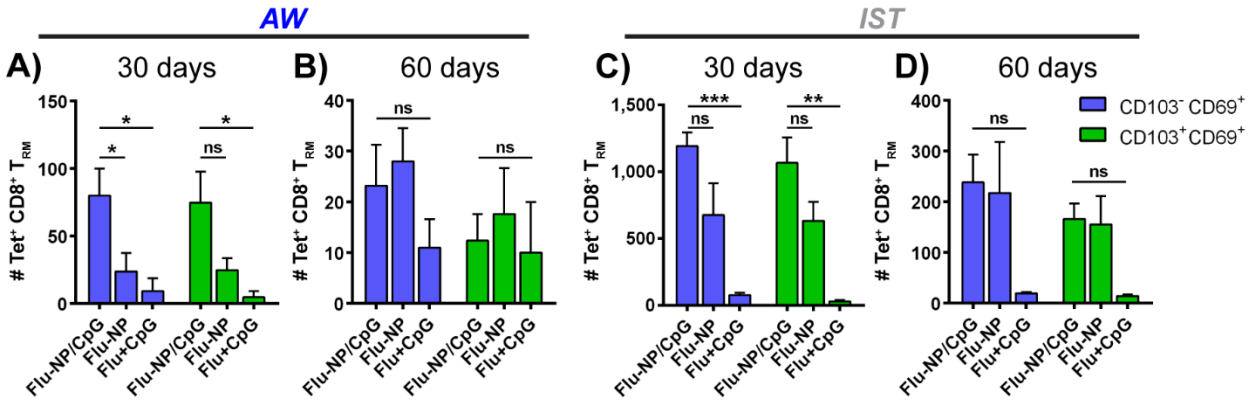

Figure 3.5 | Flu-specific CD8⁺ memory T cells express T_{RM} markers CD69 and CD103. Mice were immunized i.n. with Flu-containing formulations and lungs were analyzed on d30 or d60 *via* tetramer and surface marker staining. CD103 and CD69 were used as markers of tissue residency. **(A,B)** Number (#) of Tet⁺ CD8⁺ T cells expressing CD69±CD103 in AW were enumerated on **(A)** d30 or **(B)** d60 after immunization. **(C,D)** Number (#) of Tet⁺ CD8⁺ T cells expressing CD69±CD103 in IST were enumerated on **(C)** d30 or **(D)** d60 after immunization. Data are mean ± SEM, with *n* = 3-6 per group, and representative of two independent experiments. Immunization dose: 25 µg NP, 9.5 µg Flu, 1.4 µg CpG. Limit of detection: 1 cell (AW), 5 cells (IST/MV), 25 cells (spleen). *p<0.05, **p<0.01, ***p<0.001, by ordinary two-way ANOVA with Tukey's multiple comparisons test. ns, not significant. Statistical comparisons are shown for Flu-NP/CpG only.

Single-dose pulmonary immunization with nanoparticle vaccine protects against lethal challenge with influenza A H1N1 virus

As with previous experiments using OVA protein antigen, the ultimate test of efficacy for a vaccine is its ability to protect against infection. Thus, we sought to determine whether a single-dose of NP vaccine with Flu antigen could similarly protect against respiratory challenge. To this end, we immunized mice i.n. with Flu-NP/CpG, Flu-NP, Flu+CpG, or PBS, and on d30 or d60 post-immunization, challenged i.n. with PR8 virus. In this lethal challenge model, mice were inoculated with 200 FFU of PR8, a dose at which untreated animals experience severe weight loss and disease symptoms (**Figure B.2**). Mice were monitored daily through d21 p.i. for weight loss, morbidity, and mortality (**Figure 3.6A**).

At d30, mice immunized with either Flu-NP/CpG or Flu-NP were protected from challenge-induced weight loss relative to Flu+CpG and naïve (PBS-treated) mice (**Figure 3.6B**). Mice in the Flu-NP/CpG and Flu-NP groups lost less weight overall, and around d7-8 p.i., began to recover instead of continuing to lose weight. In addition, 83% of Flu-NP/CpG mice and 67% of Flu-NP mice survived challenge, while 100% of Flu+CpG mice and PBS mice succumbed to infection (>30% weight loss) by d7 or d8 p.i., respectively (**Figure 3.6D**).

At d60, the protective effect of the Flu-NP/CpG formulation was maintained (**Figure 3.6C**), consistent with results seen in the vaccinia challenge model described earlier. In addition, the survival

rate for the Flu-NP/CpG group remained the same (83%), but for the Flu-NP group it dropped to 33% (**Figure 3.6E**). Mice in the Flu-NP/CpG again began recovering on d7 p.i., whereas the surviving mice in the Flu-NP group did not show signs of recovery until d9-10. As before, 100% of mice in the Flu+CpG and PBS groups perished by d9 p.i. Body condition scoring of the 60-day cohort reflected the results seen in weight loss and survival, with mice in the Flu-NP/CpG group experiencing less severe symptoms and recovering more quickly relative to control groups (**Figure B.3**). Overall, these results demonstrate that a single dose of the NP vaccine formulated with a clinically relevant antigen (influenza A nucleoprotein) offers protection against lethal respiratory virus challenge. Nucleoprotein is an internal viral protein, and so it is a target for protective T cell responses. Given that T_{RM} specific for the immunodominant $CD8^+$ T cell epitope of nucleoprotein are detected at the highest frequency in lungs of mice immunized with Flu-NP/CpG, our data suggest these $CD8^+$ T_{RM} cells contribute to protection.

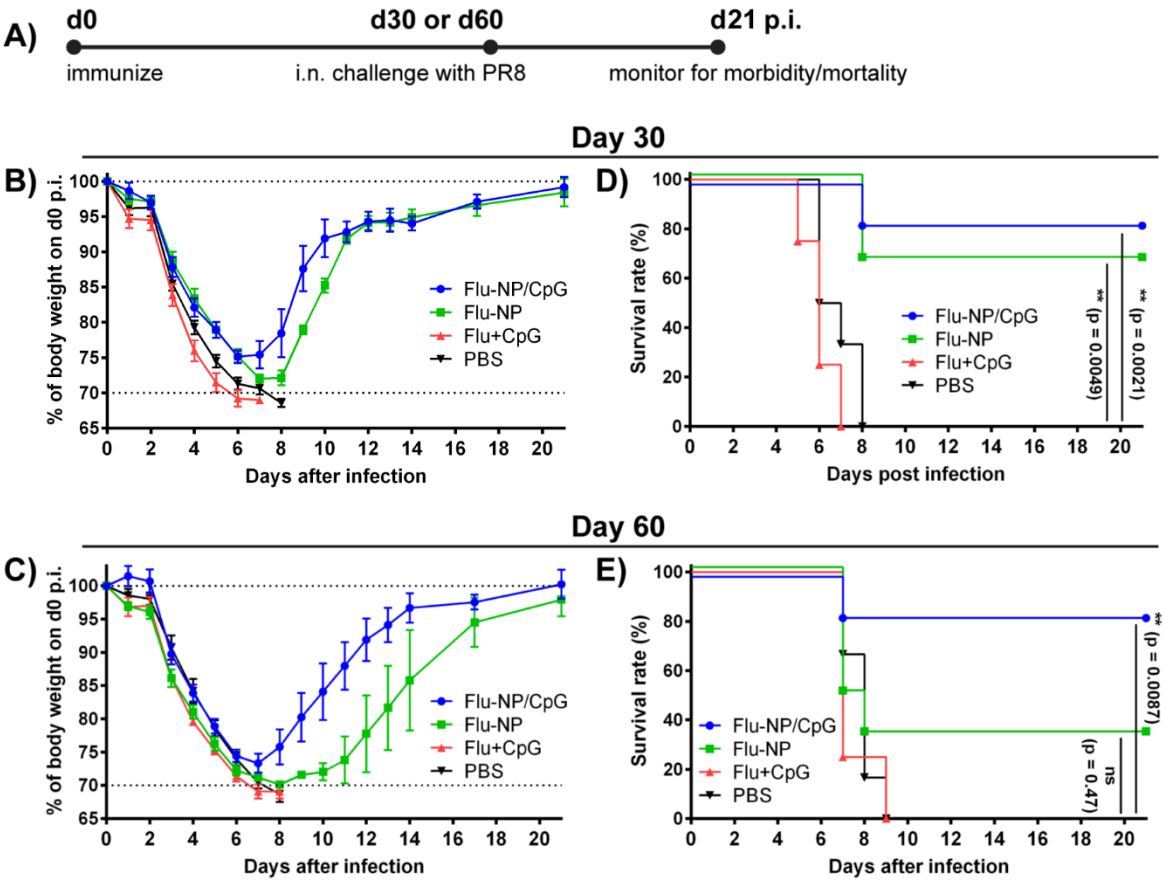

Figure 3.6 | Mice immunized with nanoparticle vaccine exhibit improved survival after intranasal challenge with influenza A H1N1 virus. (A) Mice immunized on d0 were challenged i.n. with influenza A H1N1 PR8 virus (lethal dose of 200 FFU/mouse) either 30 d or 60 d post-immunization. Mice were weighed daily and evaluated for morbidity/mortality. **(B,C)** Percent (%) weight loss in mice challenged on **(B)** d30 or **(C)** d60 after i.n. administration. **(D,E)** Survival of mice challenged on **(D)** d30 or **(E)** d60 post-immunization. Mice that exceeded 30% weight loss were considered deceased. Data are mean ±

SEM, with *n* = 4-6 per group, from two independent experiments. Immunization dose: 25 µg NP, 9.5 µg Flu, 1.4 µg CpG. Statistical significance in survival curves was determined with a Mantel-Cox log-rank test (**p<0.01; ns, not significant).

3.4 Conclusion

Respiratory infections such as influenza are a major threat to public health, and effective vaccines to prevent them are greatly needed. In particular, seasonal influenza and the threat of rapidly spreading pandemic strains place a significant burden on healthcare systems worldwide. While traditional seasonal influenza vaccines typically focus on producing humoral immunity, it is clear that T cells, particularly of those the tissue-resident variety, play a vital role in protection against this virus.[22, 63, 124] The development of universal flu vaccines that utilize conserved antigenic epitopes, particularly those that can stimulate a $CD8^+$ T cell response and provide heterosubtypic immunity against multiple virus strains—such as the nucleoprotein antigen used here—hold great promise for the future of this field.[179] It will be critical to evaluate these next-generation vaccines for their ability to generate tissue-resident memory.

In this aim, using mouse models of pulmonary immunization and respiratory virus challenge, we demonstrated that a single dose of pH-responsive nanoparticle vaccine induced a $CD8^+$ T_{RM} response that persisted for up to 60 days after immunization and was protective against both lethal and sublethal challenge with respiratory viruses (influenza and vaccinia, respectively). Antigen-specific $CD8^+$ T cells displayed surface markers characteristic of T_{RM} (CD103, CD69), and intravascular staining showed them to be resident in the lung interstitium ($CD45^-CXCR3^{lo}$) and airways ($CD45^-CXCR3^{hi}$). In contrast to other experimental T_{RM} vaccines described in the literature, for which multiple booster doses are often needed to generate an effective response, these results were obtained after a single immunization. This offers potential translational advantages, including increased compliance and the ability to more quickly manufacture and distribute a vaccine under pandemic conditions.

Several surface markers have been used to describe T_{RM} cells in various non-lymphoid tissues—in particular, CD103 and CD69.[63, 73, 93] However, these markers are not found on all T_{RM}; many T_{RM} populations located outside epithelia do not express CD103.[180] CD69 is more universally expressed and has been suggested to influence accumulation and retention of $CD8^+$ T cells in the lungs during the early stages of infection.[126] Both $CD103^-CD69^+$ and $CD103^+CD69^+$ T_{RM} subsets have been shown in the lungs.[7, 66, 181, 182] In our experiments, we found the $CD103^-CD69^+$ phenotype to be somewhat more prevalent than $CD103^+CD69^+$ in the IST and AW. It has been suggested that infiltration of tumors with $CD8^+$ T_{RM} expressing CD103 correlates to longer survival of patients with a variety of cancers, including breast, lung, ovarian, cervical, and bladder.[5] Several reports have found TGFβ is needed to induce expression of CD103 on T_{RM}, and we were unable to detect this cytokine at the timepoints tested after

immunization.[32, 96, 183] In light of this, methods to tailor the NP vaccine to stimulate TGFβ production or otherwise generate more CD103-expressing $CD8^+$ T_{RM} cells may warrant further study. It is important to note that the requirements for T_{RM} formation in different tissues, and indeed, even in different regions of the same tissue, can vary. For example, differentiation of $CD8^+$ T_{RM} in the upper respiratory tract does not seem to depend on local antigen recognition or TGFβ signaling, but in the lower respiratory tract, these both appear to be required.[96] Further study of the tissue-specific requirements for T_{RM} formation in the lungs will help inform improved design of vaccines for generating functional T_{RM} cells.

Laidlaw *et al*. reported that $CD4^+$ T cell help was critical for formation of $CD103^+$ T_{RM} in the lungs. They found that, without $CD4^+$ T cell help, $CD8^+$ T_{RM} had reduced expression of CD103 and were unable to recruit immune cells to the lungs upon challenge with influenza virus.[22] Conversely, Si *et al*. reported that their peptide nanofiber vaccine elicited functional pulmonary $CD8^+$ T_{RM} without a $CD4^+$ T cell helper epitope.[103] In the work described here, the $CD4^+$ T cell response to the NP vaccine was not studied. If the functionality of $CD8^+$ T_{RM} in the lungs is indeed dependent on $CD4^+$ T cell help, it is possible the T_{RM} phenotype generated by this NP vaccine was affected by a lack of $CD4^+$ T cells. However, since whole protein antigens containing both MHC-I and MHC-II epitopes were used, it is likely that $CD4^+$ T cells were generated.[50] In fact, it has been shown that the nucleoprotein antigen used here is an immunodominant target of $CD4^+$ T cell responses.[184] Characterization of the $CD4^+$ T cell response generated by the NP vaccine, and its effect on the phenotype of vaccine-induced $CD8^+$ T_{RM} in the lungs, merits further investigation. Nevertheless, the NP vaccine provided significant protection against challenge with multiple respiratory viruses, demonstrating its translational promise.

In conclusion, this report demonstrates generation of protective $CD8^+$ T_{RM} in the lungs with a single pulmonary dose of pH-responsive nanoparticle vaccine. Efficacy of the NP vaccine was demonstrated with both a model antigen (ovalbumin) and a clinically relevant antigen (influenza A nucleoprotein). Antigen-specific $CD8^+$ T cells in the lungs displayed characteristic T_{RM} markers at memory timepoints, and mice were protected against respiratory virus infection in both sublethal and lethal challenge models. The use of intravascular staining to identify lung-resident cells, in conjunction with staining for markers of tissue-resident memory, has enabled relationships between NP vaccine properties and the generation of protective T_{RM} to be established. In addition, successful delivery of multiple distinct antigens indicates the NP vaccine is a modular platform technology that can be used with any number of clinically-relevant protein or peptide antigens, as well as other nucleic acid adjuvants. Overall, this nanoparticle delivery system represents a promising technology for the development of T_{RM} vaccines against respiratory infections and contributes to the body of work on universal influenza vaccines.

3.5 Materials and Methods

Preparation and Characterization of Nanoparticles. Self-assembled micellar NP were formulated by first dissolving lyophilized polymer at 50 mg/ml in 100% ethanol, then rapidly pipetting dissolved polymer into 100 mM phosphate buffer (pH 7) to a final concentration of 10 mg/ml. For *in vivo* use, ethanol was removed by buffer exchange into PBS (pH 7.4) *via* 3 cycles of centrifugal dialysis (Amicon, 3 kDa MWCO, Millipore), and NP solutions were then sterilized *via* syringe filtration (Whatman, 0.22 µm, GE Healthcare). Final polymer concentration was determined with UV-Vis spectrometry (Synergy H1 Multi-Mode Reader, BioTek) by measuring absorbance of aromatic PDS groups at 280 nm. NP size was measured *via* dynamic light scattering (DLS). NP solutions were prepared at a concentration of 0.1-0.2 mg/ml in PBS (pH 7.4) and the hydrodynamic radius was measured using a Malvern Instruments Zetasizer Nano ZS Instrument (Malvern, USA).

Preparation of Antigen-Nanoparticle Conjugates. Either a model antigen, ovalbumin protein (OVA), or the influenza nucleoprotein antigen from H1N1 A/Puerto Rico/8/1934 was conjugated to pendant PDS groups on NP *via* thiol-disulfide exchange. To prepare OVA for conjugation, free amines on the protein were thiolated by incubation with ~25 molar excess of 2-iminothiolane (Traut's Reagent, Thermo Fisher Scientific) in reaction buffer (100 mM phosphate buffer, pH 8, supplemented with 1 mM EDTA) as previously described.[50] Unreacted 2-iminothiolane was removed by buffer exchanging thiolated OVA into sterile 1X PBS (pH 7.4) using Zeba™ Spin desalting columns (0.5 ml, 7 kDa MWCO, Thermo Fisher Scientific). Prior to *in vivo* use, thiolated OVA was sterilized *via* syringe filtration (0.22 µm, Millipore). Following manufacturer's instructions, the molar ratio of thiol groups to OVA protein was determined with Ellman's reagent (Thermo Fisher Scientific) to be ~3-5 thiols/OVA. Polymer NP solutions were reacted with thiolated OVA at a 5:1 molar ratio of pH-responsive polymer:OVA to make OVA-NP conjugates. Conjugation was done overnight, in the dark, at room temperature, and under sterile conditions, as previously described.[50] Antigen conjugation using FITC-labeled OVA was verified *via* non-reducing SDS-polyacrylamide gel electrophoresis (SDS-PAGE) using 4-20% Mini-Protean TGX Precast Protein Gels (Bio-Rad) (**Figure A.3A**). Gels were run at 130 V for 1 h and imaged with a Gel Doc™ EZ System (Bio-Rad). DLS was used to measure the size of OVA-NP conjugates, as described above (**Figure A.3C,** top and bottom left).

Influenza A H1N1 nucleoprotein (Flu) formulated in sterile phosphate buffer was obtained from Sino Biological (Beijing, China). To prepare Flu antigen for conjugation, free amines were thiolated by incubation with ~250 molar excess of 2-iminothiolane in reaction buffer. Unreacted 2-iminothiolane was removed by buffer exchange into sterile 1X PBS. Following manufacturer's instructions, the molar ratio of thiol groups to Flu protein was determined with a Measure-iT™ Thiol Assay Kit (Thermo Fisher

Scientific). The concentration of Flu protein after thiolation and purification was measured using the Pierce™ Rapid Gold BCA Protein Assay Kit (Thermo Fisher Scientific). In some cases, Flu was labeled with Alexa Fluor 647-NHS ester (Thermo Fisher Scientific) prior to thiolation for evaluating conjugation efficiency *via* fluorescent imaging of SDS-PAGE gels. Polymer NP solutions were reacted with thiolated Flu at a molar ratio of 5:1 pH-responsive polymer:Flu to make Flu-NP conjugates. Antigen conjugation was verified *via* SDS-PAGE (**Figure B.1A**) and gels were imaged with an IVIS Lumina III Imaging System (PerkinElmer, Waltham, MA). DLS was also used to measure the size of Flu-NP conjugates (**Figure B.1C**, top).

Formation of Nanoparticle/Adjuvant Complexes. NP/adjuvant complexation was carried out by combining CpG ODN 1826 (Invivogen) with OVA-NP or Flu-NP in PBS at room temperature for at least 30 min. Theoretical charge ratios (+/-) of 4:1 and 6:1 were tested. The charge ratio was defined as the molar ratio between protonated DMAEMA tertiary amines in the first block of the copolymer (positive charge; assuming 50% protonation at physiological pH) and phosphate groups on the CpG backbone (negative charge).[50] The charge ratios at which complete complexation of CpG to the polymer occurred were determined *via* an agarose gel retardation assay (**Figure A.3B** for OVA and **Figure B.1B** for Flu). Free CpG, OVA+CpG, Flu+CpG, and NP/CpG, OVA-NP/CpG, and Flu-NP/CpG complexes prepared at various charge ratios were loaded into lanes of a 4% agarose gel and run at 90 V for 30 min. Gels were stained with GelRed® Nucleic Acid Gel Stain (Biotium, Fremont, CA) for 20 min and visualized with a Gel Doc™ EZ System (Bio-Rad). A charge ratio of 6:1 was used for all *in vivo* experiments in order to maximize the stability of the formulations. DLS was used to measure the size of the OVA-NP/CpG formulation (**Figure A.3C,** top right) and Flu-NP/CpG formulation (**Figure B.1C**, bottom), as described above.

Animals. Male or female C57BL/6J mice were purchased from the Jackson Laboratory (Bar Harbor, ME), maintained at the animal facilities of Vanderbilt University under either conventional or animal biosafety level 2 (ABSL-2) conditions, and experimented upon in accordance with the regulations and guidelines of Vanderbilt University Institutional Animal Care and Use Committee (IACUC).

Intranasal Immunization. Endotoxin-free OVA (<1 EU/mg, EndoFit™), sterile nucleoprotein (Sino Biological), sterile buffer solutions (1X PBS, pH 7.4), and sterile polymer solutions with ethanol removed were used for vaccine formulations. Experimental groups for OVA immunization were: (**1**) nanoparticles loaded with covalently-conjugated OVA and complexed with CpG DNA (**OVA-NP/CpG**); (**2**) nanoparticles conjugated to OVA (**OVA-NP**); (**3**) a mixture of non-thiolated OVA and CpG (**OVA+CpG**); and (**4**) **PBS** for sham mice. Analogous experimental groups for Flu immunization were:

(1) Flu-NP/CpG; **(2)** Flu-NP; **(3)** Flu+CpG; and **(4)** PBS. For all groups containing "**NP**," this denotes the pH-responsive polymer. Conjugates were prepared 1-2 days before use and stored at 4 °C. OVA or Flu was thiolated and used immediately for conjugation to NP at a molar ratio of 5:1 (NP:antigen), as described above. On the day of use, CpG was complexed to conjugates at a 6:1 charge ratio *via* rapid pipetting of CpG DNA (~0.5 mg/ml) into the conjugate solution, as described above. The formulation was allowed to react for at least 30 min at room temperature for complete complexation of CpG before administration to mice.

In experiments using OVA antigen, male mice (8-12 weeks old) were anesthetized with ketamine/xylazine (10 mg/ml ketamine hydrochloride, Vedco; 1 mg/ml xylazine hydrochloride, Vanderbilt Pharmacy) by intraperitoneal (i.p.) injection (~200 µl anesthesia/22 g mouse weight). Anesthetized mice were immunized intranasally (i.n.) on day 0 with formulations containing 7.5 µg OVA and/or 1.4 µg CpG with or without 25 µg polymer. Vaccine formulations in a total volume of 80 µl PBS were delivered *via* pipette through the nostrils into the lungs of mice; inoculation with this volume allows formulations to reach the lower airways.[167] The dose was applied at the center of the nose to allow inhalation into both nostrils at a rate of ~8 µl/s. Animals were monitored either daily or thrice weekly for weight loss and signs of morbidity.

In experiments using Flu antigen, female mice (10 weeks old) were anesthetized as described and immunized i.n. on day 0 with formulations containing 9.5 µg Flu and/or 1.4 µg CpG with or without 25 µg polymer. Vaccine formulations in a total volume of 80 µl PBS were delivered through the nostrils as described.

Measurement of Antigen-Specific $CD8^+$ T Cell Response and Tissue-Resident Memory Markers. On day 30 or 60 after immunization, mice were anesthetized and intravenously (i.v.) injected with 200 µl of anti-CD45.2-APC antibody (clone 104; Tonbo) at 0.01 mg/ml (2 µg αCD45 antibody per mouse), as previously described.[66] This was done to stain marginated vascular leukocytes (MV; $CD45^+$) and differentiate them from those resident in the lung interstitium (IST; $CD45^-$).[44] To allow for circulation of αCD45 antibody, mice were rested for 3-5 min after i.v. injection and prior to CO_2 euthanasia. Lungs and spleens were then collected from each mouse. Organs were harvested and processed as previously described.[168] Briefly, lungs were minced with a scalpel and incubated for 1 h at 37 °C in complete RPMI medium (cRPMI [RPMI+10% FBS]; Gibco) supplemented with 2 mg/ml collagenase (Sigma) and 50 nM dasatinib (LC Laboratories, Woburn, MA). Lungs and spleens were treated with ACK lysing buffer (Gibco) and passed through 70 µm cell strainers to generate single cell suspensions.

Cell suspensions from lungs and spleens were stained for 1 h at 4 °C with anti-B220-FITC (clone RA3-6B2; BD Biosciences), anti-CD4-FITC (clone H129.19; BD Biosciences), anti-CD11b-FITC (clone M1/70; Tonbo), anti-CD11c-FITC (clone N418; Tonbo), anti-CD8α-Pacific Blue (clone 53-6.7; BD

Biosciences), and 1.5 µg/ml PE-labeled $OVA_{257-264}$ (SIINFEKL)-H-$2K^b$ tetramer (Tet) prepared according to a previously reported procedure.[169] In experiments utilizing mice immunized with Flu antigen, cells were instead stained with PE-labeled $Flu_{366-374}$ (ASNENMETM)-H-$2D^b$ Tet prepared using the same method. Antibodies labeled with FITC (B220/CD4/CD11b/CD11c) were referred to as the "dump" channel and were used to exclude B cells, $CD4^+$ T cells, dendritic cells, and macrophages from gating. Staining with anti-CXCR3-PerCP/Cy5.5 (clone CXCR3-173; BioLegend) was used to define $CD8^+$ T cells resident in the airways ($CXCR3^{hi}$) vs. interstitium ($CXCR3^{lo}$).[66] In experiments evaluating tissue-resident memory markers, cells from lungs and spleens were also stained with anti-CD69-PE/Cy7 (clone H1.2F3; Tonbo) and anti-CD103-Brilliant Violet 510 (clone 2E7; BioLegend).

After staining, cells were washed with FACS buffer (PBS supplemented with 2% FBS and 50 nM dasatinib) and stained with Ghost Dye™ Red 780 (Tonbo) to discriminate live *vs.* dead cells. AccuCheck counting beads (Thermo Fisher Scientific) were included in samples to allow for calculation of absolute cell counts. The frequency of antigen-specific $CD8^+$ T cells was determined by flow cytometry on a 3-laser LSR-II flow cytometer (BD). All data were analyzed using FlowJo Software (version 10.4.2; Tree Star, Inc., Ashland, OR). Cells were gated by forward and side scatter to exclude debris and doublets. Antigen-specific $CD8^+$ T cell populations were defined as follows: AW = $CXCR3^{hi}CD8\alpha^+CD45^-Tet^+$ cells in lung samples; IST = $CXCR3^{lo}CD8\alpha^+CD45^-Tet^+$ cells in lung samples; MV = $CD8\alpha^+CD45^+Tet^+$ cells in lung samples; SPL = $CD8\alpha^+Tet^+$ cells in spleen samples. All cells in the $CD8\alpha^+$ gate were also $B220^-CD4^-CD11b^-CD11c^-$ ("dump channel"). T_{RM} cells were defined as either $CD103^+CD69^+$ or $CD103^-CD69^+$ $CD8^+$ T cells in IST or AW. Representative gating for each sample type can be found in **Figures A.4B,C** and **3.2A**.

Vaccinia Virus Propagation, Intranasal Virus Challenge, and Lung Burden. Recombinant vaccinia virus expressing influenza virus nucleoprotein, ovalbumin SIINFEKL peptide, and enhanced green fluorescent protein (VV.NP-S-EGFP) was obtained through the NIH Biodefense and Emerging Infections Research Resources Repository, NIAID, NIH (NR-624; BEI Resources, Manassas, VA). The virus was grown in HeLa cells and titrated using BSC-40 cells. For titration, crystal violet stain (Eng Scientific, Clifton, NJ) was used to visualize plaques 48 h after applying serial 10-fold dilutions of the virus in HBSS+0.5% (w/v) BSA to confluent monolayers of BSC-40 cells.

For respiratory challenge, 10- to 16-week-old immunized male mice were anesthetized i.v. with ketamine/xylazine as described above and inoculated i.n. with a sublethal dose (1×10^7 pfu) of virus in 80 µl sterile PBS. Mice were monitored daily for morbidity and weight loss. On day 6 post-infection, lungs from individual mice were harvested into 2 ml HBSS (supplemented with 0.5% (w/v) BSA and 1X pen/strep, sterilized by vacuum filtration) and frozen at -80 °C.

To determine viral burden using a plaque assay, previously frozen lungs were thawed, homogenized in HBSS using a Tissue Tearor (BioSpec Products, Bartlesville, OK), and subjected to one additional freeze-thaw cycle. Serial 10-fold dilutions of lung homogenates were plated on confluent monolayers of BSC-40 cells. After 48 h, plaques were visualized by crystal violet staining.

Influenza A Virus Challenge. Influenza virus (strain A/Puerto Rico/8/1934, subtype H1N1; also known as PR8) was obtained through BEI Resources, NIAID, NIH (NR-348; Manassas, VA). For respiratory challenge, 14- to 18-week-old immunized female mice were anesthetized i.v. with ketamine/xylazine as described above and inoculated i.n. with a lethal dose (200 FFU) of virus in 80 µl sterile PBS. Mice were monitored daily through day 21 post-infection for morbidity, weight loss, and survival. After infection, mice were euthanized when weight loss exceeded 30% of initial body weight, in accordance with IACUC guidelines. In the 60-day cohort, mice were also scored daily on a scale from 1-4, with “1” indicating no outward signs of illness, “2” indicating consistently ruffled fur, “3” indicating hunched back and altered gait, and “4” indicating reduced mobility/reaction to stimulus, labored breathing, and lethargy.

Statistical Analysis. Statistical analyses were performed as indicated in figure legends. All analyses were done using GraphPad Prism software, version 6.07. Results are expressed as mean ± SEM with ****$p < 0.0001$, ***$p < 0.001$, **$p < 0.01$, *$p < 0.05$ being considered statistically significant.

CHAPTER 4

Nanoparticle-Mediated Delivery of Nucleic Acid Adjuvants to Antigen-Presenting Cells and Effects on the Lung-Resident CD8$^+$ T Cell Response

4.1 Abstract

Rational design of nanoparticle delivery platforms holds great promise for a new generation of vaccines that can efficiently generate durable and protective tissue-resident memory T cell (T_{RM}) responses. As the requirements for formation of T_{RM} cells become clearer, the engineering toolbox for T_{RM} vaccine design has also expanded. However, limited work has been done to probe the ways in which the material properties of synthetic nanoparticles can affect the resulting T_{RM} response. In addition, multiple adjuvants have shown promise as inducers of T_{RM} cells, and nanoparticle carriers offer unprecedented opportunities for localized, targeted, or dose-sparing delivery of adjuvant molecules that might otherwise be unsafe for use in humans. This work builds upon previous studies demonstrating the efficacy of a pH-responsive nanoparticle vaccine in delivering a nucleic acid adjuvant (CpG) to pulmonary antigen-presenting cells (APCs) and enhancing the downstream CD8$^+$ T_{RM} response. Here, we show that multiple nucleic acid adjuvants for distinct intracellular targets (CpG, poly(I:C), and nanoISD) can be loaded onto either the pH-responsive NP vaccine or a non-pH-responsive control particle, and that both the polymer and adjuvant used can affect the CD8$^+$ T cell response produced in the lung interstitium or vasculature. In addition, the impact of these various polymer/adjuvant formulations on antigen uptake and APC activation in the lungs and mediastinal lymph node was examined. Results of this aim indicate that polymer and adjuvant properties can have a unique effect on the immune response after immunization, and the ways in which these effects can be leveraged merits further investigation.

4.2 Introduction

Great strides have been made in recent years to understand the conditions necessary for generation and maintenance of tissue-resident memory T cells. Various innate immune cells, transcriptional factors, cytokines, and other features of the tissue environment dictate the migration and retention of T_{RM} to their home tissues, differentiation toward a T_{RM} phenotype, and long-term maintenance and/or replenishment. As our understanding of tissue-resident T cell biology grows, it presents an important opportunity to rationally design vaccines with this cell type in mind. Our previous work has shown that the pH-responsive activity of a polymeric nanoparticle could influence formation

of T_{RM} by enhancing the magnitude of the tissue-resident $CD8^+$ T cell response in lung parenchyma and airways. In addition, co-delivery of a nucleic acid adjuvant alongside protein antigen further enhanced this by increasing the magnitude, functionality, and protective capacity of the $CD8^+$ T_{RM} cell response. This presented the question of whether different adjuvants with distinct intracellular targets might have varying effects on the T_{RM} response in the lungs, and whether the material properties of the nanoparticle carrier could be altered to change that response.

Multiple innate immune cell subsets, including monocytes, alveolar macrophages, and cross-presenting dendritic cells (DCs), have been shown to play a role in priming tissue-resident T cell responses.[5, 47, 49, 61, 72, 185-188] In particular, $CD103^+$ DCs survey non-lymphoid tissues and migrate to lymph nodes, where they are efficient cross-presenters of cell-associated antigens; since cross-presentation is critical for induction of $CD8^+$ T cell responses, this makes $CD103^+$ DCs an attractive target for vaccines against intracellular pathogens, such as influenza virus or *Mycobacterium tuberculosis*.[189] In addition, $CD103^+$ DCs have been implicated in the generation of precursor T_{RM} in lymph nodes.[5, 47] Thus, effective activation and maturation of this DC subset would be a desirable feature of a potential T_{RM} vaccine. Previous *in vivo* work with our pH-responsive nanoparticle vaccine showed uptake of vaccine cargo (OVA protein and CpG adjuvant) in $CD103^+$ DCs in the lungs, as well as enhanced activation *via* CD86 expression. However, it is not yet known how cytosolic antigen delivery mediated by the pH-responsive activity of the nanoparticle might interact with the intrinsic cross-presenting mechanisms of $CD103^+$ DCs, or whether other adjuvants might differently impact uptake and activation in this DC subset. In addition, it is unknown what role other DC subsets (*i.e.*, non-cross-presenting DCs, plasmacytoid DCs) might play in the vaccine-induced immune response.

A variety of adjuvants have also been used in studies to generate T_{RM} responses, including α-galactosylceramide, IL-1β, Toll-like receptor agonists such as poly(I:C) (TLR3), MPLA (TLR4), CpG (TLR9), R848 (TLR7/8), Zymosan (TLR2/6), or combinations like poly(I:C)+anti-CD40 antibody.[8, 34, 46, 59-61, 190, 191] Because these adjuvants have unique intracellular targets that activate distinct signaling pathways, they offer an interesting opportunity to probe the ways in which innate immune activation can be leveraged to control the downstream T_{RM} response. In addition, though many experimental adjuvants have been used in pre-clinical studies, few are approved for use in humans because they are often too toxic.[87] Particulate delivery offers a potential solution to the issue of toxicity by allowing for targeted delivery of smaller doses that can be effective without causing overwhelming inflammation.[8]

The pH-responsive nanoparticle vaccine described here presents a unique opportunity to deliver adjuvants to multiple intracellular targets and examine the effect of their activation on the $CD8^+$ T_{RM} response. Although the pH-responsive activity of the material was designed for the purpose of cytosolic delivery of antigen, it is feasible that it could also deliver adjuvant to cytosolic targets, such as the RIG-I/MAVS or cGAS/STING pathways. These targets have gained much attention in recent years for

their role in both infectious diseases and cancer. For example, RIG-I signaling is important in interferon gene expression during influenza infection, and cGAS has been implicated in detection of Mtb DNA and subsequent induction of type I IFN.[192, 193] Thus, targeting these pathways may prove effective in replicating the effects of infection to produce a protective vaccine. Although the exact percentage of vaccine cargo delivered to the cytosol by the pH-responsive nanoparticle vaccine has not been quantified, we expect that there is some delivery to both the endosome and the cytosol, due to the fact that CpG, which targets TLR9 in the endosome, is an effective adjuvant when delivered with this system.[8, 50] Thus, for this aim, we chose to focus on three adjuvants with targets in either of these intracellular compartments: CpG-ODN1826 (CpG), a single-stranded DNA agonist for TLR9 in the endosome; nanoISD (ISD), a 95 base pair double-stranded immunostimulatory DNA developed in our lab that targets cGAS in the cytosol; and low molecular weight poly(I:C) (PIC), which is unique in that it can target both TLR3 in the endosome and RIG-I/MAVS in the cytosol. Previous reports have shown that both poly(I:C) and CpG can promote cross-presentation in dendritic cells.[100, 194-196] In addition, activation of the cGAS/STING pathway in DCs and subsequent production of type I IFN plays important role in cross-presentation of antigen for priming of tumor-specific $CD8^+$ T cells.[197] The NP platform employed here is useful in that it theoretically allows simple electrostatic complexation of any nucleic acid adjuvant to the cationic corona of the particle.

Here, we demonstrate that CpG, ISD, and PIC adjuvants can be stably formulated with antigen-nanoparticle conjugates and delivered intranasally to DCs in the lungs and lung-draining lymph node. Tetramer staining for antigen-specific $CD8^+$ T cells at short-term (13-day) and memory (30-day) timepoints after immunization showed these adjuvants were able to stimulate varying degrees of tissue-resident responses in the lungs. Interestingly, in some cases, immunization with these adjuvants on the non-pH-responsive control polymer seemed to have the opposite effect, boosting the response in the lung vasculature while minimizing the response in the interstitium. Antigen-specific CD8+ T cells generated in the interstitium expressed TRM markers (CD103/CD69) at both timepoints, while those in the vasculature did not. Finally, immunization resulted in enhanced expression of activation markers (CD86/CCR7) on DCs in the lungs and LN. This work lays the foundation for further studies of the effects of polymer and adjuvant properties on generation of T_{RM} immunity.

4.3 Results and Discussion

Multiple adjuvants with distinct physicochemical characteristics can be electrostatically complexed with nanoparticle carriers

Our first step in studying the effect of different adjuvants on the T_{RM} response was to determine whether immunostimulatory molecules with diverse molecular weights and structures could be electrostatically complexed with either pH-responsive (PH) or control (CT) nanoparticles. We previously demonstrated delivery of CpG1826, a class B oligodinucleotide (ODN), using this platform. CpG 1826 is a single-stranded DNA molecule and an agonist for endosomal TLR9. It has shown clinical promise, and a related class B ODN, CpG 1018, is a component of the hepatitis B vaccine Heplisav-B.[198] Poly(I:C) has shown potential in many experimental vaccines, and two derivatives, poly-IC12U (Ampligen) and poly-ICLC (Hiltonol), have been used an clinical vaccine adjuvants.[199] Since it can target both TLR3 in the endosome and RIG-I/MAVS in the cytosol, it presents a unique opportunity to study whether delivery to the endosome (CT) vs. cytosol (PH) can differentially affect the immune response. The final adjuvant we chose, nanoISD, is a 95-base pair double-stranded immunostimulatory DNA molecule and an agonist for cGAS in the cytosol; thus, it presents an opportunity to determine whether the pH-responsive polymer can deliver adjuvant to a cytosolic target. While CpG is a relatively small molecule (6364 g/mol), ISD and PIC are much larger (58,760 g/mol and ~306,866 g/mol, respectively). It is difficult to precisely determine the molecular weight of poly(I:C); the commercial adjuvant is provided as a 0.2-1 kilobase pair molecule. Thus, we estimated the average molecular weight to be that of 600 base pairs. Considering the relatively small size of the nanoparticles formed with our polymers, it was unclear whether these larger adjuvants would efficiently complex with the particles.

Polymers were synthesized and characterized by ^{1}H NMR and DLS according to previously reported procedures (**Figure C.1**).[8, 50] Both pH-responsive and CT polymers formed small NP (~20-30 diameter) (**Figure C.1C-E**) and could be covalently conjugated to thiolated OVA protein (**Figure C.2A**). Addition of OVA did not affect the size of the particles (**Figure C.2B,C**). To evaluate this the ability of OVA-loaded polymers to formulate with different adjuvants, we complexed ISD and PIC at various charge ratios (+/-) to OVA-conjugates made at either a 5:1 or 10:1 molar ratio of NP:OVA (3.6:1 or 7.2:1, respectively, for the CT polymer in order to maintain a constant dose of antigen). The charge ratios tested for both adjuvants were 6:1, 8:1, and 12:1 for PH conjugates and 5:1, 7:1, and 10:1 for CT conjugates. A gel retardation assay and dynamic light scattering was used to assess efficacy of complexation and the stability of the formulations, respectively. Both ISD (**Figure 4.1A**) and PIC (**Figure 4.1B**) completely complexed with both polymers under all reaction conditions, as indicated by a lack of nucleic acid migration from the wells of an agarose gel. Select formulations were analyzed by DLS for size and stability. Complexation of either ISD or PIC at a 6:1 charge ratio with PH conjugate (5:1 molar

ratio) resulted in negligible size change from that of conjugate without adjuvant, indicating a stable formulation (**Figure 4.1C,D**). Complexation of ISD and PIC at a 5:1 charge ratio with CT conjugate (5:1) molar ratio resulted in some size change; more so for ISD, whose size distribution increased toward a mean diameter of ~60 nm (*vs*. ~30 nm for PH formulations). Conversely, the size of OVA-CT/PIC seemed to decrease slightly toward a mean diameter of ~20-25 nm. Nevertheless, these formulation parameters were used moving forward in order to maximize the doses of adjuvant that could be delivered *in vivo*. It is possible that the slight larger size of the CT polymer, or its different chemical structure relative to the PH polymer, could have caused these differences in formulation with ISD and PIC adjuvants.

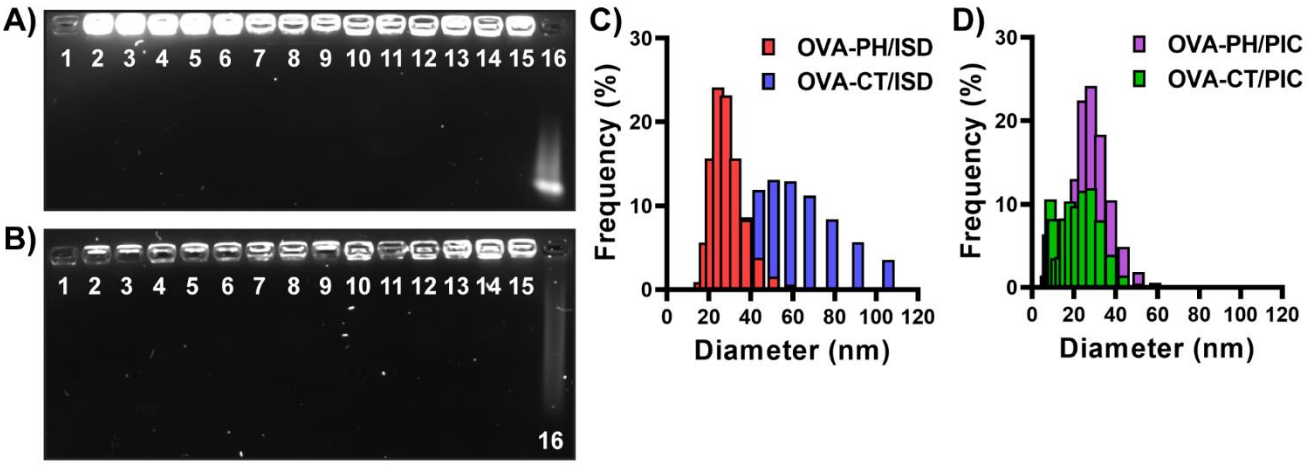

Figure 4.1 | Polymer carriers can be stably complexed with multiple nucleic acid adjuvants. **(A)** NanoISD was complexed with either PH or CT nanoparticles (with or without conjugated OVA) at various charge ratios of polymer:ISD (+/-). Gel electrophoresis and SYBR Safe staining were used to confirm adjuvant complexation. Lane **(1)** OVA-PH [5:1]; **(2)** PH/ISD [6:1]; **(3)** CT/ISD [5:1]; **(4)** OVA-PH/ISD [5:1,6:1]; **(5)** OVA-PH/ISD [10:1,6:1]; **(6)** OVA-PH/ISD [5:1,8:1]; **(7)** OVA-PH/ISD [10:1,8:1]; **(8)** OVA-PH/ISD [5:1,12:1]; **(9)** OVA-PH/ISD [10:1,12:1]; **(10)** OVA-CT/ISD [5:1,5:1]; **(11)** OVA-CT/ISD [10:1,5:1]; **(12)** OVA-CT/ISD [5:1,7:1]; **(13)** OVA-CT/ISD [10:1,7:1]; **(14)** OVA-CT/ISD [5:1,10:1]; **(15)** OVA-CT/ISD [10:1,10:1]; **(16)** free ISD. Material loaded into each lane was normalized to 0.84 µg ISD. In all formulations, lack of migration of ISD as compared to lane (16) indicates complete complexation. Conjugate without adjuvant did not show background staining (Lane 1). **(B)** Low molecular weight poly(I:C) was complexed with either PH or CT nanoparticles (with or without conjugated OVA) at various charge ratios of polymer:PIC (+/-). Gel electrophoresis and SYBR Safe staining were used to confirm adjuvant complexation. Lane **(1)** OVA-PH [5:1]; **(2)** PH/PIC [8:1]; **(3)** CT/PIC [7:1]; **(4)** OVA-PH/PIC [5:1,6:1]; **(5)** OVA-PH/PIC [10:1,6:1]; **(6)** OVA-PH/PIC [5:1,8:1]; **(7)** OVA-PH/PIC [10:1,8:1]; **(8)** OVA-PH/PIC [5:1,12:1]; **(9)** OVA-PH/PIC [10:1,12:1]; **(10)** OVA-CT/PIC [5:1,5:1]; **(11)** OVA-CT/PIC [10:1,5:1]; **(12)** OVA-CT/PIC [5:1,7:1]; **(13)** OVA-CT/PIC [10:1,7:1]; **(14)** OVA-CT/PIC [5:1,10:1]; **(15)** OVA-CT/PIC [10:1,10:1]; **(16)** free PIC. Material loaded into each lane was normalized to 0.7 µg PIC. For all formulations, lack of migration of PIC as compared to lane (16) indicates complete complexation. Conjugate without adjuvant did not show background staining (Lane 1). **(C)** Representative size distribution (number average) at pH 7.4 for pH-responsive NP (PH)

and control NP (CT) formulated with OVA antigen (5:1 molar ratio) and ISD adjuvant (PH, 6:1 charge ratio; CT, 5:1 charge ratio), as measured by DLS. **(D)** Representative size distribution (number average) at pH 7.4 for pH-responsive NP (PH) and control NP (CT) formulated with OVA antigen (5:1 molar ratio) and PIC adjuvant (PH, 6:1 charge ratio; CT, 5:1 charge ratio), as measured by DLS. Experiments were performed once.

Effect of adjuvant and nanoparticle carrier on the lung-resident CD8$^+$ T cell response

We next wished to study the effects of immunization with different adjuvant/polymer combinations on the CD8$^+$ T cell response in the lungs. For this purpose, we immunized two different cohorts of mice: the first with PIC-containing formulations delivered with either PH or CT polymers, in order to determine the effects of polymer properties on delivery of a single adjuvant; and the second with PH nanoparticles complexed with CpG, ISD, or PIC adjuvants to determine whether different ISD or PIC could generate comparable lung-resident to those seen with CpG in Aim 1. All formulations were well-tolerated in mice, with minimal weight loss and full recovery after immunization (**Figure C.3**).

In the first cohort, mice were immunized i.n. on d0 with OVA-PH/PIC, OVA-CT/PIC, OVA+PIC, OVA-PH, or PBS. We speculated that since PIC has an endosomal receptor (TLR3), soluble delivery might exhibit some efficacy. We also hypothesized that the PH and CT polymers might allow differential delivery to RIG-I in the cytosol or TLR3, respectively. On d13 after immunization, lungs, BAL, and spleens were collected and processed for staining with tetramer and surface marker antibodies, as described previously (**Figure 4.2A**). Although 13 days after after immunization would not typically be considered a “memory” timepoint, there is some evidence in the literature that T_{RM} form as soon as two weeks after immunization.[60] Thus, in addition to intravascular staining for tissue residence, we also stained for CD103 and CD69 in these experiments. At d13 after immunization, CD8$^+$ T cells expressing T_{RM} markers were abundant in the IST but not the MV (**Figure C.5**), supporting the notion these are indeed “T_{RM}” cells even at a short-term timepoint. In the AW, OVA-CT/PIC surprisingly appeared to give the highest response (**Figure 4.2B**); however, very few cells were obtained via broncheoalvolar lavage and so these numbers might not be reflective of the actual response in the airways (**Figure C.4**). In the IST, all nanoparticle-containing formulations were significantly better than the mixture of OVA+PIC. OVA-PH/PIC appeared to offer some advantage over both OVA-CT/PIC and OVA-PH, although the difference was not significant (**Figure 4.2C**). Most notably, the OVA-CT/PIC group showed a significantly higher response than other formulations in the MV (**Figure 4.2D**) and spleen (**Figure 4.2E**), indicating that the CT polymer might offer some means of enhancing systemic immunity *via* PIC delivery. In the AW, expression of CD69 was significantly higher on T_{RM} generated by particulate groups relative to OVA+PIC, and few CD103$^+$CD69$^+$ T_{RM} were generated (**Figure 4.2F**). This may again reflect overall low numbers of cells collected in the BAL. Most importantly, in the IST, OVA-PH/PIC generated

significantly more $CD69^{+}CD103^{-}$ antigen-specific $CD8^{+}$ T_{RM} than all other groups, supporting the importance of pH-responsive activity and dual-delivery in generating a lung-resident response. For the $CD103^{+}CD69^{+}$ T_{RM} phenotype in the IST, particulate formulations were superior to soluble OVA+PIC, but only OVA-PH/PIC was significantly better (**Figure 4.2G**).

In the second cohort, mice were immunized i.n. on d0 with OVA-PH/CpG, OVA-PH/ISD, OVA-PH/PIC, OVA-PH, or PBS. This experiment was done to compare pH-responsive delivery of ISD and PIC adjuvants with delivery of CpG, which has previously been proven effective (Aims 1 and 2). On d13 after immunization, lungs, BAL, and spleens were collected and processed for staining with tetramer and surface marker antibodies, as described previously (**Figure 4.3A**). In the AW, ISD was the only adjuvant to give a significantly higher response than unadjuvanted OVA-NP (**Figure 4.3B**). In the IST, both CpG and ISD generated signficantly higher responses than OVA-NP alone (**Figure 4.3C**). Interestingly, in the MV (Figure 4.3D), and to a lesser degree in the spleen (**Figure 4.3E**), delivery of ISD appeared to significantly enhance the response there relative to other adjuvants. It is unclear why ISD would promote a systemic response when delivered i.n. *via* pH-responsive polymer, and further studies to determine the mechanism behind this are warranted. The OVA-PH/ISD formulation also produced the most $CD103^{-}CD69^{+}$ T_{RM} in both the AW (**Figure 4.3F**) and IST (**Figure 4.3G**), with OVA-PH/CpG also producing a significantly higher response than OVA-PH in the IST. Numbers of $CD103^{+}CD69_{+}$ T_{RM} were signficantly higher for any group in the AW or IST, although OVA-NP/CpG did produce the highest response for this phenotype in the IST.

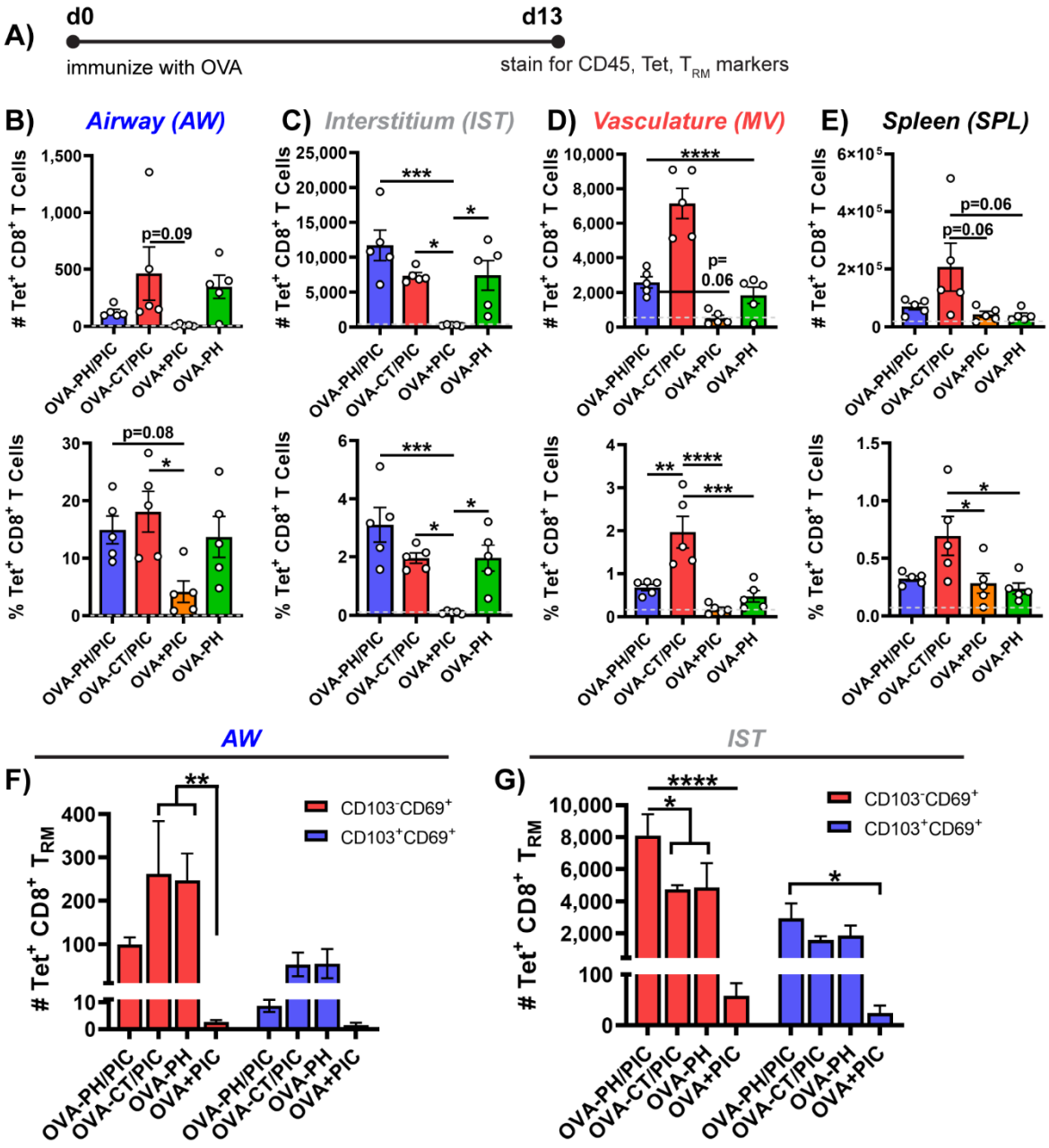

Figure 4.2| Antigen-specific CD8⁺ T cells expressing T_{RM} markers are generated after immunization with poly(I:C) adjuvant. (A) Mice were immunized i.n. with OVA-containing formulations on d0 and BAL, lungs, and spleens were analyzed on d13 *via* tetramer and surface marker staining. CD45 was used to differentiate cells in IST *vs*. MV, and CD103/CD69 were used as markers of T_{RM} cells. **(B-E)** Number (#) and frequency (%) of Tet⁺ CD8⁺ T cells in **(B)** AW, **(C)** IST, **(D)** MV, and **(E)** spleen were enumerated on d13 after i.n. administration of OVA-PH/PIC, OVA-CT/PIC, OVA-PH, or OVA+PIC. **(F,G)** Number (#) of Tet⁺ CD8⁺ T cells expressing CD69±CD103 in **(F)** AW or **(G)** IST were enumerated on d13 after immunization. Data are mean ± SEM with *n* = 5 per group. Experiment was performed once. Immunization dose: 25 µg NP, 7 µg OVA, 0.8 µg poly(I:C). *p<0.05, **p<0.01, ***p<0.001, ****p<0.0001 by **(B-E)** ordinary one-way ANOVA or **(F,G)** ordinary two-way ANOVA with Tukey's multiple comparisons test.

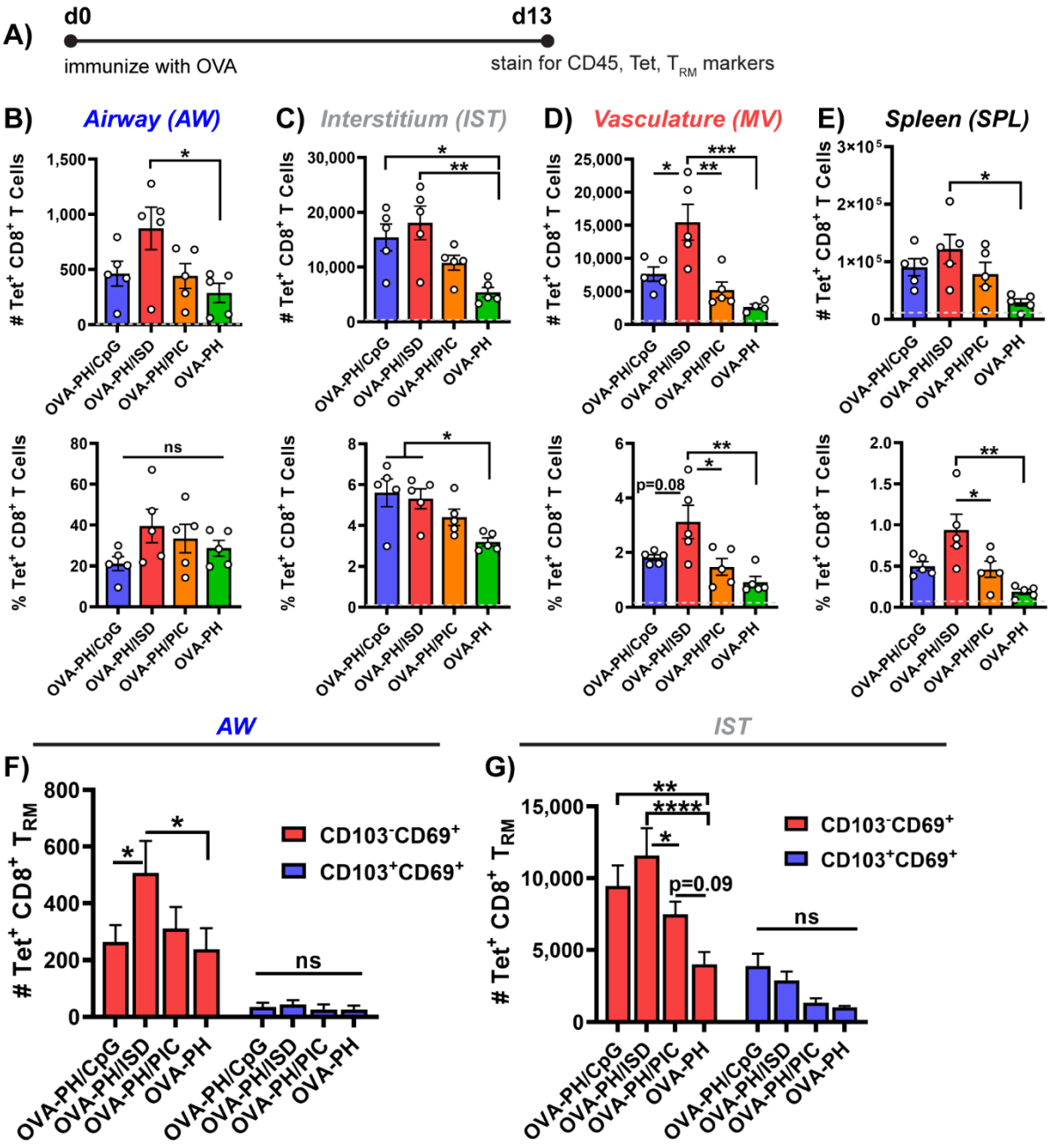

Figure 4.3 | Antigen-specific CD8⁺ T cells expressing T_{RM} markers are generated after immunization with agonists for distinct intracellular targets. (A) Mice were immunized i.n. with OVA-containing formulations on d0 and BAL, lungs, and spleens were analyzed on d13 *via* tetramer and surface marker staining. CD45 was used to differentiate cells in IST *vs*. MV, and CD103/CD69 were used as markers of T_{RM} cells. **(B-E)** Number (#) and frequency (%) of Tet⁺ CD8⁺ T cells in **(B)** AW, **(C)** IST, **(D)** MV, and **(E)** spleen were enumerated on d13 after i.n. administration of OVA-PH/CpG, OVA-PH/ISD, OVA-PH/PIC, or OVA-PH. **(F,G)** Number (#) of Tet⁺ CD8⁺ T cells expressing CD69±CD103 in **(F)** AW or **(G)** IST were enumerated on d13 after immunization. Data are mean ± SEM with *n* = 5 per group. Experiment was performed once. Immunization dose: 25 µg NP, 7 µg OVA, and 1.07 µg CpG or 1.04 µg ISD or 0.8 µg poly(I:C). *p<0.05, **p<0.01, ***p<0.001, ****p<0.0001 by **(B-E)** ordinary one-way ANOVA or **(F,G)** ordinary two-way ANOVA with Tukey's multiple comparisons test. ns, not significant.

Effect of adjuvant and nanoparticle carrier on formation of T_{RM} at a memory timepoint

We next performed similar experiments at 30 days after immunization, a true "memory" timepoints. As we have previously studied the effect of CpG adjuvant in this context (Aim 2), here we chose to focus on ISD and PIC in two separate cohorts of mice.

In the first cohort, mice were immunized i.n. on d0 with OVA-PH/ISD, OVA-CT/ISD, OVA-PH, OVA-CT or PBS. On d30 after immunization, lungs and spleens were collected and processed for staining with tetramer and surface marker antibodies, as described previously. At this timepoint, CXCR3 was used as marker of airway residence, rather than physically collecting airway fluid *via* lavage (**Figure 4.4A**). At this timepoint, the benefit of ISD appears to be diminished. There was no significance among any groups in the AW (**Figure 4.4B**); in the IST, both OVA-PH/ISD and OVA-PH were significantly better than OVA-CT, but were no different from each other (**Figure 4.4C**). The enhanced response in the MV due to ISD and/or CT polymer was not observed here (**Figure 4.4D**), although OVA-CT/ISD did generate a significantly higher response in the spleen (**Figure 4.4E**). Interestingly, in the AW, OVA-PH without adjuvant appeared to be superior for generating both phenotypes of TRM (**Figure 4.4F**). In the IST, both OVA-PH/ISD and OVA-PH produced significantly more $CD103^-CD69^+$ T_{RM} than either CT group (**Figure 4.4G**); for the $CD103^+CD69^+$ phenotype there were no significant differences, but this general trend did hold. Thus, it appears that although immunization with OVA-PH/ISD at d13 produces comparable or better antigen-specific $CD8^+$ T_{RM} responses in the IST and MV relative to OVA-NP/CpG, this benefit is not maintained through d30 after immunization. At this memory timepoint, adjuvant-free immunization with OVA-PH was equally as effective as OVA-PH/iSD.

In the second cohort, mice were immunized i.n. on d0 with OVA-PH/PIC, OVA-CT/PIC, OVA-PH, OVA-CT, OVA+PIC, or PBS. On d30 after immunization, lungs and spleens were collected and processed for staining with tetramer and surface marker antibodies (**Figure 4.5A**). In the AW, OVA-PH/PIC produced a significantly higher response than OVA-CT/PIC but was not higher than any other gorup (**Figure 4.5B**). In the IST, OVA-PH/PIC trended highest, but the difference was only significant relative to OVA-CT and OVA+PIC (**Figure 4.5C**). Interestingly, we again saw the effect of the CT polymer enhancing the response in the in the MV, although the presence of PIC adjuvant did not seem to impact this (**Figure 4.5D**). This trend remained in the spleen, and although differences were not significant in terms of cell count (#), they were significant for frequency (%) (**Figure 4.5E**). Regarding T_{RM}, again OVA-PH/PIC and OVA-PH produced significantly higher numbers of $CD103^-CD69^+$ T_{RM} in both the AW (**Figure 4.5F**) and IST (**Figure 4.5G**), indicating that pH-responsiveness is critical while PIC adjuvancy seems not to contribute. There were no significant differences between groups in the $CD103^+CD69^+$ phenotype, but OVA-PH/PIC did produce the highest response in the IST. This suggests that the presence of adjuvant may encourage expression of CD103; further studies would be needed to confirm this.

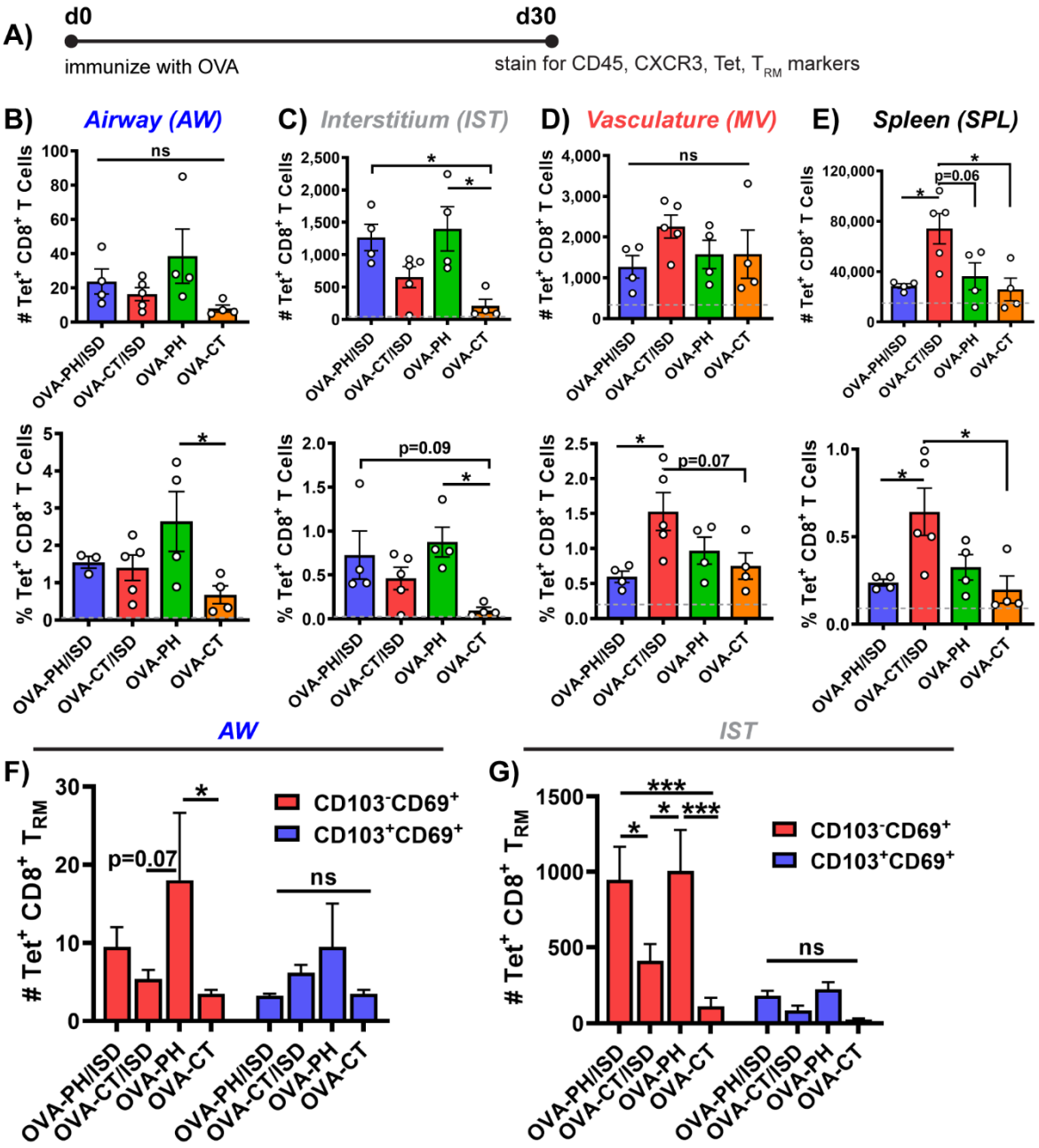

Figure 4.4 | Antigen-specific CD8⁺ T_{RM} are generated after immunization with nanoISD adjuvant. **(A)** Mice were immunized i.n. with OVA-containing formulations on d0 and lungs and spleens were analyzed on d30 *via* tetramer and surface marker staining. CD45 was used to differentiate cells in IST *vs*. MV, CXCR3 was used as a marker of airway residence, and CD103/CD69 were used as markers of T_{RM} cells. **(B-E)** Number (#) and frequency (%) of Tet⁺ CD8⁺ T cells in **(B)** AW, **(C)** IST, **(D)** MV, and **(E)** spleen were enumerated on d30 after i.n. administration of OVA-PH/ISD, OVA-CT/ISD, OVA-PH, or OVA-CT. **(F,G)** Number (#) of Tet⁺ CD8⁺ T cells expressing CD69±CD103 in **(F)** AW or **(G)** IST were enumerated on d30 after immunization. Data are mean ± SEM with *n* = 4-5 per group. Experiment was performed once. Immunization dose: 25 µg NP, 7 µg OVA, and 1.04 µg ISD. *p<0.05, ***p<0.001 by **(B-E)** ordinary one-way ANOVA or **(F,G)** ordinary two-way ANOVA with Tukey's multiple comparisons test. ns, not significant.

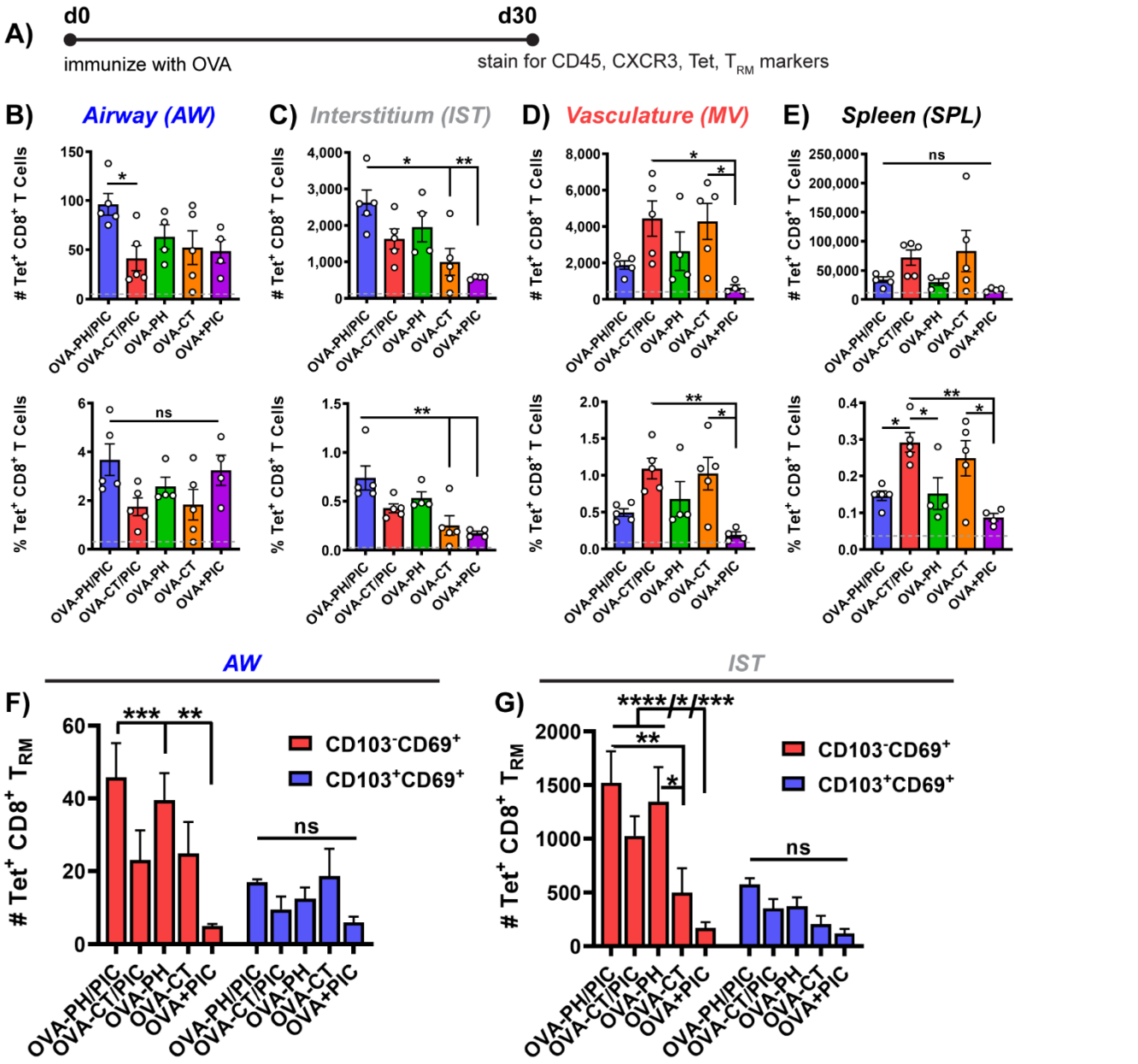

Figure 4.5 | Antigen-specific CD8⁺ T_{RM} are generated after immunization with poly(I:C) adjuvant. **(A)** Mice were immunized i.n. with OVA-containing formulations on d0 and lungs and spleens were analyzed on d30 *via* tetramer and surface marker staining. CD45 was used to differentiate cells in IST vs. MV, CXCR3 was used as a marker of airway residence, and CD103/CD69 were used as markers of T_{RM} cells. **(B-E)** Number (#) and frequency (%) of Tet⁺ CD8⁺ T cells in **(B)** AW, **(C)** IST, **(D)** MV, and **(E)** spleen were enumerated on d30 after i.n. administration of OVA-PH/PIC, OVA-CT/PIC, OVA-PH, OVA-CT, or OVA+PIC. **(F,G)** Number (#) of Tet⁺ CD8⁺ T cells expressing CD69±CD103 in **(F)** AW or **(G)** IST were enumerated on d30 after immunization. Data are mean ± SEM with *n* = 4-5 per group. Experiment was performed once. Immunization dose: 25 µg NP, 7 µg OVA, and 0.8 µg ISD. *p<0.05, **p<0.01, ***p<0.001, ****p<0.0001 by **(B-E)** ordinary one-way ANOVA or **(F,G)** ordinary two-way ANOVA with Tukey's multiple comparisons test. ns, not significant.

Effect of adjuvant and nanoparticle carrier on antigen uptake and activation of antigen-presenting cells in the lungs and lung-draining lymph node

Finally, we asked whether delivery of antigen and adjuvant with the pH-responsive polymer might differentially activate dendritic cell subsets depending on the nature of the adjuvant. To do this, we designed a flow cytometry panel to identify three DC subsets in the lungs and lung-draining lymph node (dLN). Conventional DCs (cDC) are defined by their expression of CD11c and MHC-II, while plasmacytoid DCs are defined by low expression of CD11c and high expression of CD317, or PDCA-1 (plasmacytoid dendritic cell antigen).[200] Conventional DCs can be divided into two subsets based on whether or not they typically cross-present antigen: cDC1 are cross-presenters and express XCR1, while cDC2 typically do not cross-present antigen and express SIRPα. cDC1 and cDC2 are often referred to as $CD103^+$ DCs and $CD11b^+$ DCs, respectively. While cDC1 cells are the subset most likely to be involved with formation of tissue-resident memory, it is also important to study the effects of adjuvants on other subsets as well; perhaps a particular adjuvant might be able to "convert" a DC subset not normally involved in T_{RM} formation into one that can enhance the T_{RM} response.

To investigate this, we immunized mice i.n. with pH-responsive formulations containing fluorescent antigen (OVA_{647}) and either CpG, ISD, or PIC adjuvant. LPS (10 μg) and PBS were administered as positive and negative controls, respectively. After 24 h, lungs and dLNs were harvested and processed for analysis of antigen uptake and activation marker expression (CD86/CCR7) in cDC1, cDC2, and pDC subsets. Cells were identified according to the gating strategy shown in **Figure C.6**. In the lungs, OVA uptake did not appear to vary much by cell type or adjuvant, although OVA uptake was highest in cDC2 in mice immunized with PIC (**Figures 4.6A and C.7A**). In the dLN, there was a much greater frequency of OVA^+ cells in the cDC1 subset for all adjuvants; this is likely because cDC1 are a migratory subset and so would be expected to outnumber cDC2 and pDC in this location (**Figures 4.7A and C.7B**). In the lungs, median fluorescent intensity (MFI) of OVA in OVA^+ cells was highest in pDC for all adjuvants (**Figures 4.6B and C.7C**); in the LN there was little difference, although OVA MFI was higher in the CpG group for cDC1 relative to the other cell types (**Figures 4.7B and C.7D**). In the lungs, all adjuvants enhanced CD86 expression relative to the positive control in cDC1, but no particular adjuvant stood out as best; in cDC2 and pDC, CpG appeared to be superior in stimulating CD86 expression (**Figure 4.6C,D**). CCR7 expression was negligible in the lungs for all cell subsets, as compared to both positive and negative controls (**Figure C.7E**). This was expected, as CCR7 is a migratory molecule and so cells expressing it have likely left for the dLN at this timepoint. Indeed, CCR7 expression was enhanced relative to the positive control in cells in the dLN (**Figure 4.7D,F**). In the CpG group, cDC1 had the highest CCR7 expression, whereas PIC appeared to boost its expression in the cDC2 subset comparably to that in cDC1 (**Figure 4.7D**). ISD drastically increased CCR7 expression in the pDC subset (**Figure 4.7F**). ISD and PIC stimulated greater expression of CD86 in cDC1 cells than

did CpG (**Figure 4.7C,E**). The results of these experiments demonstrate that further investigation is necessary to determine the effects of different adjuvants on uptake and activation in pulmonary dendritic cells subsets. In particular, delivery with PH vs. CT polymers should be compared to determine the degree to which pH-responsiveness drives uptake, and whether this has a significant effect on downstream activation, migration to the LN, and cross-presentation.

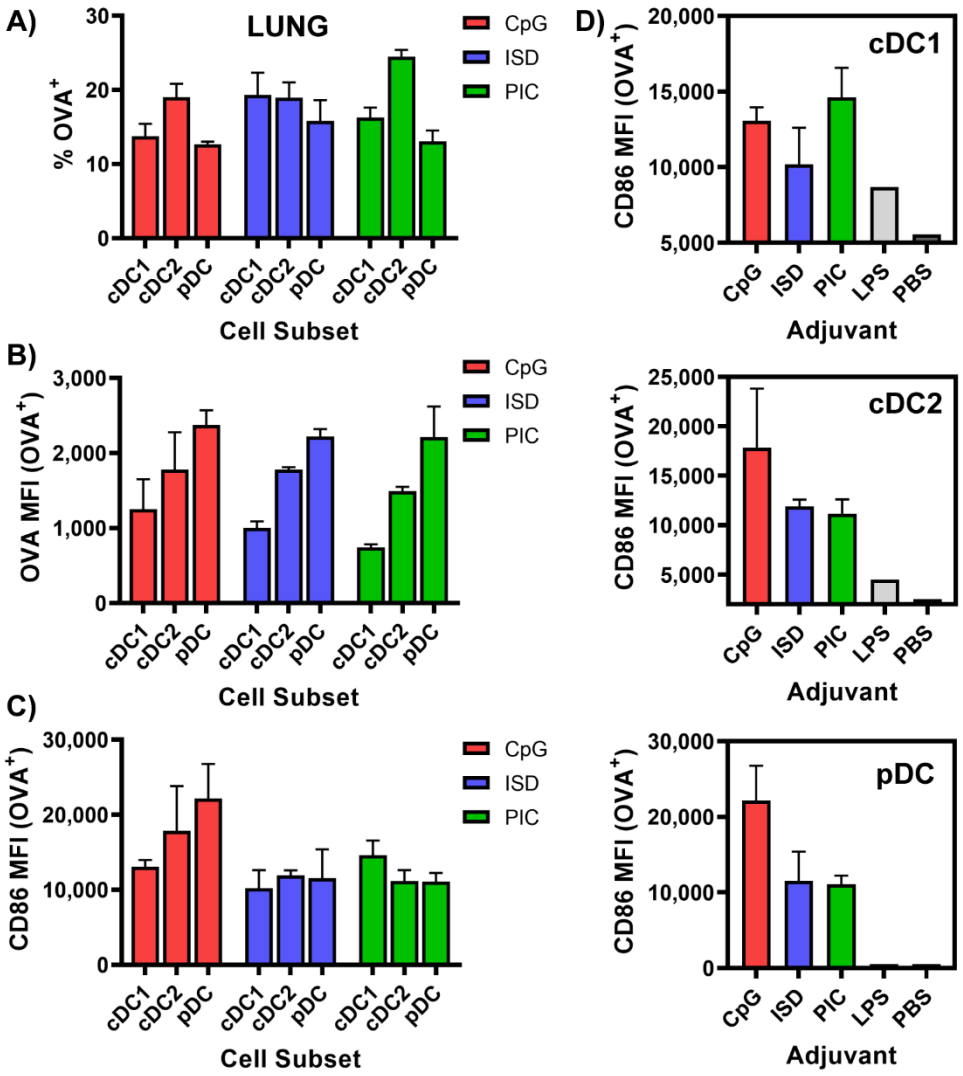

Figure 4.6 | Effects of adjuvant on uptake and activation in pulmonary dendritic cells. Mice were immunized i.n. with OVA_{647}-PH conjugates formulated with CpG, ISD, or PIC adjuvants, and lungs were harvested after 24 h. **(A)** Uptake of OVA_{647} (% OVA^+) cells in lung DC subsets. **(B)** Median fluorescence intensity (MFI) of OVA_{647} in OVA^+ cells. **(C)** MFI of CD86 in OVA^+ cells. **(D)** MFI of CD86 in individual lung DC subsets. *n* = 1-2 per group. Experiment was performed once.

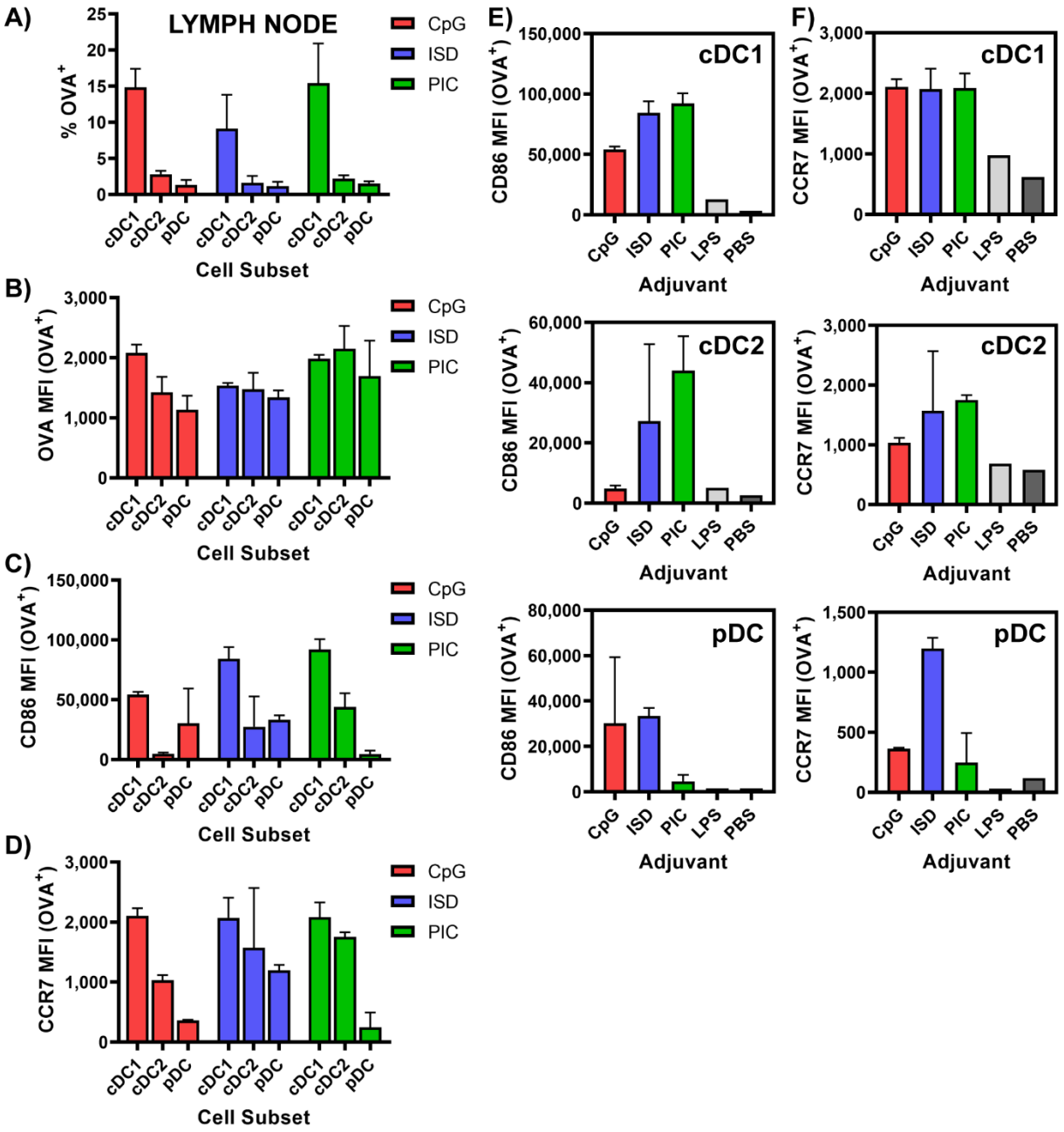

Figure 4.7 | Effects of adjuvant on uptake and activation in lymph node dendritic cells. Mice were immunized i.n. with OVA_{647}-PH conjugates formulated with CpG, ISD, or PIC adjuvants, and lung-draining lymph nodes (dLN) were harvested after 24 h. **(A)** Uptake of OVA_{647} (% OVA^+) cells in dLN DC subsets. **(B)** Median fluorescence intensity (MFI) of OVA_{647} in OVA^+ cells. **(C)** MFI of CD86 in OVA^+ cells. **(D)** MFI of CCR7 in OVA^+ cells. **(E)** MFI of CD86 in individual dLN DC subsets. **(F)** MFI of CCR7 in individual dLN DC subsets. *n* = 1-2 per group. Experiment was performed once.

4.4 Conclusion

The exact role that various APC subsets play in the development of T_{RM} remains unclear; for example, Iborra *et al*. showed that DNGR-1$^+$ cDC1 cells were necessary for T_{RM} formation in the skin and lungs after infection, whereas Dunbar *et al*. showed DCs were dispensable in lung T_{RM} formation after influenza infection, while monocytes played a central role.[47, 186] Similarly, while Macdonald *et al*. appeared to harness activation of alveolar macrophages to promote a T_{RM} response in the lungs, Goplen *et al*. demonstrated that alveolar macrophages acted as negative regulator to limit formation of CD8$^+$ T_{RM} in the lungs.[72, 201] Therefore, it is critical that tools such as the pH-responsive and control nanoparticles described here be used to probe the relationships between innate immune cell activation and T_{RM} formation. Here, we begin to show that different adjuvants might have distinct effects on expression of activation markers (CD86 and CCR7) in DC in the lungs and dLN, but further studies are needed to confirm this and to elucidate the role of pH-responsiveness in this phenomenon. Other cell subsets, such as monocytes and macrophages, should also be studied. In future experiments, it is possible that varying the degree of pH-responsiveness could be used to modulate levels of adjuvant delivery to distinct intracellular locations (endosome/cytosol). Adjuvant or polymer combinations may prove useful for generating a more holistic immune response; for example, PH nanoparticles might be used to generate tissue-resident immunity while CT nanoparticles support systemic immunity in the vasculature and spleen (**Figures 4.2 and 4.3**) Also, it is yet unknown how the pH-responsive activity of the polymer, or lack thereof, might affect the CD4$^+$ T cell response.

While nanoISD and poly(I:C) adjuvants were able to generate CD8$^+$ T_{RM} in the lungs at both short-term and long-term timepoints, it is still unclear whether these adjuvants are superior to either OVA-PH alone or the “gold standard” of CpG. Further studies comparing these adjuvants on both pH-responsive and control particles are warranted to more fully characterize the effect of each adjuvant on the T_{RM} response. It should be noted that, since CD69 is also a T cell activation marker, the presence of CD69 but not CD103 on many CD8$^+$ T cells detected at the 13-day timepoint may simply indicate T cell activation and not tissue-resident memory; however, since CD69 expression was much higher on tissue-resident cells in the lung interstitium relative to non-resident cells in the lung vasculature (**Figure C.5**), this suggests the cells in the IST at this timepoint are indeed destined to be T_{RM}. Further studies are needed to elucidate the kinetics of T_{RM} formation and differentiation after immunization with this nanoparticle vaccine. Overall, this aim lays the foundation for further studies assessing the role of adjuvant and material properties on innate immune cell activation and the downstream T_{RM} response.

4.5 Materials and Methods

RAFT Synthesis of (PDSMA-*co*-DMAEMA)-*b*-(PAA-*co*-DMAEMA-*co*-BMA). RAFT copolymerization of pyridyl disulfide ethyl methacrylate (PDSMA) and dimethylaminoethyl methacrylate (DMAEMA) was conducted under a nitrogen atmosphere in dioxane (40 wt % monomer) at 30 °C for 18 h, as previously described.[50] PDSMA monomer was synthesized according to a previously reported procedure.[163] The RAFT chain transfer agent (CTA) used was 4-cyano-4-(ethylsulfanylthiocarbonyl)sulfanylpentanoic acid (ECT) and the initiator used was 2,2'-azobis(4-methoxy-2,4-dimethylvaleronitrile) (V-70) (Wako Chemicals, Richmond, VA). The initial molar ratio of DMAEMA to PDSMA was 92:8, and the initial monomer ($[M]_0$) to CTA ($[CTA]_0$) to initiator ($[I]_0$) ratio was 100:1:0.05. The resultant poly(PDSMA-*co*-DMAEMA) macro-chain transfer agent (mCTA) was isolated by precipitation (6×) into pentane. A schematic of the mCTA polymerization reaction can be found in **Figure A.1A**.

Purified mCTA was dried *in vacuo* for one week and used for block copolymerization with DMAEMA, propylacrylic acid (PAA), and butyl methacrylate (BMA) to create a pH-responsive polymer, as described previously.[50, 164] DMAEMA (30%), PAA (30%), and BMA (40%) ($[M]_0/[mCTA]_0 = 450$) were added to the mCTA dissolved in dimethylacetamide (DMAc) (40 wt % monomer and mCTA) along with V-70 initiator ($[mCTA]_0/[I]_0 = 2.5$). Polymerization took place under a nitrogen atmosphere for 24 h at 30 °C. The resultant diblock copolymer was isolated by dialysis against acetone using a 3.5 kDa MWCO membrane, followed by dialysis against deionized water. The purified diblock copolymer was lyophilized for 72 h prior to use. A schematic of the pH-responsive polymerization reaction can be found in **Figure A.1B**. Polymer composition, monomer conversion, and molecular weight of the diblock copolymer were characterized by ^{1}H NMR spectroscopy ($CDCl_3$) on a Bruker AV400 spectrometer (**Figure C.1A**). Characterization was done according to previously published methods.[50]

RAFT Synthesis of (PDSMA-*co*-DMAEMA)-*b*-(BMA). Purified mCTA used for the synthesis described above was also used for block copolymerization with poly(butyl methacrylate) (pBMA) to create a non-pH-responsive control polymer. Monomer was added to mCTA ($[M]_0/[mCTA]_0 = 300$) and dissolved in dioxane (40 wt % monomer and mCTA) along with V-70 initiator ($[mCTA]_0/[I]_0 = 20$), then polymerized under a nitrogen atmosphere for 24 h at 35 °C. The resultant diblock copolymer was isolated by dialysis as described above. The purified polymer was then lyophilized, and its composition and molecular weight were analyzed using ^{1}H NMR ($CDCl_3$) spectroscopy (**Figure C.1B**), according to previously published methods.[165] The control polymerization reaction can be seen in **Figure A.1C**.

Preparation and Characterization of Nanoparticles. Self-assembled micellar nanoparticles (NP) were obtained by first dissolving lyophilized polymer at 50 mg/ml in 100% ethanol, then rapidly pipetting dissolved polymer into 100 mM phosphate buffer (pH 7) to a final concentration of either 10 mg/ml (pH-responsive polymer) or 5 mg/ml (control polymer). For *in vivo* studies, ethanol was removed by buffer exchange into PBS (pH 7.4) *via* 3 cycles of centrifugal dialysis (Amicon, 3 kDa MWCO, Millipore), and NP solutions were then sterilized *via* syringe filtration (Whatman, 0.22 µm, GE Healthcare). Final polymer concentration was determined with UV-Vis spectrometry (Synergy H1 Multi-Mode Reader, BioTek) by measuring absorbance of aromatic PDS groups at 280 nm. Size of the NP was measured *via* dynamic light scattering (DLS). NP solutions were prepared at a concentration of 0.1-0.2 mg/ml in PBS (pH 7.4) and the hydrodynamic radius was measured using a Malvern Instruments Zetasizer Nano ZS Instrument (Malvern, USA). Representative DLS data for both polymers at physiological pH (7.4) can be found in **Figure C.1C-E**.

Preparation of Antigen-Nanoparticle Conjugates. A model antigen, ovalbumin protein (OVA), was conjugated to pendant PDS groups on NP *via* thiol-disulfide exchange. For conjugate characterization and *in vivo* studies, endotoxin-free (<1 EU/mg) EndoFit™ OVA (Invivogen) was used. In some experiments, OVA was labeled with Alexa Fluor 647-NHS ester for evaluating conjugation efficiency *via* fluorescent imaging of SDS-PAGE gels, or for tracking conjugates after *in vivo* administration. Following manufacturer's instructions, dye was added to OVA for a degree of labeling of ~0.5 AF647/OVA.

To prepare OVA for conjugation, free amines on the protein were thiolated by incubation with ~25 molar excess of 2-iminothiolane (Traut's Reagent, Thermo Fisher Scientific) in reaction buffer (100 mM phosphate buffer, pH 8, supplemented with 1 mM EDTA) as previously described.[50] Unreacted 2-iminothiolane was removed by buffer exchanging thiolated OVA into 1X PBS (pH 7.4) using Zeba™ Spin desalting columns (0.5 ml, 7 kDa MWCO, Thermo Fisher Scientific). For *in vivo* studies, thiolated OVA was sterilized *via* syringe filtration (0.22 µm, Millipore). Following manufacturer's instructions, the molar ratio of thiol groups to OVA protein was determined with Ellman's reagent (Thermo Fisher Scientific) to be ~3-5 thiols/OVA. Polymer NP solutions were reacted with thiolated OVA at a molar ratio of 5.1:1 (pH-responsive NP:OVA) or 3.85:1 (control NP:OVA) to make OVA-PH and OVA-CT conjugates, respectively. The conjugation ratio for the control polymer was adjusted to maintain a constant dose of antigen for both carriers. Conjugation was done overnight, in the dark, at room temperature, and under sterile conditions (when needed), as previously described.[50] Antigen conjugation was verified *via* non-reducing SDS-polyacrylamide gel electrophoresis (SDS-PAGE) using 4-20% Mini-Protean TGX Precast Protein Gels (Bio-Rad) (**Figure C.2A**). Gels were run at 130 V for 1 h and imaged with an IVIS Lumina III Imaging System (PerkinElmer, Waltham, MA). DLS was used to measure the size of OVA-NP conjugates, as described above (**Figure C.2B,C**).

Formation of Nanoparticle/Adjuvant Complexes. NP/adjuvant complexation was carried out by combining CpG ODN 1826 (Invivogen), nanoISD (formulated in-lab), or low-molecular weight poly(I:C) (PIC; Invivogen) with PH, CT, OVA-PH, or OVA-CT in PBS at room temperature for at least 30 min. Theoretical charge ratios (+/-) of 6:1, 8:1, and 12:1 were tested for complexation with PH; ratios of 5:1, 7:1, and 10:1 were tested for complexation with CT. The charge ratio was defined as the molar ratio between protonated DMAEMA tertiary amines in the first block of the copolymer (positive charge; assuming 50% protonation at physiological pH) and phosphate groups on the nucleic acid backbone (negative charge).[50] CpG was considered to have 20 negative charges; ISD had 190 negative charges, and PIC had an average of 1200 negative charges. The charge ratios at which complete complexation of adjuvant to the polymer occurred were determined *via* an agarose gel retardation assay (**Figure 4.1A,B**). Formulations prepared at various charge ratios were loaded into lanes of a 4% agarose gel and run at 90 V for 30 min. Gels were stained with SYBR Safe DNA Gel Stain (Thermo Fisher Scientific) for 30 min and visualized with a Gel Doc™ EZ System (Bio-Rad). A charge ratio of ~6:1 (PH) or ~5:1 (CT) was used for all *in vivo* formulations in order to maximize the stability of the formulation and maintain consistent adjuvant doses. DLS was used to measure the size of the formulations (**Figure 4.1C,D**), as described above.

Animals. Female C57BL/6J mice were purchased from the Jackson Laboratory (Bar Harbor, ME), maintained at the animal facilities of Vanderbilt University under either conventional conditions, and experimented upon in accordance with the regulations and guidelines of Vanderbilt University Institutional Animal Care and Use Committee (IACUC).

Immunization. Endotoxin-free OVA (<1 EU/mg, EndoFit™), sterile buffer solutions (1X PBS, pH 7.4), and sterile polymer solutions with ethanol removed were used for vaccine formulations. Mice were immunized with either pH-responsive NP (PH) or control NP (CT) formulated with OVA and with or without either CpG, ISD, or PIC adjuvants. Conjugates were prepared 1-2 days before use and stored at 4 °C. OVA was thiolated and used immediately for conjugation to NP at a molar ratio of 5.1:1 or 3.85:1 (NP:OVA), as described above. On the day of use, CpG, ISD, or PIC was complexed to conjugates at a 6:1 or 5:1 charge ratio *via* rapid pipetting of adjuvant (~0.5 mg/ml) into the conjugate solution, as described above. The formulation was allowed to react for at least 30 min at room temperature for complete complexation of adjuvant before administration to mice.

Female mice (8-10 weeks old) were anesthetized with ketamine/xylazine (10 mg/ml ketamine hydrochloride, Vedco; 1 mg/ml xylazine hydrochloride, Vanderbilt Pharmacy) by i.p. injection (~200 µl anesthesia/22 g mouse weight). Anesthetized mice were immunized i.n. on day 0 with formulations containing 7 µg OVA, 25 µg polymer, and 1.07 µg CpG or 1.04 µg ISD or 0.8 µg PIC. Vaccine

formulations in a total volume of 75 µl PBS were delivered *via* pipette through the nostrils into the lungs of mice; inoculation with this volume allows formulations to reach the lower airways.[167] The dose was applied drop-wise at the center of the nose to allow inhalation into both nostrils at a rate of ~4 µl/s. Animals were monitored either daily or thrice weekly for weight loss and signs of morbidity.

Measurement of Antigen-Specific CD8$^+$ T Cell Responses and T_{RM} Markers. On day 13 or day 30 after immunization, mice were anesthetized and intravenously (i.v.) injected with 200 µl of anti-CD45.2-APC antibody (clone 104; Tonbo) at 0.01 mg/ml (2 µg αCD45 antibody per mouse), as previously described.[66] This was done to stain marginated vascular leukocytes (MV; CD45$^+$) and differentiate them from those resident in the lung interstitium (IST; CD45$^-$).[44] To allow for circulation of αCD45 antibody, mice were rested for 3-5 min after i.v. injection and prior to CO_2 euthanasia. For experiments done at day 13, prior to organ harvest, lungs of euthanized mice were flushed with ~1 ml of PBS to collect broncheoalveolar lavage fluid (BAL) from the airway compartment (AW) while maintaining IST and MV populations in the lung parenchyma. For experiments done at day 30, lungs were not lavaged and CXCR3 was used as a marker of airway residence.[66] Lungs and spleens were then harvested and processed as previously described.[168] Briefly, lungs were minced with a scalpel and incubated for 1 h at 37 °C in complete RPMI medium (cRPMI [RPMI+10% FBS]; Gibco) supplemented with 2 mg/ml collagenase (Sigma) and 50 nM dasatinib (LC Laboratories, Woburn, MA). Lungs and spleens were treated with ACK lysing buffer (Gibco) and passed through 70 µm cell strainers to generate single cell suspensions.

Cell suspensions from BAL, lungs, and spleens were stained for 1 h at 4 °C with anti-B220-FITC (clone RA3-6B2; BD Biosciences), anti-CD4-FITC (clone H129.19; BD Biosciences), anti-CD11b-FITC (clone M1/70; Tonbo), anti-CD11c-FITC (clone N418; Tonbo), anti-CD8α-Pacific Blue (clone 53-6.7; BD Biosciences), and 1.5 µg/ml PE-labeled $OVA_{257-264}$ (SIINFEKL)-H-2K^b tetramer (Tet) prepared according to a previously reported procedure.[169] Antibodies labeled with FITC (B220/CD4/CD11b/CD11c) were referred to as the "dump" channel and were used to exclude B cells, CD4$^+$ T cells, dendritic cells, and macrophages from gating. Staining with anti-CXCR3-PerCP/Cy5.5 (clone CXCR3-173; BioLegend) was used to define CD8$^+$ T cells resident in the airways (CXCR3^{hi}) vs. interstitium (CXCR3^{lo}).[66] To measure tissue-resident memory markers, cells from lungs and spleens were also stained with anti-CD69-PE/Cy7 (clone H1.2F3; Tonbo) and anti-CD103-Brilliant Violet 510 (clone 2E7; BioLegend).

After staining, cells were washed with FACS buffer (PBS supplemented with 2% FBS and 50 nM dasatinib) and stained with Ghost Red 780 (Tonbo) to discriminate live *vs.* dead cells. AccuCheck counting beads (Thermo Fisher Scientific) were included in samples to allow for calculation of absolute cell counts. The frequency of antigen-specific CD8$^+$ T cells was determined using a 3-laser LSR-II flow cytometer (BD). All data were analyzed using FlowJo Software (version 10.4.2; Tree Star, Inc., Ashland,

OR). Cells were gated by forward and side scatter to exclude debris and doublets. Viable antigen-specific $CD8^+$ T cell populations were defined as follows: AW = $CD8\alpha^+CD45^-Tet^+$ cells in BAL samples (or $CXCR3^{hi}$ in lung samples); IST = $CD8\alpha^+CD45^-Tet^+$ cells in lung samples (sometimes also $CXCR3^{lo}$); MV = $CD8\alpha^+CD45^+Tet^+$ cells in lung samples; SPL = $CD8\alpha^+Tet^+$ cells in spleen samples. All cells in the $CD8\alpha^+$ gate were also $B220^-CD4^-CD11b^-CD11c^-$ ("dump channel"). Representative gating for each sample type can be found in **Figure A.4A-C**.

Uptake and Activation in Innate Immune Cells in the Lungs and Lymph Node. To identify the effects of various adjuvants delivered by the NP vaccine on innate immune cell uptake and activation in lungs and lung-draining lymph nodes (dLN), mice were immunized with fluorescently labeled OVA_{647}-PH/CpG, OVA_{647}-PH/ISD, OVA_{647}-PH/PIC, LPS (10 μg; positive control) or PBS (negative control). In the fluorescent formulations, OVA was labeled with Alexa Fluor 647 as described above (OVA_{647}). After 24 h, mice were euthanized and lungs and dLN were harvested. Lungs were processed as described above to obtain single-cell suspensions. Lymph nodes were gently pressed through a 70 μm strainer, collected, centrifuged, and resuspended in FACSB to create single-cell suspensions. Lung and dLN samples were stained for flow cytometric analysis of dendritic cell subsets using the following panel: **(1)** cross-presenting conventional dendritic cells (**cDC1**): $XCR1^+CD11c^+MHCII^+$; **(2)** non-cross-presenting conventional dendritic cells (**cDC2**): $SIRP\alpha^+CD11c^+MHCII^+$; **(3)** plasmacytoid dendritic cells (**pDC**): $CD317^+CD11c^{lo}$. These cell subsets were assessed for percentage of OVA uptake, MFI of OVA in OVA^+ cells, and expression of activation markers CD86 and CCR7. The following antibodies were used: anti-XCR1-PE (BioLegend; ZET), anti-CCR7-PE/Cy7 (BioLegend; 4B12), anti-SIRPα-PerCP/Cy5.5 (BioLegend; P84), anti-CD11c-APC/Cy7 (BD; HL3), anti-I-A/I-E-Alexa Fluor 488 (BioLegend; M5/114.15.2), anti-CD317-Brilliant Violet 650 (BioLegend; 927), and anti-CD86-Brilliant Violet 421 (BioLegend; GL-1). Ghost Dye™ Violet 510 (Tonbo) was used to discriminate live *vs.* dead cells. Samples were stained with viability dye for 30 min at 4 °C, washed with FACS buffer (PBS+2% FBS, 50 nM dasatinib), incubated with Fc-block (anti-CD16/CD32, clone 2.4G2; Tonbo) for 15 min at 4 °C, and then stained for 1 h at 4 °C with the antibody panel listed above. Finally, cells were washed once, resuspended in FACS buffer, and analyzed by flow cytometry. Data were collected using a 3-laser Fortessa (BD) and analyzed with FlowJo software (v.10.4.2). Representative gating for identification of cell subsets can be found in **Figure C.6**.

Statistical Analysis. Statistical analyses were performed as indicated in figure legends. All analyses were done using GraphPad Prism software, version 6.07. Results are expressed as mean ± SEM with ****$p < 0.0001$, ***$p < 0.001$, **$p < 0.01$, *$p < 0.05$ being considered statistically significant.

CHAPTER 5

Conclusion

5.1 Chapter Summaries

Prior to initiating this work, several outstanding research questions were established: can this pH-responsive polymer nanoparticle system be used for mucosal (intranasal) immunization and co-delivery of antigen and adjuvant to the lungs? If so, can it be used to generate $CD8^+$ T_{RM} cells in the lungs, and are these cells protective against challenge with respiratory viruses? And finally, how can the material and delivery properties of the nanoparticle carrier (i.e., pH-responsive activity and nature of adjuvants delivered) be utilized to tune the T_{RM} response? What is the connection between activation of innate immunity and downstream production of T_{RM} cells? Consequently, several specific aims were designed to address and answer these questions by combining principles of materials engineering and drug delivery with recent advances in the field of T_{RM} biology (**Figure 5.1**).

In the first aim of this dissertation (Chapter 2), we demonstrate that intranasal delivery of antigen and adjuvant with a pH-responsive nanoparticle delivery platform can enhance the magnitude and functionality of the lung tissue-resident $CD8^+$ T cell response. This is the first comprehensive characterization of this nanomaterial in the context of mucosal delivery, and represents an advance over the typical approach of systemic immunization. In addition, we show that particulate delivery can enhance both co-localization and retention of vaccine cargo in pulmonary innate immune cells, including key subsets such as cross-presenting $CD103^+$ dendritic cells, and that delivery with the nanoparticle stimulates an acute cytokine profile that may promote formation of tissue-resident memory T cells. Persistent antigen stimulation and an array of cytokines have been reported to be crucial in stimulating pulmonary T_{RM} immunity, and so this work demonstrates that the nanoparticle vaccine holds potential as a platform for generating protective T_{RM} responses. Importantly, its pH-responsiveness and capacity for dual-delivery are essential to its efficacy in this setting. In addition, the use of nanoparticle-based delivery platforms offers potential advantages, such dose-sparing, targeted delivery, improved antigen cross-presentation, and scale-up for manufacturing.

The second central hypothesis of this work (Chapter 3) was that the lung tissue-resident $CD8^+$ T cells generated by the nanoparticle vaccine were in fact T_{RM} cells that could mediate protection against challenge with respiratory pathogens. To investigate this, we utilized lethal and sublethal models of murine respiratory infection and, importantly, demonstrated protection against influenza A virus, a clinically relevant pathogen. Our work represents the first demonstration that this pH-responsive nanoparticle vaccine can confer significant protection against respiratory virus infection, and to our knowledge, is one of the only reports that accomplished this with a single dose of the vaccine. Tissue-

resident $CD8^+$ memory T cells expressing T_{RM} markers CD69 and CD103 were found in the lungs. Measurement of these markers, in combination with intravascular staining for tissue-residency, has enabled relationships between NP vaccine properties and generation of T_{RM} to be established.

The third portion of this work (Chapter 4) built upon previous observations of vaccine-induced DC activation in the lungs by further investigating the relationships between pH-responsive activity, adjuvant delivery, and T_{RM} formation. We demonstrated that multiple adjuvants with diverse physicochemical characteristics could be loaded onto both pH-responsive and control particles and delivered to dendritic cell subsets in the lungs and lymph nodes, where they promoted antigen uptake and APC activation. These adjuvant/polymer formulations also stimulated varying levels of $CD8^+$ T_{RM} in the lungs. Defining the T_{RM} response to a variety of mucosal adjuvants will help to inform future vaccine design approaches for generating tissue-resident T cell memory.

The work presented here has broad implications for the fields of materials science, immunoengineering, and vaccine development (**Figure 5.1**). We have demonstrated for the first time that the material property of a vaccine delivery platform has a direct effect on the generation of tissue-resident T cell memory. This paves the way for investigation of the ways in which other engineered materials can promote formation of this key memory subset. We have shown that, with a rational design approach, mucosal subunit vaccines can be created that are safe, immunogenic, and capable of producing $CD8^+$ T cells. This offers a potential avenue for delivery of mucosal adjuvants that are otherwise unsafe for use. Overall, the nanoparticle vaccine described here represents a platform technology with enormous potential for use in myriad immunotherapeutic applications.

5.2 Shortcomings

Overall, this work has demonstrated the ability of a pH-responsive nanoparticle vaccine to generate $CD8^+$ T_{RM} cells in the lungs and confer protection against infection with respiratory viruses. While this represents a significant contribution to the field of T_{RM}-focused vaccine design, there are also shortcomings to this work that warrant discussion.

First, although RAFT polymerization offers a controlled synthesis method for generation of replicable polymers with uniform size and polydispersity, the polymer carriers used here still present certain barriers to scale-up and translation.[202, 203] These polymers suffer from batch-to-batch variability, and we have observed the control polymer in particular appears to be quite sensitive to reaction time. Various batches of polymer made in the course of this work suffered from issues with formulation (crashing out) or sterilization (unable to pass easily through a syringe filter due to formation of large species). Although we were able to formulate both pH-responsive and control nanoparticles with diverse protein antigens and nucleic acid adjuvants, based on extensive characterization via dynamic light

scattering and gel assays, we did observe some differences in formulation stability for certain polymer batches and adjuvants. It is possible that heterogeneity between formulations may have affected resultant immune responses, introducing a confounding variable in our data. Greater optimization of the reproducibility of polymer synthesis would be needed before this vaccine platform could be scaled up for clinical use.

Toxicity of the nanoparticle vaccine might also present a barrier to clinical translation. Although we present data indicating the polymer was well-tolerated in mice, with quick recovery from weight loss, an acute and localized cytokine response, and minimal immunopathology in the lungs, it must be acknowledged that the safety requirements for prophylactic vaccines are much more stringent than those of other immunotherapies. Almost exclusively, healthy individuals are the ones to receive vaccines (including infants), and so even the slightest degree of toxicity will be unacceptable. Future iterations of this vaccine should attempt to eliminate weight loss entirely. In addition, while the nanoparticle vaccine was well-tolerated in mice, only a small dose could be used; larger doses of nanoparticle were found to be immediately lethal in dosing pilot studies. Thus, redesigning the polymer to mitigate toxicity, such as with a PEGylated outer layer, may be necessary for clinical translation.[204]

In addition, while an important advance of this work is the demonstration that mucosal delivery of the nanoparticle vaccine can generate T_{RM} cells, the method used here for intranasal immunization (instillation of liquid into the lungs) is not clinically feasible in humans. Ideally, future work will investigate the feasibility of formulating this vaccine as an aerosol. An advantage of aerosol formulations is that they can be administered without the use of needles, which offers the potential for increased patient compliance and improved vaccine availability in areas with a lack of trained healthcare workers.

Although this work extensively characterized the $CD8^+$ T_{RM} response to immunization, there remain additional experiments that can be done to unambiguously prove that the conferred protection is mediated by functional T_{RM} cells. While our choice of viruses for challenge experiments indirectly indicated that protection was facilitated by $CD8^+$ T cells, we have not ruled out that humoral or $CD4^+$ T cell immunity may also play a role—and indeed, it would likely be beneficial if they did. Often, a holistic immune response is preferable over one that engages a single arm of the immune system.[12] In other reports in the literature, techniques such as $CD8^+$/$CD4^+$ T cell depletion with antibodies, or treatment with FTY720, have been used to explicitly show that protection is mediated by T_{RM} cells. It will be important in the future to characterize the $CD4^+$ T cell response to this vaccine, particularly in the context of certain diseases such as tuberculosis. In addition, we only evaluated the T_{RM} response prior to infection; it may also be useful to characterize the recall response in the lungs after challenge, in order to further demonstrate functionality of the T_{RM} cells upon pathogen encounter.

Finally, many of the $CD8^+$ T_{RM} generated in the lungs by our vaccine lacked the adhesion molecule CD103. While this is not necessarily problematic, there is evidence that $CD103^+$ T_{RM} are

preferred for effective tumor immunity.[5] The lack of CD103 observed may be related to our inability to detect TGFβ after immunization, since this cytokine is required for CD103 expression. Indeed, in preliminary experiments with both prophylactic and therapeutic tumor models of metastatic lung cancer, we were surprised to find that our nanoparticle vaccine provided little benefit. It is possible that increasing the number of $CD103^+$ T_{RM} produced would improve its potential as a cancer vaccine.

5.3 Future Work

Additional studies building on the research described in this dissertation will further characterize the innate and adaptive immune responses elicited by the nanoparticle vaccine. With regard to adaptive immunity, while studying the $CD4^+$ T cell response to the vaccine was outside the scope of this dissertation, it will be important to characterize this in the future to obtain a more complete picture of the cellular response generated. Although $CD4^+$ T_{RM} are less well-characterized than $CD8^+$ T_{RM}, they do appear to play an important role in protective immunity against diseases like tuberculosis, for which an improved vaccine is greatly needed. It has previously been shown that this vaccine platform can stimulate an IFNγ-producing $CD4^+$ T cell response in the spleen, so it is likely to generate one in the lungs as well.[50] Demonstrating this would further support the platform's utility as a T_{RM} vaccine for diverse pathogens. Future studies examining the efficacy of the nanoparticle vaccine in other models of infection, including Mtb, are also warranted. In addition, since $CD103^+CD8^+$ T_{RM} play a critical role in cancer immunity, this vaccine may also be studied in models of mucosal tumors.

In the work presented here, $CD8^+$ T_{RM} in the lungs presented both $CD103^+$ and $CD103^-$ phenotypes. While a lack of CD103 expression may not be detrimental, $CD103^+$ T_{RM} have been reported to improve responses to both influenza infection and cancer.[5, 22] Therefore, strategies to increase the expression of CD103 on vaccine-induced T_{RM} may warrant investigation. In particular, it is well-established that TGFβ signaling is central to CD103 induction, and we were not able to detect TGFβ in the lungs, airways, or serum at several timepoints after immunization (data not shown). It is possible that we either need to look at different timepoints or use a more sensitive method of detection. If further studies still cannot detect this cytokine, strategies to increase TGFβ production by the nanoparticle vaccine may be pursued; however, because TGFβ is involved in an enormous variety of cell signaling pathways and disease states, it is likely further clarity on the precise role of TGFβ in T_{RM} formation will be needed before this can be accomplished. Perhaps direct delivery of TGFβ in conjunction with the vaccine could be considered.

While the work in this dissertation focused primarily on the immune response in the lungs, it will be important for future studies to also assess immune activity in the mediastinal (lung-draining) lymph node. In particular, since cross-presenting DCs are an important cell type in generating T_{RM} responses,

future studies should examine the effects of various adjuvant and polymer combinations on antigen cross-presentation in this LN. This has been previously accomplished *in vivo* after OVA immunization using an antibody for H-2K^b/SIINFEKL.[205] Because the pH-responsive property of the polymer used acts as a "substitute" for natural cross-presentation mechanisms to deliver antigen to the cytosol, it is unclear whether use of this polymer as a vaccine mitigates the importance of natural cross-presenting DCs in T_{RM} formation. Perhaps it supplements cross-presentation by these DCs, or it boosts the ability of non-cross-presenting DCs to elicit T_{RM}. Batf3-knockout mice, which lack cross-presenting DCs, may be used as a tool to study the relative contributions of natural cross-presenting mechanisms and pH-responsive activity to the resulting T_{RM} response after nanoparticle vaccination.

While cross-presenting DCs are often cited as the most important cell type for generation of T_{RM}, recently other innate immune cells have been implicated in this process as well. Namely, monocytes may promote tissue-resident T cell formation, and macrophages may positively or negatively regulate it.[72, 185, 201] Future work would benefit from more closely studying uptake and activation in these cell types along with DCs, and the ways in which material and adjuvant properties can regulate the activity of each of these cell types. In addition, further characterization of the cytokines produced and innate immune pathways activated by nanoparticle-mediated delivery of various adjuvants may help inform the choice of adjuvants or synergistic adjuvant combinations that can activate the appropriate innate immune cells and promote a T_{RM} response.

A driving hypothesis behind the comparison of pH-responsive and control carriers in Aim 3 was the idea that altering the pH-responsiveness of the polymer can modulate delivery of adjuvants to distinct intracellular compartments. For example, a highly pH-responsive polymer may increase delivery to the cytosol, while a low degree of pH-responsiveness may favor endosomal delivery. Future work should build on this by synthesizing a library of polymers with varying degrees of pH-responsiveness (*e.g.*, high/medium/low, rather than simply on/off as was done in Aim 3) and using them to deliver adjuvants that localize to different targets in the cell. Showing a connection between this and the downstream T_{RM} response would further support the notion that material properties can be used to modulate tissue-resident immunity.

Finally, in Aim 3, we observed an unusual phenomenon: the control polymer appeared to be superior at generating a CD8$^+$ T cell response in the lung vasculature, while it is generally ineffective at eliciting lung-tissue resident CD8$^+$ T cells. It would be interesting to investigate the reason for this. It could perhaps be due to the less cationic nature of the control polymer making it less mucoadhesive and better able to enter the vasculature. It could also be related to the size of the nanoparticle—in the experiments where this phenomenon was observed, DLS sometimes showed control polymer formulations to be slightly larger than pH-responsive formulations. This might impact localization of the vaccine or the cell populations it interacts with. The polymer itself might also have intrinsic immune

activating effects. Thus, this “control” material might offer potential usefulness in other vaccine applications outside of generating T_{RM} cells.

With regard to the future of nanoparticle technologies for T_{RM} vaccines, several approaches may be taken to tune and improve the immune response, including the use of adjuvant combinations to activate specific innate immune signals and generate a cytokine milieu supportive of T_{RM} cells; the use of targeting strategies to specifically deliver vaccines to key APC subsets, including cross-presenting dendritic cells, monocytes, or macrophages; and the engineering of materials with stimuli-responsive or controlled release properties that can overcome drug delivery barriers, such as by increasing antigen cross-presentation in the local lymph nodes and antigen residence time at the site of immunization, both of which have been implicated in the generation of T_{RM} cells in specific tissues (**Figure 5.1**). As we move away from live vaccine vectors and further toward widespread use of subunit vaccines, the ideal goal will be to recapitulate “real viruses” are closely as possible with engineered subunit platforms. This may be done by adding an increasing number of functionalities to the vaccine delivery platform; for example, in the case of this dissertation, dual-delivery of adjuvant along with the vaccine antigen was employed to mimic the immunostimulatory effect of a virus’s pathogen-associated molecular patterns (PAMPs). One possibility for the next iteration, for example, would be to also load antibodies onto the nanoparticle as a moiety for targeting cross-presenting dendritic cells (e.g., anti-DEC205 or anti-Clec9A antibodies). In this way, similar to how viruses possess receptors with tropisms for specific cell types, subunit vaccines can be targeted for uptake in specific cell subsets. Another option would be to load multiple synergistic adjuvants onto the nanoparticle in order to fine-tune activation of the innate immune response and more closely mimic the array of PAMPs present on pathogen surfaces. However, there will likely be a point of diminishing returns at which the design and manufacture of pathogen-mimetic subunit vaccines becomes too complex to be sustainable. It will also be important to consider hurdles in translation and regulatory approval for these vaccines. A key effort in the future of vaccine design will be to identify this point of diminishing returns and design sophisticated materials that can push the envelope as far as possible toward increasingly complex vaccine formulations.

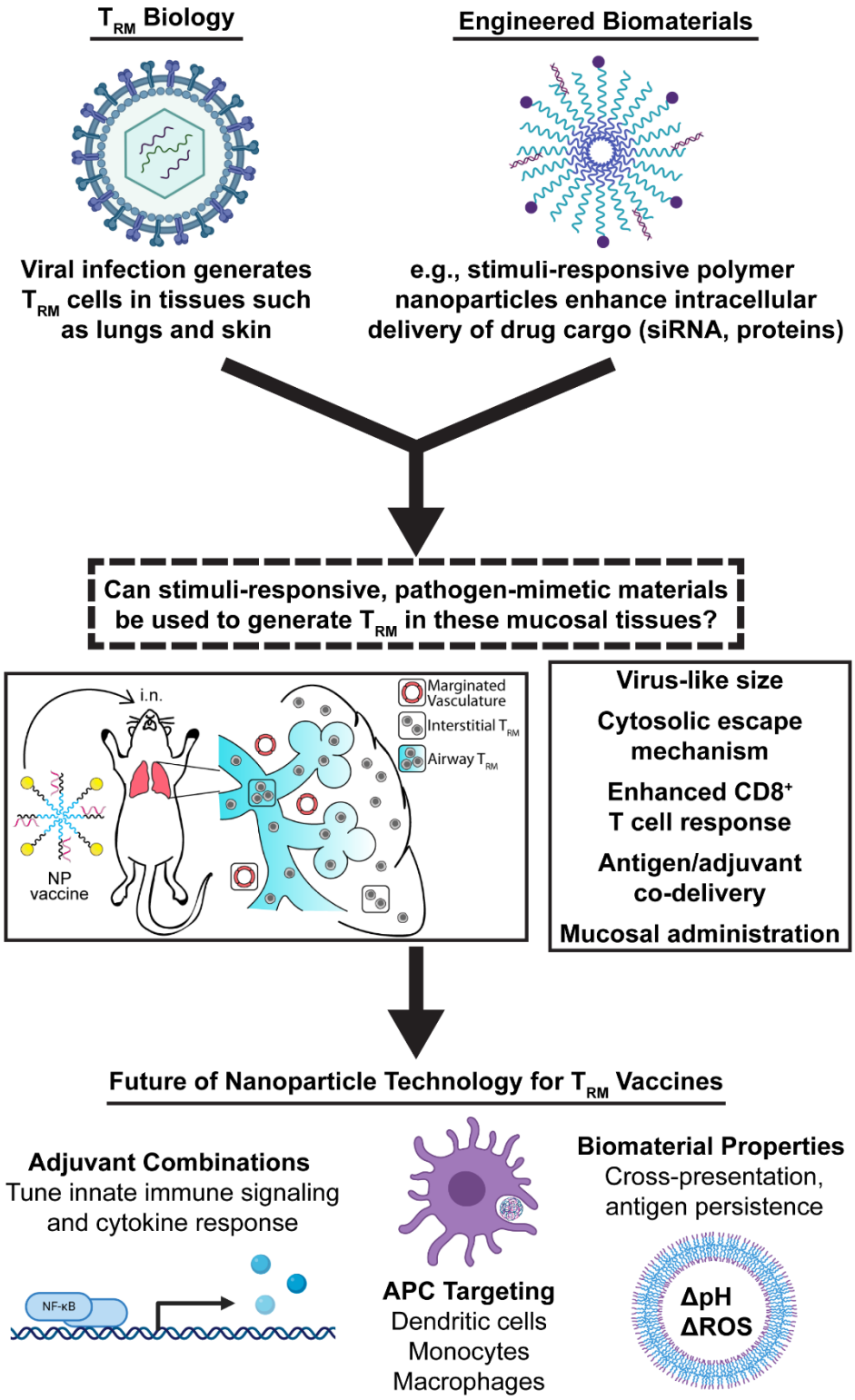

Figure 5.1 | Past-present-future of nanoparticle technology for T_{RM} vaccines. Graphical abstract demonstrating the state of the field prior to this dissertation; the contributions of this work to the field; and perspectives on possible future directions in the development of engineered nanoparticle vaccines for generating T_{RM} cells. Figure created with Biorender.com.

5.4 Concluding Remarks

The field of immunology is ever-expanding, providing new knowledge that can be utilized by scientists and engineers to create the next generation of vaccines and immunotherapeutics. The work described in this dissertation has focused on harnessing this toolbox to probe the relationships between nanoparticle-mediated vaccine delivery and tissue-resident memory T cells. We have presented the novel application of a pH-responsive nanomaterial for use in mucosal delivery of vaccine antigens and adjuvants, and we have shown that this material can be used to create a vaccine that produces T_{RM} cells and protects against respiratory viral infection. This dissertation has also laid the foundation for studying links between innate immune activation and tissue-resident immunity. Each component of this work further illuminates the relationships between innate and adaptive immunity, and the ways in which immunoengineering can harness intrinsic immune mechanisms to create a new generation of safer and more effective vaccines. While vaccine science has in some ways progressed slowly, it has also experienced major breakthroughs—such as the eradication of smallpox in 1980. Today, we face major challenges in the field, including creation of the first HIV and malaria vaccines, improving the BCG vaccine for tuberculosis, developing universal influenza vaccines that can protect us from a worldwide pandemic, and the major global public health crisis of COVID-19. Advances have already been made in tackling some of these challenges; for example, the first ever approved malaria vaccine is currently undergoing pilot trials in Malawi, Ghana, and Kenya. As scientists and engineers come together in an increasingly interdisciplinary field, we are better equipped than ever to overcome these important public health challenges.

APPENDIX A

SUPPLEMENTARY MATERIAL FOR CHAPTER 2

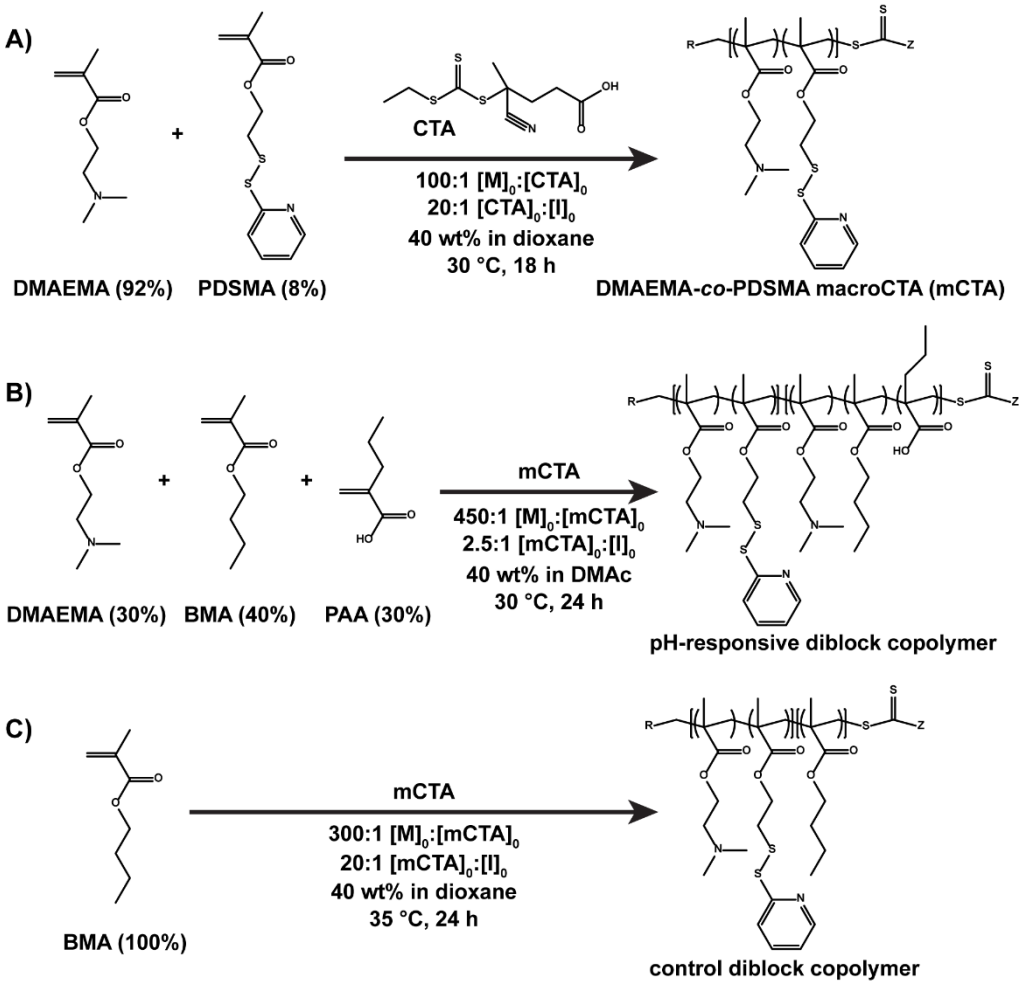

Figure A.1 | RAFT synthesis of pH-responsive and control polymers for dual-delivery of protein antigen and nucleic acid adjuvant. (A) Synthesis scheme and reaction conditions for DMAEMA-*co*-PDSMA macro-chain transfer agent (mCTA). **(B)** Synthesis of pH-responsive diblock copolymer, (DMAEMA-*co*-PDSMA)-*b*-(PAA-*co*-DMAEMA-*co*-BMA). **(C)** Synthesis of control diblock copolymer, (DMAEMA-*co*-PDSMA)-*b*-BMA.

Table A.1 | Summary of polymer properties.

	pH-responsive polymer			Control polymer		
	1st block (mCTA)	2nd block	Diblock copolymer (1+2)	1st block (mCTA)	2nd block	Diblock copolymer (1+2)
Molecular weight (g/mol)	11,370	18,470	29,840	12,870	29,600	42,470
Polydispersity index (PDI)	1.04	—	1.51	1.04	—	1.09

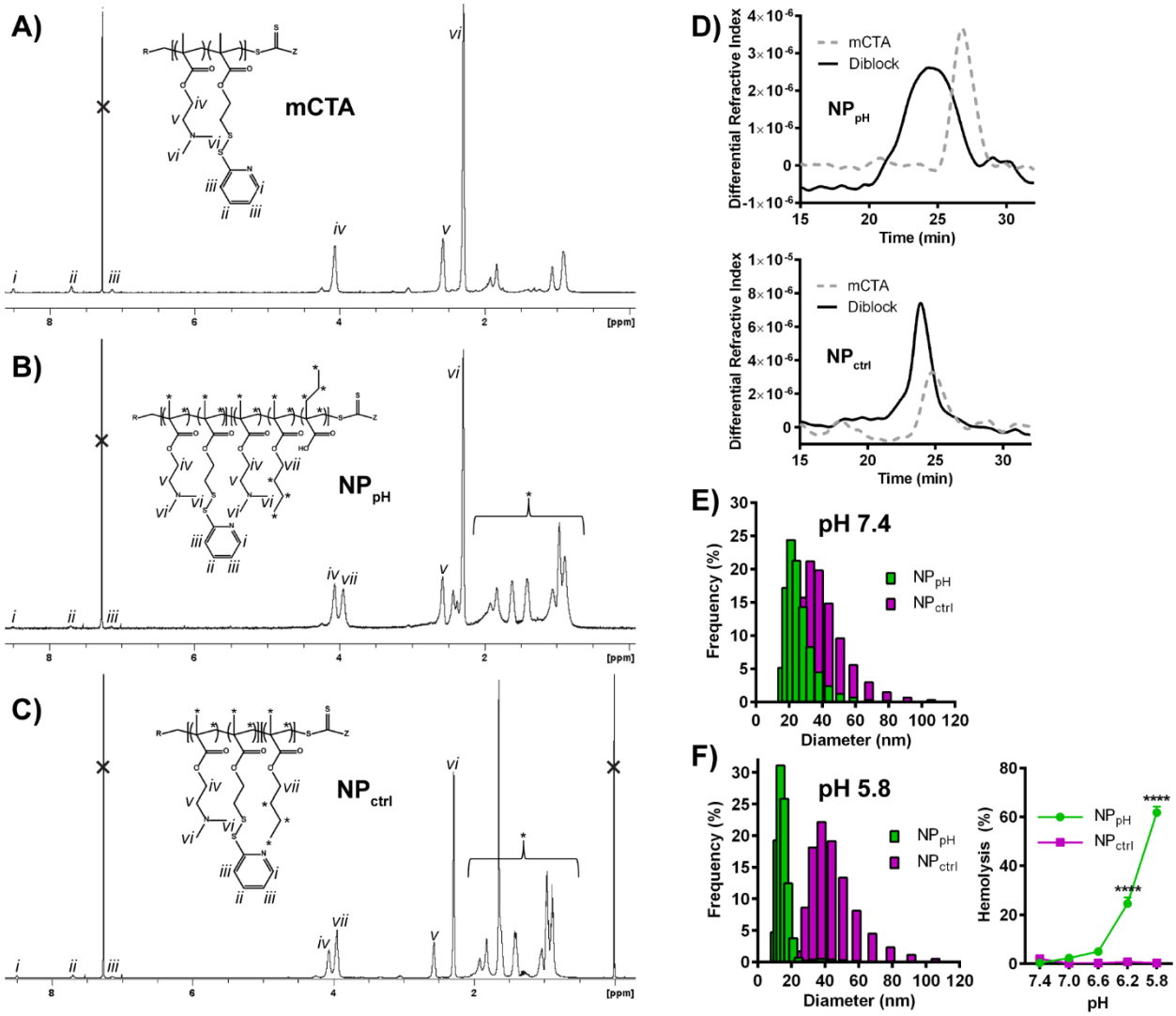

Figure A.2 | Polymer and nanoparticle characterization for pH-responsive and control carriers. **(A-C)** Representative ^{1}H-NMR ($CDCl_3$) of **(A)** DMAEMA-*co*-PDSMA macroCTA, **(B)** pH-responsive diblock copolymer, and **(C)** control diblock copolymer. **(D)** Representative GPC traces for mCTA and diblock copolymer, pH-responsive (top) and control (bottom). **(E)** Representative size distribution (number average) at pH 7.4 for pH-responsive NP (NP_{pH}) and control NP (NP_{ctrl}) as measured by DLS. **(F)** Left: representative size distribution (number average) at pH 5.8 for NP_{pH} and NP_{ctrl}, indicating pH-dependent change in particle morphology; right: erythrocyte lysis assay demonstrates pH-dependent membrane destabilizing activity of NP_{pH} but not NP_{ctrl} (10 µg/ml polymer). Data are mean ± SEM with *n* = 4 per group. ****p<0.0001 by ordinary two-way ANOVA with Sidak's multiple comparisons test.

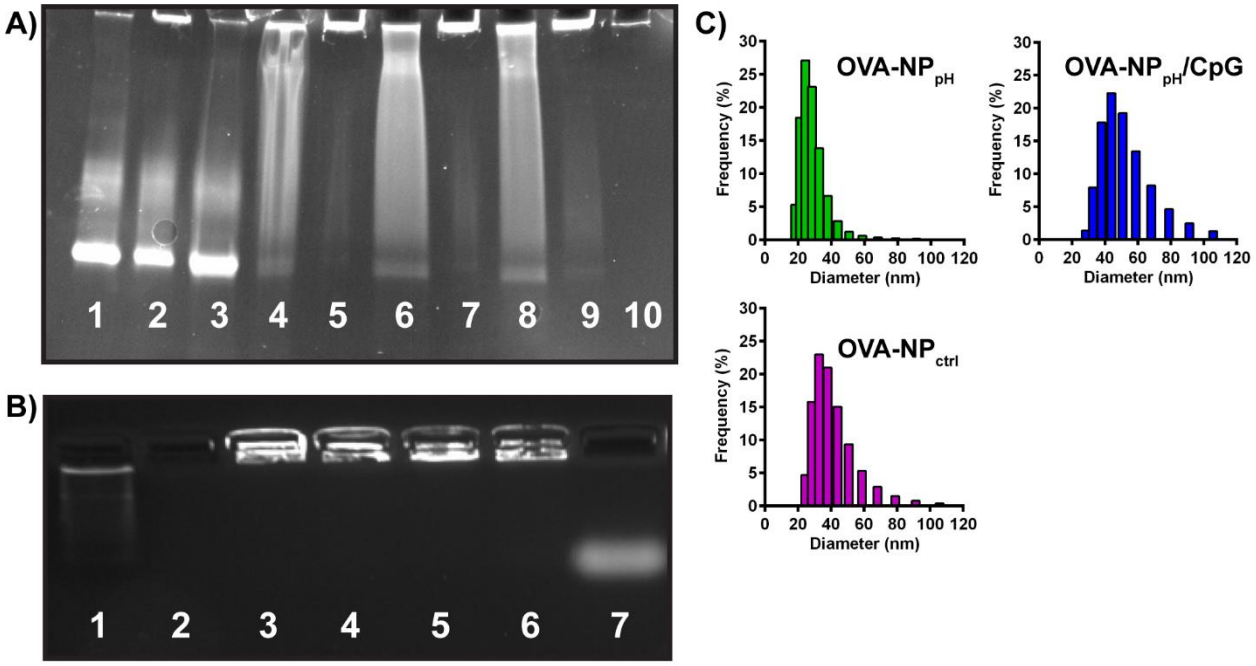

Figure A.3 | OVA-nanoparticle conjugation, adjuvant complexation, and vaccine characterization. (A) Thiolated OVA protein labeled with FITC was reacted with NP made from pH-responsive polymer (NP_{pH}) or control polymer (NP_{ctrl}) to form conjugates at various molar ratios of OVA:polymer. SDS-PAGE was used to confirm antigen conjugation. Lane (1) free OVA protein; (2) mixture of OVA+NP_{ctrl}; (3) mixture of OVA+NP_{pH}; (4) OVA-NP_{pH} (1:20 molar ratio); (5) OVA-NP_{ctrl} (1:14); (6) OVA-NP_{pH} (1:10); (7) OVA-NP_{ctrl} (1:7); (8) OVA-NP_{pH} (1:5); (9) OVA-NP_{ctrl} (1:3.5); (10) free NP_{ctrl}. Material loaded into each lane was normalized to 5 µg OVA. Thiolated OVA was confirmed to conjugate to both NP_{pH} and NP_{ctrl} at all molar ratios tested (lanes 4-9), and non-thiolated OVA did not conjugate with either polymer (lanes 2-3). The NP itself was not fluorescent (lane 10). **(B)** CpG DNA was complexed with nanoparticles (NP_{pH}) and conjugates (OVA-NP_{pH}, 1:5) at various charge ratios of polymer:CpG (+/-). Gel electrophoresis and GelRed staining were used to confirm adjuvant complexation. Lane (1) 20 bp ladder; (2) OVA-NP; (3) NP/CpG (6:1 +/-); (4) NP/CpG (4:1); (5) OVA-NP/CpG (6:1); (6) OVA-NP/CpG (4:1); (7) free CpG. Material loaded into each lane was normalized to 2.3 µg CpG. CpG complexed with both NP and OVA-NP at both charge ratios, as shown by lack of migration from the wells of the gel (lanes 3-6). Free CpG migrated from the well due to its net negative charge (lane 7). OVA-NP did not show background staining from GelRed (lane 2). **(C)** Representative size distributions (number average) at pH 7.4 for OVA-NP_{pH} (1:5 molar ratio), OVA-NP_{ctrl} (1:3.5 molar ratio), and OVA-NP_{pH}/CpG (1:5 molar ratio, 6:1 charge ratio), as measured by DLS.

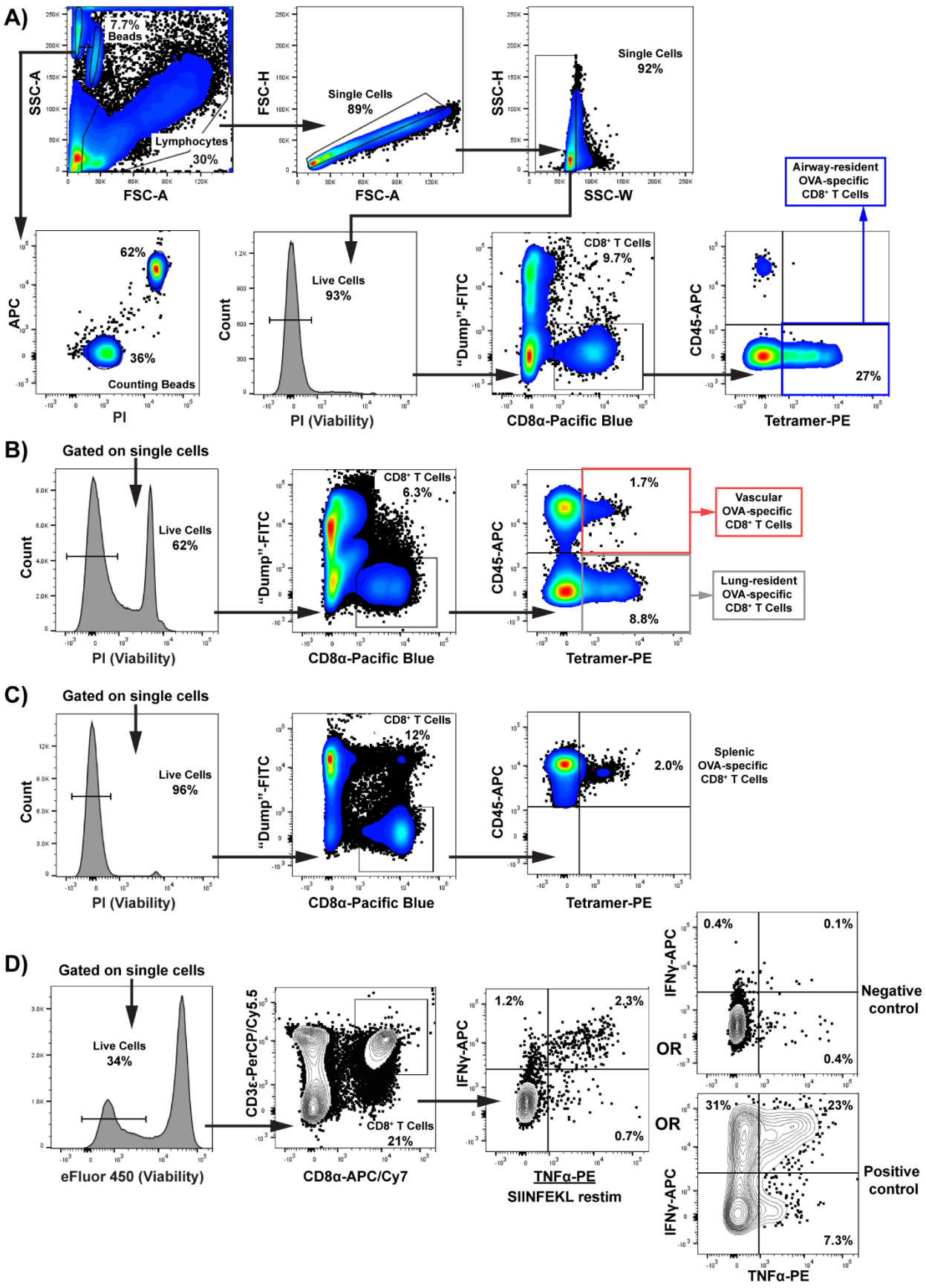
A)
7.7%
Beads
Lymphocytes
30%
SSC-A
FSC-A
Single Cells
89%
FSC-H
FSC-A
Single Cells
92%
SSC-H
SSC-W
62%
36%
Counting Beads
APC
PI
Live Cells
93%
Count
PI (Viability)
CD8⁺ T Cells
9.7%
"Dump"-FITC
CD8α-Pacific Blue
Airway-resident
OVA-specific
CD8⁺ T Cells
27%
CD45-APC
Tetramer-PE
B)
Gated on single cells
Live Cells
62%
Count
PI (Viability)
CD8⁺ T Cells
6.3%
"Dump"-FITC
CD8α-Pacific Blue
1.7%
8.8%
CD45-APC
Tetramer-PE
Vascular
OVA-specific
CD8⁺ T Cells
Lung-resident
OVA-specific
CD8⁺ T Cells
C)
Gated on single cells
Live Cells
96%
Count
PI (Viability)
CD8⁺ T Cells
12%
"Dump"-FITC
CD8α-Pacific Blue
2.0%
CD45-APC
Tetramer-PE
Splenic
OVA-specific
CD8⁺ T Cells
D)
Gated on single cells
Live Cells
34%
eFluor 450 (Viability)
CD3ε-PerCP/Cy5.5
CD8⁺ T Cells
21%
CD8α-APC/Cy7
1.2%
2.3%
0.7%
IFNγ-APC
TNFα-PE
SIINFEKL restim
0.4%
0.1%
0.4%
IFNγ-APC
OR
Negative
control
31%
23%
7.3%
IFNγ-APC
OR
Positive
control
TNFα-PE

Figure A.4 | Gating strategies for flow cytometric analysis of antigen-specific CD8$^+$ T cells and intracellular cytokine production in airways, lungs, and spleens. Representative plots are from mice immunized with OVA-NP$_{pH}$/CpG. **(A-C)** Events were first gated on lymphocytes (SSC-A *vs*. FSC-A), then single cells were isolated *via* gating FSC-H *vs*. FSC-A and SSC-H *vs*. SSC-W. Single cells negative for propidium iodide (PI) were live cells. Viable CD8$^+$ T cells were positive for CD8α-Pacific Blue and negative for the "dump" channel (B220/CD4/CD11b/CD11c-FITC). Two populations of counting beads were gated for calculating absolute cell counts. **(A)** Analysis of airway (AW)-resident OVA-specific CD8$^+$ T cells in BAL. AW population was negative for i.v. stain (CD45-APC$^-$) and positive for PE-labeled SIINFEKL/MHC-I tetramer (tetramer-PE$^+$). **(B)** Analysis of lung interstitium (IST)-resident and marginated vascular (MV) OVA-specific CD8$^+$ T cells in lungs. IST population was CD45-APC$^-$ and tetramer-PE$^+$. MV population was CD45$^+$tetramer$^+$. **(C)** Analysis of systemic OVA-specific CD8$^+$ T cells in spleens. Spleen population was tetramer-PE$^+$ after being gated on CD8α. **(D)** For ICCS, counting beads, "dump" channel, and i.v. staining were not used. After gating for lymphocytes and singlets, viability was determined using eFlour 450, and viable CD8$^+$ T cells were CD3ε$^+$CD8α$^+$. Cells were then gated on TNFα-PE and IFNγ-APC to assess cytokine production. Plots shown here are from a lung sample; the same gating was used for spleens. BAL was not collected for ICCS experiments. Cells were restimulated with SIINFEKL peptide, cRPMI (negative control), or PMA/ionomycin (positive control).

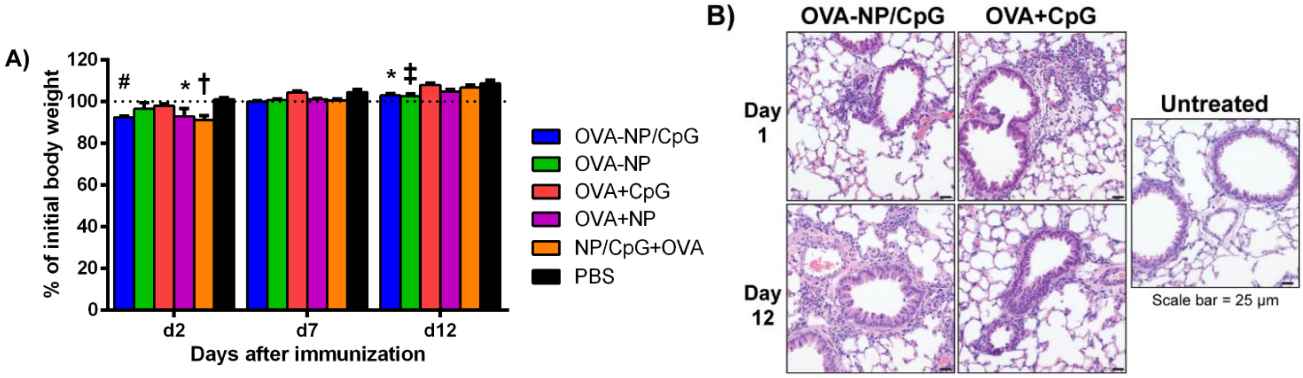

Figure A.5 | Minimal toxicity after pulmonary immunization with pH-responsive formulations. (A) Weight loss shown as percent of body weight on day of immunization (d0). Dose: 25 μg NP, 7.5 μg OVA, 1.4 μg CpG. Mice were immunized with pH-responsive formulations: OVA-NP/CpG, OVA-NP, OVA+CpG, OVA+NP, NP/CpG+OVA, or PBS (control). Data are mean ± SEM and pooled from five independent experiments, with n = 2-18 per group. *p<0.05, ‡p<0.01, †p<0.001, #p<0.0001, by ordinary two-way ANOVA with Tukey's multiple comparisons test. Significance is indicated relative to the PBS control group. All unlabeled groups are ns (not significant). **(B)** H&E staining of lungs harvested at d1 or d12 after immunization with either OVA-NP/CpG or OVA+CpG (n = 2 per group). Untreated lung for comparison. Scale bar = 25 μm.

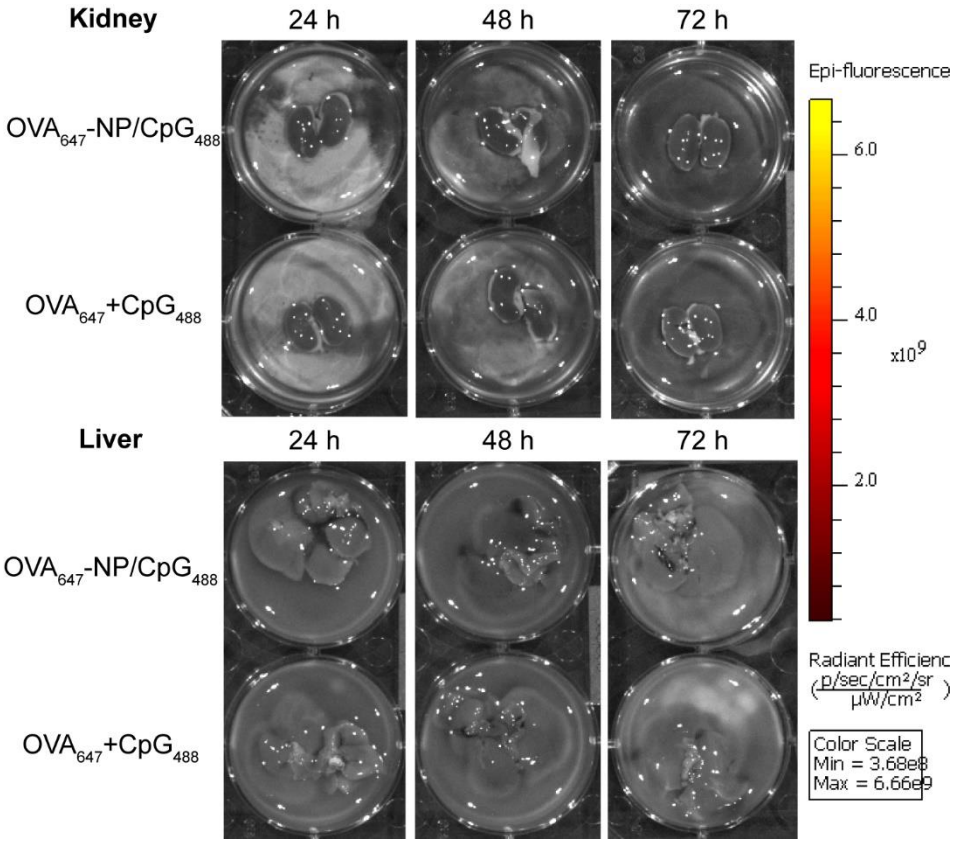

Figure A.6 | IVIS imaging of livers and kidneys in immunized mice. Fluorescence was negligible at all time points in kidneys and livers of mice receiving i.n. administration of either OVA_{647}-NP/CpG_{488} or OVA_{647}+CpG_{488}, indicating localized pulmonary delivery and uptake with minimal systemic distribution.

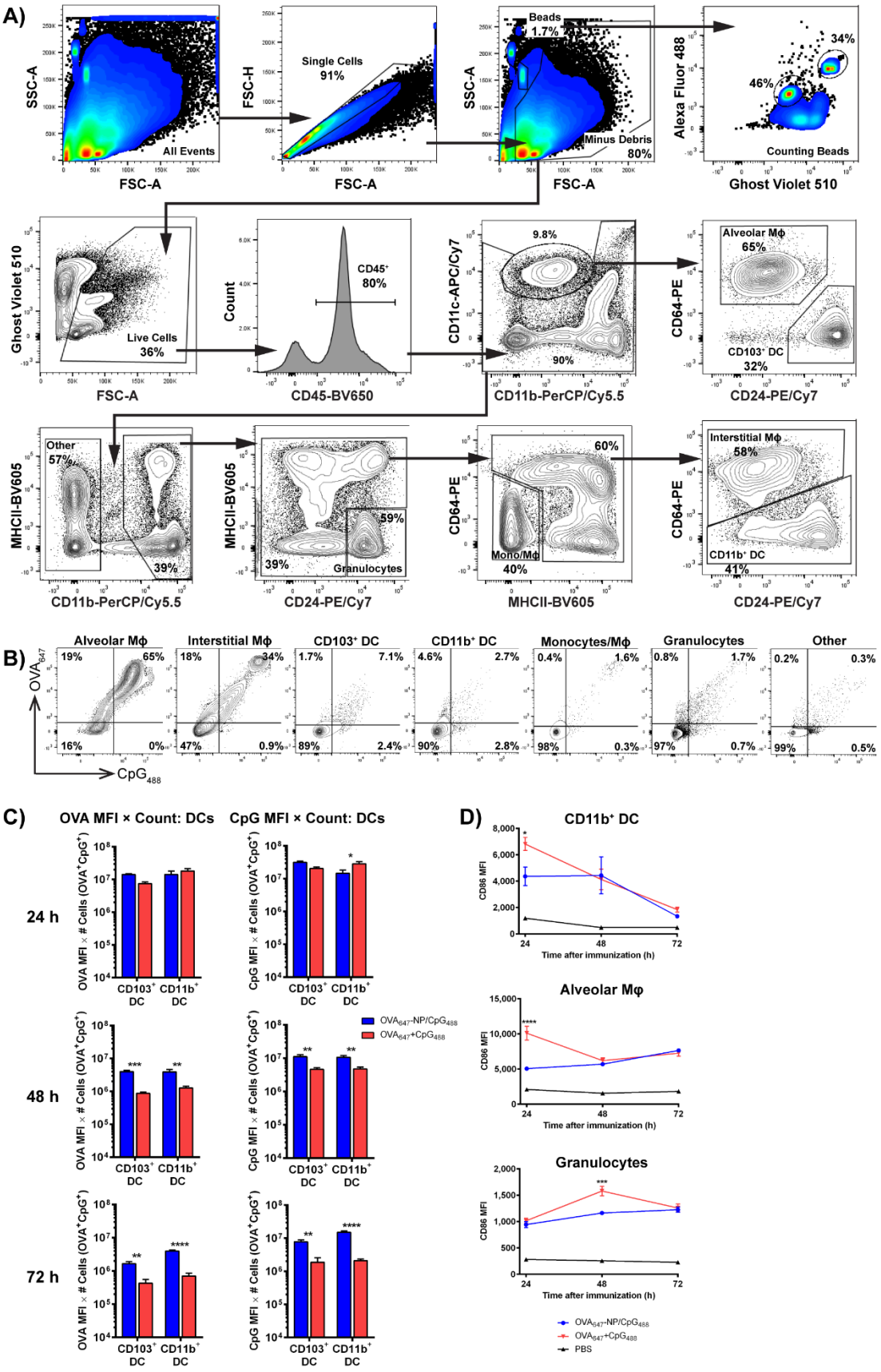
A)
SSC-A
All Events
FSC-A
FSC-H
Single Cells
91%
FSC-A
SSC-A
Beads
1.7%
Minus Debris
80%
FSC-A
Alexa Fluor 488
34%
46%
Counting Beads
Ghost Violet 510
Live Cells
36%
FSC-A
Count
CD45+
80%
CD45-BV650
CD11c-APC/Cy7
9.8%
90%
CD11b-PerCP/Cy5.5
CD64-PE
Alveolar Mφ
65%
CD103+ DC
32%
CD24-PE/Cy7
MHCII-BV605
Other
57%
39%
CD11b-PerCP/Cy5.5
MHCII-BV605
59%
39%
Granulocytes
CD24-PE/Cy7
CD64-PE
60%
Mono/Mφ
40%
MHCII-BV605
CD64-PE
Interstitial Mφ
58%
CD11b+ DC
41%
CD24-PE/Cy7
B)
Alveolar Mφ
Interstitial Mφ
CD103+ DC
CD11b+ DC
Monocytes/Mφ
Granulocytes
Other
OVA647
CpG488
19%
65%
16%
0%
18%
34%
47%
0.9%
1.7%
7.1%
89%
2.4%
4.6%
2.7%
90%
2.8%
0.4%
1.6%
98%
0.3%
0.8%
1.7%
97%
0.7%
0.2%
0.3%
99%
0.5%
C)
OVA MFI × Count: DCs
CpG MFI × Count: DCs
24 h
48 h
72 h
OVA MFI × # Cells (OVA+CpG+)
CpG MFI × # Cells (OVA+CpG+)
CD103+ DC
CD11b+ DC
OVA647-NP/CpG488
OVA647+CpG488
D)
CD11b+ DC
Alveolar Mφ
Granulocytes
CD86 MFI
Time after immunization (h)
OVA647-NP/CpG488
OVA647+CpG488
PBS

Figure A.7 | Gating strategy for flow cytometric analysis of OVA_{647} and CpG_{488} in pulmonary innate immune cells, representative dot plots showing uptake in pulmonary cells, relative OVA and CpG uptake in DC subsets, and CD86 expression in selected subsets. The gating strategy shown here was adapted from Misharin *et al*.[56] Flow plots are from mice immunized with pH-responsive OVA_{647}-NP/CpG_{488}. **(A)** All events were gated on single cells (FSC-H *vs*. FSC-A), then debris was gated out (SSC-A *vs*. FSC-A). Two populations of counting beads were gated for use in calculating absolute cell counts. Viable single cells were gated using Ghost Dye™ Violet 510. Viable $CD45^+$ cells were then gated using a variety of surface markers to identify pulmonary immune cell subsets. **(B)** Representative dot plots showing OVA_{647} *vs*. CpG_{488} uptake for each cell type. Double-positive cells (OVA^+CpG^+) were indicative of vaccine cargo co-localization. **(C)** Relative OVA and CpG uptake in $CD103^+$ DC and $CD11b^+$ DC for each formulation was calculated as OVA MFI × # OVA^+CpG^+ cells and CpG MFI × # OVA^+CpG^+ cells. **(D)** CD86 MFI in $CD11b^+$ DCs, alveolar macrophages, and granulocytes. Data are mean ± SEM with *n* = 3-4 per group. *p<0.05, **p<0.01, ***p<0.001, ****p<0.0001 by **(C)** ordinary two-way ANOVA with Sidak's multiple comparisons test, or **(D)** ordinary two-way ANOVA comparing OVA-NP/CPG *vs*. OVA+CpG, with Tukey multiple comparisons test.

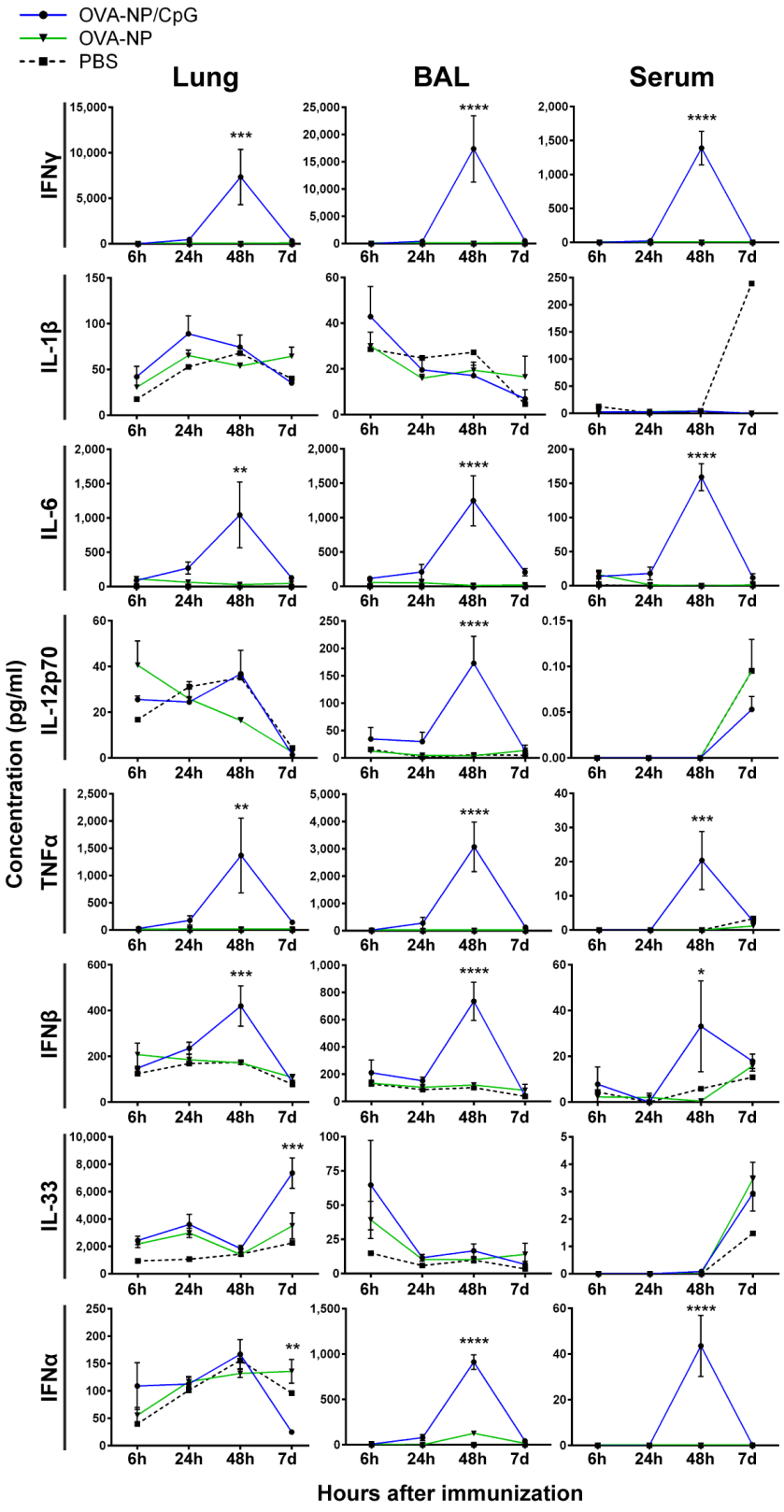

Figure A.8 | Presence of CpG adjuvant is needed to stimulate an acute cytokine response to the nanoparticle vaccine. Cytokines associated with $CD8^+$ T cells (IFNγ, IL-1β, IL-6, IL-12p70) and T_{RM} generation (TNFα, IFNβ, IL-33, IFNα) were measured in lungs, BAL, and serum obtained 6 h, 24 h, 48 h, or 7 d after immunization with either OVA-NP/CpG or OVA-NP. Data are mean ± SEM and

representative of two independent experiments, with *n* = 4-5 per group. Immunization dose: 25 μg NP, 7.5 μg OVA, 1.4 μg CpG. *p<0.05, **p<0.01, ***p<0.001, ****p<0.0001, by ordinary two-way ANOVA with Tukey's multiple comparisons test. Statistical differences shown are for comparison of OVA-NP/CpG *vs*. OVA-NP.

APPENDIX B

SUPPLEMENTARY MATERIAL FOR CHAPTER 3

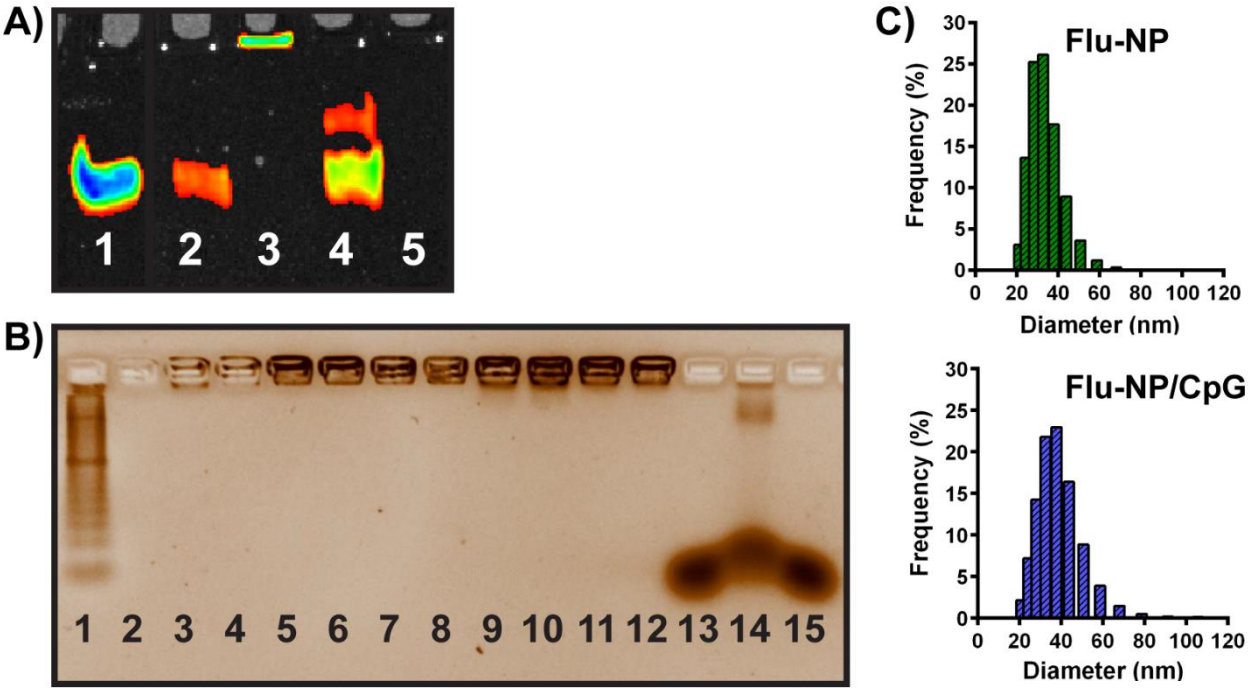

Figure B.1 | Flu-nanoparticle conjugation, adjuvant complexation, and vaccine characterization. **(A)** Thiolated Flu protein labeled with AF647 was reacted with NP made from pH-responsive polymer at a molar ratio of 5:1 (protein:polymer) to form conjugates. SDS-PAGE was used to confirm antigen conjugation. Lane (1) free Flu protein; (2) thiolated Flu protein; (3) Flu-NP conjugate; (4) Flu-NP conjugate + TCEP; (5) free NP. Material loaded into each lane was normalized to 3.5 µg Flu protein. Thiolated Flu was confirmed to conjugate to NP (lane 3), as incubation with TCEP to disrupt the disulfide bridges between thiolated protein and NP resulted in reappearance of the free protein band (lane 4, compare with lane 1). Thiolating the protein did not cause significant self-aggregation (lane 2). The NP itself was not fluorescent (lane 5). **(B)** CpG DNA was complexed with nanoparticles (NP) and conjugates (OVA-NP or Flu-NP, 1:5) at various charge ratios of polymer:CpG (+/-). Gel electrophoresis and GelRed staining were used to confirm adjuvant complexation. Lane (1) 20 bp ladder; (2) OVA-NP; (3-4) Flu-NP; (5) NP/CpG (6:1); (6) NP/CpG (4:1); (7) OVA-NP/CpG (6:1); (8) OVA-NP/CpG (4:1); (9) Flu-NP/CpG (6:1); (10) Flu-NP/CpG (4:1); (11) Flu-NP/CpG (6:1); (12) Flu-NP/CpG (4:1); (13) OVA+CpG; (14) Flu+CpG; (15) free CpG. CpG complexed with NP, OVA-NP, and Flu-NP at both charge ratios, as shown by lack of migration from the wells of the gel (lanes 5-12). Free CpG and CpG mixed with OVA or Flu protein migrated from the well due to its net negative charge (lanes 13-15), indicating the NP is necessary for complete electrostatic complexation. Antigen-NP conjugates did not show background staining from GelRed (lanes 2-4). **(C)** Representative size distributions (number average) at pH 7.4 for Flu-NP (1:5 molar ratio) and Flu-NP/CpG (1:5 molar ratio, 6:1 charge ratio), as measured by DLS.

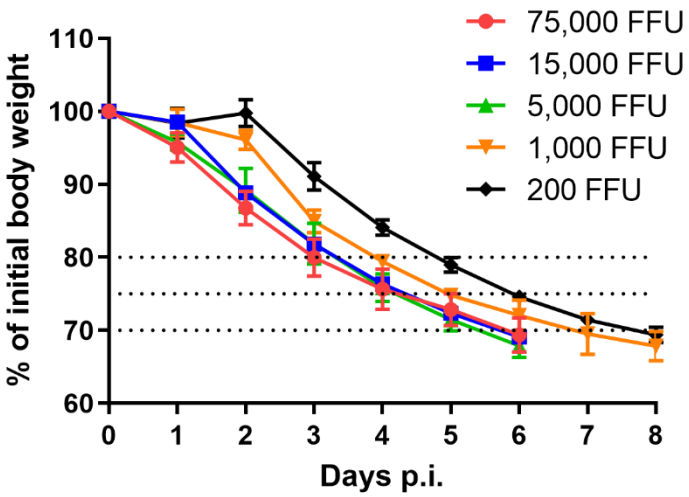

Figure B.2 | Lethal dosing study with PR8 virus. Doses from 200-75,000 FFU were tested via i.n. challenge in naïve mice in order to determine the ideal dose for exhibiting weight loss, morbidity, and mortality (>30% weight loss and euthanasia as per IACUC guidelines). A dose of 200 FFU was determined to accomplish this in the appropriate timeframe. Dotted lines added for ease of identifying the days on which mice reached certain weight loss points. *n* = 5 per group; p.i.: post-infection.

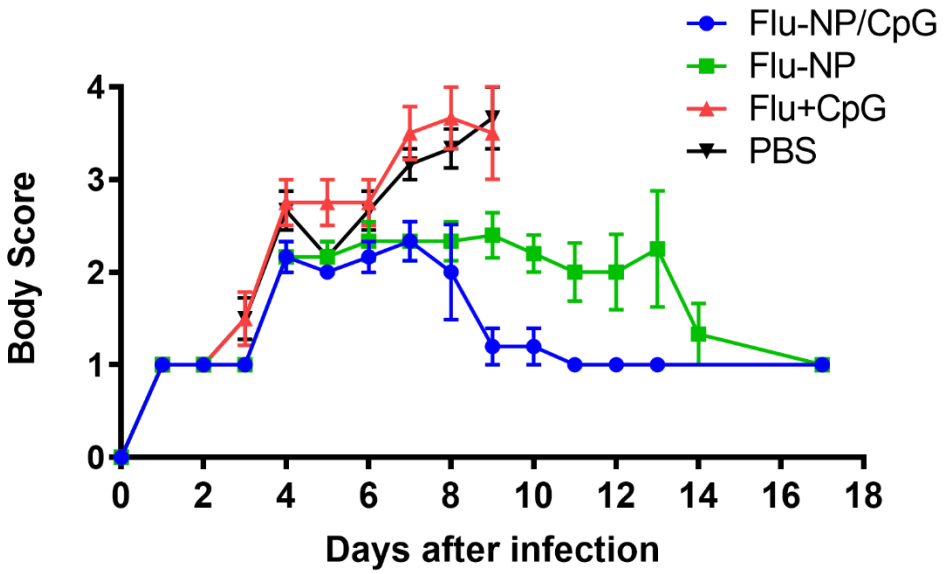

Figure B.3 | Body scoring of mice challenged with influenza virus after immunization. Mice were immunized i.n. on d0 with Flu-NP/CpG, Flu-NP, Flu+CpG, and PBS. On d60 after immunization, mice were challenged i.n. with PR8 virus (200 FFU/mouse) and scored daily based on signs of illness. Mice that exceeded 30% weight loss were considered deceased and were no longer included in scoring. Consistent with weight loss data, mice immunized with Flu-NP/CpG experienced less severe illness and recovered more quickly relative to other groups.

APPENDIX C

SUPPLEMENTARY MATERIAL FOR CHAPTER 4

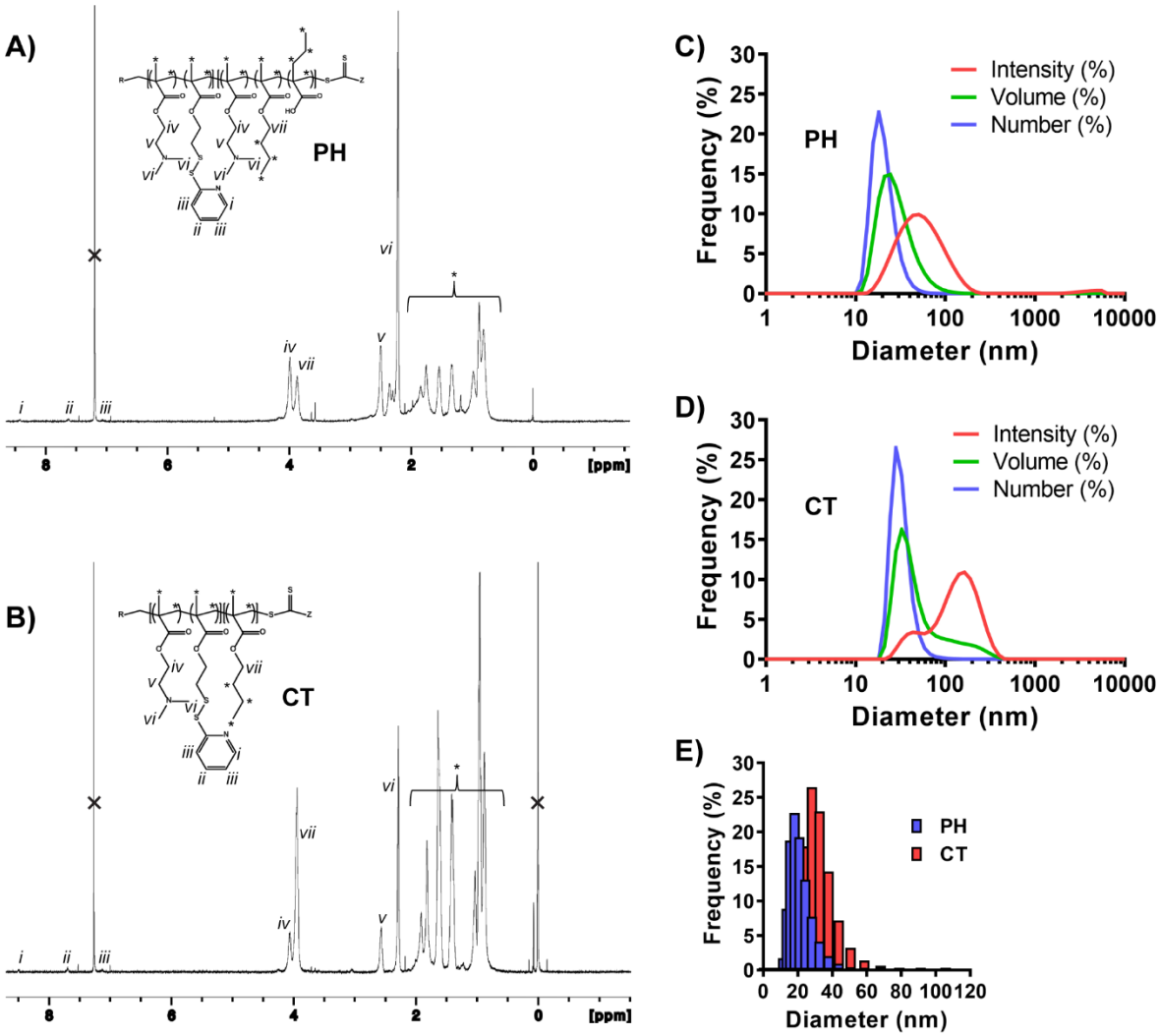

Figure C.1 | Polymer and nanoparticle characterization for pH-responsive and control carriers. **(A,B)** Representative ^{1}H-NMR ($CDCl_3$) of **(A)** pH-responsive diblock copolymer and **(B)** control diblock copolymer. **(C,D)** Representative size distribution at pH 7.4 for **(C)** pH-responsive NP (PH) and **(D)** control NP (CT) as measured by DLS. **(E)** Size distribution comparison (number average) for PH and CT nanoparticles as measured by DLS. NMR was used to determine the molecular weight of the PH polymer (31,500 g/mol) and the CT polymer (43,674 g/mol).

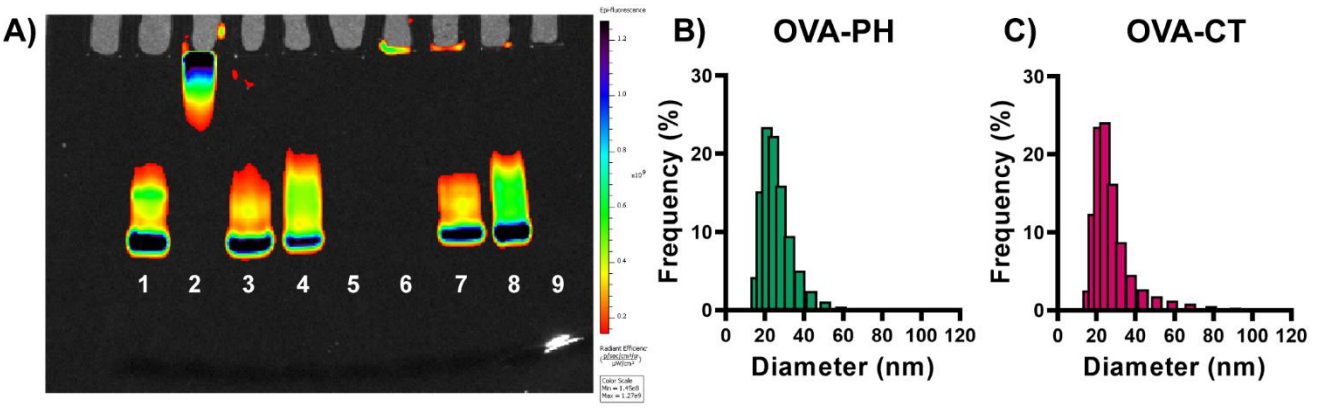

Figure C.2 | Characterization of OVA-nanoparticle conjugation with pH-responsive and control carriers. (A) Thiolated OVA protein labeled with AF647 was reacted with PH or CT NP at a molar ratio of 5.1:1 (PH:OVA) or 3.85:1 (CT:OVA) to form conjugates. The conjugation ratio for CT NP was adjusted in order to maintain a constant dose of antigen (7 µg) on the amount of polymer administered *in vivo* (25 µg). SDS-PAGE was used to confirm antigen conjugation. Lane (1) free OVA protein; (2) OVA-PH conjugate; (3) OVA-PH + TCEP; (4) OVA+PH mixture; (5) PH NP; (6) OVA-CT conjugate; (7) OVA-CT + TCEP; (8) OVA+CT mixture; (9) CT NP. Material loaded into each lane was normalized to 2.25 µg OVA. Thiolated OVA was confirmed to conjugate to both PH and CT NP due to lack of a free OVA band (compare lanes 2, 6 to lane 1). Incubation with TCEP disrupted the disulfide bridges between thiolated protein and NP, resulting in reappearance of the free protein band (lanes 3 and 7). Non-thiolated OVA did not conjugate with the NP (lanes 4 and 8), and the NP itself was not fluorescent (lanes 5 and 9).

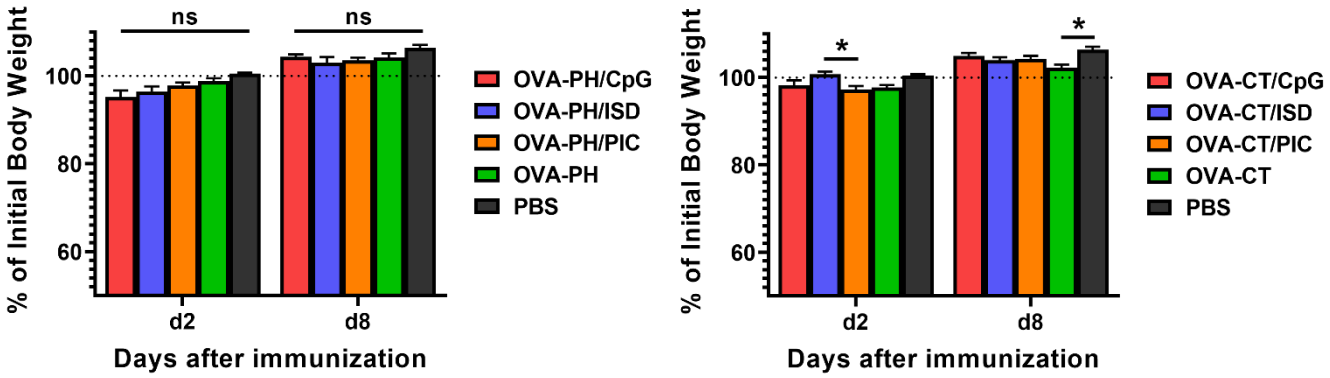

Figure C.3 | Weight loss after immunization with various adjuvant and polymer combinations. Weight loss shown as percent of body weight on day of immunization (d0). Dose: 25 µg NP, 7 µg OVA, 1.07 µg CpG or 1.04 µg ISD or 0.8 µg PIC. Mice were immunized with formulations containing pH-responsive NP (top) or control NP (bottom). Data are mean ± SEM and pooled from four independent experiments, with n = 4-18 per group. *p > 0.05.

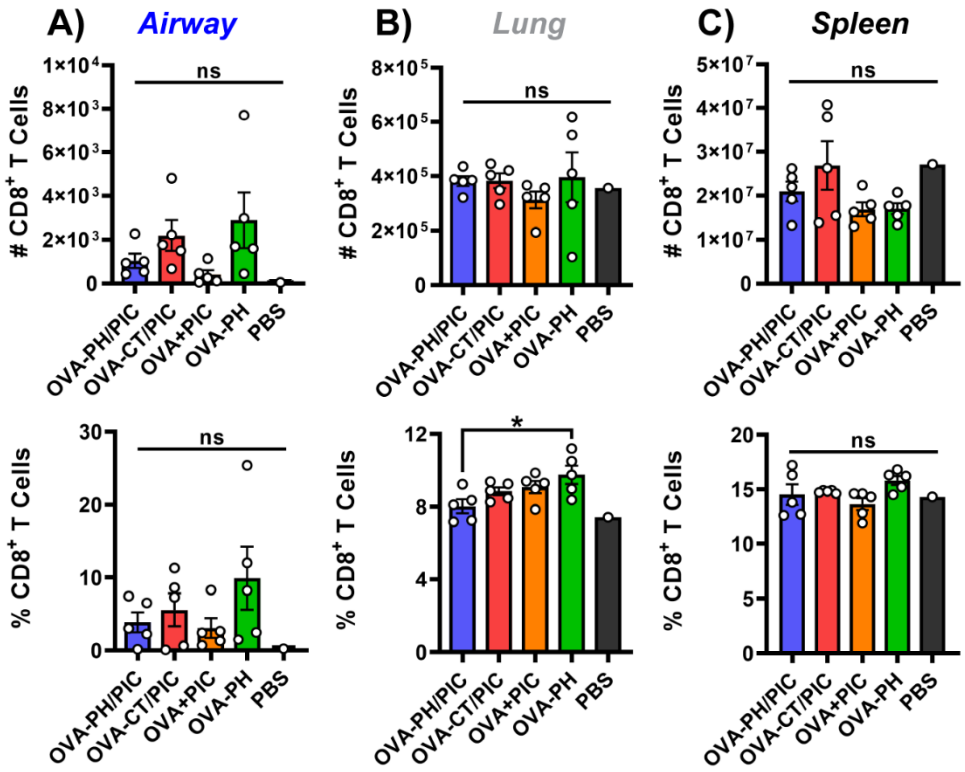

Figure C.4 | Total number (#) and frequency (%) of CD8⁺ T cells in airways, lungs, and spleens after immunization. Total number and percentage of CD8⁺ T cells were quantified in **(A)** BAL fluid, **(B)** lungs, and **(C)** spleens using flow cytometry. CD8⁺ T cells were defined as CD8α⁺B220⁻CD4⁻CD11b⁻CD11c⁻. Low numbers of CD8⁺ T cells obtained from BAL fluid may indicate a need for alternate collection methods. Notably, there are negligible CD8⁺ T cells present in the airways of a naïve mouse at steady state (PBS).

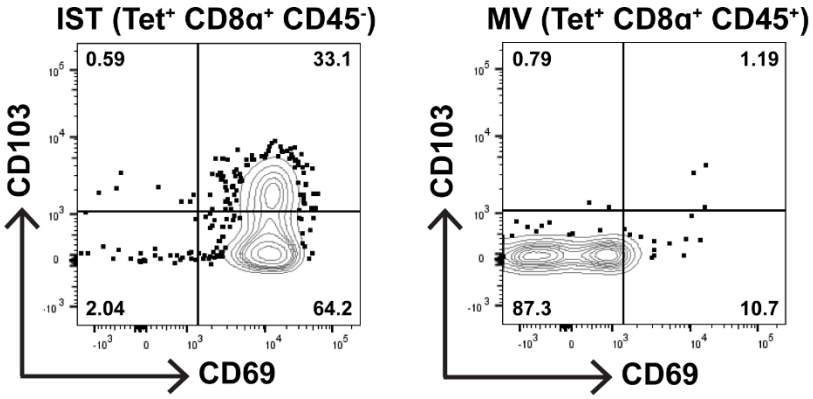

Figure C.5 | Antigen-specific CD8⁺ T cells expressing T_{RM} markers are found in the lung interstitium but not lung vasculature. T_{RM} cells were defined as those expressing CD103 and/or CD69. Antigen-specific CD8⁺ T cells in the lung interstitium (IST) were defined as Tet⁺CD8α⁺CD45⁻ (left), while those in the lung vasculature (MV) were defined as Tet⁺CD8α⁺CD45⁺. Representative dot plots are from mice analyzed 13 days after immunization with poly(I:C)-containing formulations.

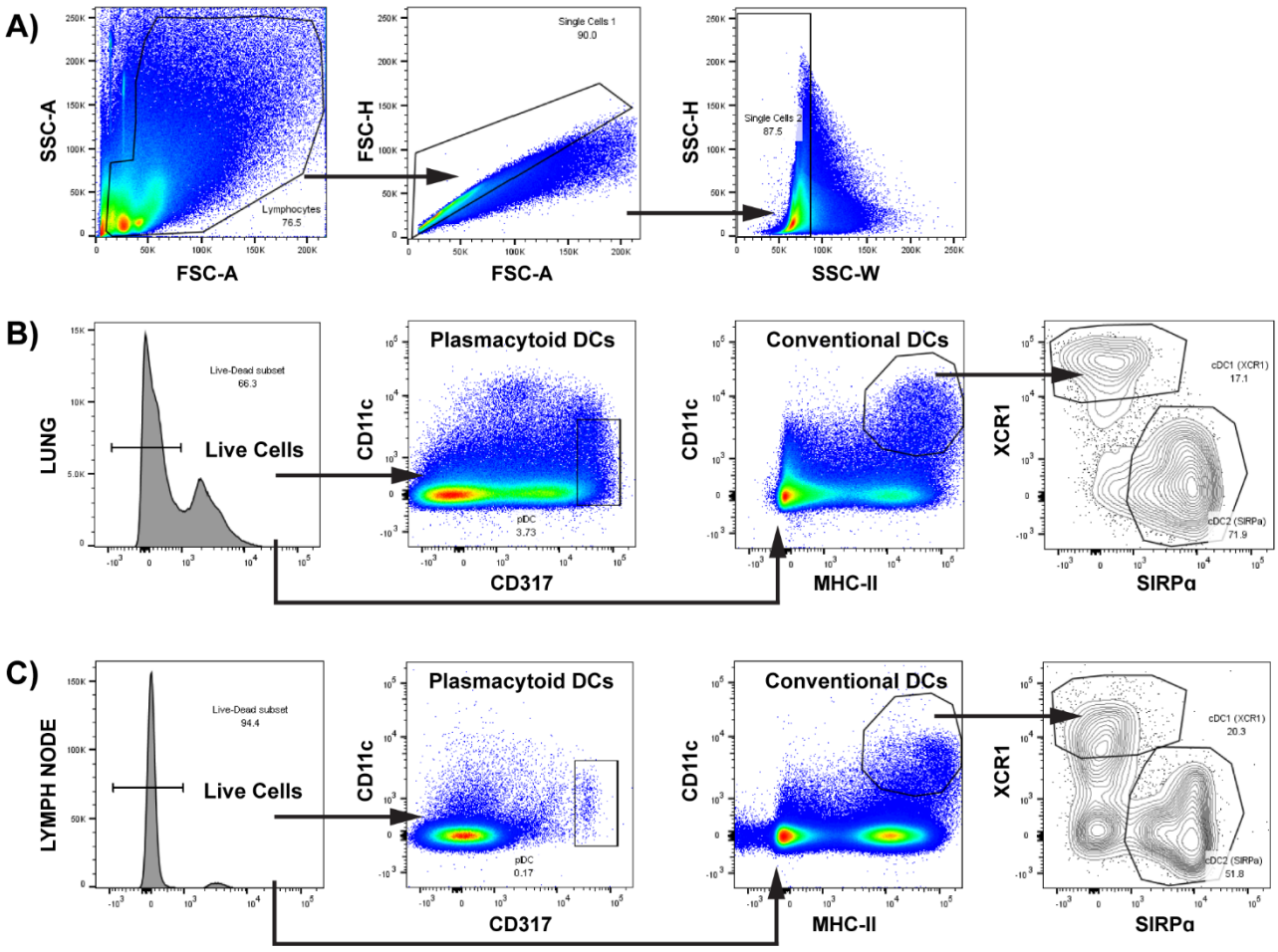

Figure C.6 | Gating strategy for identification of dendritic cell subsets in the lungs and lymph node. Representative flow plots are from mice immunized with pH-responsive NP formulations. **(A)** All events were gated minus debris (SSC-A *vs*. FSC-A), then single cell events were isolated (FSC-H *vs*. FSC-A, SSC-H *vs*. SSC-W). **(B)** In the lungs, viable single cells were identified using Ghost Dye™ Violet 510. Live cells were then gated using a variety of surface markers to identify pulmonary immune cell subsets. **(C)** In the lung-draining lymph node, viable single cells were identified using Ghost Dye™ Violet 510. Live cells were then gated using a variety of surface markers to identify lymphoid immune cell subsets. In both organs, cell subsets were identified by the following phenotypes: plasmacytoid DC (pDC) = $CD11^{lo}CD317^{+}$; conventional DC (cDC) = $CD11c^{+}MHCII^{+}$; cross-presenting cDC1 = $XCR1^{+}CD11c^{+}MHCII^{+}$; non-cross-presenting cDC2 = $SIRP\alpha^{+}CD11c^{+}MHCII^{+}$

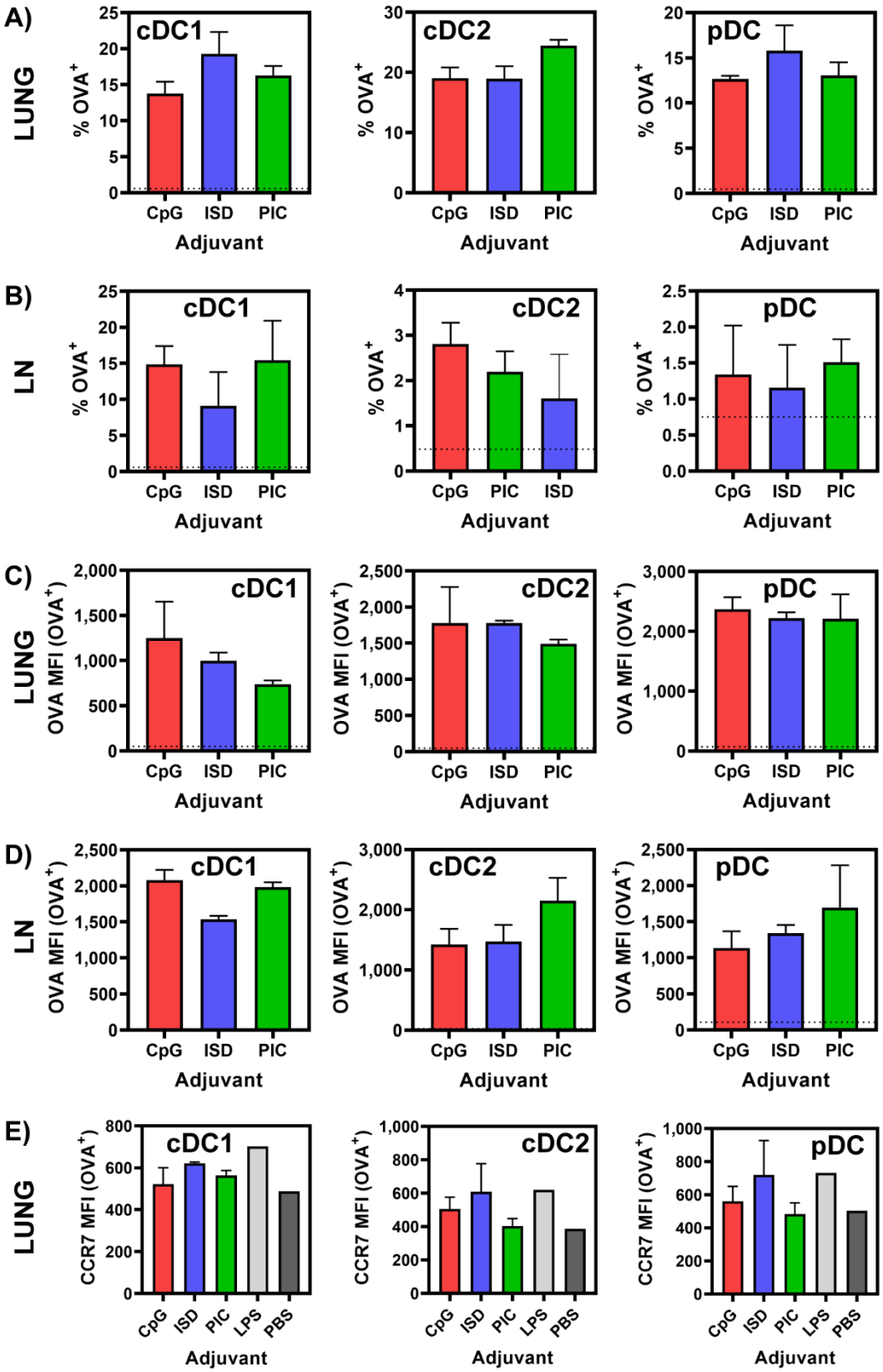

Figure C.7 | OVA uptake, OVA MFI, and CCR7 MFI in lung and lymph node dendritic cells. Mice were immunized i.n. with OVA-PH/CpG, OVA-PH/ISD, or OVA-PH/PIC containing AF647-labeled OVA; LPS and PBS were used for positive and negative controls, respectively. Lungs and mediastinal lymph

nodes were harvested 24 h after immunization and analyzed by flow cytometry for uptake of OVA647 and expression of CD86/CCR7. **(A)** Percent OVA^+ DCs in the lungs. **(B)** Percent OVA^+ DCs in the LN. **(C)** OVA MFI (OVA^+ cells) in the lungs. **(D)** OVA MFI (OVA^+ cells) in the LN. **(E)** CCR7 MFI (OVA^+ cells) in the lungs; *n* = 1-2 per group.

REFERENCES

1. Clemens, E.; Van De Sandt, C.; Wong, S.; Wakim, L.; Valkenburg, S., Harnessing the Power of T Cells: The Promising Hope for a Universal Influenza Vaccine. *Vaccines* **2018,** *6* (2), 18.
2. Behar, S. M.; Woodworth, J. S.; Wu, Y., Next generation: tuberculosis vaccines that elicit protective CD8 + T cells. **2007,** *6* (3), 441-456.
3. Egelston, C. A.; Avalos, C.; Tu, T. Y.; Rosario, A.; Wang, R.; Solomon, S.; Srinivasan, G.; Nelson, M. S.; Huang, Y.; Lim, M. H.; Simons, D. L.; He, T.-F.; Yim, J. H.; Kruper, L.; Mortimer, J.; Yost, S.; Guo, W.; Ruel, C.; Frankel, P. H.; Yuan, Y.; Lee, P. P., Resident memory CD8+ T cells within cancer islands mediate survival in breast cancer patients. *JCI Insight* **2019,** *4* (19).
4. Garber, K., Pursuit of tumor-infiltrating lymphocyte immunotherapy speeds up. *Nat Biotechnol* **2019,** *37* (9), 969-971.
5. Amsen, D.; van Gisbergen, K.; Hombrink, P.; van Lier, R. A. W., Tissue-resident memory T cells at the center of immunity to solid tumors. *Nat Immunol* **2018,** *19* (6), 538-546.
6. Esser, M. T.; Marchese, R. D.; Kierstead, L. S.; Tussey, L. G.; Wang, F.; Chirmule, N.; Washabaugh, M. W., Memory T cells and vaccines. *Vaccine* **2003,** *21* (5-6), 419-430.
7. Takamura, S.; Kohlmeier, J. E., Establishment and Maintenance of Conventional and Circulation-Driven Lung-Resident Memory CD8+ T Cells Following Respiratory Virus Infections. *Frontiers in Immunology* **2019,** *10*.
8. Knight, F. C.; Gilchuk, P.; Kumar, A.; Becker, K. W.; Sevimli, S.; Jacobson, M. E.; Suryadevara, N.; Wang-Bishop, L.; Boyd, K. L.; Crowe, J. E., Jr.; Joyce, S.; Wilson, J. T., Mucosal Immunization with a pH-Responsive Nanoparticle Vaccine Induces Protective CD8(+) Lung-Resident Memory T Cells. *ACS Nano* **2019,** *13* (10), 10939-10960.
9. Haddadi, S.; Vaseghi-Shanjani, M.; Yao, Y.; Afkhami, S.; D'Agostino, M. R.; Zganiacz, A.; Jeyanathan, M.; Xing, Z., Mucosal-Pull Induction of Lung-Resident Memory CD8 T Cells in Parenteral TB Vaccine-Primed Hosts Requires Cognate Antigens and CD4 T Cells. *Front Immunol* **2019,** *10*, 2075.
10. Haynes, B. F.; Bradley, T., Broadly Neutralizing Antibodies and the Development of Vaccines. *JAMA* **2015,** *313* (24), 2419.
11. Mathew, N. R.; Angeletti, D., Recombinant Influenza Vaccines: Saviors to Overcome Immunodominance. *Frontiers in Immunology* **2020,** *10* (2997).
12. Fang, M.; Sigal, L. J., Antibodies and CD8+ T cells are complementary and essential for natural resistance to a highly lethal cytopathic virus. *J Immunol* **2005,** *175* (10), 6829-36.
13. Moyle, P. M.; Toth, I., Modern Subunit Vaccines: Development, Components, and Research Opportunities. *ChemMedChem* **2013,** *8* (3), 360-376.
14. Hogenesch, H.; O'Hagan, D. T.; Fox, C. B., Optimizing the utilization of aluminum adjuvants in vaccines: you might just get what you want. *npj Vaccines* **2018,** *3* (1).
15. Szabo, P. A.; Miron, M.; Farber, D. L., Location, location, location: Tissue resident memory T cells in mice and humans. *Science Immunology* **2019,** *4* (34), eaas9673.
16. Sallusto, F.; Geginat, J.; Lanzavecchia, A., Central Memory and Effector Memory T Cell Subsets: Function, Generation, and Maintenance. *Annual Review of Immunology* **2004,** *22* (1), 745-763.
17. Mueller, S. N.; Mackay, L. K., Tissue-resident memory T cells: local specialists in immune defence. *Nature Reviews Immunology* **2016,** *16* (2), 79-89.
18. Schenkel, J. M.; Masopust, D., Tissue-resident memory T cells. *Immunity* **2014,** *41* (6), 886-97.
19. Buggert, M.; Nguyen, S.; Salgado-Montes De Oca, G.; Bengsch, B.; Darko, S.; Ransier, A.; Roberts, E. R.; Del Alcazar, D.; Brody, I. B.; Vella, L. A.; Beura, L.; Wijeyesinghe, S.; Herati, R. S.; Del Rio Estrada, P. M.; Ablanedo-Terrazas, Y.; Kuri-Cervantes, L.; Sada Japp, A.; Manne, S.; Vartanian, S.; Huffman, A.; Sandberg, J. K.; Gostick, E.; Nadolski, G.; Silvestri, G.; Canaday, D. H.; Price, D. A.; Petrovas, C.; Su, L. F.; Vahedi, G.; Dori, Y.; Frank, I.; Itkin, M. G.; Wherry, E. J.; Deeks, S. G.; Naji, A.; Reyes-Terán, G.; Masopust, D.; Douek, D. C.; Betts, M. R., Identification and characterization of HIV-specific resident memory CD8 + T cells in human lymphoid tissue. *Science Immunology* **2018,** *3* (24), eaar4526.
20. Haddadi, S.; Thanthrige-Don, N.; Afkhami, S.; Khera, A.; Jeyanathan, M.; Xing, Z., Expression and role of VLA-1 in resident memory CD8 T cell responses to respiratory mucosal viral-vectored immunization against tuberculosis. *Scientific Reports* **2017,** *7* (1).
21. Jozwik, A.; Habibi, M. S.; Paras, A.; Zhu, J.; Guvenel, A.; Dhariwal, J.; Almond, M.; Wong, E. H. C.; Sykes, A.; Maybeno, M.; Del Rosario, J.; Trujillo-Torralbo, M.-B.; Mallia, P.; Sidney, J.; Peters, B.; Kon, O. M.; Sette, A.; Johnston, S. L.; Openshaw, P. J.; Chiu, C., RSV-specific airway resident memory CD8+ T cells and differential disease severity after experimental human infection. *Nature Communications* **2015,** *6* (1), 10224.

22. Laidlaw, B. J.; Zhang, N.; Marshall, H. D.; Staron, M. M.; Guan, T.; Hu, Y.; Cauley, L. S.; Craft, J.; Kaech, S. M., CD4+ T Cell Help Guides Formation of CD103+ Lung-Resident Memory CD8+ T Cells during Influenza Viral Infection. **2014,** *41* (4), 633-645.
23. Walk, J.; Stok, J. E.; Sauerwein, R. W., Can Patrolling Liver-Resident T Cells Control Human Malaria Parasite Development? *Trends in Immunology* **2019,** *40* (3), 186-196.
24. Jeyanathan, M.; Yao, Y.; Afkhami, S.; Smaill, F.; Xing, Z., New Tuberculosis Vaccine Strategies: Taking Aim at Un-Natural Immunity. *Trends in Immunology* **2018,** *39* (5), 419-433.
25. Savas, P.; Virassamy, B.; Ye, C.; Salim, A.; Mintoff, C. P.; Caramia, F.; Salgado, R.; Byrne, D. J.; Teo, Z. L.; Dushyanthen, S.; Byrne, A.; Wein, L.; Luen, S. J.; Poliness, C.; Nightingale, S. S.; Skandarajah, A. S.; Gyorki, D. E.; Thornton, C. M.; Beavis, P. A.; Fox, S. B.; Darcy, P. K.; Speed, T. P.; Mackay, L. K.; Neeson, P. J.; Loi, S., Single-cell profiling of breast cancer T cells reveals a tissue-resident memory subset associated with improved prognosis. *Nature Medicine* **2018,** *24* (7), 986-993.
26. Enamorado, M.; Iborra, S.; Priego, E.; Cueto, F. J.; Quintana, J. A.; Martínez-Cano, S.; Mejías-Pérez, E.; Esteban, M.; Melero, I.; Hidalgo, A.; Sancho, D., Enhanced anti-tumour immunity requires the interplay between resident and circulating memory CD8+ T cells. *Nature Communications* **2017,** *8* (1).
27. Sandoval, F.; Terme, M.; Nizard, M.; Badoual, C.; Bureau, M. F.; Freyburger, L.; Clement, O.; Marcheteau, E.; Gey, A.; Fraisse, G.; Bouguin, C.; Merillon, N.; Dransart, E.; Tran, T.; Quintin-Colonna, F.; Autret, G.; Thiebaud, M.; Suleman, M.; Riffault, S.; Wu, T. C.; Launay, O.; Danel, C.; Taieb, J.; Richardson, J.; Zitvogel, L.; Fridman, W. H.; Johannes, L.; Tartour, E., Mucosal Imprinting of Vaccine-Induced CD8+ T Cells Is Crucial to Inhibit the Growth of Mucosal Tumors. **2013,** *5* (172), 172ra20-172ra20.
28. Djenidi, F.; Adam, J.; Goubar, A.; Durgeau, A.; Meurice, G.; De Montpréville, V.; Validire, P.; Besse, B.; Mami-Chouaib, F., CD8+CD103+ Tumor–Infiltrating Lymphocytes Are Tumor-Specific Tissue-Resident Memory T Cells and a Prognostic Factor for Survival in Lung Cancer Patients. *The Journal of Immunology* **2015,** *194* (7), 3475-3486.
29. Topham, D. J.; Reilly, E. C.; Emo, K. L.; Sportiello, M., Formation and Maintenance of Tissue Resident Memory CD8+ T Cells after Viral Infection. *Pathogens* **2019,** *8* (4).
30. Sandoval, F.; Terme, M.; Nizard, M.; Badoual, C.; Bureau, M. F.; Freyburger, L.; Clement, O.; Marcheteau, E.; Gey, A.; Fraisse, G.; Bouguin, C.; Merillon, N.; Dransart, E.; Tran, T.; Quintin-Colonna, F.; Autret, G.; Thiebaud, M.; Suleman, M.; Riffault, S.; Wu, T. C.; Launay, O.; Danel, C.; Taieb, J.; Richardson, J.; Zitvogel, L.; Fridman, W. H.; Johannes, L.; Tartour, E., Mucosal imprinting of vaccine-induced CD8(+) T cells is crucial to inhibit the growth of mucosal tumors. *Sci Transl Med* **2013,** *5* (172), 172ra20.
31. Masopust, D.; Vezys, V.; Wherry, E. J.; Barber, D. L.; Ahmed, R., Cutting edge: gut microenvironment promotes differentiation of a unique memory CD8 T cell population. *J Immunol* **2006,** *176* (4), 2079-83.
32. Mackay, L. K.; Rahimpour, A.; Ma, J. Z.; Collins, N.; Stock, A. T.; Hafon, M. L.; Vega-Ramos, J.; Lauzurica, P.; Mueller, S. N.; Stefanovic, T.; Tscharke, D. C.; Heath, W. R.; Inouye, M.; Carbone, F. R.; Gebhardt, T., The developmental pathway for CD103(+)CD8+ tissue-resident memory T cells of skin. *Nat Immunol* **2013,** *14* (12), 1294-301.
33. Turner, D. L.; Farber, D. L., Mucosal Resident Memory CD4 T Cells in Protection and Immunopathology. *Frontiers in Immunology* **2014,** *5*.
34. Stary, G.; Olive, A.; Radovic-Moreno, A. F.; Gondek, D.; Alvarez, D.; Basto, P. A.; Perro, M.; Vrbanac, V. D.; Tager, A. M.; Shi, J.; Yethon, J. A.; Farokhzad, O. C.; Langer, R.; Starnbach, M. N.; von Andrian, U. H., A mucosal vaccine against Chlamydia trachomatis generates two waves of protective memory T cells. *Science* **2015,** *348* (6241), aaa8205.
35. Wilk, M. M.; Misiak, A.; McManus, R. M.; Allen, A. C.; Lynch, M. A.; Mills, K. H. G., Lung CD4 Tissue-Resident Memory T Cells Mediate Adaptive Immunity Induced by Previous Infection of Mice with Bordetella pertussis. *The Journal of Immunology* **2017**, 1602051.
36. Glennie, N. D.; Yeramilli, V. A.; Beiting, D. P.; Volk, S. W.; Weaver, C. T.; Scott, P., Skin-resident memory CD4+T cells enhance protection againstLeishmania majorinfection. *The Journal of Experimental Medicine* **2015,** *212* (9), 1405-1414.
37. Bull, N. C.; Kaveh, D. A.; Garcia-Pelayo, M. C.; Stylianou, E.; McShane, H.; Hogarth, P. J., Induction and maintenance of a phenotypically heterogeneous lung tissue-resident CD4+ T cell population following BCG immunisation. *Vaccine* **2018,** *36* (37), 5625-5635.
38. Bull, N. C.; Stylianou, E.; Kaveh, D. A.; Pinpathomrat, N.; Pasricha, J.; Harrington-Kandt, R.; Garcia-Pelayo, M. C.; Hogarth, P. J.; McShane, H., Enhanced protection conferred by mucosal BCG vaccination associates with presence of antigen-specific lung tissue-resident PD-1(+) KLRG1(-) CD4(+) T cells. *Mucosal Immunol* **2019,** *12* (2), 555-564.

39. Sakai, S.; Kauffman, K. D.; Schenkel, J. M.; McBerry, C. C.; Mayer-Barber, K. D.; Masopust, D.; Barber, D. L., Cutting Edge: Control of Mycobacterium tuberculosis Infection by a Subset of Lung Parenchyma-Homing CD4 T Cells. *The Journal of Immunology* **2014,** *192* (7), 2965-2969.
40. Teijaro, J. R.; Turner, D.; Pham, Q.; Wherry, E. J.; Lefrançois, L.; Farber, D. L., Cutting Edge: Tissue-Retentive Lung Memory CD4 T Cells Mediate Optimal Protection to Respiratory Virus Infection. *The Journal of Immunology* **2011,** *187* (11), 5510-5514.
41. Chapman, T. J.; Topham, D. J., Identification of a Unique Population of Tissue-Memory CD4+ T Cells in the Airways after Influenza Infection That Is Dependent on the Integrin VLA-1. *The Journal of Immunology* **2010,** *184* (7), 3841-3849.
42. Liu, Y.; Ma, C.; Zhang, N., Tissue-Specific Control of Tissue-Resident Memory T Cells. *Crit Rev Immunol* **2018,** *38* (2), 79-103.
43. Fan, X.; Alexander, Hallmarks of Tissue-Resident Lymphocytes. *Cell* **2016,** *164* (6), 1198-1211.
44. Anderson, K. G.; Mayer-Barber, K.; Sung, H.; Beura, L.; James, B. R.; Taylor, J. J.; Qunaj, L.; Griffith, T. S.; Vezys, V.; Barber, D. L.; Masopust, D., Intravascular staining for discrimination of vascular and tissue leukocytes. *Nat Protoc* **2014,** *9* (1), 209-22.
45. Anderson, K. G.; Sung, H.; Skon, C. N.; Lefrancois, L.; Deisinger, A.; Vezys, V.; Masopust, D., Cutting edge: intravascular staining redefines lung CD8 T cell responses. *J Immunol* **2012,** *189* (6), 2702-6.
46. Li, A. V.; Moon, J. J.; Abraham, W.; Suh, H.; Elkhader, J.; Seidman, M. A.; Yen, M.; Im, E. J.; Foley, M. H.; Barouch, D. H.; Irvine, D. J., Generation of effector memory T cell-based mucosal and systemic immunity with pulmonary nanoparticle vaccination. *Sci Transl Med* **2013,** *5* (204), 204ra130.
47. Iborra, S.; Martinez-Lopez, M.; Khouili, S. C.; Enamorado, M.; Cueto, F. J.; Conde-Garrosa, R.; Del Fresno, C.; Sancho, D., Optimal Generation of Tissue-Resident but Not Circulating Memory T Cells during Viral Infection Requires Crosspriming by DNGR-1(+) Dendritic Cells. *Immunity* **2016,** *45* (4), 847-860.
48. Wakim, L. M.; Smith, J.; Caminschi, I.; Lahoud, M. H.; Villadangos, J. A., Antibody-targeted vaccination to lung dendritic cells generates tissue-resident memory CD8 T cells that are highly protective against influenza virus infection. *Mucosal Immunol* **2015,** *8* (5), 1060-71.
49. Fernandez-Ruiz, D.; Ng, W. Y.; Holz, L. E.; Ma, J. Z.; Zaid, A.; Wong, Y. C.; Lau, L. S.; Mollard, V.; Cozijnsen, A.; Collins, N.; Li, J.; Davey, G. M.; Kato, Y.; Devi, S.; Skandari, R.; Pauley, M.; Manton, J. H.; Godfrey, D. I.; Braun, A.; Tay, S. S.; Tan, P. S.; Bowen, D. G.; Koch-Nolte, F.; Rissiek, B.; Carbone, F. R.; Crabb, B. S.; Lahoud, M.; Cockburn, I. A.; Mueller, S. N.; Bertolino, P.; McFadden, G. I.; Caminschi, I.; Heath, W. R., Liver-Resident Memory CD8(+) T Cells Form a Front-Line Defense against Malaria Liver-Stage Infection. *Immunity* **2016,** *45* (4), 889-902.
50. Wilson, J. T.; Keller, S.; Manganiello, M. J.; Cheng, C.; Lee, C. C.; Opara, C.; Convertine, A.; Stayton, P. S., pH-Responsive nanoparticle vaccines for dual-delivery of antigens and immunostimulatory oligonucleotides. *ACS Nano* **2013,** *7* (5), 3912-25.
51. Scott, E. A.; Stano, A.; Gillard, M.; Maio-Liu, A. C.; Swartz, M. A.; Hubbell, J. A., Dendritic cell activation and T cell priming with adjuvant- and antigen-loaded oxidation-sensitive polymersomes. *Biomaterials* **2012,** *33* (26), 6211-9.
52. Casey, K. A.; Fraser, K. A.; Schenkel, J. M.; Moran, A.; Abt, M. C.; Beura, L. K.; Lucas, P. J.; Artis, D.; Wherry, E. J.; Hogquist, K.; Vezys, V.; Masopust, D., Antigen-independent differentiation and maintenance of effector-like resident memory T cells in tissues. *J Immunol* **2012,** *188* (10), 4866-75.
53. Shin, H.; Iwasaki, A., A vaccine strategy that protects against genital herpes by establishing local memory T cells. *Nature* **2012,** *491* (7424), 463-7.
54. Mackay, L. K.; Stock, A. T.; Ma, J. Z.; Jones, C. M.; Kent, S. J.; Mueller, S. N.; Heath, W. R.; Carbone, F. R.; Gebhardt, T., Long-lived epithelial immunity by tissue-resident memory T (TRM) cells in the absence of persisting local antigen presentation. *Proc Natl Acad Sci U S A* **2012,** *109* (18), 7037-42.
55. Wakim, L. M.; Woodward-Davis, A.; Bevan, M. J., Memory T cells persisting within the brain after local infection show functional adaptations to their tissue of residence. *Proc Natl Acad Sci U S A* **2010,** *107* (42), 17872-9.
56. Iijima, N.; Iwasaki, A., T cell memory. A local macrophage chemokine network sustains protective tissue-resident memory CD4 T cells. *Science* **2014,** *346* (6205), 93-8.
57. Zammit, D. J.; Turner, D. L.; Klonowski, K. D.; Lefrancois, L.; Cauley, L. S., Residual antigen presentation after influenza virus infection affects CD8 T cell activation and migration. *Immunity* **2006,** *24* (4), 439-49.
58. Zacharias, Z. R.; Ross, K. A.; Hornick, E. E.; Goodman, J. T.; Narasimhan, B.; Waldschmidt, T. J.; Legge, K. L., Polyanhydride Nanovaccine Induces Robust Pulmonary B and T Cell Immunity and Confers Protection Against Homologous and Heterologous Influenza A Virus Infections. *Front Immunol* **2018,** *9*, 1953.
59. Lapuente, D.; Storcksdieck Genannt Bonsmann, M.; Maaske, A.; Stab, V.; Heinecke, V.; Watzstedt, K.; Hess, R.; Westendorf, A. M.; Bayer, W.; Ehrhardt, C.; Tenbusch, M., IL-1beta as mucosal vaccine adjuvant: the

specific induction of tissue-resident memory T cells improves the heterosubtypic immunity against influenza A viruses. *Mucosal Immunol* **2018,** *11* (4), 1265-1278.
60. Holz, L. E.; Prier, J. E.; Freestone, D.; Steiner, T. M.; English, K.; Johnson, D. N.; Mollard, V.; Cozijnsen, A.; Davey, G. M.; Godfrey, D. I.; Yui, K.; Mackay, L. K.; Lahoud, M. H.; Caminschi, I.; McFadden, G. I.; Bertolino, P.; Fernandez-Ruiz, D.; Heath, W. R., CD8(+) T Cell Activation Leads to Constitutive Formation of Liver Tissue-Resident Memory T Cells that Seed a Large and Flexible Niche in the Liver. *Cell Rep* **2018,** *25* (1), 68-79 e4.
61. Thompson, E. A.; Darrah, P. A.; Foulds, K. E.; Hoffer, E.; Caffrey-Carr, A.; Norenstedt, S.; Perbeck, L.; Seder, R. A.; Kedl, R. M.; Loré, K., Monocytes Acquire the Ability to Prime Tissue-Resident T Cells via IL-10-Mediated TGF-β Release. *Cell Reports* **2019,** *28* (5), 1127-1135.e4.
62. Irvine, D. J.; Swartz, M. A.; Szeto, G. L., Engineering synthetic vaccines using cues from natural immunity. *Nature Materials* **2013,** *12* (11), 978-990.
63. Zens, K. D.; Chen, J. K.; Farber, D. L., Vaccine-generated lung tissue-resident memory T cells provide heterosubtypic protection to influenza infection. *JCI Insight* **2016,** *1* (10).
64. Lycke, N., Recent progress in mucosal vaccine development: potential and limitations. *Nat Rev Immunol* **2012,** *12* (8), 592-605.
65. Zhao, J.; Zhao, J.; Mangalam, A. K.; Channappanavar, R.; Fett, C.; Meyerholz, D. K.; Agnihothram, S.; Baric, R. S.; David, C. S.; Perlman, S., Airway Memory CD4(+) T Cells Mediate Protective Immunity against Emerging Respiratory Coronaviruses. *Immunity* **2016,** *44* (6), 1379-91.
66. Gilchuk, P.; Hill, T. M.; Guy, C.; McMaster, S. R.; Boyd, K. L.; Rabacal, W. A.; Lu, P.; Shyr, Y.; Kohlmeier, J. E.; Sebzda, E.; Green, D. R.; Joyce, S., A Distinct Lung-Interstitium-Resident Memory CD8(+) T Cell Subset Confers Enhanced Protection to Lower Respiratory Tract Infection. *Cell Rep* **2016,** *16* (7), 1800-9.
67. Muruganandah, V.; Sathkumara, H. D.; Navarro, S.; Kupz, A., A Systematic Review: The Role of Resident Memory T Cells in Infectious Diseases and Their Relevance for Vaccine Development. *Front Immunol* **2018,** *9*, 1574.
68. Wilk, M. M.; Mills, K. H. G., CD4 TRM Cells Following Infection and Immunization: Implications for More Effective Vaccine Design. *Front Immunol* **2018,** *9*, 1860.
69. Wang, L.; Zhu, C.; Zhang, T.; Tian, Q.; Zhang, N.; Morrison, S.; Morrison, R.; Xue, M.; Zhong, G., Nonpathogenic Colonization with Chlamydia in the Gastrointestinal Tract as Oral Vaccination for Inducing Transmucosal Protection. *Infect Immun* **2018,** *86* (2).
70. Zheng, X.; Oduro, J. D.; Boehme, J. D.; Borkner, L.; Ebensen, T.; Heise, U.; Gereke, M.; Pils, M. C.; Krmpotic, A.; Guzman, C. A.; Bruder, D.; Cicin-Sain, L., Mucosal CD8+ T cell responses induced by an MCMV based vaccine vector confer protection against influenza challenge. *PLoS Pathog* **2019,** *15* (9), e1008036.
71. Dekhtiarenko, I.; Ratts, R. B.; Blatnik, R.; Lee, L. N.; Fischer, S.; Borkner, L.; Oduro, J. D.; Marandu, T. F.; Hoppe, S.; Ruzsics, Z.; Sonnemann, J. K.; Mansouri, M.; Meyer, C.; Lemmermann, N. A. W.; Holtappels, R.; Arens, R.; Klenerman, P.; Früh, K.; Reddehase, M. J.; Riemer, A. B.; Cicin-Sain, L., Peptide Processing Is Critical for T-Cell Memory Inflation and May Be Optimized to Improve Immune Protection by CMV-Based Vaccine Vectors. *PLOS Pathogens* **2016,** *12* (12), e1006072.
72. Macdonald, D. C.; Singh, H.; Whelan, M. A.; Escors, D.; Arce, F.; Bottoms, S. E.; Barclay, W. S.; Maini, M.; Collins, M. K.; Rosenberg, W. M., Harnessing alveolar macrophages for sustained mucosal T-cell recall confers long-term protection to mice against lethal influenza challenge without clinical disease. *Mucosal Immunol* **2014,** *7* (1), 89-100.
73. Morabito, K. M.; Ruckwardt, T. R.; Redwood, A. J.; Moin, S. M.; Price, D. A.; Graham, B. S., Intranasal administration of RSV antigen-expressing MCMV elicits robust tissue-resident effector and effector memory CD8+ T cells in the lung. *Mucosal Immunol* **2017,** *10* (2), 545-554.
74. McMaster, S. R.; Wein, A. N.; Dunbar, P. R.; Hayward, S. L.; Cartwright, E. K.; Denning, T. L.; Kohlmeier, J. E., Pulmonary antigen encounter regulates the establishment of tissue-resident CD8 memory T cells in the lung airways and parenchyma. *Mucosal Immunol* **2018,** *11* (4), 1071-1078.
75. Van Braeckel-Budimir, N.; Varga, S. M.; Badovinac, V. P.; Harty, J. T., Repeated Antigen Exposure Extends the Durability of Influenza-Specific Lung-Resident Memory CD8(+) T Cells and Heterosubtypic Immunity. *Cell Rep* **2018,** *24* (13), 3374-3382 e3.
76. Morabito, K. M.; Ruckwardt, T. J.; Bar-Haim, E.; Nair, D.; Moin, S. M.; Redwood, A. J.; Price, D. A.; Graham, B. S., Memory Inflation Drives Tissue-Resident Memory CD8(+) T Cell Maintenance in the Lung After Intranasal Vaccination With Murine Cytomegalovirus. *Front Immunol* **2018,** *9*, 1861.
77. Anderson, K. G.; Masopust, D., Editorial: Pulmonary resident memory CD8 T cells: here today, gone tomorrow. *Journal of Leukocyte Biology* **2014,** *95* (2), 199-201.

78. Slütter, B.; Van Braeckel-Budimir, N.; Abboud, G.; Varga, S. M.; Salek-Ardakani, S.; Harty, J. T., Dynamics of influenza-induced lung-resident memory T cells underlie waning heterosubtypic immunity. *Science Immunology* **2017,** *2* (7), eaag2031.
79. Florido, M.; Muflihah, H.; Lin, L. C. W.; Xia, Y.; Sierro, F.; Palendira, M.; Feng, C. G.; Bertolino, P.; Stambas, J.; Triccas, J. A.; Britton, W. J., Pulmonary immunization with a recombinant influenza A virus vaccine induces lung-resident CD4(+) memory T cells that are associated with protection against tuberculosis. *Mucosal Immunol* **2018,** *11* (6), 1743-1752.
80. Tan, H. X.; Wheatley, A. K.; Esterbauer, R.; Jegaskanda, S.; Glass, J. J.; Masopust, D.; De Rose, R.; Kent, S. J., Induction of vaginal-resident HIV-specific CD8 T cells with mucosal prime-boost immunization. *Mucosal Immunol* **2018,** *11* (3), 994-1007.
81. Cuburu, N.; Graham, B. S.; Buck, C. B.; Kines, R. C.; Pang, Y. Y.; Day, P. M.; Lowy, D. R.; Schiller, J. T., Intravaginal immunization with HPV vectors induces tissue-resident CD8+ T cell responses. *J Clin Invest* **2012,** *122* (12), 4606-20.
82. Cuburu, N.; Kim, R.; Guittard, G. C.; Thompson, C. D.; Day, P. M.; Hamm, D. E.; Pang, Y. S.; Graham, B. S.; Lowy, D. R.; Schiller, J. T., A Prime-Pull-Amplify Vaccination Strategy To Maximize Induction of Circulating and Genital-Resident Intraepithelial CD8(+) Memory T Cells. *J Immunol* **2019,** *202* (4), 1250-1264.
83. Petitdemange, C.; Kasturi, S. P.; Kozlowski, P. A.; Nabi, R.; Quarnstrom, C. F.; Reddy, P. B. J.; Derdeyn, C. A.; Spicer, L. M.; Patel, P.; Legere, T.; Kovalenkov, Y. O.; Labranche, C. C.; Villinger, F.; Tomai, M.; Vasilakos, J.; Haynes, B.; Kang, C. Y.; Gibbs, J. S.; Yewdell, J. W.; Barouch, D.; Wrammert, J.; Montefiori, D.; Hunter, E.; Amara, R. R.; Masopust, D.; Pulendran, B., Vaccine induction of antibodies and tissue-resident CD8+ T cells enhances protection against mucosal SHIV-infection in young macaques. *JCI Insight* **2019,** *4* (4).
84. Fausther-Bovendo, H.; Kobinger, G. P., Pre-existing immunity against Ad vectors. *Human Vaccines & Immunotherapeutics* **2014,** *10* (10), 2875-2884.
85. Van Der Loo, J. C. M.; Wright, J. F., Progress and challenges in viral vector manufacturing. *Human Molecular Genetics* **2016,** *25* (R1), R42-R52.
86. Woodrow, K. A.; Bennett, K. M.; Lo, D. D., Mucosal Vaccine Design and Delivery. *Annu Rev Biomed Eng* **2012,** *14* (1), 17-46.
87. Lawson, L. B.; Norton, E. B.; Clements, J. D., Defending the mucosa: adjuvant and carrier formulations for mucosal immunity. *Current Opinion in Immunology* **2011,** *23* (3), 414-420.
88. Yewdell, J. W., Designing CD8+ T cell vaccines: it's not rocket science (yet). *Curr Opin Immunol* **2010,** *22* (3), 402-10.
89. Foged, C.; Hansen, J.; Agger, E. M., License to kill: Formulation requirements for optimal priming of CD8(+) CTL responses with particulate vaccine delivery systems. *Eur J Pharm Sci* **2012,** *45* (4), 482-91.
90. Koup, R. A.; Douek, D. C., Vaccine design for CD8 T lymphocyte responses. *Cold Spring Harb Perspect Med* **2011,** *1* (1), a007252.
91. Foged, C., Subunit vaccines of the future: the need for safe, customized and optimized particulate delivery systems. *Ther Deliv* **2011,** *2* (8), 1057-77.
92. Mohsen, M. O.; Zha, L.; Cabral-Miranda, G.; Bachmann, M. F., Major findings and recent advances in virus–like particle (VLP)-based vaccines. *Seminars in Immunology* **2017,** *34*, 123-132.
93. Lee, Y. N.; Lee, Y. T.; Kim, M. C.; Gewirtz, A. T.; Kang, S. M., A Novel Vaccination Strategy Mediating the Induction of Lung-Resident Memory CD8 T Cells Confers Heterosubtypic Immunity against Future Pandemic Influenza Virus. *J Immunol* **2016,** *196* (6), 2637-45.
94. Hodgins, B.; Pillet, S.; Landry, N.; Ward, B. J., Prime-pull vaccination with a plant-derived virus-like particle influenza vaccine elicits a broad immune response and protects aged mice from death and frailty after challenge. *Immun Ageing* **2019,** *16*, 27.
95. Schwarz, B.; Morabito, K. M.; Ruckwardt, T. J.; Patterson, D. P.; Avera, J.; Miettinen, H. M.; Graham, B. S.; Douglas, T., Viruslike Particles Encapsidating Respiratory Syncytial Virus M and M2 Proteins Induce Robust T Cell Responses. *ACS Biomater Sci Eng* **2016,** *2* (12), 2324-2332.
96. Takamura, S., Niches for the Long-Term Maintenance of Tissue-Resident Memory T Cells. *Front Immunol* **2018,** *9*, 1214.
97. Reagin, K. L.; Klonowski, K. D., Incomplete Memories: The Natural Suppression of Tissue-Resident Memory CD8 T Cells in the Lung. *Front Immunol* **2018,** *9*, 17.
98. Gola, A.; Silman, D.; Walters, A. A.; Sridhar, S.; Uderhardt, S.; Salman, A. M.; Halbroth, B. R.; Bellamy, D.; Bowyer, G.; Powlson, J.; Baker, M.; Venkatraman, N.; Poulton, I.; Berrie, E.; Roberts, R.; Lawrie, A. M.; Angus, B.; Khan, S. M.; Janse, C. J.; Ewer, K. J.; Germain, R. N.; Spencer, A. J.; Hill, A. V. S., Prime and target immunization protects against liver-stage malaria in mice. *Sci Transl Med* **2018,** *10* (460).

99. Woodworth, J. S.; Cohen, S. B.; Moguche, A. O.; Plumlee, C. R.; Agger, E. M.; Urdahl, K. B.; Andersen, P., Subunit vaccine H56/CAF01 induces a population of circulating CD4 T cells that traffic into the Mycobacterium tuberculosis-infected lung. *Mucosal Immunol* **2017,** *10* (2), 555-564.
100. Zhu, Q.; Egelston, C.; Gagnon, S.; Sui, Y.; Belyakov, I. M.; Klinman, D. M.; Berzofsky, J. A., Using 3 TLR ligands as a combination adjuvant induces qualitative changes in T cell responses needed for antiviral protection in mice. *J Clin Invest* **2010,** *120* (2), 607-16.
101. Mestecky, J.; Russell, M. W., Induction of mucosal immune responses in the human genital tract. *FEMS Immunol Med Microbiol* **2000,** *27* (4), 351-5.
102. Sato, A.; Suwanto, A.; Okabe, M.; Sato, S.; Nochi, T.; Imai, T.; Koyanagi, N.; Kunisawa, J.; Kawaguchi, Y.; Kiyono, H., Vaginal memory T cells induced by intranasal vaccination are critical for protective T cell recruitment and prevention of genital HSV-2 disease. *J Virol* **2014,** *88* (23), 13699-708.
103. Si, Y.; Wen, Y.; Kelly, S. H.; Chong, A. S.; Collier, J. H., Intranasal delivery of adjuvant-free peptide nanofibers elicits resident CD8(+) T cell responses. *J Control Release* **2018,** *282*, 120-130.
104. Hart, P.; Copland, A.; Diogo, G. R.; Harris, S.; Spallek, R.; Oehlmann, W.; Singh, M.; Basile, J.; Rottenberg, M.; Paul, M. J.; Reljic, R., Nanoparticle-Fusion Protein Complexes Protect against Mycobacterium tuberculosis Infection. *Mol Ther* **2018,** *26* (3), 822-833.
105. Fromen, C. A.; Rahhal, T. B.; Robbins, G. R.; Kai, M. P.; Shen, T. W.; Luft, J. C.; DeSimone, J. M., Nanoparticle surface charge impacts distribution, uptake and lymph node trafficking by pulmonary antigen-presenting cells. *Nanomedicine* **2016,** *12* (3), 677-687.
106. Stano, A.; Scott, E. A.; Dane, K. Y.; Swartz, M. A.; Hubbell, J. A., Tunable T cell immunity towards a protein antigen using polymersomes vs. solid-core nanoparticles. *Biomaterials* **2013,** *34* (17), 4339-46.
107. Frey, M.; Bobbala, S.; Karabin, N.; Scott, E., Influences of nanocarrier morphology on therapeutic immunomodulation. *Nanomedicine (Lond)* **2018**.
108. Convertine, A. J.; Benoit, D. S. W.; Duvall, C. L.; Hoffman, A. S.; Stayton, P. S., Development of a novel endosomolytic diblock copolymer for siRNA delivery. *Journal of Controlled Release* **2009,** *133* (3), 221-229.
109. Gebhardt, T.; Palendira, U.; Tscharke, D. C.; Bedoui, S., Tissue-resident memory T cells in tissue homeostasis, persistent infection, and cancer surveillance. *Immunol Rev* **2018,** *283* (1), 54-76.
110. Shin, H.; Iwasaki, A., Tissue-resident memory T cells. *Immunol Rev* **2013,** *255* (1), 165-81.
111. Mueller, S. N.; Gebhardt, T.; Carbone, F. R.; Heath, W. R., Memory T cell subsets, migration patterns, and tissue residence. *Annu Rev Immunol* **2013,** *31*, 137-61.
112. Ariotti, S.; Haanen, J. B.; Schumacher, T. N., Behavior and function of tissue-resident memory T cells. *Adv Immunol* **2012,** *114*, 203-16.
113. Buggert, M.; Nguyen, S.; Salgado-Montes de Oca, G.; Bengsch, B.; Darko, S.; Ransier, A.; Roberts, E. R.; Del Alcazar, D.; Brody, I. B.; Vella, L. A.; Beura, L.; Wijeyesinghe, S.; Herati, R. S.; Del Rio Estrada, P. M.; Ablanedo-Terrazas, Y.; Kuri-Cervantes, L.; Sada Japp, A.; Manne, S.; Vartanian, S.; Huffman, A.; Sandberg, J. K.; Gostick, E.; Nadolski, G.; Silvestri, G.; Canaday, D. H.; Price, D. A.; Petrovas, C.; Su, L. F.; Vahedi, G.; Dori, Y.; Frank, I.; Itkin, M. G.; Wherry, E. J.; Deeks, S. G.; Naji, A.; Reyes-Teran, G.; Masopust, D.; Douek, D. C.; Betts, M. R., Identification and characterization of HIV-specific resident memory CD8(+) T cells in human lymphoid tissue. *Sci Immunol* **2018,** *3* (24).
114. Haddadi, S.; Thanthrige-Don, N.; Afkhami, S.; Khera, A.; Jeyanathan, M.; Xing, Z., Expression and role of VLA-1 in resident memory CD8 T cell responses to respiratory mucosal viral-vectored immunization against tuberculosis. *Sci Rep* **2017,** *7* (1), 9525.
115. Jozwik, A.; Habibi, M. S.; Paras, A.; Zhu, J.; Guvenel, A.; Dhariwal, J.; Almond, M.; Wong, E. H.; Sykes, A.; Maybeno, M.; Del Rosario, J.; Trujillo-Torralbo, M. B.; Mallia, P.; Sidney, J.; Peters, B.; Kon, O. M.; Sette, A.; Johnston, S. L.; Openshaw, P. J.; Chiu, C., RSV-specific airway resident memory CD8+ T cells and differential disease severity after experimental human infection. *Nat Commun* **2015,** *6*, 10224.
116. Laidlaw, B. J.; Zhang, N.; Marshall, H. D.; Staron, M. M.; Guan, T.; Hu, Y.; Cauley, L. S.; Craft, J.; Kaech, S. M., CD4+ T cell help guides formation of CD103+ lung-resident memory CD8+ T cells during influenza viral infection. *Immunity* **2014,** *41* (4), 633-45.
117. Savas, P.; Virassamy, B.; Ye, C.; Salim, A.; Mintoff, C. P.; Caramia, F.; Salgado, R.; Byrne, D. J.; Teo, Z. L.; Dushyanthen, S.; Byrne, A.; Wein, L.; Luen, S. J.; Poliness, C.; Nightingale, S. S.; Skandarajah, A. S.; Gyorki, D. E.; Thornton, C. M.; Beavis, P. A.; Fox, S. B.; Kathleen Cuningham Foundation Consortium for Research into Familial Breast, C.; Darcy, P. K.; Speed, T. P.; Mackay, L. K.; Neeson, P. J.; Loi, S., Single-cell profiling of breast cancer T cells reveals a tissue-resident memory subset associated with improved prognosis. *Nat Med* **2018,** *24* (7), 986-993.
118. Enamorado, M.; Iborra, S.; Priego, E.; Cueto, F. J.; Quintana, J. A.; Martinez-Cano, S.; Mejias-Perez, E.; Esteban, M.; Melero, I.; Hidalgo, A.; Sancho, D., Enhanced anti-tumour immunity requires the interplay between resident and circulating memory CD8(+) T cells. *Nat Commun* **2017,** *8*, 16073.

119. Djenidi, F.; Adam, J.; Goubar, A.; Durgeau, A.; Meurice, G.; de Montpreville, V.; Validire, P.; Besse, B.; Mami-Chouaib, F., CD8+CD103+ tumor-infiltrating lymphocytes are tumor-specific tissue-resident memory T cells and a prognostic factor for survival in lung cancer patients. *J Immunol* **2015,** *194* (7), 3475-86.
120. Nizard, M.; Roussel, H.; Diniz, M. O.; Karaki, S.; Tran, T.; Voron, T.; Dransart, E.; Sandoval, F.; Riquet, M.; Rance, B.; Marcheteau, E.; Fabre, E.; Mandavit, M.; Terme, M.; Blanc, C.; Escudie, J. B.; Gibault, L.; Barthes, F. L. P.; Granier, C.; Ferreira, L. C. S.; Badoual, C.; Johannes, L.; Tartour, E., Induction of resident memory T cells enhances the efficacy of cancer vaccine. *Nat Commun* **2017,** *8*, 15221.
121. Sakai, S.; Kauffman, K. D.; Schenkel, J. M.; McBerry, C. C.; Mayer-Barber, K. D.; Masopust, D.; Barber, D. L., Cutting edge: control of Mycobacterium tuberculosis infection by a subset of lung parenchyma-homing CD4 T cells. *J Immunol* **2014,** *192* (7), 2965-9.
122. Pizzolla, A.; Nguyen, T. H.; Sant, S.; Jaffar, J.; Loudovaris, T.; Mannering, S. I.; Thomas, P. G.; Westall, G. P.; Kedzierska, K.; Wakim, L. M., Influenza-specific lung-resident memory T cells are proliferative and polyfunctional and maintain diverse TCR profiles. *J Clin Invest* **2018,** *128* (2), 721-733.
123. Park, S. L.; Buzzai, A.; Rautela, J.; Hor, J. L.; Hochheiser, K.; Effern, M.; McBain, N.; Wagner, T.; Edwards, J.; McConville, R.; Wilmott, J. S.; Scolyer, R. A.; Tuting, T.; Palendria, U.; Gyorki, D.; Mueller, S. N.; Huntington, N. D.; Bedoui, S.; Holzel, M.; Mackay, L. K.; Waithman, J.; Gebhardt, T., Tissue-resident memory CD8(+) T cells promote melanoma-immune equilibrium in skin. *Nature* **2018**.
124. Wu, T.; Hu, Y.; Lee, Y. T.; Bouchard, K. R.; Benechet, A.; Khanna, K.; Cauley, L. S., Lung-resident memory CD8 T cells (TRM) are indispensable for optimal cross-protection against pulmonary virus infection. *J Leukoc Biol* **2014,** *95* (2), 215-24.
125. Perdomo, C.; Zedler, U.; Kuhl, A. A.; Lozza, L.; Saikali, P.; Sander, L. E.; Vogelzang, A.; Kaufmann, S. H.; Kupz, A., Mucosal BCG Vaccination Induces Protective Lung-Resident Memory T Cell Populations against Tuberculosis. *mBio* **2016,** *7* (6).
126. Takamura, S.; Yagi, H.; Hakata, Y.; Motozono, C.; McMaster, S. R.; Masumoto, T.; Fujisawa, M.; Chikaishi, T.; Komeda, J.; Itoh, J.; Umemura, M.; Kyusai, A.; Tomura, M.; Nakayama, T.; Woodland, D. L.; Kohlmeier, J. E.; Miyazawa, M., Specific niches for lung-resident memory CD8+ T cells at the site of tissue regeneration enable CD69-independent maintenance. *J Exp Med* **2016,** *213* (13), 3057-3073.
127. McMaster, S. R.; Wilson, J. J.; Wang, H.; Kohlmeier, J. E., Airway-Resident Memory CD8 T Cells Provide Antigen-Specific Protection against Respiratory Virus Challenge through Rapid IFN-gamma Production. *J Immunol* **2015,** *195* (1), 203-9.
128. Kinnear, E.; Lambert, L.; McDonald, J. U.; Cheeseman, H. M.; Caproni, L. J.; Tregoning, J. S., Airway T cells protect against RSV infection in the absence of antibody. *Mucosal Immunol* **2018,** *11* (1), 290.
129. Neutra, M. R.; Kozlowski, P. A., Mucosal vaccines: the promise and the challenge. *Nat Rev Immunol* **2006,** *6* (2), 148-58.
130. Woodrow, K. A.; Bennett, K. M.; Lo, D. D., Mucosal vaccine design and delivery. *Annu Rev Biomed Eng* **2012,** *14*, 17-46.
131. Perrie, Y.; Mohammed, A. R.; Kirby, D. J.; McNeil, S. E.; Bramwell, V. W., Vaccine adjuvant systems: enhancing the efficacy of sub-unit protein antigens. *Int J Pharm* **2008,** *364* (2), 272-80.
132. Foged, C.; Hansen, J.; Agger, E. M., License to kill: Formulation requirements for optimal priming of CD8(+) CTL responses with particulate vaccine delivery systems. *European journal of pharmaceutical sciences : official journal of the European Federation for Pharmaceutical Sciences* **2012,** *45* (4), 482-491.
133. Swartz, M. A.; Hirosue, S.; Hubbell, J. A., Engineering approaches to immunotherapy. *Science Translational Medicine* **2012,** *4* (148), 148rv9.
134. Bookstaver, M. L.; Tsai, S. J.; Bromberg, J. S.; Jewell, C. M., Improving Vaccine and Immunotherapy Design Using Biomaterials. *Trends Immunol* **2018,** *39* (2), 135-150.
135. Sahdev, P.; Ochyl, L. J.; Moon, J. J., Biomaterials for nanoparticle vaccine delivery systems. *Pharm Res* **2014,** *31* (10), 2563-82.
136. Kapadia, C. H.; Tian, S.; Perry, J. L.; Sailer, D.; Christopher Luft, J.; DeSimone, J. M., Extending antigen release from particulate vaccines results in enhanced antitumor immune response. *J Control Release* **2018,** *269*, 393-404.
137. de Titta, A.; Ballester, M.; Julier, Z.; Nembrini, C.; Jeanbart, L.; van der Vlies, A. J.; Swartz, M. A.; Hubbell, J. A., Nanoparticle conjugation of CpG enhances adjuvancy for cellular immunity and memory recall at low dose. *Proc Natl Acad Sci U S A* **2013,** *110* (49), 19902-7.
138. Nembrini, C.; Stano, A.; Dane, K. Y.; Ballester, M.; van der Vlies, A. J.; Marsland, B. J.; Swartz, M. A.; Hubbell, J. A., Nanoparticle conjugation of antigen enhances cytotoxic T-cell responses in pulmonary vaccination. *Proc Natl Acad Sci U S A* **2011,** *108* (44), E989-97.

139. Qiu, F.; Becker, K. W.; Knight, F. C.; Baljon, J. J.; Sevimli, S.; Shae, D.; Gilchuk, P.; Joyce, S.; Wilson, J. T., Poly(propylacrylic acid)-peptide nanoplexes as a platform for enhancing the immunogenicity of neoantigen cancer vaccines. *Biomaterials* **2018,** *182*, 82-91.
140. Ballester, M.; Nembrini, C.; Dhar, N.; de Titta, A.; de Piano, C.; Pasquier, M.; Simeoni, E.; van der Vlies, A. J.; McKinney, J. D.; Hubbell, J. A.; Swartz, M. A., Nanoparticle conjugation and pulmonary delivery enhance the protective efficacy of Ag85B and CpG against tuberculosis. *Vaccine* **2011,** *29* (40), 6959-66.
141. Wakim, L. M.; Gupta, N.; Mintern, J. D.; Villadangos, J. A., Enhanced survival of lung tissue-resident memory CD8(+) T cells during infection with influenza virus due to selective expression of IFITM3. *Nat Immunol* **2013,** *14* (3), 238-45.
142. Coffman, R. L.; Sher, A.; Seder, R. A., Vaccine adjuvants: putting innate immunity to work. *Immunity* **2010,** *33* (4), 492-503.
143. Kim, T. S.; Hufford, M. M.; Sun, J.; Fu, Y. X.; Braciale, T. J., Antigen persistence and the control of local T cell memory by migrant respiratory dendritic cells after acute virus infection. *J Exp Med* **2010,** *207* (6), 1161-72.
144. Ho, N. I.; Huis In 't Veld, L. G. M.; Raaijmakers, T. K.; Adema, G. J., Adjuvants Enhancing Cross-Presentation by Dendritic Cells: The Key to More Effective Vaccines? *Front Immunol* **2018,** *9*, 2874.
145. Riehn, M.; Cebula, M.; Hauser, H.; Wirth, D., CpG-ODN Facilitates Effective Intratracheal Immunization and Recall of Memory against Neoantigen-Expressing Alveolar Cells. *Front Immunol* **2017,** *8*, 1201.
146. Khan, T. N.; Mooster, J. L.; Kilgore, A. M.; Osborn, J. F.; Nolz, J. C., Local antigen in nonlymphoid tissue promotes resident memory CD8+ T cell formation during viral infection. *J Exp Med* **2016,** *213* (6), 951-66.
147. Misharin, A. V.; Morales-Nebreda, L.; Mutlu, G. M.; Budinger, G. R.; Perlman, H., Flow cytometric analysis of macrophages and dendritic cell subsets in the mouse lung. *Am J Respir Cell Mol Biol* **2013,** *49* (4), 503-10.
148. Topham, D. J.; Reilly, E. C., Tissue-Resident Memory CD8(+) T Cells: From Phenotype to Function. *Front Immunol* **2018,** *9*, 515.
149. Ben-Sasson, S. Z.; Hogg, A.; Hu-Li, J.; Wingfield, P.; Chen, X.; Crank, M.; Caucheteux, S.; Ratner-Hurevich, M.; Berzofsky, J. A.; Nir-Paz, R.; Paul, W. E., IL-1 enhances expansion, effector function, tissue localization, and memory response of antigen-specific CD8 T cells. *J Exp Med* **2013,** *210* (3), 491-502.
150. Cox, M. A.; Harrington, L. E.; Zajac, A. J., Cytokines and the inception of CD8 T cell responses. *Trends Immunol* **2011,** *32* (4), 180-6.
151. Curtsinger, J. M.; Agarwal, P.; Lins, D. C.; Mescher, M. F., Autocrine IFN-gamma promotes naive CD8 T cell differentiation and synergizes with IFN-alpha to stimulate strong function. *J Immunol* **2012,** *189* (2), 659-68.
152. Henry, C. J.; Ornelles, D. A.; Mitchell, L. M.; Brzoza-Lewis, K. L.; Hiltbold, E. M., IL-12 produced by dendritic cells augments CD8+ T cell activation through the production of the chemokines CCL1 and CCL17. *J Immunol* **2008,** *181* (12), 8576-84.
153. Lee, Y. J.; Won, T. J.; Hyung, K. E.; Jang, Y. W.; Kim, S. J.; Lee do, I.; Park, S. Y.; Hwang, K. W., IL-6 induced proliferation and cytotoxic activity of CD8(+) T cells is elevated by SUMO2 overexpression. *Arch Pharm Res* **2016,** *39* (5), 705-12.
154. Skon, C. N.; Lee, J. Y.; Anderson, K. G.; Masopust, D.; Hogquist, K. A.; Jameson, S. C., Transcriptional downregulation of S1pr1 is required for the establishment of resident memory CD8+ T cells. *Nat Immunol* **2013,** *14* (12), 1285-93.
155. Pesce, I.; Monaci, E.; Muzzi, A.; Tritto, E.; Tavarini, S.; Nuti, S.; De Gregorio, E.; Wack, A., Intranasal administration of CpG induces a rapid and transient cytokine response followed by dendritic and natural killer cell activation and recruitment in the mouse lung. *J Innate Immun* **2010,** *2* (2), 144-59.
156. Lopes, P. P.; Todorov, G.; Pham, T. T.; Nesburn, A. B.; Bahraoui, E.; BenMohamed, L., Laser Adjuvant-Assisted Peptide Vaccine Promotes Skin Mobilization of Dendritic Cells and Enhances Protective CD8(+) TEM and TRM Cell Responses against Herpesvirus Infection and Disease. *J Virol* **2018,** *92* (8).
157. Lee, Y. T.; Suarez-Ramirez, J. E.; Wu, T.; Redman, J. M.; Bouchard, K.; Hadley, G. A.; Cauley, L. S., Environmental and antigen receptor-derived signals support sustained surveillance of the lungs by pathogen-specific cytotoxic T lymphocytes. *J Virol* **2011,** *85* (9), 4085-94.
158. Alpar, H. O.; Somavarapu, S.; Atuah, K. N.; Bramwell, V. W., Biodegradable mucoadhesive particulates for nasal and pulmonary antigen and DNA delivery. *Adv Drug Deliv Rev* **2005,** *57* (3), 411-30.
159. Joffre, O. P.; Segura, E.; Savina, A.; Amigorena, S., Cross-presentation by dendritic cells. *Nat Rev Immunol* **2012,** *12* (8), 557-69.
160. Griffiths, K. L.; Ahmed, M.; Das, S.; Gopal, R.; Horne, W.; Connell, T. D.; Moynihan, K. D.; Kolls, J. K.; Irvine, D. J.; Artyomov, M. N.; Rangel-Moreno, J.; Khader, S. A., Targeting dendritic cells to accelerate T-cell activation overcomes a bottleneck in tuberculosis vaccine efficacy. *Nat Commun* **2016,** *7*, 13894.

161. Beauchamp, N. M.; Yammani, R. D.; Alexander-Miller, M. A., CD8 marks a subpopulation of lung-derived dendritic cells with differential responsiveness to viral infection and toll-like receptor stimulation. *J Virol* **2012,** *86* (19), 10640-50.
162. Perrier, S., 50th Anniversary Perspective: RAFT Polymerization—A User Guide. *Macromolecules* **2017,** *50* (19), 7433-7447.
163. Sevimli, S.; Knight, F. C.; Gilchuk, P.; Joyce, S.; Wilson, J. T., Fatty Acid-Mimetic Micelles for Dual Delivery of Antigens and Imidazoquinoline Adjuvants. *ACS Biomater Sci Eng* **2017,** *3* (2), 179-194.
164. Convertine, A. J.; Diab, C.; Prieve, M.; Paschal, A.; Hoffman, A. S.; Johnson, P. H.; Stayton, P. S., pH-responsive polymeric micelle carriers for siRNA drugs. *Biomacromolecules* **2010,** *11* (11), 2904-11.
165. Jacobson, M. E.; Wang-Bishop, L.; Becker, K. W.; Wilson, J. T., Delivery of 5′-triphosphate RNA with endosomolytic nanoparticles potently activates RIG-I to improve cancer immunotherapy. *Biomaterials Science* **2018**.
166. Murthy, N.; Robichaud, J. R.; Tirrell, D. A.; Stayton, P. S.; Hoffman, A. S., The design and synthesis of polymers for eukaryotic membrane disruption. *J Control Release* **1999,** *61* (1-2), 137-43.
167. Miller, M. A.; Stabenow, J. M.; Parvathareddy, J.; Wodowski, A. J.; Fabrizio, T. P.; Bina, X. R.; Zalduondo, L.; Bina, J. E., Visualization of murine intranasal dosing efficiency using luminescent Francisella tularensis: effect of instillation volume and form of anesthesia. *PLoS One* **2012,** *7* (2), e31359.
168. Gilchuk, P.; Knight, F. C.; Wilson, J. T.; Joyce, S., Eliciting Epitope-Specific CD8+ T Cell Response by Immunization with Microbial Protein Antigens Formulated with alpha-Galactosylceramide: Theory, Practice, and Protocols. *Methods Mol Biol* **2017,** *1494*, 321-352.
169. Rodenko, B.; Toebes, M.; Hadrup, S. R.; van Esch, W. J.; Molenaar, A. M.; Schumacher, T. N.; Ovaa, H., Generation of peptide-MHC class I complexes through UV-mediated ligand exchange. *Nat Protoc* **2006,** *1* (3), 1120-32.
170. Steel, J., A paradigm shift in vaccine production for pandemic influenza. *Ann Transl Med* **2015,** *3* (12), 165.
171. Slutter, B.; Pewe, L. L.; Kaech, S. M.; Harty, J. T., Lung airway-surveilling CXCR3(hi) memory CD8(+) T cells are critical for protection against influenza A virus. *Immunity* **2013,** *39* (5), 939-48.
172. Bailey, E. S.; Choi, J. Y.; Fieldhouse, J. K.; Borkenhagen, L. K.; Zemke, J.; Zhang, D.; Gray, G. C., The continual threat of influenza virus infections at the human-animal interface: What is new from a one health perspective? *Evol Med Public Health* **2018,** *2018* (1), 192-198.
173. Li, Z. T.; Zarnitsyna, V. I.; Lowen, A. C.; Weissman, D.; Koelle, K.; Kohlmeier, J. E.; Antia, R., Why Are CD8 T Cell Epitopes of Human Influenza A Virus Conserved? *J Virol* **2019,** *93* (6).
174. Grant, E.; Wu, C.; Chan, K. F.; Eckle, S.; Bharadwaj, M.; Zou, Q. M.; Kedzierska, K.; Chen, W., Nucleoprotein of influenza A virus is a major target of immunodominant CD8+ T-cell responses. *Immunol Cell Biol* **2013,** *91* (2), 184-94.
175. Grant, E. J.; Quinones-Parra, S. M.; Clemens, E. B.; Kedzierska, K., Human influenza viruses and CD8(+) T cell responses. *Curr Opin Virol* **2016,** *16*, 132-142.
176. Sridhar, S.; Begom, S.; Bermingham, A.; Hoschler, K.; Adamson, W.; Carman, W.; Bean, T.; Barclay, W.; Deeks, J. J.; Lalvani, A., Cellular immune correlates of protection against symptomatic pandemic influenza. *Nat Med* **2013,** *19* (10), 1305-12.
177. McMichael, A. J.; Gotch, F. M.; Noble, G. R.; Beare, P. A., Cytotoxic T-cell immunity to influenza. *N Engl J Med* **1983,** *309* (1), 13-7.
178. Townsend, A. R.; Rothbard, J.; Gotch, F. M.; Bahadur, G.; Wraith, D.; McMichael, A. J., The epitopes of influenza nucleoprotein recognized by cytotoxic T lymphocytes can be defined with short synthetic peptides. *Cell* **1986,** *44* (6), 959-68.
179. Wang, Y.; Deng, L.; Kang, S. M.; Wang, B. Z., Universal influenza vaccines: from viruses to nanoparticles. *Expert Rev Vaccines* **2018,** *17* (11), 967-976.
180. Beura, L. K.; Rosato, P. C.; Masopust, D., Implications of Resident Memory T Cells for Transplantation. *Am J Transplant* **2017,** *17* (5), 1167-1175.
181. Mueller, S. N.; Mackay, L. K., Tissue-resident memory T cells: local specialists in immune defence. *Nat Rev Immunol* **2016,** *16* (2), 79-89.
182. Shane, H. L.; Klonowski, K. D., Every breath you take: the impact of environment on resident memory CD8 T cells in the lung. *Front Immunol* **2014,** *5*, 320.
183. Bergsbaken, T.; Bevan, M. J., Proinflammatory microenvironments within the intestine regulate the differentiation of tissue-resident CD8(+) T cells responding to infection. *Nat Immunol* **2015,** *16* (4), 406-14.
184. Chen, L.; Zanker, D.; Xiao, K.; Wu, C.; Zou, Q.; Chen, W., Immunodominant CD4+ T-Cell Responses to Influenza A Virus in Healthy Individuals Focus on Matrix 1 and Nucleoprotein. **2014,** *88* (20), 11760-11773.
185. Chu, K.-L.; Batista, N. V.; Girard, M.; Watts, T. H., Monocyte-Derived Cells in Tissue-Resident Memory T Cell Formation. *The Journal of Immunology* **2020,** *204* (3), 477-485.

186. Dunbar, P. R.; Cartwright, E. K.; Wein, A. N.; Tsukamoto, T.; Tiger Li, Z.-R.; Kumar, N.; Uddbäck, I. E.; Hayward, S. L.; Ueha, S.; Takamura, S.; Kohlmeier, J. E., Pulmonary monocytes interact with effector T cells in the lung tissue to drive TRM differentiation following viral infection. *Mucosal Immunology* **2019**.
187. Desai, P.; Tahiliani, V.; Stanfield, J.; Abboud, G.; Salek-Ardakani, S., Inflammatory monocytes contribute to the persistence of CXCR3hi CX3CR1lo circulating and lung-resident memory CD8+ T cells following respiratory virus infection. *Immunology and Cell Biology* **2018,** *96* (4), 370-378.
188. Menares, E.; Galvez-Cancino, F.; Caceres-Morgado, P.; Ghorani, E.; Lopez, E.; Diaz, X.; Saavedra-Almarza, J.; Figueroa, D. A.; Roa, E.; Quezada, S. A.; Lladser, A., Tissue-resident memory CD8(+) T cells amplify anti-tumor immunity by triggering antigen spreading through dendritic cells. *Nat Commun* **2019,** *10* (1), 4401.
189. Mayer, C. T.; Ghorbani, P.; Nandan, A.; Dudek, M.; Arnold-Schrauf, C.; Hesse, C.; Berod, L.; Stuve, P.; Puttur, F.; Merad, M.; Sparwasser, T., Selective and efficient generation of functional Batf3-dependent CD103+ dendritic cells from mouse bone marrow. *Blood* **2014,** *124* (20), 3081-3091.
190. Nizard, M.; Diniz, M. O.; Roussel, H.; Tran, T.; Ferreira, L. C.; Badoual, C.; Tartour, E., Mucosal vaccines: novel strategies and applications for the control of pathogens and tumors at mucosal sites. *Hum Vaccin Immunother* **2014,** *10* (8), 2175-87.
191. Caminschi, I.; Lahoud, M. H.; Pizzolla, A.; Wakim, L. M., Zymosan by-passes the requirement for pulmonary antigen encounter in lung tissue-resident memory CD8(+) T cell development. *Mucosal Immunol* **2019,** *12* (2), 403-412.
192. Mäkelä, S. M.; Österlund, P.; Westenius, V.; Latvala, S.; Diamond, M. S.; Gale, M.; Julkunen, I., RIG-I Signaling Is Essential for Influenza B Virus-Induced Rapid Interferon Gene Expression. *Journal of Virology* **2015,** *89* (23), 12014-12025.
193. Robert; Samantha; Donna; Jacqueline; Elie; Olivas, J.; Russell; Christina; Herbert; Jeffery, The Cytosolic Sensor cGAS Detects Mycobacterium tuberculosis DNA to Induce Type I Interferons and Activate Autophagy. *Cell Host & Microbe* **2015,** *17* (6), 811-819.
194. Maurer, T.; Heit, A.; Hochrein, H.; Ampenberger, F.; O'Keeffe, M.; Bauer, S.; Lipford, G. B.; Vabulas, R. M.; Wagner, H., CpG-DNA aided cross-presentation of soluble antigens by dendritic cells. *Eur J Immunol* **2002,** *32* (8), 2356-64.
195. Kuchtey, J.; Chefalo, P. J.; Gray, R. C.; Ramachandra, L.; Harding, C. V., Enhancement of dendritic cell antigen cross-presentation by CpG DNA involves type I IFN and stabilization of class I MHC mRNA. *J Immunol* **2005,** *175* (4), 2244-51.
196. Datta, S. K.; Redecke, V.; Prilliman, K. R.; Takabayashi, K.; Corr, M.; Tallant, T.; DiDonato, J.; Dziarski, R.; Akira, S.; Schoenberger, S. P.; Raz, E., A subset of Toll-like receptor ligands induces cross-presentation by bone marrow-derived dendritic cells. *J Immunol* **2003,** *170* (8), 4102-10.
197. Li, A.; Yi, M.; Qin, S.; Song, Y.; Chu, Q.; Wu, K., Activating cGAS-STING pathway for the optimal effect of cancer immunotherapy. *J Hematol Oncol* **2019,** *12* (1), 35.
198. Splawn, L. M.; Bailey, C. A.; Medina, J. P.; Cho, J. C., Heplisav-B vaccination for the prevention of hepatitis B virus infection in adults in the United States. *Drugs Today (Barc)* **2018,** *54* (7), 399-405.
199. Martins, K. A.; Bavari, S.; Salazar, A. M., Vaccine adjuvant uses of poly-IC and derivatives. *Expert Rev Vaccines* **2015,** *14* (3), 447-59.
200. Merad, M.; Sathe, P.; Helft, J.; Miller, J.; Mortha, A., The dendritic cell lineage: ontogeny and function of dendritic cells and their subsets in the steady state and the inflamed setting. *Annu Rev Immunol* **2013,** *31*, 563-604.
201. Goplen, N. P.; Huang, S.; Zhu, B.; Cheon, I. S.; Son, Y. M.; Wang, Z.; Li, C.; Dai, Q.; Jiang, L.; Sun, J., Tissue-Resident Macrophages Limit Pulmonary CD8 Resident Memory T Cell Establishment. *Frontiers in Immunology* **2019,** *10*.
202. Chiefari, J.; Chong, Y. K.; Ercole, F.; Krstina, J.; Jeffery, J.; Le, T. P. T.; Mayadunne, R. T. A.; Meijs, G. F.; Moad, C. L.; Moad, G.; Rizzardo, E.; Thang, S. H., Living Free-Radical Polymerization by Reversible Addition−Fragmentation Chain Transfer: The RAFT Process. *Macromolecules* **1998,** *31* (16), 5559-5562.
203. Micic, N.; Young, A.; Rosselgong, J.; Hornung, C. H., Scale-up of the Reversible Addition-Fragmentation Chain Transfer (RAFT) Polymerization Using Continuous Flow Processing. *Processes* **2014,** *2* (1), 58-70.
204. Suk, J. S.; Xu, Q.; Kim, N.; Hanes, J.; Ensign, L. M., PEGylation as a strategy for improving nanoparticle-based drug and gene delivery. *Advanced Drug Delivery Reviews* **2016,** *99*, 28-51.
205. Wilson, D. S.; Hirosue, S.; Raczy, M. M.; Bonilla-Ramirez, L.; Jeanbart, L.; Wang, R.; Kwissa, M.; Franetich, J. F.; Broggi, M. A. S.; Diaceri, G.; Quaglia-Thermes, X.; Mazier, D.; Swartz, M. A.; Hubbell, J. A., Antigens reversibly conjugated to a polymeric glyco-adjuvant induce protective humoral and cellular immunity. *Nat Mater* **2019,** *18* (2), 175-185.